From AMPAR lateral diffusion to whisker perception : a new model for cortical remapping

Tiago Campelo

université de BORDEAUX

Thèse présentée

Pour obtenir le grade de

Docteur de L'Université de Bordeaux

École Doctorale

Science de la Vie et de la Santé

Par Tiago CAMPELO

From AMPAR lateral diffusion to whisker perception: A new model for cortical remapping

Sous la direction de : Dr. Daniel CHOQUET

Soutenue le 7 Octobre 2019

Membres du jury :

Richard Huganir	Prof., PhD	Johns Hopkins University (EU)	Examinateur
Anthony Holtmaat	Prof., PhD	Université de Genève (CH)	Examinateur
Jérôme Baufreton	D.R., PhD, H.D.R.	CNRS/Université de Bordeaux (FR)	Examinateur
Isabelle Férézou	C.R., PhD, H.D.R.	CNRS/Université Paris-Sud (FR)	Rapporteur
Julie Perroy	D.R., PhD, H.D.R.	CNRS/Université de Montpellier (FR)	Rapporteur
Frédéric Gambino	C.R., PhD	CNRS/Université de Bordeaux (FR)	Invité

Interdisciplinary Institute for Neuroscience (IINS)

CNRS UMR 5297

Université de Bordeaux

Centre Broca Nouvelle-Aquitaine

146 rue Léo Saignat

33076 Bordeaux (France)

Table of contents

Résumé

De la diffusion latérale des récepteurs AMPA à la perception des whiskers : un nouveau modèle de cartographie corticale

Les champs récepteurs corticaux se réorganisent en réponse aux changements de l'environnement. Par exemple, suite à une lésion périphérique, les modalités sensorielles préservées gagnent de l'espace cortical au détriment de celles lésées. L'étude du cortex somatosensoriel en tonneau des rongeurs a fourni des données importantes pour la compréhension des mécanismes synaptiques à l'origine de cette réorganisation corticale. En condition normale, les neurones de chaque colonne corticale répondent préférentiellement à la stimulation d'une seule vibrisse principale ("*Principal Whisker, PW*"). Au contraire, suite à l'amputation de l'ensemble des vibrisses sauf une ("*Single Whisker Experience, SWE*"), les neurones des colonnes associées aux vibrisses amputées répondent à la stimulation de la vibrisse conservée, à l'origine du renforcement et de l'expansion des représentations corticales des vibrisses conservées.

Bien que des preuves indirectes aient révélées un rôle de la potentialisation à long terme ("*Long-Term Potentiation, LTP*") de synapses préexistantes dans la modification des cartes corticales, probablement *via* une augmentation du nombre des récepteurs AMPA (AMPARs) aux synapses, un lien direct entre la LTP, la réorganisation des cartes corticales, et l'adaptation des comportements sensori-moteurs suite à une altération des entrées sensorielles n'a pas encore été démontré. L'objectif de cette thèse a donc été de mettre en évidence cette relation de façon expérimentale et en condition physiologique. Pour cela, nous avons mis au point une stratégie *in vivo* combinant des enregistrements électrophysiologiques, de l'imagerie biphotonique et l'analyse du comportement d'exploration chez la souris contrôle ("*Full Whisker Experience, FWE*) et amputée de certaines vibrisses (SWE).

Nous avons d'abord confirmé que la stimulation rythmique de la PW ("*Rhytmic Whisker Swtimulation, RWS*") renforce les synapses excitatrices (RWS-LTP) *in vivo* des souris anesthésiées FWE. Au contraire des souris FWE, les neurones pyramidaux des souris SWE présentent une augmentation de l'excitabilité neuronale et une absence de RWS-LTP, indiquant ainsi que les synapses corticales associées à la vibrisse intacte ont été potentialisées en réponse au protocole SWE. Pour mieux comprendre l'implication de la RWS-LTP dans la réorganisation des cartes corticales et l'adaptation des comportements sensori-moteurs, nous avons développé une nouvelle approche pour manipuler la LTP *in vivo* grâce à l'immobilisation des AMPARs par des anticorps extracellulaires ("*cross-linking*"). En effet, notre équipe a montré précédemment que le *cross-linking* des AMPARs empêche la LTP *in vitro*. Par ailleurs, une accumulation des AMPARs au niveau post-synaptique a été démontrée *in vivo* par imagerie biphotonique au cours d'une stimulation RWS, suggérant un rôle de la mobilité de ces récepteurs dans cette RWS-LTP. Au cours de cette thèse, nous avons démontré que le *cross-linking* des AMPARs *in vivo* bloque également l'expression de la RWS-LTP, mais sans affecter la transmission synaptique basale, ni l'induction de la RWS-LTP, indiquant ainsi que la mobilité des AMPARs est également

fondamental pour l'expression de la LTP *in vivo*. De façon importante, le *cross-linking* des AMPARs de façon chronique, au cours du SWE, permet non seulement de rétablir la RWS-LTP et l'excitabilité neuronale, et donc de bloquer la réorganisation corticale, mais aussi de modifier les capacités de récupération sensori-motrices des souris amputées.

Dans l'ensemble, nos données démontrent pour la première fois un rôle critique et direct de la RWS-LTP dans le réarrangement des circuits en réponse à l'amputation de certaines vibrisses. La réorganisation des cartes corticales serait ainsi assurée par le renforcement de la transmission synaptique, et constituerait alors un mécanisme compensatoire pour optimiser le comportement sensorimoteur de l'animal lors de l'altération des entrées sensorielles.

Mots clés : Récepteurs AMPA ; Plasticité synaptique ; LTP ; Réorganisation des cartes corticales ; Imagerie et Electrophysiologie *In vivo*

Abstract

From AMPAR lateral diffusion to whisker perception: a new model for cortical remapping

Neuronal receptive fields in the cerebral cortex change in response to peripheral injury, with active modalities gaining cortical space at the expense of less active ones. Experiments on the mouse whisker-to-barrel cortex system provided important evidences about the synaptic mechanisms driving this cortical remapping. Under normal conditions, neurons in each barrel-column have receptive fields that are strongly tuned towards one principal whisker (PW). However, trimming all the whiskers except one **(single-whisker experience, SWE)** causes layer (L) 2/3 pyramidal neurons located in the deprived and spared-related columns to increase their response towards the spared input. This results in a strengthening and expansion of the spared whisker representation within the barrel sensory map. Indirect evidences suggest that these cortical alterations might depend on the **activity-dependent potentiation of pre-existing excitatory synapses (LTP)**, likely through increased levels of postsynaptic **AMPA receptors (AMPARs).** However, a clear link between LTP, cortical remapping, and the adaptation of sensorimotor skills following altered sensory experience has not yet convincingly been demonstrated. Here, we combined *in vivo* whole-cell recordings, 2-Photon calcium imaging and a whisker-dependent behavior protocol to directly demonstrate this relationship. It has been described that rhythmic whisker stimulation potentiates cortical synapses **(RWS-LTP*)*** *in vivo*. An accumulation of postsynaptic AMPARs during similar sensory stimulation was also reported by imaging evidences. Our data demonstrates that this potentiation is occluded by SWE, suggesting that cortical synapses are already potentiated by this trimming protocol. This is translated into an increased fraction of whisker-evoked somatic spikes in the spared column and sensorimotor recovery by the spared whisker. To better understand the implication of LTP in cortical remapping, we developed a novel approach to manipulate LTP *in vivo* without affecting overall circuit properties. Our team showed previously that the blockage of AMPARs synaptic recruitment by extracellular antibody cross-linking prevents LTP *in vitro*. Here, we report that *in vivo* cross-linking of AMPARs blocks the expression but not the induction of RWS-LTP, suggesting that the synaptic recruitment of AMPARs is fundamental for *in vivo* LTP as well. Moreover, chronic AMPAR cross-linking during SWE reverts RWS-LTP occlusion and the increased fraction of whisker-evoked somatic spikes caused by whisker trimming. As consequence, the sensorimotor performance by the spared whisker is altered by the blockage of cortical remapping. Altogether, these evidences led us to define a critical role for synaptic LTP on circuit re-arrangement after whisker trimming. Our data shows that LTP-driven cortical remapping is a compensatory mechanism to optimize animal's sensorimotor behavior upon altered sensory experience.

Keywords: AMPAR; Synaptic Plasticity; LTP; Cortical Remapping; *In vivo* Patch Clamp; *In vivo* 2-Photon imaging

Acknowledges / Remerciements

What an adventure! This doctorate was the biggest personal and professional challenge of my whole life. I would have never guess that, when I came to Bordeaux for a master's internship, I would be staying for a doctorate! I wouldn't bet that, four years later, I would be shifting from the nanoscale provided by super-resolution microscopy towards the challenge of working *in vivo*. I would like to deeply thank Doctor Daniel Choquet for trusting me in a way that no one ever did. I will never forget his words when he offered me this PhD position. Thank you for everything you taught me, the support, guidance, and daily inspiration… You definitively made me a better person and scientist. Thank you also for letting me attend several scientific meetings, and to present our work to an incredible and exciting community. Also, thank you for the opportunity of launching this challenging but exciting collaboration with Gambino's team.

This was truly a collaborative project. Therefore, I would like to thank my PhD co-supervisor, Doctor Frédéric Gambino. Thank you for being so patient and for teaching me all the theoretical, technical, and analytical background necessary to accomplish all the goals of my PhD project. I have to highlight how precious your help was, from the first cranial window implantation, to the first RWS-LTP that we ever recorded! I couldn't believe that, after four years of work, I would accomplish everything that we did. A huge part of this success is, without any doubt, yours. Thank you for your professionalism and, for along this journey, never letting me down. Thank you for sharing your passion for science with me… It was (and it is) a profound inspiration.

Besides my PhD advisors, I would like to thank to all the members of thesis committee: Professor. Richard Huganir, Professor Anthony Holtmaat, Doctor Isabelle Férézou, Doctor Julie Perroy, and Doctor Jérôme Baufreton, for kindly offering their time to evaluate my work. I am deeply honored that you accepted to be present during my PhD defense, from which we will hopefully build an exciting scientific discussion.

Despite the scientific knowledge that I gathered throughout this adventure, I also realized that science is not only possible but certainly more fun when shared. This work is not only my thesis, but a collaborative work of many people. I would like to deeply thank Elisabete Augusto for teaching and helping me with all the Gap Crossing experiments here performed. To Nicolas Chenouard (spelled with my really bad French accent) for his sorcery on MatLab, he magically analyzed all the intrinsic optical imaging data. To Aron de Miranda (valeu cara!) for sharing his incredible knowledge on single-unit recordings, and the daily motivation that was essential to survive the last year of my thesis. To Côme Camus, a bright master student, who helped me with the somatic 2-Photon calcium imaging. To comrade Vladimir Kouskoff (or Dimitri, I am always confused) for the scientific, philosophical, and geoolitical discussions throughout my PhD. To Mattia (Pau) Aime, a true friend for life, for teaching me that during a PhD, and in life in general, one has to "fino alla fine".

I am also very grateful to all the members of the Choquet's laboratory, the ones with who I shared my master's and PhD thesis, for the technical support, scientific discussion, and friendship

along this incredible adventure. To cite a few: Benjamin Compans, always there for any situation and for all the help he gave me! Thank you dude! Christelle Breillat, our incredible lab manager, for saving my life a countless number of times. Natacha Retailleau, for taking care of me as a younger brother, since my first day in the lab. Julia Goncalves, for sharing both the masters and PhD thesis with me. A special thanks to Hajer El oussini for taking her precious time and helping me with the prototype for the Gap Crossing apparatus used in this project. Her work was very important to accomplish all the behavioral experiments here performed.

A special thanks to Rémi Sterling for supporting directly or indirectly all of my experiments. Also a huge thanks to Mélanie Dessans for the friendship and for saving my bureaucratic life over and over again… Ultimately saving me from gettting arrested due to tax evasion issues!

A word of gratitude to Élisabeth Normand and Christelle Martin for the help and training with the ethical conduct in the care and use of animals for research purposes. Also a special thanks to Doctor Yann Humeau for the scientific discussions and for taking his time to help me with the *in vitro* electrophysiology at the very beginning of my PhD thesis. Thank you, Doctor Fabrice Cordelières, for building the custom made ImageJ plug-in that we used to analyze the preliminary dendritic calcium imaging data.

"Work hard, party harder". This was the way that I decided to face my PhD, in every sense of the quote. Therefore, I would like to thank my good friends, cosmonaut Filipe de Nunes Vicente, the Baleares majesty Tomas Jorda Siquiera, and to the apocalypse knight José Cruz (ganda Zé!), for significantly reducing my lifespan. Thank you all for the good moments, parties, and for turning me into a major Petit Quebec's stockholder. Queria também agradecer a toda a comunidade portuguesa de neurociências em Bordéus, o meu muito sincero obrigado por todo o apoio – Ânia das bolachas, Alexandra, Diogo, Eva (pelas sem ou cem rótulo), Joana (pela ajuda sempre, mas sobretudo no meu mestrado), Nânci, Inês, e Steve! Foi bom ter um grande pedaço do nosso pequeno país sempre presente.

Dedico esta tese a toda a minha família! Quando abandonei a minha casa, há cinco anos atrás, não fazia ideia quão difícil seria estar longe dos meus, das minhas tradições e costumes. Tenho o maior orgulho nos meus pais que sempre trabalharam arduamente para me permitirem a melhor educação possível. À minha mãe, a minha maior conselheira e o meu porto de abrigo, obrigado por estares sempre comigo. Ao meu pai, o maior exemplo da minha vida… Nem com mil doutoramentos serei metade do homem que tu és ! Obrigado pela dedicação, exemplo de trabalho e pela amizade. Ao meu irmão e ao resto da família, especialmente o pequeno grande Afonso, obrigado pela alegria que é voltar a casa. O meu coração é completo muito por vossa causa. Espero que o orgulho de ver esta etapa terminada recompense o facto de um dia ter partido… Mas sempre com a certeza de que, por mais voltas que o mundo dê, terei sempre um pequeno pedaço ao qual eu posso chamar de casa.

Aos meus bons amigos dureza que sempre me souberam e saberão bem receber quando retornado à pátria-mãe. À malta do Arredas por continuarem a organizar a festa que me permite recarregar energias para um novo ano de trabalho.

Remerciement aussi à la personne plus important de la planète, et qui m'a aidé à survivre à cette aventure. Merci Ophélie pour la compréhension, la soutenance et l'amour tous les jours de notre vie. Merci de tolérer mon humeur, les week-ends et les vacances passés sur l'ordinateur ! Je n'aurais pas pu survivre à cette aventure sans ton soutien ... Merci de m'avoir montré que la vie c'est bien plus qu'une pièce noire remplie de microscopes ... Grâce à toi, je sais que la vie a plus de couleurs de ce que j'avais imaginé ! Je suis impatient pour partager beaucoup d'autres aventures près de toi ! Et je suis très heureux de partir pour la prochaine étape à ton côté, je ne saurais pas quoi faire tout seul…Tu es une personne incroyable et je suis très chanceux de partager ma vie avec toi.

Last but not the least, thank you Doctor Daniel Choquet, Doctor Frédéric Gambino, Elisabete Augusto, Aron de Miranda, and Benjamin Compans for the feedback and the critical reviewing of this thesis.

List of abbreviations

AB	Atipamazole/buprenorphine mixture
AMPAR	α-amino-3-hydroxy-5-methyl-4-isoxazolepropionic acid
BC	Barrel Cortex
BDNF	Brain-derived neurotrophic factor
C.W.	Cranial Window
Ca2+	Calcium
CALI	Chromophore-assisted light inactivation
CaMKII	Ca2+/calmodulin-dependent protein kinase II
CCD	Charted-Coupled Device
CNS	Central nervous system
CP-AMPARs	Calcium permable AMPARs
CREB	cAMP-response element-binding protein
CTD	Cytoplasmic C-terminal domain
DC	Discrimination Coefficient
DVN	Deep Vribirssal Nerve
DWE	Dual-whisker experience
eGFP	Enhanced green fluorescent protein
ePSP	evoked Postsynaptic Potential
ER	Endoplasmic reticulum
FPS	Frames per second
FW	Full whisker
FWE	Full-whisker experience
FWHM	Full-width at half maximum
GABA	γ-aminobutyric acid
GC	Gap Crossing
GD	Gap Distance
GKAP	Guanylate-Kinase-Associated Protein
HFS	High-frequency stimulation
I.M.	Intramuscularly
I.P.	Intraperitoneal
IgGs	Imunoglobulin (here used as antibody)
iGluRs	Ionotropic glutamate receptors
IOI	Intrinsic optical imaging
IOS	Intrinsic optical signals
IR	Infrared
iRT	Intermediate Reticular Nucleus
IV curve	Input-Output Curve

K+	Potassium
KARs	Kainate Receptors
KI	Knock-in
L	Layer
LBD	Ligand-binding domain
LFS	Low-frequency stimulation
LTD	Long-term depression
LTP	Long-term potentiation
M1	Primary Motor Cortex
MAGUK	Membrane-Associated Guanylate Kinases
MB	Medotomidine/buprenorphine mixture
MD	Monocular deprivation
Mg2+	Magnesium
MGluRs	Metabotropic glutamate receptors
mPFC	Medial Prefrontal Cortex
Na+	Sodium
NMDAR	N-Methyl-D-aspartic acid
NOS	Nitric oxide synthase
NTD	N-terminal domain
NW	No Whiskers
PDMS	Polydimethylsiloxane
PKA	cAMP-dependent protein kinase
PKC	Protein kinase C
POm	Posteromedial
PrV	Principalis Nucleus
PSD	Postsynaptic density
PSP	Postsynaptic Potential
RA	Radpidly Adapting
ROIs	Regions of interest
RSW	Rhythmic whisker stimulation
RT	Room temperature
RWS	Rhythmic whisker stimulation
RWS-LTP	Rhythmically whisker stimulation-induced LTP
S.C.	Subcutaneous
S2	Secondary Somatosensory Cortex
SA	Slowly Adapting
SpVc	Spinal Trigeminal caudalis Nucleus
SpVi	Spinal Trigeminal Interpolaris Nucleus
SpVo	Spinal Trigeminal Oralis Nucleus
sRWS	Short rhythmic whisker stimulation

sRWS	Short Rhythmic Whisker Stimulation (8 Hz, 2.5 sec.)
STDP	Spike timing-dependent plasticity
SVN	Superficial Vibrissal Nerve
SWE	Single-whisker experience
SWE	Single-whisker experience
TARPs	Transmembrane AMPAR regulatory protein
TeTx	Tetanus Toxin
TMD	Transmembrane domain
TN	Trigeminal Nucleus
U.V.	Ultraviolet
Vm	Membrane potential
Vm	Membrane potential
VPM	Ventral Posterior Medial
VPMdm	Dorsomedial Ventral Posterior Medial
VPMvl	Ventrolateral Ventral Posterior Medial
VTA	Ventral Tegmental Area
wC2	whisker C2
WT	Wild type
X-SWE	Chronic antibody injection during SWE

List of figures

Fig. 27) Pipeline of *in vivo* 2-Photon dendritic imaging;

Fig. 28) The Gap Crossing apparatus and associated behavior protocol;

Fig. 29) SWE drives map plasticity in the barrel cortex;

Fig. 30) SWE alters circuit-wide whisker computation;

Fig. 31) SWE increased whisker-evoked somatic spikes and alters whisker-evoked PSPs;

Fig. 32) SWE occludes sensory-evoked LTP;

Fig. 33) SWE alters pyramidal neurons excitability and RWS-evoked cumulative depolarization;

Fig. 34) *In vivo* AMPAR cross-linking in the barrel cortex;

Fig. 35) AMPAR cross-linking does not alter excitatory nor inhibitory components of whisker-evoked PSPs;

Fig. 36) *In vivo* 2-Photon dendritic calcium imaging with AMPAR cross-linking;

Fig. 37) AMPAR cross-linking blocks RWS-LTP expression;

Fig. 38) AMPAR cross-linking does not alter the induction of RWS-LTP;

Fig. 39) Chronic AMPAR cross-linking during SWE;

Fig. 40) Chronic AMPAR-crosslinking reduces SWE-induced neuronal response potentiation of the spared whisker;

Fig. 41) Chronic AMPAR-crosslinking reverts RWS-LTP occlusion after SWE;

Fig. 42) Resume of all RWS-LTP experiments;

Fig. 43) Gap Crossing as a whisker-dependent behavioral task;

Fig. 44) Map plasticity compensates a learned whisker-dependent behavior;

Fig. 45) LTP facilitates the recovery of altered whisker-dependent behaviors during the early phases of SWE;

Fig. 46) LTP-driven map plasticity does not alter the decision latency, neither GD exploration;

Fig. 47) MK801 intracellular application abolishes NMDAR-mediated plateau potentials and reveals a high-frequency AMPAR component;

Fig. 48) AMPAR cross-linking reveals a postsynaptic short-term depression induced by sRWS;

Fig. 49) Proposed model for sRWS-evoked short-term plasticity on L2/3 synapses;

Fig. 50) Single-unit recordings in the barrel cortex to explore the neuronal correlates of SWE and GC behavior;

Fig. 51) Towards an unsupervised analysis of whisker motion during GC behavior.

Introduction

1. Cortical Remapping

1.1 Cortical representations have well-defined topography

The external world is rich in sensory stimuli, ranging from auditory to visual cues. To survive, animals have to precisely integrate this multisensory information and adjust their behavior accordingly. Cortical representations of both motor and sensory modalities are performed in non-overlapping regions, where neurons with the same function co-localize[1]. This provides not only an efficient computation with a minimal wiring cost within a local circuit, but also across hierarchically related brain regions. Such functional segregation, known as "cortical maps", reflect either (1 – motor maps) the coupling between motor neurons and independent muscles or (2 – sensory maps) the stimulus-specific computation by the neocortex[2]. Our knowledge of cortical maps has incredibly evolved over the last decades (reviewed elsewhere[3]) The first indirect evidence for cortical maps came from Hughlings Jackson's work with epileptic patients[4]. His observations suggested that the stereotyped progression of sensations and movements upon a seizure, closely matches the spread of activity across the maps in the neocortex. The first detailed map of the motor cortex was then confirmed by Sherrington and colleagues, using electrical stimulation on the cortex of primates[5]. Functional maps were finally experimentally demonstrated in humans by Penfield and Boldrey in 1937[6]. They characterized somatotopic maps for tactile sensation in the anterior parietal cortex, based on percepts induced by cortical stimulation on epileptic patients. This map was represented as the cortical homunculus, where the relative amount of cortical area used to gather information from the sensory epithelium is illustrated (fig. 1A). Notably, human sensory maps are not isomorphic, presenting a notable expansion of behaviorally important regions, such as the face, lips, and hands. Later on, a similar functional organization was recorded in anesthetized monkeys, suggesting a common somatotopy across primates[7]. A subsequent study confirmed the presence of somatosensory maps in rodents, where whiskers representations predominate (fig. 1B)[8,9]. Nowadays, it is considered that all the mammalian species have homunculi with different shapes but with a common-theme: body parts with strong behavioral relevance have extended cortical representations[10].

Our understanding of **cortical maps** has changed drastically over the last decades. It is currently assumed that maps are crudely defined during the development, **but can be profoundly reshaped throughout adulthood. More than fixed anatomical entities, cortical maps can be altered by the subject-environment interaction, or radically changed upon altered sensory experience**. **This functional malleability, defined as cortical remapping, not only allows animals to adapt to their environment, but also to injury (e.g., stroke).** The next paragraph will cover a brief historical overview of the groundbreaking work essential to define map plasticity as a fundamental cortical mechanism in the adult brain.

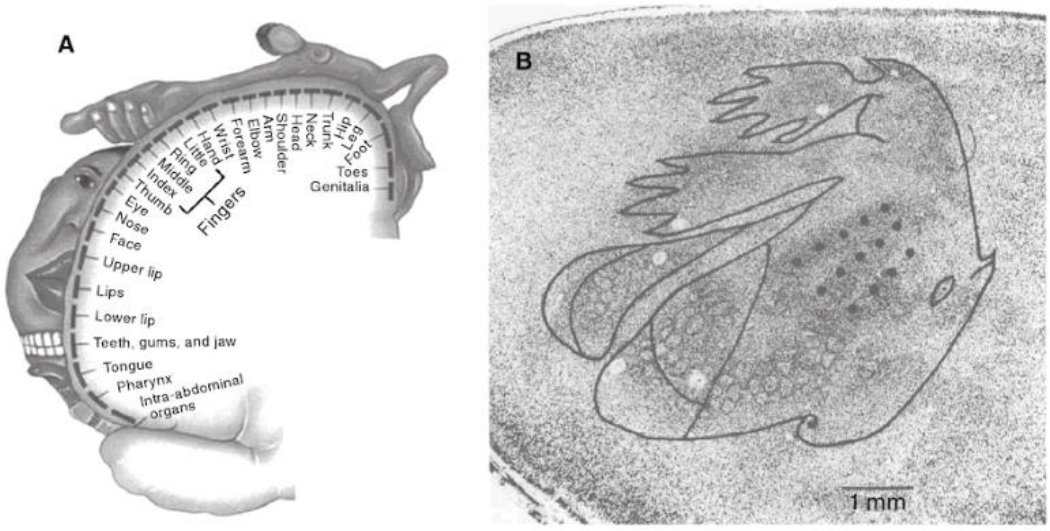

Fig. 1) Representation of the body surface in human and rodent somatosensory cortex. A) The cortical homunculus as described by Penfield and Rasmussen (1950). The human somatosensory cortex has a clearly magnification for areas devoted to the face, lips, and hands representation. **B)** A Nissl-stained section of the rat somatosensory cortex with the body representation superimposed (drawing). A clear magnification of the cortical area devoted to compute whiskers is observed. Figure reproduced from reference Fox, K & Woolsey, T. (2008) Cambridge Univ. Press.

1.2 Cortical remapping in the adult brain – a brief historical perspective

Cortical remapping was classically described to occur exclusively during a restricted period of the animal's life, early during development (Hubel and Wiesel doctrine)[11]. This critical period corresponded to a brief time-window where cortical maps could be dramatically remapped upon altered sensory experience (e.g., monocular deprivation). After that, especially during adulthood, this capacity was believed to dramatically decrease, rendering cortical maps insensitive to experience. Even if critical development periods are important, we **now know that the neocortical architecture can be altered throughout adulthood.** Bellow, the seminal work that allowed this change in paradigm will be presented (also reviewed here[3,12]).

The first evidence for functional remapping in the adult brain came from a study of cortical representations of the body surface in monkeys[13]. Merzenich and colleagues demonstrated that, upon finger amputation, the somatosensory representation of the spared inputs expanded into the deprived region. This observation was similar to the Hubel and Wiesel's postulates, however with a remarkable difference: it occurred after the critical developmental period, in the adult brain. Two different mechanisms that could explain adult cortical remapping were proposed by the authors: (1) either a simple anatomical competition between inputs or (2) an activity-dependent recruitment of the deprived region by the spared input. To test which of the hypothesis was correct, they performed an experiment where two fingers were surgically fused (syndactyly) to compromise

competition between inputs[14]. They found that, after syndactyly, somatosensory neurons acquired the capacity to respond to both fingers, with a concomitant merging of the cortical maps. This was the first evidence that remapping requires an activity-dependent temporal correlation between sensory inputs and cortical regions to occur. A distinct set of experiments, showed a similar injury-induced cortical remapping in different sensory cortices[15,16]. Therefore, remapping was not limited to the somatosensory cortex, but expressed throughout the neocortex. A further study on the cat visual cortex helped to refine the activity-dependence for cortical remapping proposed by Merzenich and colleagues. Alteration on the visual maps upon lesion was not due to changes in the location or number of cortical neurons, but rather due to a progressive shifting of their responses towards the spared input[15,17]. These initial observations paved the way to our current knowledge on the cellular and circuit underpinnings of adult cortical remapping (discussed on chapter 3). Later on, map plasticity was described to occur not only to peripheral, but also in response to lesions in central somatosensory areas (e.g., focal lesion)[18,19]. Furthermore, cortical remapping was described to occur not only in response to injury but naturally during behavior. In agreement, when adult monkeys used precise fingertips to receive food rewards, the representation of the corresponding skin regions in the cortex expanded[20].

From this brief historical perspective, one can easily identify **common aspects of adult cortical remapping: (1) it is a canonical mechanism across different sensory modalities; (2) it requires activity-dependent and time correlated alterations of cortical representations; (3) occurs during peripheral or central injury; (4) but also naturally during behavior, due to sensory overuse; (5) cortical areas computing overused sensory modalities, or behaviorally more relevant, increase their representation, while (6) regions responding to deprived inputs shrink their cortical maps.** Therefore**, neocortical architecture is continuously redefined throughout life, where sensory representations in cortical maps are continuously modified**. **These alterations do not involve dramatic alterations in anatomy, but rather subtle activity-dependent adjustments of neuronal responses. This increases learning abilities and perceptual functions by adapting neuronal responses according to the environmental context or after injury.** The next section will describe recent evidences of cortical remapping in the human brain, both in physiological and pathological conditions. The latter is an area of intense research, where approaches promoting cortical remapping are seen as promising therapeutic venues to improve patient's recovery. This will help to illustrate the importance of fundamental research on map plasticity, and how studies on simpler models (e.g., rodents) can significantly impact human conditions.

1.3 Experience-dependent and injury-induced cortical remapping in the adult human brain

Functional imaging studies revealed that, similar to other primates, **experience-dependent cortical remapping also occurs in the adult human brain** (reviewed by[3,12,19]). For instance, prolonged and synchronous stimulation of multiple fingers has been reported to result in a merging of their cortical representations[21]. Along the same line, sensory overrepresentation on stringed

instrument players or Braille readers also alters the cortical map of the predominantly used finger[22,23]. A similar re-organization was reported to occur in the auditory cortex of musicians, with an enlargement of the cortical region computing the specific tones of the played instrument[24]. On the contrary, focal hand dystonia (loss of muscular control in highly practiced movements), leads to a disordered cortical representation of the fingers[25]. Remarkably, cortical maps from patients with congenital syndactyly were reported to be restored after a corrective surgery[26]. Altogether, these studies corroborate an evidence also reported in non-human primates: the activity-dependence and time correlation of the sensory inputs for cortical maps formation.

Besides experience-dependence**, cortical remapping has been also implicated in recovery from different pathological conditions.** The best example for injury-related map plasticity is the recovery from the leading cause of adult disability: stroke (reviewed here[27]). It is now believed that the stroke-injured brain partially restores its normal functions due to motor map plasticity[28,29]. The general principle is that, upon central brain damage, cortical remapping operates to recruit additional cortical areas to compensate behavioral demand. In agreement, rehabilitation strategies are based on repetitive, and intensive, task-specific motor training to promote plasticity-induced recovery of the affected movement[29]. Another interesting area of research for remapping-induced functional recovery is the alternative treatments to threat amblyopia, also known as the lazy eye[30]. In this case, researchers can use visual training (e.g., video games) to enhance visual cortex plasticity in amblyopic adult patients. This promising approach has been described to significantly improve several visual dysfunctions associated to this pathology[31].

The effect of map plasticity in the human brain can also have a deleterious effect[3,19]. This mechanism can under certain conditions alter the normal computation in the neocortex. The best example of this malplasticity is the **phantom limb pain syndrome** (see for review[32]). This pathology refers to pain in an amputated part of the body, and assumed to be related to changes in cortical maps. A good example of this aberrant remapping, came from a study with arm amputees[33]. In this case, amputation-induced plasticity lead to an aberrant cortical expansion of the facial cortical representation into the deafferented (arm) region. This type of malplasticity is believed to evoke a spatial sensation of the missing limb that, along with an incongruent proprioceptive feedback, might evoke pain[19,32]. It is important to state, however, that a clear link between phantom limb syndrome and cortical remapping does not exist. Even more complicated, some cases of this pathological condition were reported to occur without any cortical re-organization[34].

Despite these heroic advances, still little is known about the fundamental synaptic, cellular, and circuit mechanisms underlying cortical remapping, neither their importance for adaptive behaviors. This is due, in part, to the implicit difficulties of using humans and non-human primates to answer these questions. Fortunately, **cortical remodeling was also described to occurs in different sensory cortices from rodents**[12,35]. Indeed, the bulk of the current knowledge about the underpinnings of map plasticity were gathered from these simpler models.

The final section of this chapter will (1) introduce important concepts on synaptic plasticity and (2) describe how these mechanisms underlie the functional changes induced by cortical remapping.

1.4 Towards the synaptic and neuronal substrates of cortical remapping

The last section described the most obvious consequence of cortical remapping: the functional alterations at the circuit level. It was referred that, **depending on the experience, sensory maps can either be expanded or shrinked. Importantly, these are not simple anatomical alterations, but activity-dependent alterations of the neocortical architecture**. However, a fundamental question still has to be answered: what ultimately underlies this circuit refinement? The solution to this conundrum lies on the most fundamental unit of a brain circuit – the synapse.

Neurons are highly specialized cells from the nervous system. Each individual neuron communicates with hundreds to thousands of others, shaping complex neuronal circuits. This communication occurs in a sophisticated cellular contact, known **as synapse**[36,37]. Synapses are generally formed by the axon terminal of the presynaptic neuron and the dendrites of the postsynaptic ones. They can be either electrical or chemical in nature. In an electrical synapse, both pre- and postsynaptic membranes are connected by gap junctions – clusters of transcellular channels composed by connexins[38]. This membrane apposition allows an electrical coupling between neurons, where voltage changes in the presynaptic cells are directly perceived by the postsynaptic one. In a chemical synapse, presynaptic electrical activity is rather converted into the release of a chemical signal by the axon[37]. Neurotransmitter released into the synaptic cleft binds then to specific receptors accumulated in the postsynaptic membrane. A complete overview of the molecular machinery involved on the glutamatergic synaptic transmission is provided in chapter 4. Receptor binding to its specific agonist triggers a complex cascade of signal transduction in the postsynapse and a complex decoding of the original synaptic input[36,37]. This allows neurons to adjust the efficacy of their individual synapses accordingly to the ongoing activity, by a process known as synaptic plasticity.

"Neurons that fire together wire together" - the fundamental principle of the Hebbian theory for synaptic plasticity and associative learning[39]. Donald Hebb postulated that "*when an axon of cell A is near enough to excite a cell B and repeatedly or persistently takes part in firing it, some growth process or metabolic change takes place in one or both cells such that A's efficiency, as one of the cells firing B, is increased*". This postulate implies that, upon tight temporal correlation between presynaptic firing and postsynaptic activity, a given synapse increases its gain (i.e., it gets potentiated). As consequence, the likelihood of neuron A to drive neuron B increases, in an input-specific way. This input specificity implies that modifications can be induced in one set of synapses on a neuron without affecting other synapses. The first evidence for this theory came from Bliss and Lømo experiments in 1973[40]. **They demonstrated that upon high-frequency activation of excitatory synapses in the hippocampus, postsynaptic responses**

increased in a long-lasting manner. A similar effect was described, two decades later, in the neocortex[9,41]**. This phenomenon, coined as long-term potentiation (LTP), has been exhaustively characterized, and is currently considered the cellular substrate for memory formation and retrieval (fig. 2A)**[42,43]. A conceptual limitation of LTP is that, in the absence of a counterbalance, it can lose its significance due to a generalized increase of synaptic gains. Therefore, an inverse mechanism to LTP has to exist in order to efficiently code information at the neuronal level. This mechanism is **known as long-term depression (LTD)**, by which the efficacy of synaptic transmission can be decreased in an activity-dependent and long-lasting manner (fig. 2B)[44,45]. Mechanistically, LTD can either be input-specific (homosynaptic) or expressed in different synapses than the one activated upon a presynaptic spike (heterosynpatic)[46].

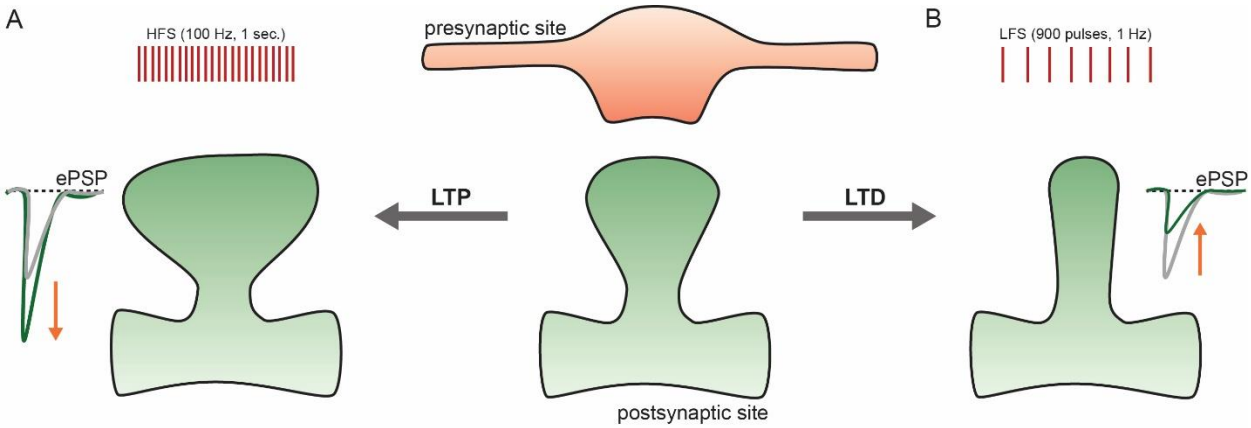

Fig. 2) A model of bidirectional synaptic plasticity. The fundamental properties of the communication between neurons are not fixed, but rather dynamic, due to synaptic plasticity. Depending on the pattern of activity, synapses (green) can be either increase (LTP) or decrease (LTD) their efficacy. **A)** Synaptic LTP is induced by a high-frequency (HFS) coupling of pre- and post-synaptic activity. This leads to global alterations on the postsynaptic site (detailed on chapter 4), that ultimately increase the evoked postsynaptic potential (ePSP). **B)** Synaptic LTD is induced by low frequency stimulation (LFS), with concomitant decrease of ePSP. Changes on ePSP relative to basal state are indicated by the orange arrow.

It is important to state that these forms of synaptic plasticity are induced by (likely) non-natural patterns of presynaptic activity. A more physiological model of strengthening/weakening synapses exist by a mechanism known as **spike timing-dependent plasticity (STDP)**[47]. The induction of STDP relies on the **frequency or time synchrony of both pre- and postsynaptic activity.** In terms of frequency, STDP can induce (1) LTP, by a high-frequency burst of pre-before-post pairing or (2) LTD, upon high-frequency post-before-pre pairing of neuronal responses[47,48]. Regarding the timing, STDP can induce (1) LTP, if a presynaptic spike precedes for a few milliseconds or coincides with a postsynaptic depolarization, or (2) LTD, if postsynaptic activity occurs first than the presynaptic one[47,49].

A different type of synaptic plasticity, importantly mostly lacking input-specificity, known as **homeostatic plasticity**, was more recently described[50]. The principal form of homeostatic plasticity is the "synaptic scaling", **where the strength of all synapses are increased (scaling**

up) or decreased (scaling down) to normalize neuronal responses to a steady-state level[51,52]. In agreement, permanent reduction in neuronal activity drives scaling up at the single-neuron level, while increased excitability causes a scaling down. The timescale of this form of plasticity is much slower than the one for LTP or LTD and, by consequence, useful to achieve homeostasis at the circuit level.

A key aspect of synaptic plasticity is that, when considered at the circuit level, it provides the computational flexibility required for animal behavior. The basic properties of neuronal circuits can be defined by the complex pattern of synaptic weights connecting each individual cells[44]. As described, these weights are not simply genetically-encoded, but importantly shaped by ongoing activity. All forms of synaptic plasticity orchestrate the temporal and spatial flow of information in a given neuronal circuit – in a more efficient way that a simple (anatomical) recruitment or removal of neurons would allow. This not only ensures an optimal information storage at the circuit-level, but also a developmental and experience-dependent network refinement critical for **behavioral flexibility.**

One of the first evidences that synaptic plasticity underlies cortical remapping came from Merzenich and colleagues work with syndactyly in adult owl monkeys[14]. After three decades, we now know that the activity-driven remapping proposed by the authors is, at the neuronal level, a consequence of synaptic plasticity. **A huge part of this knowledge came from studies that took advantage of the simple neuronal circuits underlying sensory processing in rodents** (fig. 3). Even if important differences exist across rodent sensory cortices, they share common mechanisms for map plasticity. Indeed, upon altered sensory experience, cortical remapping is believed to **(1) initially require alterations of pre-existing synapses; (2) involve formation of new synapses and (3) at larger time-scales, drive circuit-wide structural alterations in axons and dendrites**[19,53,54]. **At the single-cell level, the combination of these mechanisms is believed to shift neuronal responses (i.e., response tuning) towards the active sensory input.** Moreover, the rule of thumb for the synaptic alterations during map plasticity states that **(1) LTP drives the cortical representation of the spared/used input, while (2) LTD is used to shrink the representation upon sensory deprivation**[54]. It is worth mentioning that this is, however, an oversimplied view of the problem. Indeed, cortical remapping might rather rely on complex spatiotemporal interactions between different synaptic mechanisms, occurring in distinct cell types. Other local (e.g., vasculature modifications) or brain-wide mechanisms (e.g., neuromodulation) might also directly impact the expression of cortical remapping (discussed on chapter 3).

One of the most popular models to study cortical remapping is the whisker-to-barrel system. This remarkable circuit allows not only the recording of well-defined neuronal responses to naturally occurring stimulus, **but also to induce map plasticity by simple whisker trimming.** The barrel system has in addition a well-defined somatotopy, developmental, and synaptic plasticity alterations, that allows to study cortical remapping in behaviorally relevant conditions. An exhaustive description of the synaptic, cellular, and circuit mechanisms of whisker-related map

plasticity will be provided on chapter three. This will be complemented with information from other sensory regions, where certain aspects of remapping have been preferentially studied. To better understand how a system is modified, one has to know how it normally works. Therefore, a complete overview of the anatomy and physiology of the whisker-to-barrel system will be provided on the next chapter. This will prepare the reader to better understand how barrel cortex computation is altered by sensory-experience.

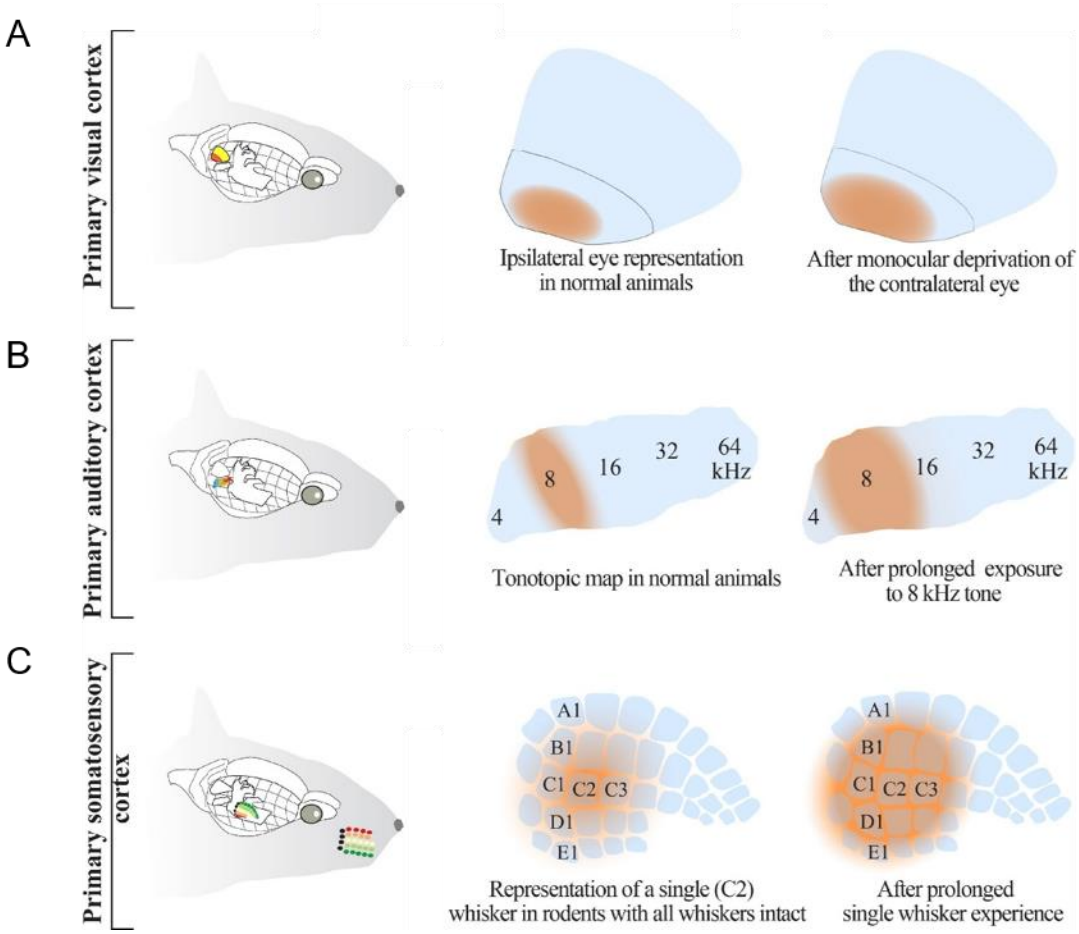

Fig. 3) Cortical remapping across primary sensory cortices in rodents. Cortical remapping has been exhaustively studied on the **A)** visual cortex - monocular deprivation increases the cortical representation of the spared (contralateral eye); **B)** auditory cortex – where sensory over-representation of a given tone (e.g., 8 kHz) increases its cortical representation or **C)** barrel cortex – whisker representations can be dramatically changed upon whisker trimming (detailed on chapter 2 and 3). Adapted from Kole, K. *et al.*, (2018) Neurosci. Biobehav. Rev.

2 The barrel cortex – an anatomical and functional description

2.1 Whiskers provide tactile sensorimotor information

Rodents are nocturnal animals. Virtually all the aspects of their behavior, from eating to reproduction, are modulated by the near absence of light. To overcome this limitation, rodents developed a complex somatosensory system. **By using their whiskers as tactile organs, they replaced the dependence on vision as the major sensory modality for environmental exploration**[9,55].

Mice have a group of **30 to 35 mystacial vibrissae that can be deflected by muscles in and around the whisker pad to acquire tactile information** (fig. 4A)[9,56]. All the main whiskers are organized in a well-defined matrix of 5 rows classified from A to E (dorso-ventral), and 7 principal arcs with a caudo-rostral distribution. An additional arc containing four additional whiskers (α, β, γ and δ) aligned between the rows is present in the caudal part of the matrix. Individual whiskers have defined length and thickness, with caudal whiskers being longer than the rostral ones[57]. Whisker follicles have a conical shape able to detect subtle variation of object's surface textures[9,58]. As whiskers palpates a surface, their tip can be halt in a texture-dependent time function, after which it can slip from surface grains. Therefore, each texture results in a unique "kinetic signature" defined by the stick-slip events[59,60]. **This allows mice not only to compute textures, shapes or distances between objects, but also to mediate social interaction**[61].

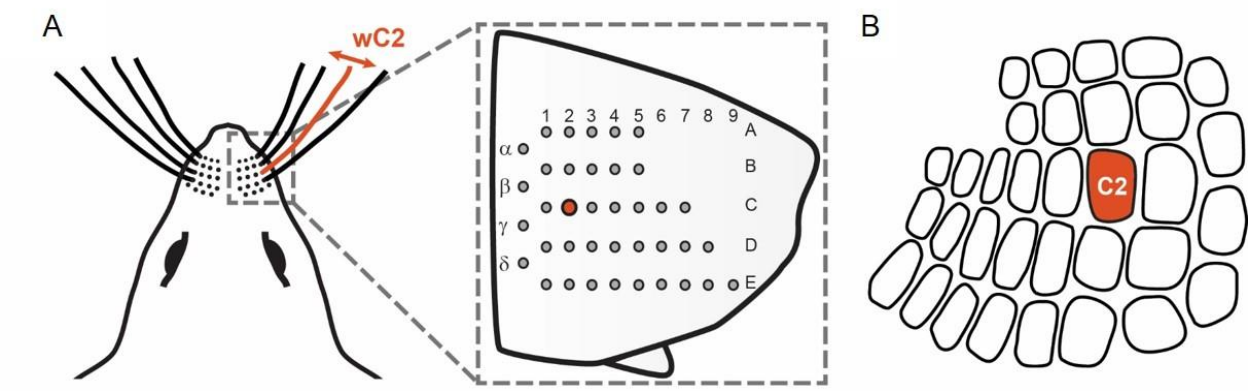

Fig. 4) The exquisite somatotopy of the whisker-to-barrel system. A) Mice have a complex two dimensional grid of whiskers that can be moved in the tridimensional space by muscles in the whisking pad. The whisker pad is organized in five rows of 9 to 5 whiskers in both sides of the snout. In orange, the whisker C2 (wC2) is represented. **B)** Stimulation of wC2 is computed by the C2 barrel due to the exquisite somatotopy of the whisker-to-barrel system.

Rodent's change the *modus operandi* of their whiskers accordingly to their behavioral needs – in a similar way that humans adopt a large spectrum of sensorimotor strategies to optimize perception. Briefly, whisker-mediated perception can be divided in two different categories: (1) generative mode and (2) receptive mode (reviewed elsewhere [62]). In the first mode, animal actively use their whiskers (whisking) to seek the contact, and to optimize object perception. This implies that sensory systems integrate motor information to correctly compute the

incoming information. The mechanism underlying sensorimotor integration will be discussed later on this chapter (see section 2.4). In the receptive mode, rodents have their whiskers immobilized to optimize the sensing from a physical entity (e.g., predator) moving in their direction.

Active whisking infers a rhythmic use of the whiskers by rodents in the rostro-caudal axis at a relative low frequency (5-15Hz)[9,55]. **During exploration, they can adjust the movement of their whiskers to make smaller movement at higher frequencies (15-25 Hz)**[63]. The combination of active whisking and the precise time-locking of stick-slip events efficiently converts tactile into neuronal information[62]. This active motion of whiskers is accompanied by head movement, and posture adjustment to guide the animal throughout the environment. Similarly, obstacles recognition requires synchronization of respiration, head, and whisking to generate an object perception[64,65]. Importantly, the dynamics of whisker movement are greatly dependent on the animal behavioral state. In agreement, a decreased whisking amplitude has been described to occur once the animal gets familiar with its environment[66].

Tactile information perceived by the whiskers on the mice's snout is primarily computed in the barrel cortex, a subpart of the somatosensory cortex (S1). The exquisite somatotopy between individual whiskers and their cortical computation placed the barrel cortex as one of the best models to study the synaptic mechanisms of cortical remapping (fig.4B). The cortical area devoted to the barrel cortex comprises 2.1 to 2.8 mm^2 and represents around 13 % of the total cortical surface[8,67]. This indirectly demonstrates the importance of whiskers as tactile organs for rodents, as hands are important for humans and other primates. Additional neocortical structures, and subcortical structures are also recruited for a complete sensorimotor transformation of the whisker-tactile information.

This chapter will start with an overview of the brain regions implicated on the primary processing of whisker-related tactile information. Then, the principal anatomical pathways that route neuronal information from the whiskers to the neocortex will be described. This picture will be further complemented with a complete description of the intra- and inter-laminar connectivity of the cortical structures implicated on whisker processing. This anatomical description will be then enriched by a functional picture of the cortical processing in response to a minimal whisker deflection and during complex forms of whisker-dependent behaviors. This functional characterization will be complemented with a non-exhaustive description of the most studied subcortical circuits implicated on the whole-body integration of whisker sensorimotor information. Finally, this chapter will be ended with a discussion of the recent and conflictual views that place the barrel cortex as more than a simple sensorial decoder.

2.2 From whiskers to the cerebral cortex – a circuit overview

Whiskers are attached to the skin by a complex structure defined as the follicle-sinus complex – an oval structure formed by two pockets (one inside the other) originated from dermis and epidermis (fig.5A). Both pockets are separated by a cavity known as the sinus[9]. The overall complex is wrapped with striate muscles able to precisely control whisker movements (reviewed elsewhere[68,69]). They can be roughly divided into two different families accordingly to their function: (1) intrinsic muscles which contraction leads to whisker's protraction and (2) extrinsic muscles which movement is linked to retraction. Both type of muscles are innervated by cholinergic motor neurons located in the lateral facial nucleus whose activity orchestrate whisker movements[70]. They receive synaptic inputs on different somatodendritic domains from different whisker premotor neurons projecting from different brain regions (described here[71]). Interestingly, motor neurons innervating intrinsic muscles projected preferentially from the intermediate reticular nucleus of the brainstem (IRt), while the ones innervating extrinsic muscles from the spinal trigeminal interpolaris nucleus (SPVi, see below)[68].

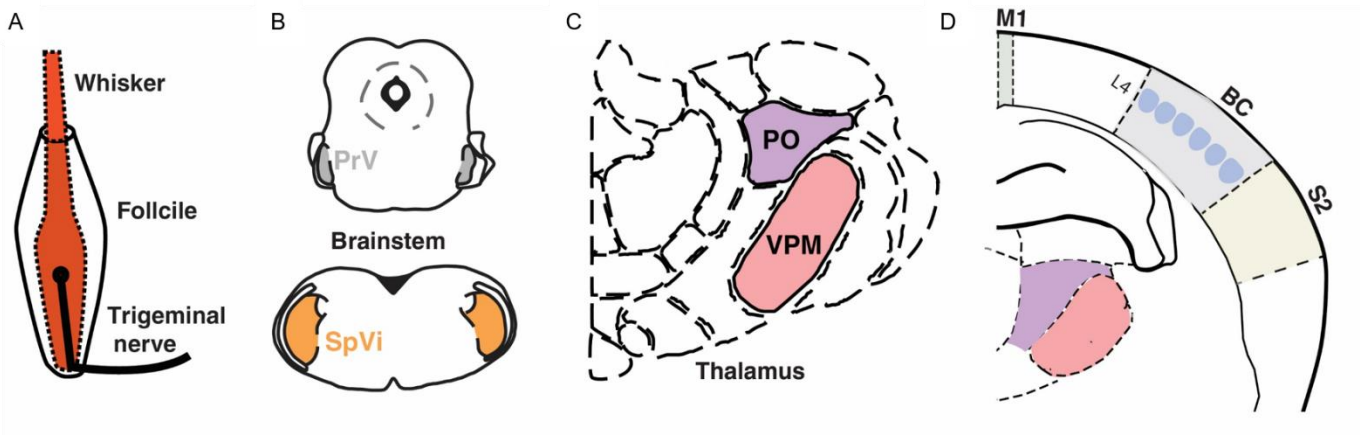

Fig. 5) From whiskers to the neocortex: a circuit overview. A) Whiskers are tactile organs attached to mice's skin by the follicle-sinus complex. Whisker movement is translated into neuronal activity by mechanogated ion channels and the consequence depolarization transmitted along the trigeminal nerve to the **B)** brainstem trigeminal complex. Here are represented the principalis nucleus (PrV, top) and the interpolaris of the spinal one (SpVi, bottom). **C)** Upon TN processing, whisker-related information is sent to the thalamus. More concretely, to the VPM (light pink) and the medial part of PO (purple) nuclei. **D)** After subcortical processing, whisker-related information is finally computed in the three major neocortical regions: (blue) the barrel cortex (BC) characterized by the L4 barrels; S2 (yellow) and M1 (green). M1 position does not correspond to the precise stereotaxic coordinates. Figure C adapted from Allen Brain Atlas (section 71/132) and D from Paxinos Brain Atlas (Coronal slice from bregma: -1.34 mm).

Individual follicle-sinus complexes are innervated by both the superficial vibrissa nerve (SVN) and the deep vibrissal nerve (DVN)[72,73]. The SVN and DVN fibers can have (1) Merkel cell endings, which are slowly adapting (SA) or (2) lanceolate endings, which are rapidly adapting (RA) mechanoreceptors[9,69]. As consequence, lanceolate endings compute mostly unexpected whisker movements, while Merkel cell endings will primarily detect ongoing ones. The cell bodies

of these fibers are predominantly located in the trigeminal ganglion. As these axonal projections do not branch, each neuron in the trigeminal ganglion receives a single-whisker input[9]. Mechanical movements of the whisker activate the different mechanogated ion channels in both DVN and SVN nerve endings[74]. The resulting depolarization drives an action potential on these sensory neurons that is propagated towards the infraorbital branch of the trigeminal nerve projecting to the brainstem.

Trigeminal afferents carry a strict mono-whisker input to the brainstem trigeminal complex (TN), which consist of one principalis nucleus (PrV) and of three spinal nuclei (oralis, SpVo; interpolaris, SpVi; and caudalis, SpVc) (fig.5B)[75]. Upon entering the brainstem, primary afferents axons bifurcate to an ascending fiber to PrV and a descending fiber to the spinal portions of TN. All the nuclei, except SpVo and the rostral part of SpVi, have a have a well-defined somatotopy where trigeminothalamic neurons are organized in barrelets[76,77]. The organization of barrelets has an inverted somatotopy, with rostral whiskers having a medial representation and dorsal whiskers a ventral one. Each barrelet has its maximal response tuned towards the principal whisker, forming a complete whisker map. However, neurons in TN can also be multi-whisker decoders and integrate information from more than one whisker[78]. For instance, while the PrV nucleus is dominated by single-whisker neurons, SpVi neurons can have large receptive fields comprising up to 16 whiskers[79,80]. After being processed in TN, tactile information is then relayed to the contralateral somatosensory thalamus. This is performed by efferent projections from distinct TN nuclei and originates different anatomical pathways for whisker computation (detailed below).

The thalamic decoding of whisker-related information is performed by two different nuclei: the ventral posteromedial (VPM) and the posteromedial (POm) (fig.5C)[9,74]. The VPM receives major projections from PrV and SpVi nuclei of the brainstem[9]. This thalamic structure is organized into banana-shaped tubes with 1-200 μm in diameter defined as barreloids[81,82]. These barreloids are prominent in the dorsomedial part of VPM (VPMdm), with a less obvious representation in the ventrolateral part (VPMvl). The barreloid area can be further divided into "head", "core", and "tail" sub-regions from where the different pathways of whisker computation further diverge[9,83]. VPMdm neurons respond preferentially to the principal whisker, where it evokes stronger responses than the surrounding ones[84]. The POm lacks somatotopic organization, receives projections mainly from multi-whisker SpVi neurons, and computes multi-whisker information[9,75,83]. Moreover, POm is under direct control of a strong cortical feedback (see below). Thalamic neurons from both structures project to different brain regions devoted to compute distinct properties of the whisking behavior (detailed on section 2.3).

Most of the primary computation of the tactile information received from whiskers on the animal's snout is performed by the barrel cortex (fig.5D)[9]. Similar to other cortical areas, this region is an assembly of six different layers (L), dorsoventrally designated L1 to L6. All of them have a distinct architecture due to the presence of different cell types and connectivity patterns. Up to 80% of the barrel cortex cells are excitatory and localized from L2 to L6 (detailed

on fig. 6A[41])[85]. They are mostly **pyramidal neurons**, and are characterized by **(1) a typical triangular shape of their soma; (2) well-defined apical dendrite that projects vertically towards the cortical surface and (3) several basal dendrites that projects laterally from the base of their cellular body.** An additional type of glutamatergic cells, known as spiny stellate neurons, is specifically found on L4[86,87]. The information flow across different excitatory cells is fine-tuned regulated by inhibitory interneurons. Even if in significant less number, interneurons are present within all layers of the barrel cortex[88]. They can be roughly divided in three different families accordingly to the expression of specific molecular markers: **(1) ionotropic serotonin receptor 5-HT_{3A}R and nicotinic acetylcholine receptors; (2) calcium-binding protein parvalbumin (PV) or (3) somatostatin (SST)-expressing interneurons**[89]. The cells are GABAergic non-pyramidal cells with a complex dendritic and axonal arborization (detailed on fig. 6B[42]). Their atypical morphology places inhibitory interneurons as "maestros" of local excitatory microcircuits activity. In agreement, a strong local inhibition has been described to render the firing rate of different L2/3 pyramidal neurons sparse[90,91] (see section 2.4). Inhibitory gating is important in all cortical layers, especially on L1 where all the cells are considered to be GABAergic. This inhibition has been elegantly described as a master regulator of dendritic mechanisms and synaptic plasticity of L2/3 pyramidal neurons (detailed on chapter 3)[92].

The barrels that gives the name to this cortical region are located in L4[9]. There, a characteristic cluster of L4 neuronal dendrites and VPM axons can be found in a barrel-like shape. The space between and around the different barrels is defined as septa, which mainly receive multi-whisker inputs (see below) [93]. This septal circuitry is more prominent in rats than in mice. Barrels are organized in rows and arcs in a same way than the whiskers on the animal's snout. This results from the circuitry's exquisite somatotopy and ensures that each individual barrel receives a predominant input from its principal whisker[94]. **Besides the barrel cortex, whisker-related information is processed by additional cortical regions such as the secondary somatosensory (S2) and primary motor (M1).**

Fig. 6) Different categories of Barrel Cortex excitatory neurons and inhibitory interneurons (fig. on the next page). A) Classification of different sub-classes of barrel cortex pyramidal neurons accordingly to their dendritic morphology. L4 has three different morphological classes of excitatory intratelencephalic (IT) neurons: pyramidal, star pyramidal, and spiny stellate. Additional IT neurons are found in L2, L3, L5A and L5B. Contrarily to L4, these neurons have a remarkable intralaminar and intracolumnar branching. Additionally, pyramidal tract (PT) neurons of L5B and corticothalamic (CT) neurons of L6 are also represented. Figure adapted from Harris, K. D. & Shepherd, G. M. (2015) Nature Neurosci. **B)** Besides their biochemical profile, inhibitory interneurons can be further divided accordingly to their dendritic (*red*) and axonal (*blue*) morphologies. A sub-division accordingly to their preferential postsynaptic target can be made: ChC (chandelier or axo-axonic) cells forming synapses in the axon initial segment and controlling the input/output function of pyramidal neurons; BC (basket cells) that form synapses with the soma and proximal dendrites of pyramidal cells or other interneurons. A good example of BC cells is the PV+ fast spiking interneurons; NGFC (Neurogliaform cell) have a spider web-like axonal arborization targeting basal and proximal apical oblique dendrites; MC (Martinotti cell) are belloning to the family of interneurons targeting exclusively distal dendritic compartments; VIP (Vasoactive intestinal polypeptide cell) neurons targeting specifically other types of interneurons. Figure adapted from Feldmeyer, D. *et al.,* (2018) Neuroscience.

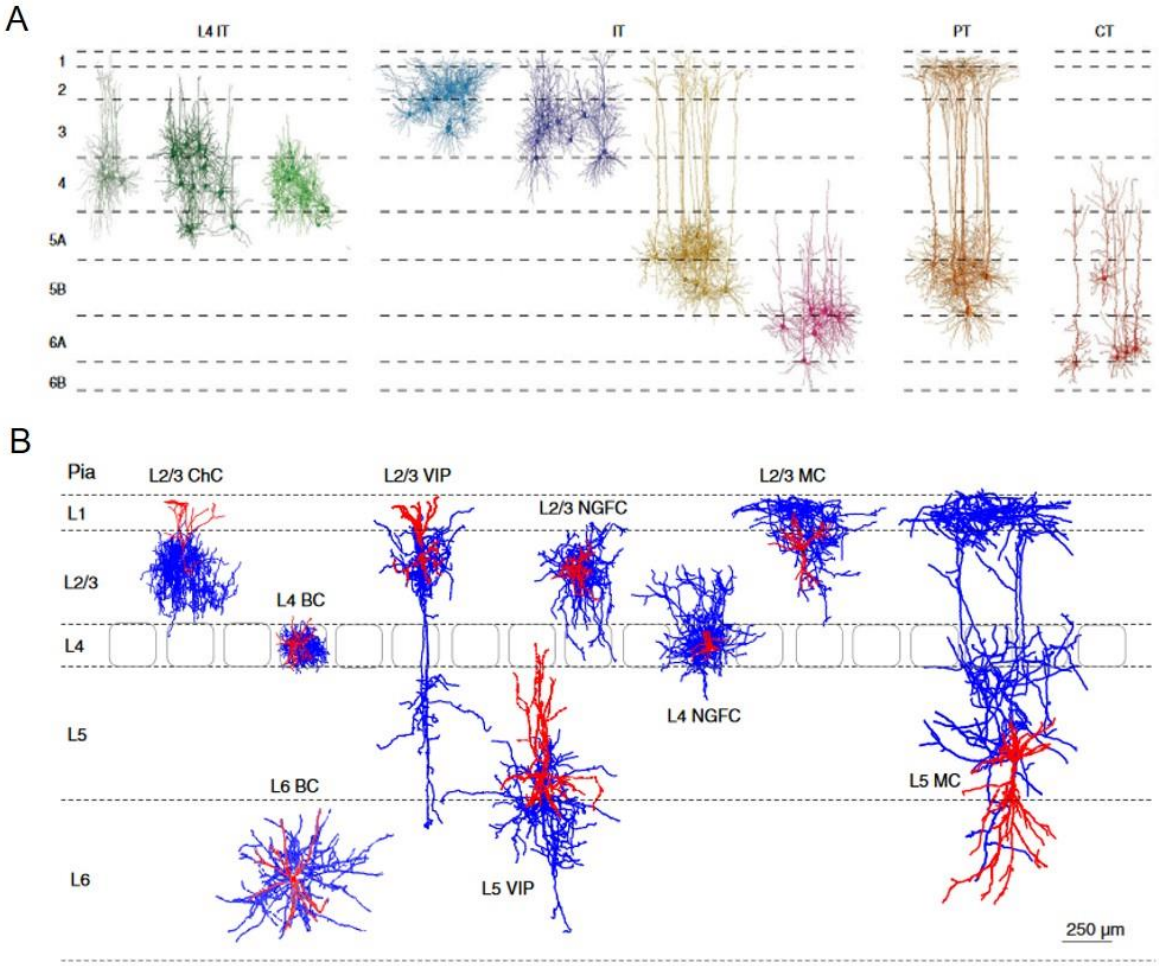

The next section will describe the different anatomical pathways that convey information from the whiskers to the different neocortical structures and their implication for tactile perception.

2.3 Trigemino-thalamo-cortical pathways for whisker-related tactile information

Whisker-related information is relayed by four trigemino-thalamo-cortical pathways: two lemniscal, a paralemniscal, and an extralemnsical (fig.7). All of them share the same trigeminal afferent but significantly divergence from TN's processing, their thalamic nuclei, and their neocortical target structures/layers[9,74,83,95]. Ultimately, all the different anatomical pathways convey different aspects of the whisker sensation.

The lemniscal pathway is the main source of single-whisker information to the barrel cortex. It departs from single-whisker neurons in PrV, and is carried via the barreloid cores in VPMdm to the barrel cortex[96,97]. There, VPM inputs predominantly target L4 and L6A and to a lesser extent L3 and L5B. As previously mentioned, VPM inputs into L4 show a barrel-column related projection due to a high clustering at individual barrels. A second lemniscal pathway

emerging from the barreloid heads in VPMdm and innervating neurons in L4 septal regions is also described[98,99]. The lemniscal pathways has been hypothesized to mediate whisking-touch computation[100].

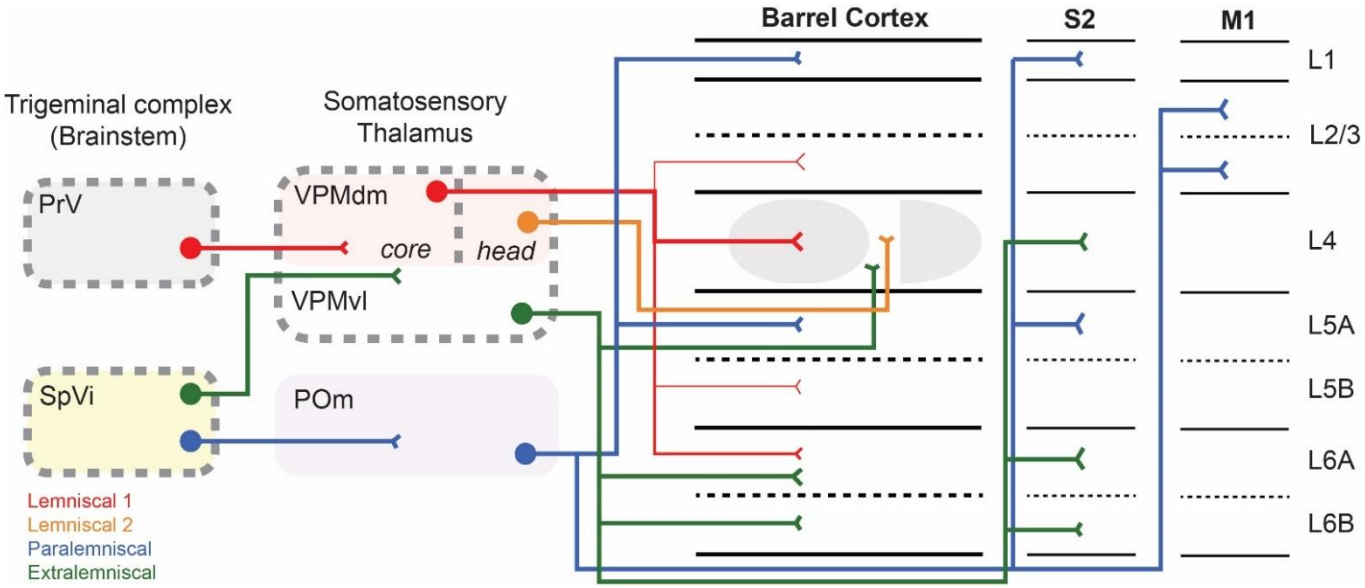

Fig. 7) The four different anatomical pathways that convey tactile information from the whiskers to the neocortex. Overview of the different trigemino-thalamo-cortical circuits conveying whisker-tactile information to the barrel cortex and other neocortical regions: lemniscal 1 (red), lemniscal 2 (orange), paralemniscal (blue) and extralemniscal (green).

The paralemniscal pathway originates from multi-whisker neurons in the caudal part of SpVi and projects to the barrel cortex via POm projections to L1, L5a and septal regions of L4[9,75,93]. In L1 and superficial L2, POm axons preferentially target apical dendrites of L2/3 and L5 pyramidal neurons, and L1 and L2 interneurons. Interestingly, the VPM (lemniscal) and POm (paralemniscal) projections into this cortical area shows a largely complementary distribution[83]. Indeed, POm projections do not cluster and have an important lateral spread across neighboring barrels. As POm afferents have a limited whisker somatotopy, they might be suitable to integrate information across the entire barrel cortex. Besides the barrel cortex, information from the paralemnsical pathway can be directly relayed to Layer L1 and L5A of S2 and Layer 2/3 of M1[9,69,75,83].

The extralemniscal pathway departs from multi-whisker neurons in the caudal region of SpVi, projects to VPMvl, and then to different neocortical regions: (1) L4 septa and L6 of the barrel cortex and (2) L4 and L6 of the S2 cortex[69,83,101]. This pathway might relay information about whisker-to-object contact[100].

After describing the vertical flow of whisker information, the next section will focus on its final cortical computation. Pioneer experiments from Hutson and Masterton elegantly demonstrated the complex role of the barrel cortex during whisker perception[102]. In this study, a complete ablation of the barrel cortex dramatically impaired performance when the animal had to

actively use their whiskers (gap crossing), but not to detect a passive whisker deflection. This led the authors to enlarge the role of this cortical region, from a simple sensory decoder to a complex sensorimotor integrator (but see[103]). The next section will detail the anatomical connection of a whisker-barrel column and its interactions with the barrel field and other brain structures (check for additional reviews [9,69,83,95]). This will help to set the stage for a functional cortical processing of whisker-tactile information introduced later on this chapter.

2.4 Anatomical deconstruction of a cortical barrel column

As aforementioned, virtually all layers of the barrel cortex receive input from either VPM or POm thalamic neurons. However, the highest density of thalamocortical axons can be found in L4 – the major input layer[104]. **There, VPM axons make synapses on dendrites from L4 spiny stellate cells oriented towards the center of the barrel**[9]. This ensures that neurons from individual barrels collect their major synaptic drive from the principal whisker, preserving circuitry somatotopy. A smaller percentage (less than 10%) of VPM thalamic afferents also innervate L4 inhibitory interneurons[45]. **The L4 acts as an "information hub" from where thalamocortical excitation spreads to both supra- and infragranular layers. Axons from this layer are highly confined within the barrel-column and can project (1) to basal dendrites of L5A and L5B pyramidal neurons; (2) apical tuft dendrites of L6A pyramidal cells and (3) massively to L2/3 (circuit described on fig. 8)**[83]**. The L4 to L2/3 synaptic inputs are made the basal dendritic arbor and its drive built by a mixture of AMPAR and NMDAR components**[87]**. These synapses are relatively reliable but evoke a small excitatory postsynaptic potential (PSP)**[46]**.** Therefore, the convergence of inputs from L4 axons is critical to efficiently activate L2/3 neurons. The within-barrel confinement of L4 afferents ensures an activation that is whisker-to-barrel specific. **Axonal projections and dendritic morphologies from L2/3 pyramidal neurons are complex, illustrating the role of this cortical layer as a key integrator/decoder of the barrel cortex. Their axons can horizontally project into layers 2/3 and L5 of the entire barrel field or form long-range projections to the ipsilateral S2 and M1 cortex**[83,95]**. Their dendrites have an intricate morphology, with an extensive branching of distal dendrites into L1**[105,106]. This branching turns possible a cross-talk between the lemniscal and the extralemniscal pathway, important to mediate sensory-evoked synaptic plasticity (chapter 3). **Therefore, L2/3 neuronal firing can be transmitted (1) locally to other L2/3 cells of the same barrel; (2) to other whisker-related cortical regions (see below); (3) horizontally across different barrel columns, to integrate multi-whisker inputs and (4) vertically to L5A and L5B**[83]**.** The layer 5 can be considered as the main output layer of the barrel cortex. For the sake of simplicity, only the fundamental computation principles of this layer will be here described. A complete characterization of the different L5 pyramidal neurons and their role on the layer computation can be found elsewhere[83]. Dendrites of L5B pyramidal cells project via a thick basal dendrite to L1, where they form extensive branching (tufts) into this superficial layer[83,95]. Interestingly, the thalamic input on those cells appears to be segregated into different domains: while VPM inputs are performed mostly into the thick basal dendrite, POm axons form connections preferentially

into the distal tufts[83]. The importance of such segregation for whisker computation has been described in an elegant study[107]. These authors showed that during a whisker detection task, there is a collaborative activation of both VPM and POm inputs to drive L5 pyramidal neurons activity. As a consequence, the manipulation of POm activity into distal tufts lead to a change on whisker perception by the animal. The hypothetical implication of a similar mechanism on L2/3 pyramidal neurons is discussed in chapter 3. The connectivity of L5 cells is more widespread than those of L2/3. They project (1) to other L5 neurons; (2) massively back L2/3; (3) to the contralateral barrel cortex via corpus callosum; (4) to the ipsilateral whisker-related M1 cortex; (5) different subcortical regions (e.g., thalamic nuclei) and (6) back to the POm nucleus of the thalamus[83]. The last projection has been hypothesized as an important corticothalamic loop, where VPM inputs from L5 are able to regulate POm activity[108]. The description of the barrel cortex connectivity finishes into the deeper layer, L6 – the dominant source of corticothalamic projections. Similar to other sensory cortices, L6 is considered as an element of a feedback loop that modulates the response of the thalamus accordingly to ongoing sensory information. The vast majority of cellular heterogeneity in L6 can be roughly divided in 2 different groups accordingly to their axonal projections: intracortical or corticothalamical[83]. The first type of cells have their axons mainly within L5 and L6 of the barrel cortex[109]. They project across the barrel field to mediate transcolumnar interactions and some of them form long-range collaterals projecting to S2 and M1 cortex[83]. The second type can be subdivided on neurons that (1) target exclusively to VPM and have intracortical axon collaterals to L4 within the barrel column; (2) project to both VPM and POm nucleus; (3) have ascending collaterals terminating in L5 and L4 that diffuse across several barrels and (4) target VPMvl and therefore the origin of the extralemnsical pathway[83].

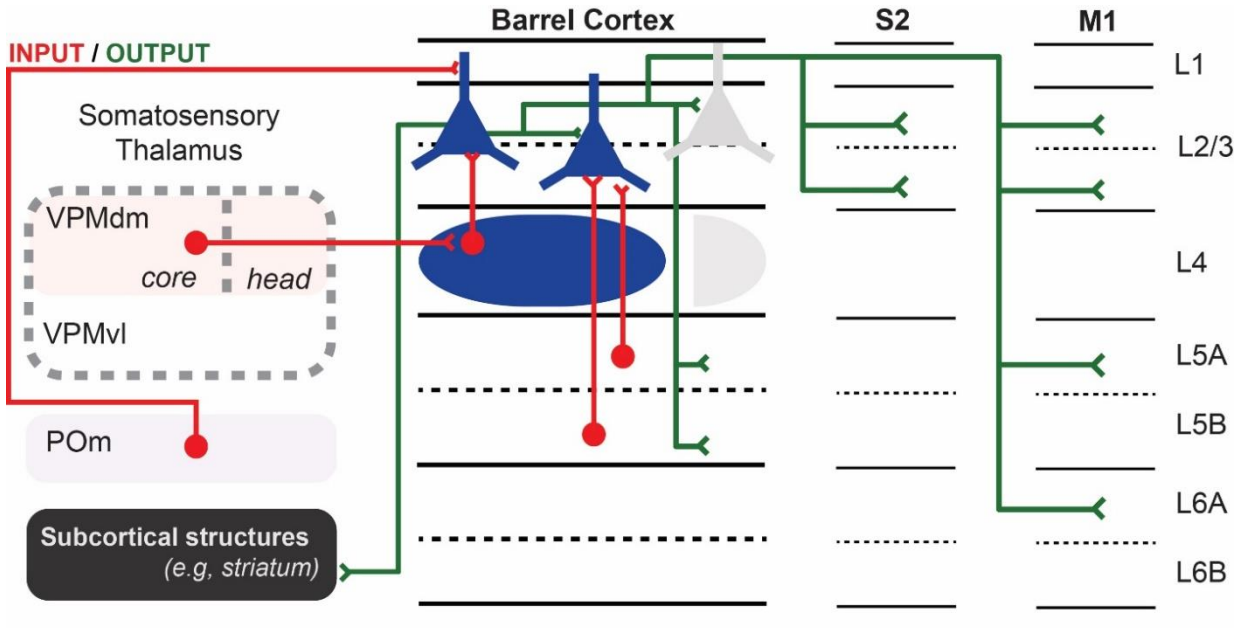

Fig. 8) Input/output connectivity of L2/3 pyramidal neurons (legend on the next page).

Fig. 8) Input/output connectivity of L2/3 pyramidal neurons. The major inputs (red) onto L2/3 pyramidal neurons (blue and grey) are made by (1) lemniscal inputs onto basal dendrites from L4 projections; (2) direct paralemniscal inputs into distal dendrites and (3) direct inputs from L5 pyramidal neurons. Upon spiking, L2/3 activity can be propagated (green) to (1) other pyramidal neurons in the same barrel (blue-blue connection); (2) pyramidal neurons in a neighbor barrel column (blue-grey connection); (3) to L5 pyramidal neurons; (4) to L2/3 pyramidal neurons of S2 and (5) L2/3, L5A, L6A pyramidal neurons of M1 cortex.

Besides this complex intracortical connectivity, some layers in the barrel cortex also have long-range connections to other neocortical regions (described above). From those targeted cortical regions the most prominent and well-described are S2 and M1.

Axonal projections from the barrel cortex to the ipsilateral S2 have a well-defined somatotopy[110]. The major inputs into S2 are originated from L2/3, L5, and L6 pyramidal neurons from barrel and septal systems [83,110]. Receptive fields in S2 are larger than in the barrel cortex, with neurons tuned to several adjacent whiskers[111]. Co-activation of barrel cortex and S2 has been described to code information about texture and animal's decision (see section 2.5). As discussed above, whisker-related information can be directly transferred to S2 via the extralemniscal pathway. Moreover, direct projections between S2, M1 and several other subcortical regions do also occur[69,83,110].

Somatosensation in rodents depends not only on the core processing of the tactile information but also on the precise adjustment of the whisker motion as a behavior function. Animals have to adjust the movement of their whiskers accordingly to the ongoing sensorial experience to optimize the tactile perception. A huge deal of this motor control is performed by M1 cortex (but see[112]). Not surprisingly, direct inputs between this region and the barrel cortex have been well-described (reviewed elsewhere[68,69,83]). Projections from the barrel cortex are performed from a subset of L2/3 and L5 pyramidal neurons and target neurons in the same layers of M1[110,113,114]. Object contact upon active whisker exploration evoke somatotopic responses in S1 and M1, suggesting that this cortical region also has a sensory whisker map[115]. Conversely, ipsilateral M1-to-barrel cortex projections are made into L2/3 and L5 but also in L6 and L1 due to axon collaterals[112,114,116]. Inputs from L1 in M1 are directly made into the apical dendrites of L2/3 and L5 cells in the barrel cortex. As aforementioned, L5 neurons also receive direct inputs from POm axons in the same dendritic domain. Considering that (1) POm neurons might code whisker position and (2) M1 projections translate the voluntary whisker control, it is possible that the cooperation between those two inputs compute information related to whisker movement and position[83]. M1 might also control bilateral coordination of whisker movement due to projections to the interconnection of the two M1 cortices in the different brain hemispheres via the claustrum[117]. In agreement, M1 ablation does not abolish whisking, but does impair whisking coordination, synchrony and kinematics[118]. The M1 cortex is additionally involved in different feedback loops, including reciprocal connections with the thalamus, basal ganglia and cerebellum[69].

The next section will describe the functional computation resulting from the intricate anatomical circuitry mediating whisker-related tactile information. It will start to describe the excitatory wave flowing through these circuits in response to a minimal stimulation and how

inhibition importantly regulates it. Then, it will describe the different strategies of the neocortex to compute different whisking strategies on the behaving mice. A special focus will be made on how the triad barrel cortex-S2-M1 might be well-suited to mediate the early stages of sensorimotor transformations of whisker-related sensory information to a goal-directed motor output.

2.5) Cortical processing of whisker-tactile information

The fastest cortical response evoked by a single deflection of the principal whisker occurs in L4 of the principal barrel and peaks within 10 ms after stimulation[119]. Then, a wave of activity radiates out to the neighboring barrels, spreading across the entire barrel field and to other cortical regions (fig. 9A)[115,120]. If a surrounding whisker is instead stimulates, the evoked response recorded in the main barrel has smaller amplitude and larger latency to peak[121–123]. Remarkably, deflection of a surrounding whisker decreases the response evoked by the principal whisker in the respective barrel[124,125]. How the anatomical pathways conveying information from the whiskers to the cortex help to understand these stereotyped responses?

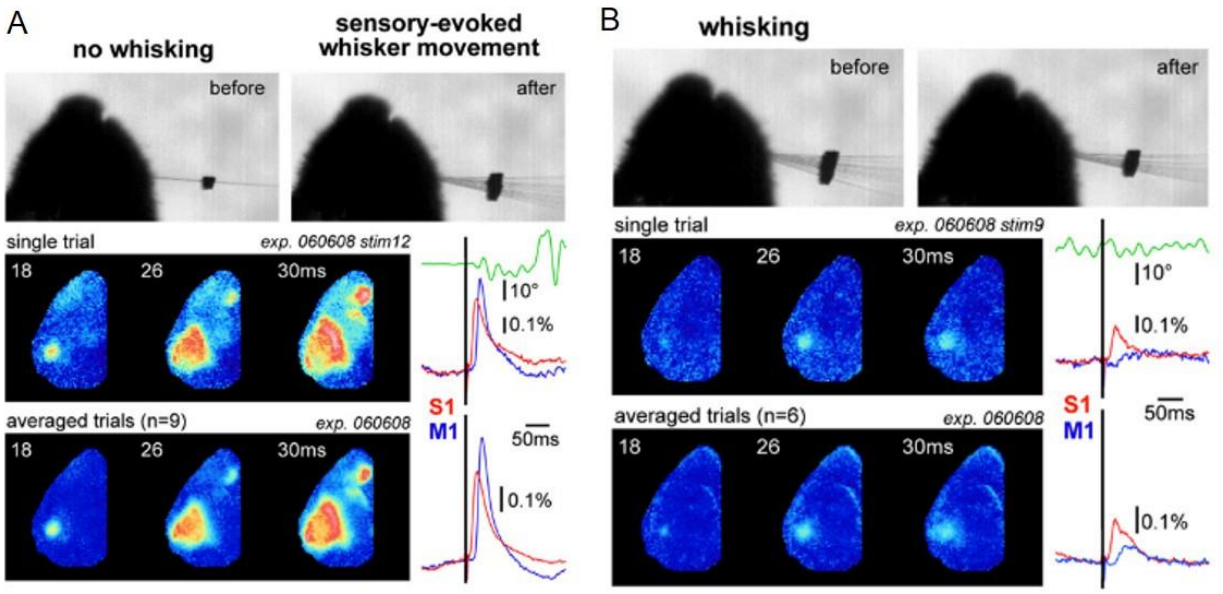

Fig. 9) Cortical computation of whisker-tactile information is behavior-state dependent. A) During quite wakefulness (no active whisking), C2 whisker deflection droves whisker-evoked activity with a complex temporal profile: (1) restricted to the main barrel; (2) spread all over the barrel field and (3) relayed to other neocortical regions (e.g., Motor Cortex). **B)** If the same whisker stimulation protocol is performed during active whisking, a different cortical response is recorded. Adapted from Ferezou, I *et al.* (2007) Neuron.

Whisker deflection evokes a wave of excitation that propagates, from the peripheral receptor to the cortex, by different anatomical pathways. If more than one whisker are stimulated, either principal- and surrounding-whiskers responses can be seen as early as in TN processing (see above). How can this functional divergence be conciliated with the strict anatomical somatotopy of the barrel cortex? A good starting point to answer this question lies on the lemniscal input into L4 – relaying volume transmission of whisker-tactile information. Thalamic VPMdm neurons

respond on average to principal-whisker stimulation with a latency of 4-6ms[126]. If a surrounding-whisker is stimulated, this response gets more delayed and variable (up 7-15 ms). These differences on latency are instrumental to restrict the transmission of principal-whisker information through the lemniscal pathway. Individual thalamic inputs in L4 recipient cells are week – 1 mV PSP on average[104]. As consequence, an efficient activation of L4 neurons requires many and synchronous thalamic inputs. **The delay of thalamic neurons to process surrounding responses makes this requirement exclusively accomplished by principal-whisker responses. Therefore, L4 pyramidal neurons act as a filter where principal-whisker responses are selected from a background of surrounding ones.** This is further refined by strong inhibitory feedback inputs from the reticular nucleus to sharpen the timing of VPM neurons firing[84,104]. In layer IV, the average latency for EPSPs after whisker stimulation is 10 ms and 72 ms for action potential generation[119]. Similar short latencies are also described to L5 and L6[96,116]. From here, the information wave is propagated to L2/3 with a 3.5-4 ms delay (to L4 activation) and before any horizontal transfer to neighbor columns[119,126]. This initial vertical representation of the whisker-tactile information is in agreement with Mouncastle postulates defining the barrel column as the fundamental unit for sensory processing[127].

This one-to-one relationship between whiskers and cortical columns might be hypothetically useful to extract the location (e.g., touch) of individual peripheric receptors with a minimal computation effort[9]. **However, during active exploration, whiskers have dynamic spatiotemporal distribution to a given object – making location a relative measure. Therefore, information from individual whiskers have to be integrated to extract behavior-relevant neuronal information[128,129].** The sources for multi-whisker integration can have either a cortical or subcortical origin. The L2/3 has the highest proportion of cells in the barrel cortex prone to integrate information from different cortical columns[130]. Their intricate morphology allows the horizontal spread across columns of the original (main-whisker) information[115,120]. The latency of this spreading is dependent on the spatial position of the recorded cell to the main-column: 1-2.5 ms if located on the near side or 9-15 ms if on the far side)[123]. The excitation wave generated in the main-barrel can be propagated across the entire barrel field, with a preferential propagation along the rows[131]. **Elegant work further extended the knowledge of the functional column by demonstrating that this excitation can be subsequently propagated by long-range projections to other brain regions (e.g., M1)[115].** Another source of multi-whisker integration and transfer to the cortex relies on the paralemniscal pathway[97]. As discussed, POm neurons respond equally to stimulation of different whiskers and their projections to the barrel cortex lack somatotopy. Considering that POm receives direct inputs from S2 and M1, it is conceivable that this source of multi-whisker information can be implicated on certain forms of whisker behavior. A consequence of the complex receptive fields of L2/3 neurons was well-illustrated by Clancy and colleagues[132]. These authors demonstrated that, even if in average principal-whisker responses are predominant, main-barrel responses are very heterogeneous. As consequence, L2/3 neuronal responses to whisker-deflection are distributed across the main- and the surrounding-barrels. This

is in agreement with other studies showing that nearby L2/3 cells can preferentially respond to different whiskers[133,134].

Another pivotal player on this functional processing lies on a different class of neurons – the inhibitory interneurons (reviewed here[89,135]). GABAergic interneurons have been considered as the "ying and yang" regulators of different neocortical regions involved in sensory processing (reviewed elsewhere[136]). In the barrel cortex, whisker stimulation recruits an inhibitory drive that damps down and critically sharpens the excitatory response in virtually all the layers[9]. In L2/3, the frequency of spontaneous action potentials (APs) of interneurons is almost ten times higher compared to pyramidal neurons[90]. If scaled to the population size, this means that interneurons APs closer resemble the number of excitatory ones. Moreover, interneurons inactivation via pharmacological or optogenetical approaches consistently increase the firing rate of pyramidal neurons[90,137]. **This suggests that the sparse firing of pyramidal neurons (see below) is a consequence of a strong inhibitory drive. In agreement, a strong bidirectional connection between pyramidal neurons and PV interneurons has been described**[138,139]. Both inhibitory and excitatory drive from or into pyramidal neurons or PV interneurons have very rapid kinetics[139]. Such connectivity might place PV neurons as network pacemakers by providing strong and rapid feedback inhibition. Importantly, **the effect of sensory stimulation has different consequences on the different subclasses of interneurons: while SST neurons are inhibited upon whisker stimulation, PV, and $5HT_{3A}R$ are depolarized**[90,137]**.** This differences of activity result from different synaptic inputs as described on chapter 3. Interestingly, the receptive field organization of inhibition closer resembles the one for excitation: the principal whisker evokes the greatest inhibition and the adjacent whisker a smaller one[123]. Likewise, deflection of a surrounding whisker before stimulating the principal one, decreases the response recorded in the principal barrel[124,125]. Contrarily, the blockage of interneurons activity (e.g., bicuculline) greater enhances the horizontal spread of whisker-evoked excitation in both superficial and deeper layers of the principal barrel[140]. Altogether, these evidences suggest that lateral inhibition across barrel columns can sharpen whiskers receptive fields in the barrel cortex. How this lateral inhibition can be affected by altered sensory experience and their implication on cortical remapping are discussed on chapter 3. In conclusion, inhibitory circuits are able to orchestrate pyramidal neurons synaptic integration, response gain, spike timing, and receptive field size[3,135].

It should be noted that the previous functional description is linked to a minimal and likely non-ethological pattern of whiskers stimulation. **Functional processing of whisker-related information is now appreciated to greatly depend on the whisker stimulation protocol (e.g., single versus multiwhisker), anesthesia levels (if used) or on the animal's behavior state (fig.9B)**[84,115,141]. These differences have been reported to occur in both excitatory and inhibitory types of neurons in the barrel cortex[90,137]. Therefore, it is important to discuss the recent findings on the strategies used by the neocortex to compute complex whisking on the behaving mice. A detailed discussion on how different stimulus features (e.g., direction) are encoded cortically and subcortically is out of the scope of this discussion (reviewed elsewhere[142]).

Most of the current knowledge on how the neocortex actively process whisker-related information comes from experiments on head-restrained behaving mice (see for review[143]). Here, one can directly couple (1) neuroethological relevant forms of whisker behavior to (2) 2-Photon somatic calcium imaging of large populations of superficial cortical neurons[143,144]. This approach revealed that different populations of L2/3 neurons have distinct patterns of activity varying accordingly to their functionality (e.g., neurons computing whisking)[145]. The activity of the recorded neurons was sparse (17% of the population, in agreement with[91]) and their function spatially intermingled. A seminal work proposed that this distribution can underlie a distinct, and largely non-overlapping connectivity to different neocortical regions[143,146]. These authors used two-color retrograde labelling to show a sparse and intermingled L2/3 pyramidal population, sending inputs mutually exclusive to S2 ("BC-S2 neurons") or to M1 ("BC-M1 neurons"). Once again, the activity of BC-S2 or BC-M1 neurons greatly depended on their behavioral functionality: (1) neurons encoding whisking were generally BC-S2; (2) higher-fraction of BC-M1 neurons were activated by whisker touch during object location, while (3) touch-related responses during a texture discrimination task was preferentially encoded by BC-S2 neurons. Another type of behavior function that one can extract is the discrimination coefficient (DC) – how well neuronal activity predicts a "hit" or a "correct rejection" during a Go/No Go task (active control of whiskers)[143]. The DC is non-homogeneously distributed in L2/3 cells of the barrel cortex, and neurons with high DC are a small fraction of the recorded population[146–148]. This division can be further refined if the different subtypes of pyramidal neurons are considered: for object location a higher number of BC-M1 neurons showed high DC compared to BC-S2, while this is opposed for texture discrimination[146]. This suggests that computation of object location in the barrel cortex is incredibly complex. **Whisker-mediated touch events are represented in L2/3 in sparse, distributed, intermingled and heterogeneous manner. This information is then sent either to M1 or S2, where different aspects of the whisker sensorimotor transformation are made in a behavior-dependent manner.** Importantly, these interactions can also be altered by learning and hypothetically by sensorial experience[149].

Besides the barrel cortex, whisker-related information is additionally computed in M1 and S2 (detailed above). Somatic calcium imaging of L2/3 in M1 showed a salt-and-pepper representation of touch and whisking on the behaving mice[150]. Moreover, axonal imaging of M1 neurons projecting back to S1 during object localization task showed a large spectrum of activity[151]. Indeed, this feedback inputs were sensitive to object location due to touch-related signaling but also to whisker movement and licking. Hence, the cortico-cortical loop between M1 and the barrel cortex might importantly update the touch information that is primarily computed in the barrel cortex. Simultaneous imaging of S1 and S2 L2/3 neuronal populations during a texture-discrimination task revealed a coordinated activity between the two regions[152]. This coordination was preferential to sensory- and decision-related components of the behavior task. Another study imaging S2 axons projecting into S1 demonstrated that this inputs have a movement- and choice-related activity[153]. Therefore, it is conceivable that the cortico-cortical loop

between S2 and S1 can compute and integrate either sensory- and choice-related information during touch perception.

The next session will complement the neocortical circuits with a non-exhaustive description of subcortical networks. This places the neocortex as the "tip of the iceberg" for the complexity of processing whisker-related neuronal information. The chapter will be closed with a discussion of the recent alternative views that turns the barrel cortex as more than a simple sensorial decoder.

2.6) Sensorimotor transformation of whisker-tactile information depends on a complex network of different subcortical structures

The complete whisker sensorimotor transformation has a rich repertoire of both cortical and subcortical brain regions (reviewed elsewhere[69,110]) (fig.10). Altogether, these regions work in collaboration to mediate a whole-body adjustment for a goal-oriented motor output accordingly to the ongoing sensorial information. **The interaction between cortico-cortical and cortico-subcortical loops allow the animal to adapt the whisker movement in order to optimize the tactile experience.** Not surprisingly, brain regions involved in different aspects of motor behavior (e.g., initiation), bilateral coordination, and neuromodulatory regulation of brain-states (e.g., alertness) have been directly or indirectly implicated on the processing of whisker-tactile information. In this section, a brief discussion of prominent subcortical circuits will be made.

A brain region receiving important inputs from individual barrel columns of the barrel cortex is located in the dorsolateral striatum: caudate-putamen[154,155]. Axonal projections from barrel neurons underlying this corticostriatal feedforward loops are predominantly from deeper layers of the cortex. Excitatory top-down control from the barrel cortex to the basal ganglia forms an important gateway for motor control and action selection. Interestingly, neurons in the caudate-putamen can influence back the neocortex due to a disynaptic circuit involving the globus pallidus and the sensory thalamus[59,69].

Axons prevenient from the deeper layers of the barrel cortex are also found in the superior colliculus, pons, and red nucleus[69]. The superior colliculus is directly implicated in spatial orientation, and can be related to orientation of whisker movement towards an object that attracted animal's attention. In agreement, barrel cortex axons projecting to this brain region have been implicated on the signal of salient sensory information[156,157]. Therefore, it is conceivable that this corticotectal loop might orchestrate attention and body movement towards a stimulus of interest[158,159]. The pons is connected via contralateral pontocerebellar projections to the cerebellum – an important region for motor refinement and learning[69,110]. Moreover, the corticopontine from the barrel cortex might be well-suited in fine-scale motor control output for a whole-body optimization of the sensory experience[110]. In agreement, if these projections are abolished by lesion, rodent's behavior during a gap crossing task is affected[160].

Sensory decision-making behavioral tasks not only depends on the context, attention, and motivation but particularly in rule-learning. This high-level aspects of goal-directed behavior might be directly under regulation of both medial prefrontal cortex (mPFC) and the hippocampus[144]. Both structures developed whisker-sensory responses with learning and their inactivation strongly impaired behavior on a whisker-dependent decision-making task[161]. This led the authors to hypothesize that the circuit barrel cortex-mPFC-hippocampus might be important to compute of learned, context-dependent transformation of ongoing sensory information into orchestrated whole-body goal-directed motor output. It should be noted that, besides this recent advances, the fundamental circuit mechanisms linking sensory processing in the barrel cortex to high-order brain functions (e.g., reward) remains largely unknown.

The final section of this chapter will discuss a barrel-centric computation of high-order neuronal processes. Recent findings have suggested that the barrel cortex might compute within its circuit certain aspects of the animal behavior that are not directly predict by its anatomy. These non-canonical computational strategies might enrich the repertoire of possibilities for an efficient sensorimotor conversion of whisker-related tactile information. This discussion will be concluded with the controversial view of a whisker-dependent sensation in the absence of the barrel cortex.

2.7) Alternative views and functions of the barrel cortex

The previous sections discussed the classical-view of the barrel cortex as the primary processing hub for whisker-related information from which then information is transmitted to other brain regions. However, recent evidences indicate that additional "non-canonical" computations might also occur. This may be well-illustrated with a recent study showing that the barrel cortex can directly and independently generate whisker movement[112]. The authors demonstrated that this cortical region can directly evoke whisker retraction, creating an important negative feedback mechanism for sensorimotor integration. This (1) non only questioned the dogmatic view of M1 cortex as the major regulator of whisker movement, but also (2) raises the need to reformulate the current concept of functional maps and their downstream alterations during cortical remapping. Another good example of a non-canonical computation is the direct reward-coding on the distal dendrites of L2/3 and L5 pyramidal neurons[162]. This study described reward-dependent dendritic spikes on these neurons that emerged gradually with the training in a task-specific manner. In other words, this suggests that more than its primary function as sensory modality, the barrel cortex can additionally encode association and behavioral-related saliency. Therefore, reward coding can be locally computed in the barrel cortex either in parallel- or independent-manner to subcortical processing. Additionally, the barrel cortex might be able to integrate multisensory information. In agreement, auditory-evoked neuronal responses were reported to occur in both the whisker-related thalamus and on the barrel cortex itself[163,164]. This multisensory integration can either be seen as a cooperative mechanism between different stimuli to increase environment's perception or a consequence of the animal's internal state (e.g., expectation).

Virtually all the ideas discussed on the current chapter have been challenged by a recent controversial work describing a rapid recovery of perception, movement, and learning in the absence of the barrel cortex[165]. Altogether, these evidences raise the need to re-revisit some of the basic concepts of barrel cortex processing. The implication of this brain region on whisker perception might be more complex than what is predicted from its anatomy and largely behavior-dependent. Therefore, it is important to study the neuronal mechanisms of primary sensory coding by the barrel cortex in contexts of pure neuroethology. This not only has the potential to change our current knowledge on the basic processing for whisker-related information but also to pave the way for more unexpected computational strategies awaiting to be unrevealed.

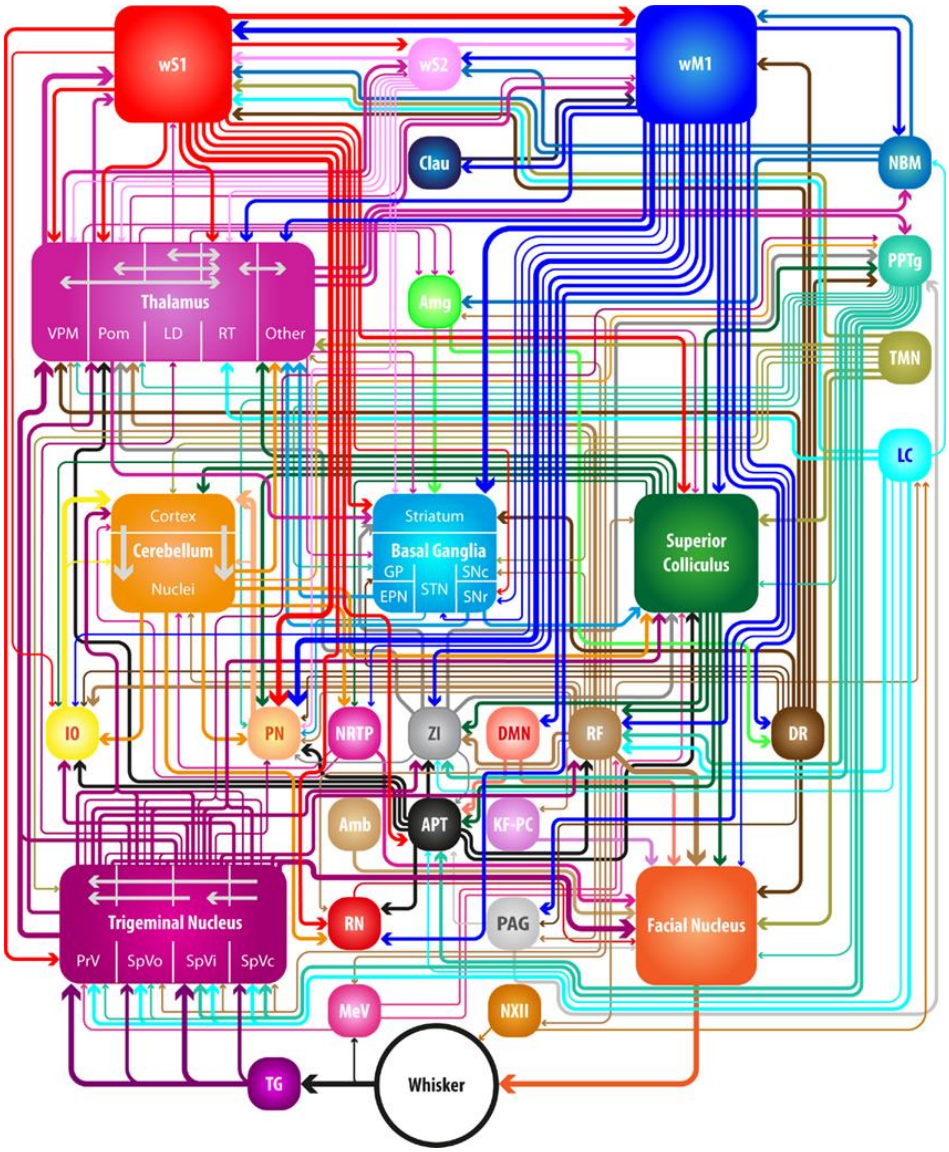

Fig. 10) Overview of the cortical and subcortical networks involved on the sensorimotor transformation of whisker-tactile information. Many different brain regions are required to control whisker movement in a behavior-dependent manner. The requirement of each independent structure to the overall sensorimotor transformation is largely behavior and brain-state dependent. Figure adapted from Bosman, L. W. J. (2011) Front. In Integr. Neurosc.

3. Barrel cortex – a circuit model for synaptic and cortical plasticity

3.1 Whisker trimming induces map plasticity in the barrel cortex

Studies on the barrel cortex have provided valuable information regarding the molecular, cellular, and circuit underpins of map plasticity. This system allows to induce cortical remapping by simple trimming or plucking a subset of whiskers[9]. The consequences of whisker manipulation are complex and largely dependent on the used protocol (fig.11) (for review [2,3]). For instance, **single-whisker experience (SWE), where all the whiskers but one are trimmed, results in a functional expansion of the spared barrel** (barrel expansion, section 3.5)[166]. Conversely, deprivation of all except two neighboring whiskers (DWE), forces the cortical representation of the two spared inputs to merge[167]. These effects resemble the ones described by Merzenich and colleagues upon amputation or syndactyly experiments on monkeys (section 1.2). More complex patterns of trimming do exist, ranging from single or multiple row sparing/deprivation, to more complex protocol (e.g., chessboard pattern of deprivation)[9,35]. **Independently of the protocol, the computational alterations induced by whisker trimming can be described as follows: the initial decrease of neuronal responses within the deprived barrel is followed by increased spared input-driven neuronal responses in both the spared and the deprived column**[168,169]. By other words, sensory inputs, which under normal conditions (full-whisker, FW) drive subthreshold responses in the deprived barrel, become suprathreshold upon whisker trimming. This results in a prominent functional remodeling, with a decreased cortical representation of the deprived whisker, while increasing the spared one[3]. Important to state that this effect largely depends on the animal's age[3,9,54]. Indeed, both weakening and potentiation are present in juvenile (less than two months), whereas response potentiation is predominant during adulthood. This rule is not valid for sensory-induced remapping without whisker trimming. In agreement, prolonged passive whisker stimulation, with all the sensory inputs preserved, induced rather a shrinkage of the cortical representation[170]. Similarly, enriched environment sharpens receptive fields on FW naïve animals[171]. Altogether, these evidences suggest that **trimming-induced map plasticity likely depend on a complex interplay of factors, far more complex that simple alterations on pyramidal neuron's computation.**

How can whisker-dependent cortical remapping be conciliated with the remarkable somatotopy of the whisker-to-barrels system? Can barrel cortex anatomy and physiology explain the circuit alterations upon altered sensory experience? A good starting point to answer these questions are the broad receptive fields of L2/3 pyramidal neurons (for reviews, see[3,9,19,172]). Their receptive fields are complex, containing: (1) major main-whisker component, dictated by whisker-to-barrel somatotopy, but also (2) a highly variable surrounding-whisker component (section 2.5). At the dendritic level, this implies that single-neurons receive inputs from both the principal and surrounding whiskers due to intracortical and thalamocortical projections. These incredible anatomical and functional signatures might be one of the major substrates for map plasticity in the

barrel cortex. When all the whiskers are preserved, L2/3 synapses are preferentially tuned towards the principal-whisker, even if weaker responses for the surrounding-whisker do exist. One can easily imagine a response filtering at dendritic level, where suprathreshold inputs are picked from a variable background of subthreshold ones. This variability explains why neuronal responses evoked by whisker stimulation are distributed across the principal- and surrounding-barrel[132]. **Upon whisker trimming, this tight equilibrium is compromised, and the synaptic weights shifted towards the spared input. Ultimately, this alterations of response tuning underlies the cortical remapping seen upon whisker trimming. This is well illustrated by the finding described by Margolis and colleagues[173]. These authors reported that, upon whisker trimming, neurons that normally would respond to the deprived whisker, shifted their response towards the neighbor spared one – therefore expanding the cortical representation of the spared whisker.**

The shift of neuronal response tuning induced by whisker trimming results of a complex spatiotemporal interplay of synaptic and circuit mechanisms, involving different cell types. The next sections will deconstruct, piece-by-piece, this intricate mechanism. First, a detailed review of the synaptic and cellular alterations underlying cortical remapping in the barrel cortex will be described. An important focus on the time-dependent evolution of the map plasticity will be made: from the initial alterations on pre-existing synapses to the longer time-scale refinement of the circuit. Then, this information will be conciliated at the circuitry level, to describe the local and brain-wide consequences of whisker-related map plasticity.

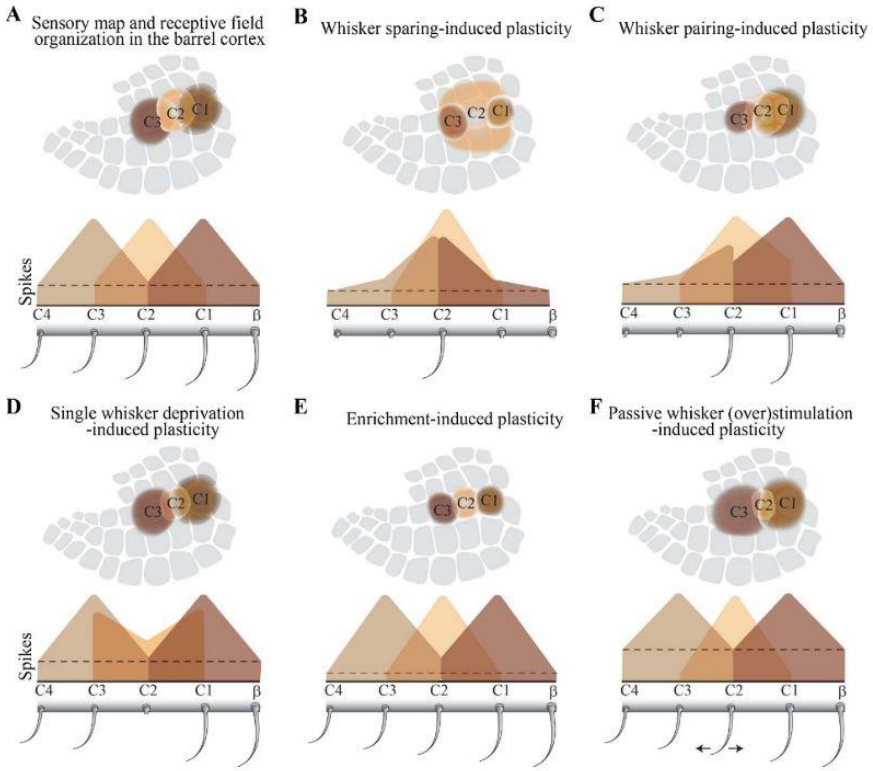

Fig. 11) Map plasticity in the barrel cortex (legend on the next page).

Fig. 11) Map plasticity in the barrel cortex. Different whisker trimming protocols induce distinct effects on functional representations in the barrel cortex. Cortical remapping can be also induced by sensory overuse, without whisker trimming. **A)** Barrel cortex somatotopy underlies the one-to-one relationship between whiskers and barrels; **B)** Single-whisker Experience (SWE) expands the cortical representation of the spared whisker; **C)** Dual-whisker Experience (DWE) overlaps the cortical representations of the spared whiskers; **D)** Single-whisker deprivation shrinks the spared barrel, with an expansion of the representation of the neighboring ones **E)** Map plasticity induced by environmental-enrichment sharpens the representation of all the individual barrels, while **F)** chronic whisker stimulation sharpens the cortical representation of the activated input. Figure reproduced from Kole, K. *et al.* (2018) Neurosci. Biobehav. Rev.

3.2 Synaptic and cellular mechanisms of cortical remapping

The functional expression of map plasticity requires different synaptic mechanisms as well as multiple cellular types. Even more complicated is to understand how these factors interact with each other as a function of time, to convert the initial alterations on pre-existing synapses, into circuit-wide alterations. To deconvolute this problem, we will focus our attention into the workhorses of barrel cortex's computation – the pyramidal neurons.

The effect of map plasticity on excitatory transmission can be roughly described by a five component model proposed by professor Feldman (fig. 12) [54]. The five cornerstones of this models are: whisker trimming dependent – (1) rapid depression of neuronal responses to the deprived input (LTD), followed by (2) slower potentiation of spared-input responses in both deprived and spared barrel column (LTP). Both components result from an activity-dependent competition between active and inactive inputs, which is therefore Hebbian in nature. (3) Homeostatic regulation, scaling up or down, to an increase (i.e., sensory overuse) or decrease (i.e., deprivation) of the neuronal excitability; (4) Behavior dependent – synaptic LTP induced by the activity-dependent and temporal correlation of sensory inputs without trimming (e.g., passive whisker stimulation). (5) synaptic LTP induced by reinforcement-dependent mechanisms (e.g., reward), dependent on neuromodulation. Below, I will discuss all the synaptic and cellular mechanisms of map plasticity in a different order that here presented.

3.2.1 Hebbian-type synaptic plasticity

Increased cortical representation of the spared input is believed to involve synaptic LTP[174]. This synaptic mechanism has been reported to occur in the barrel cortex by an extensive body of research (see for a review[9,175]). **The two most striking evidences come from recent *in vivo* studies, showing that rhythmic whisker stimulation (RWS) potentiate L2/3 cortical synapses by a LTP-like manner** (section 3.5)[176,177]. This is in agreement with a previous *in vitro* studies, where synaptic LTP has been indirectly demonstrated to occur by prolonged sensory experience[178,179]. Previous studies have demonstrated that synaptic LTP can be induced in the barrel cortex by electrically stimulating inter- and intracolumnar projections[180–182]. This form of synaptic LTP share similarities with the one reported in the hippocampus, such as: (1) NMDAR-dependence (*in vitro* and *in vivo* evidences[176,177,182]); Ca2+/calmodulin-dependent protein kinase II (CaMKII)-dependence[169,181,183], and (3) bidirectional regulation by LTD[184]. A striking difference

is also reported, due to the presence of a strong pre-synaptic component[185,186]. If the same pre-synaptic effect occurs *in vivo* during sensory-evoked LTP is currently unknown.

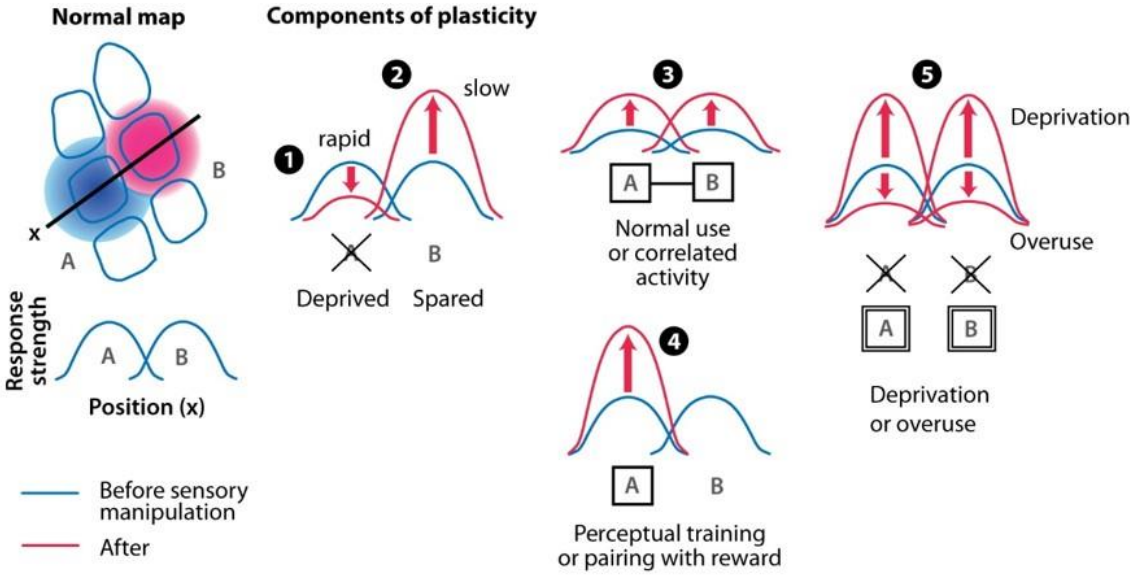

Fig. 12) The five synaptic components of map plasticity (Feldman's model): The five synaptic components at play upon altered sensory experience are **1)** A rapid depression of neuronal responses in the deprived barrel, **(2)** followed by a slower potentiation of the spare representation (comprising the concomitant barrel expansion); **3)** Synaptic LTP induced by activity-dependent and temporal correlation of the sensory inputs (without trimming). **4)** Synaptic LTP induced by reinforcement-dependent mechanisms (e.g. reward) and **5)** Homeostatic scaling up or down in response to sensory deprivation or overuse, respectively. Figure reproduced from Feldman, D. E. (2019) Annu. Rev. Neurosci.

Although the relationship between this form of LTP and map plasticity has been assumed for decades, no direct evidence exists at the time of writing. For example, Finnerty and collaborators demonstrated that upon single row sparing, the synaptic transmission between spared L2/3-L2/3 pyramidal neurons is increased[187]. On SWE-subjected mice, an increase of the firing rate of L2/3 pyramidal neurons in the spared barrel is reported to occur after 24h of trimming[188]. This increased of spiking probabilities was hypothesized to be driven by a LTP-like mechanisms, because (1) increased the reliability of the neuronal responses on a trial-to-trial basis was increased; (2) spike latencies were reduced and (3) the transmission of stimulus-related information propagation through L2/3 network was improved. The dependence of SWE-induced cortical remapping, at least on the spared barrel, is confirmed by two other studies[189,190]. A similar effect also occurs in the deprived barrel, where the probability of inducing LTP *in vitro* is reported to increase after whisker deprivation[186]. However, the best hints that map plasticity depends on synaptic LTP came from three independent studies[169,181,183]. In all of them, the blockage of synaptic LTP using a non-functional form of CaMKII impaired the SWE-induced functional barrel expansion (mechanism detailed on chapter 4) (fig.13). Altogether, these data suggest that the functional barrel expansion after whisker trimming likely relies on LTP-driven increased excitability on the spared barrel that, somehow, is propagated to the neighboring columns. **While**

of the role of intracortical projections for this radial expansion appear critical, the synaptic mechanisms driving it are less well-described (see below). It is worth to mention that, virtually all the evidences for a role of synaptic LTP during map plasticity, result mostly from *in vitro* approaches, or largely nonspecific manipulations (e.g. CaMKII mutants). Therefore, despite these heroic advances, a definitive demonstration of LTP during map plasticity on the alive animal remains to be made.

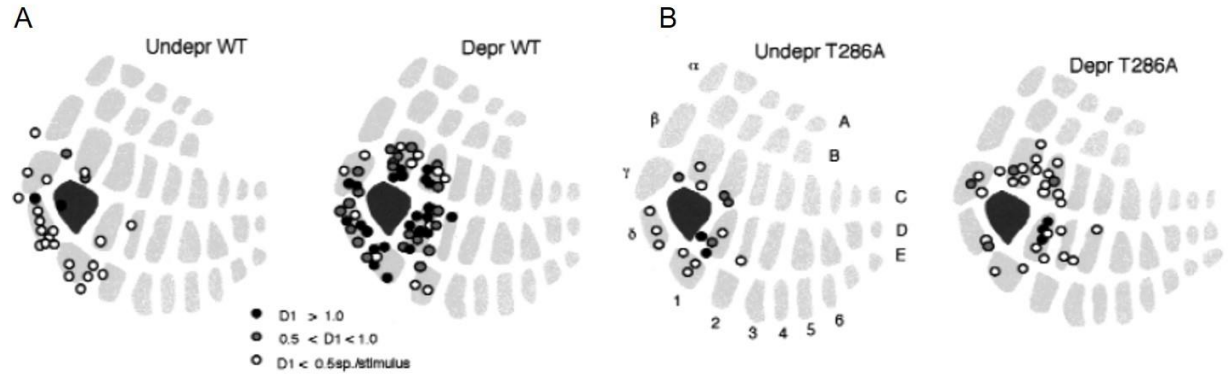

Fig. 13) A CaMKII mutant (synaptic LTP blocked) impairs the expansion of the spared barrel during SWE. Single-neuron recordings in the barrel in D1 barrel before and after SWE. The color of each circle corresponds to intensity of the neuronal response evoked by the spared whisker (white: small; black: large). **A)** On the *wild type* (WT) background, SWE expands the spared barrel. This is due to a functional recruitment of deprived neurons, as indicated by the increased responses to the spared whisker on the neighboring barrels (black dots). **B)** This functional expansion is impaired in CaMKII mutant (T286A) animals. This mutation abolishes the kinase activity, prevents synaptic plasticity (likely LTP) and, therefore, map plasticity. Figure reproduced from Glazewski *et al.* (2000) Nat. Neurosci.

The other Hebbian-type synaptic mechanism underlying map plasticity is LTD. Several different forms of LTD, induced by distinct molecular mechanisms, have been reported to occur in the barrel cortex (reviewed here[9,54]). **A large body of evidences suggest that, upon whisker trimming, response deprivation to the deprived whisker requires synaptic LTD in L4-L2/3 and L2/3-L2/3 synapses**[54]. For example, whisker deprivation was reported to drive synaptic LTD on L4-L2/3 synapses while left unchanged L4-L4 synaptic weights[191]. This decreases the neuronal responses to the deprived whisker in its corresponding main barrel, as recorded after whisker regrowth[191]. This evidence for trimming-induced synaptic LTD in the deprived barrel was corroborated by two further studies[192,193]. A similar experience-dependent synaptic LTD was reported to occur across different sensory cortices. This is well-illustrated by Heynen and collaborators experiments on the visual cortex during monocular deprivation (MD, lid suture)[194]. They found that this form of visual cortex plasticity critically depends on a homosynaptic form of synaptic LTD. A different variant of synaptic LTD driven by sensory experience was also reported to occur in the auditory cortex[195]. Froemke and colleagues elegantly demonstrated that LTP induced by a well-defined pitch was matched by a heterosynaptic form of LTD of the neuronal responses to the original best frequency. A similar mechanism might exist in the barrel cortex as suggested by experiments using chessboard pattern of whisker deprivation[9]. A

different synergetic effect between synaptic LTP and LTD also occurs after SWE. In agreement, it has been reported that the magnitude of synaptic LTD is higher for deprived cells close to the spared barrel[191]. **Altogether, these results suggest a complex role of synaptic LTD during map plasticity**.

3.2.2 Homeostatic plasticity

Homeostatic plasticity is another form of activity-dependent mechanism, which is non-Hebbian in nature, that could explain some properties of map plasticity[54,196]. Unfortunately, this mechanism is poorly understood in the barrel cortex. However, homeostatic plasticity was proposed to occur in the visual cortex after MD[197]. This form of sensory deprivation was described to increase neuronal excitability, circuit spontaneous activity, as well as visual-evoked neuronal responses. Imaging evidences raises the possibility that a similar mechanism can occur after full-whisker deprivation (i.e., trimming all the whiskers) in the barrel cortex[179]. In this study, an overall and non-specific increase of synaptic weights lacking input-specificity was reported to occur after prolonged sensory deprivation. However, limited conclusions can be made, since this work was performed under highly non-physiological conditions. Therefore, whether a similar effect occurs in vivo, remains currently unknown. **Additionally, professor Feldman proposed a role of homeostatic plasticity on the potentiation of the neuronal responses to the spared input**[54]**.** He proposed that this might be consequent to a generalized increase of synapses strength (lacking input specificity and/or increased intrinsic excitability. Even if this might be an obvious mechanism in the visual system, no data supports this hypothesize in the barrel cortex.

3.2.3 Intrinsic cell excitability

Additional mechanisms of plasticity without input-specificity and reported to occur during whisker map plasticity are alterations of cell intrinsic excitability. Cortical neurons can undergo experience-dependent regulation of voltage-gated ion channels, expressed as alterations on membrane excitability[198]. By increasing or decreasing intrinsic excitability, incoming synaptic inputs can have a completely different relationships with somatic spike output[199]. It has been demonstrated that long periods of rhythmic firing in L5 barrel cortex pyramidal neurons modulate their membrane excitability *in vivo*[200]. A similar mechanism also occurs during map plasticity, where SWE is reported to increase the threshold for action potential generation[201]. Altogether, these results raise the need to carefully interpret the effects of map plasticity at the synaptic level. Indeed, these alterations can be amplified or even filtered by whole-cell adjustments to the ongoing circuit activity.

3.2.4 Spike-timing dependent plasticity

Besides activity-dependent mechanisms, map plasticity can also result from the relative time correlation between two synaptic inputs – a mechanisms known as spike-timing dependent plasticity (STDP). STDP underlies a brief millisecond-scale time-window, where the pre-to-post firing correlation can change synaptic fate. A good physiological example occurs in

the auditory cortex, where STDP-LTP can be induced by pairing an auditory-cue with a consequent postsynaptic depolarization[202]. In agreement, STDP has been described to be an important mechanism to define neuronal receptive fields in both auditory and visual cortices[203,204]. The best example for a role of STDP in the barrel cortex comes from Celikel and colleagues seminal work[205]. On FW animals, L4 axonal spike (VPM driven) precedes postsynaptic L2/3 depolarization. Therefore, during normal conditions, the L4-L2/3 temporal correlation is set to drive STD-LTP (pre-before-post spiking). However, upon single-whisker deprivation, the timing of this activation is critically inverted: due to the absence of L4 activity, the L2/3 will be activated by intracortical inputs from neighboring barrel columns. The consequence of this, as elegantly described by Celikel and colleagues, is a decrease of synaptic weights of L4-L2/3 synapses by STDP-LTD[206]. An additional study, coupling postsynaptic depolarization followed by passive whisker deflection (post-before-pre) also reports induction of STDP-LTD in L2/3 neurons[207]. Gambino and colleagues demonstrates that STDP-LTP can be induced if the order of whisker/post-synaptic depolarization is reverted[208]. Moreover, STDP is an interesting mechanism for map plasticity in the barrel cortex, because: (1) it can occur as a consequence (i.e., positive feedback) or in parallel with activity-dependent and structural changes and (2) it can be mediated by L2/3 postsynaptic NMDAR-dendritic depolarization (see section 3.5) and, as consequence, without necessarily requiring spike rate alterations (in agreement with Celikel and colleagues[206]). It would be of great interest to determine the relationship between Hebbian plasticity and STDP, and if this can underlie circuit-wide alterations upon whisker trimming.

3.3 Map plasticity effects on inhibitory microcircuits

Synaptic modifications induced by altered sensory experience are not restricted to excitatory neuronal networks. **The other side of the coin for map plasticity importantly lies on inhibition** (nicely reviewed here[172,196,209]). As described on chapter 2.5, inhibitory cells embedded on barre cortex microcircuits orchestrate several functions: it closes matches the excitation, regulates the integration of excitatory inputs at the dendritic level, and sharpens neuronal receptive fields (i.e., specifies suprathreshold input). Moreover, inhibition tightly regulate when and how a given excitatory cells fires, and as a consequence, defining STDP rules[196]. **On the reverse order of thinking, altering inhibitory tuning of excitatory microcircuits can have important repercussions on pyramidal cell's function, and more importantly, plasticity. Therefore, the yin-yang relationship between excitation and inhibition is a cornerstone of injury- and learning-induced map plasticity** (see neuromodulation, section 3.3). Here, we will focus our attention on how the destabilization of this balance can change whisker cortical representations.

Perisomatic inhibitory drive of PV-positive basket cells into pyramidal neurons has been described to decrease upon sensory deprivation[210]. The effect of this trimming-induced disinhibition at the excitatory level is complex. For instances, in the behaving rat, removal of the principal whisker leads to a decrease excitability in the main-barrel, while increasing the excitability in the neighboring ones[211]. The increase of excitability in the spared barrel has been hypothesize to have a component of disinhibition[188]. By other words, increased whisker-evoked

neuronal responses to the spared whisker can result from a collaboration between synaptic LTP and local disinhibition[54]. On the other hand, disinhibition on the deprived barrel has been linked to act as a fast homeostatic mechanism[212,213]. In agreement, inhibitory drive onto pyramidal neurons has been described to decrease, matching the level of reduced excitation, stabilizing circuit excitability. This is proposed to normalize levels of excitation in the absence of sensory input, before the onset of synaptic LTD, and map plasticity.

Another important role for disinhibition is on the remodeling of neuronal receptive fields induced by whisker trimming. It has been known for a long time that lateral inhibition can be reduced by whisker deprivation[211]. However, the importance of this disinhibition on pyramidal neuron's computation has only recently been described[208]. In FW conditions, STDP-LTP induction is restricted to the principal-whisker stimulation, as predicted by the one-to-one relationship between whiskers and barrels. However, upon dual whisker trimming, the circuit becomes more promiscuous, and STDP-LTP possible to be induced by surround-whisker stimulation. This was associated with a decreased surrounding whisker-evoked inhibition, and proposed to be an important mechanism to drive receptive field's rearrangement[208]. A similar mechanism might also occur in the visual cortex[214]. An elegant mechanism proposed by Sammons and Keck for disinhibition in the visual cortex is represented on figure 14[215]. They propose that the association between structural disinhibition (see below) and synaptic plasticity (Hebbian and/or STDP) is essential for alteration of neuron's receptive fields and, as consequence, map plasticity. It remains to be demonstrated if a similar mechanism also occurs in the barrel cortex. Another exciting possibility for disinhibition occurs in another subcellular compartment, millimeters afar from the soma – on the distal apical dendrites. It has been recently appreciated that inhibitory inputs can be directly made on neuronal dendrites, or even directly in dendritic spines[216,217]. There, this inhibitory drive is critical to keep NMDAR activity, and dendritic excitability under tight control. On the visual cortex, a reduction of dendritic inhibitory inputs has been reported to occur after monocular deprivation[218,219]. This reduction occurred faster than changes on dendritic spines (excitatory), and proposed by van Versendaal and colleagues to facilitate the strengthening of specific visual inputs without requiring important alteration on the excitatory circuitry[218]. Considering the tight-regulation of local dendritic computation by inhibitory circuits in the barrel cortex, it is tempting to assume that dendritic disinhibition might be common to both cortices (see section 3.5).

Fig. 14) Sammons and Keck model for disinhibition-mediated map plasticity (figure on the next page). A) Before retinal lesion, the visual circuit is built by green or blue neurons (triangles) with different receptive fields. **B)** After retinal injury, the input to the green cell (defined as lesion projecting zone, LPZ) is lost. At the same time, inhibitory input (red circles) into green cells is decreased, along with pruning of axons from LPZ neurons (green dotted lines) **C)** Blue neurons located outside LTZ send new inputs into the green cells. This is proposed to be directed by an inhibitory gradient. There, novel synaptic inputs with green cells will be made, shifting their receptive fields (i.e., input remapping). **D)** This new inputs recruit green LPZ neurons into the blue network, increasing the cortical representation of the blue stimulus. This new network is proposed to be stabilized by a new steady-state of inhibition. Figure reproduced from Sammons & Keck (2015) Curr. Opin. Neurobiol.

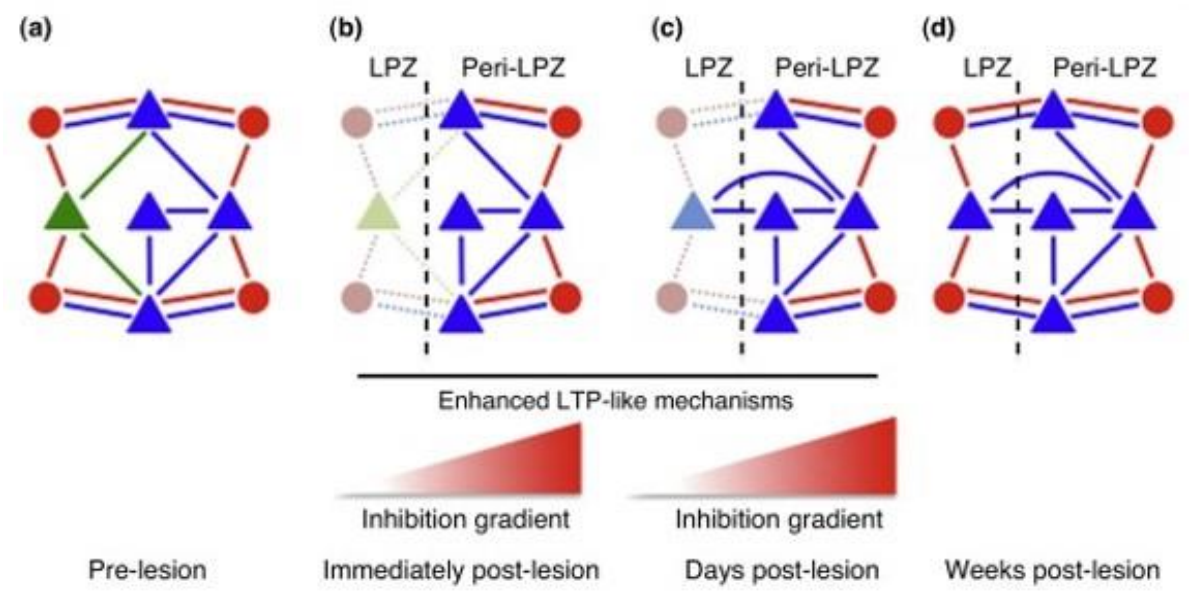

Fig. 14) Sammons and Keck model for disinhibition-mediated map plasticity.

3.4 Non-neuronal correlates of map plasticity

Besides both excitatory and inhibitory neurons, cortical remapping can additionally induce alterations in neuroglial cells – astrocytes, microglia, or oligodendrocites (reviewed elsewhere[35]). In a simplified view, neuroglia has a large spectrum of roles in the brain, ranging from neurotransmitter recycling, neurovascular coupling, metabolic regulation, to control of axonal myelination[220]. These functions are good candidates to explain some of the early and long-term functional alterations induced upon whisker trimming. Unfortunately, our current knowledge on how experiences alters neuroglial cells function is still very primitive. Nevertheless, we now know that map plasticity has more than a neuro-centric locus, importantly requiring a plethora of different cell types to be manifested[9,35].

3.5 Long-lasting alterations of map plasticity

The described excitatory and inhibitory alterations are likely to occur at short time-scale after altered sensory experience. Therefore, **to make cortical remapping long lasting, alterations of the genetic-wired neocortical architecture most occur. These mechanisms, described as a late-phase plasticity, are primed by the initial synaptic alterations and require a large network of molecules and genes. Ultimately, late-phase plasticity drives long-lasting structural changes at the single-cell and circuit level to make map plasticity last.**

Structural plasticity on dendritic spines and axons are one of the best documented forms of long-lasting alterations underlying map plasticity (reviewed here[53]). In the same way that two are required for tango, structural alterations on axons or dendritic spines are a good-readout of how neuronal activity alters synaptic fate. The advent of *in vivo* 2-Photon calcium imaging turned possible to chronically image the same population of axons and spines, and to determine how map plasticity change their dynamics. This allowed not only to understand the immediate consequences

of synaptic plasticity, but also how experience shapes neocortical fine-architecture. Dendritic spines have a spectrum of shapes, ranging from highly mobile filopodia-like to more stable mushroom-like[53]. Structural modifications on dendritic spines and axons have been extensively studied in the barrel cortex. During FW conditions, L2/3 dendritic arbors are very stable across time, upon learning, or even after sensory experience (e.g., environmental enrichment)[221,222]. This is explained by a remarkable stability of pre-existing mushroom-like spines, and to the short lifespan of the newly formed spines. A similar stability is also seen in thalamocortical axons[223]. The exception to this are the intracortical axons of L2/3 and L5 pyramidal neurons, with a higher turnover rate over one month of imaging. Therefore, even if the overall neuronal circuit is not changed during normal conditions, it has some components prone to be changed by experience. This is especially true for L2/3 pyramidal neurons, proving once again how plastic this cortical layer can be.

Not surprisingly, structural dynamics of both dendritic spines and axonal boutons are altered by whisker trimming[9,53]. In agreement, prolonged sensory deprivation decreases spine elimination, with the concomitant increase of spine number and density[53,224]. This is well-illustrated by an elegant study performing spine quantification after a chessboard pattern of whisker deprivation (fig. 15)[224]. Whisker trimming increased formation and stabilization of newly formed filopodia-like spines, along with a stabilization of pre-existing mushroom-like ones. Important to note that this is not a generalized effect, but rather affecting a small fraction of the spine population (less than 10%). Structural alterations caused by whisker trimming are not restricted to postsynaptic spines, but also found on axons of both excitatory and inhibitory cells. For example, the density of horizontal projections from spared pyramidal neurons into the deprived columns is increased after whisker plucking[225]. **This is accompanied by a retraction of inhibitory axons on the deprived barrel, possibly leading to disinhibition on excitatory cells as reported in the visual cortex[218]. Such loss of inhibitory inputs can create a permissive environment for a synaptic gain or loss and, as consequence, explain the structural postsynaptic changes[226]. Therefore, structural modifications upon whisker trimming likely relies on the orchestrated long-lasting changes of both excitatory and inhibitory cortical building blocks.** If this is caused or consequent to all the aforementioned plasticity mechanisms remains to be determined.

Formation of new spines and axonal re-organization require metabolically-expensive alterations of neuronal morphology. Therefore, **these long-lasting alterations might require not only structural changes, but also alterations on broad cellular mechanisms. Not surprisingly, map plasticity in the barrel cortex has been linked to alterations on the patterns of gene expression** (reviewed elsewhere[9,35]). In agreement, different immediate early genes are described to be upregulated upon whisker-trimming (e.g., c-FOS) in the spared barrel[227]. A similar effect is reported to the cAMP-response element-binding protein (CREB), that increases its expression 12h after SWE[168]. This expression accompanied an increased excitability of L2/3 pyramidal neurons and was restricted to the cortex, unchanging any subcortical structure. An interesting mediator of

CREB signaling is the brain-derived neurotrophic factor (BDNF)[228]. BDNF expression is increased upon altered sensory experience[229]. Considering the synaptogenic effect of BDNF, this molecule might be essential to stabilize newly-formed spines after altered sensory experience[230]. In conclusion, transcriptomic changes during map plasticity might be essential to convert the transient changes on synaptic weights on long-lasting cellular and circuit alterations.

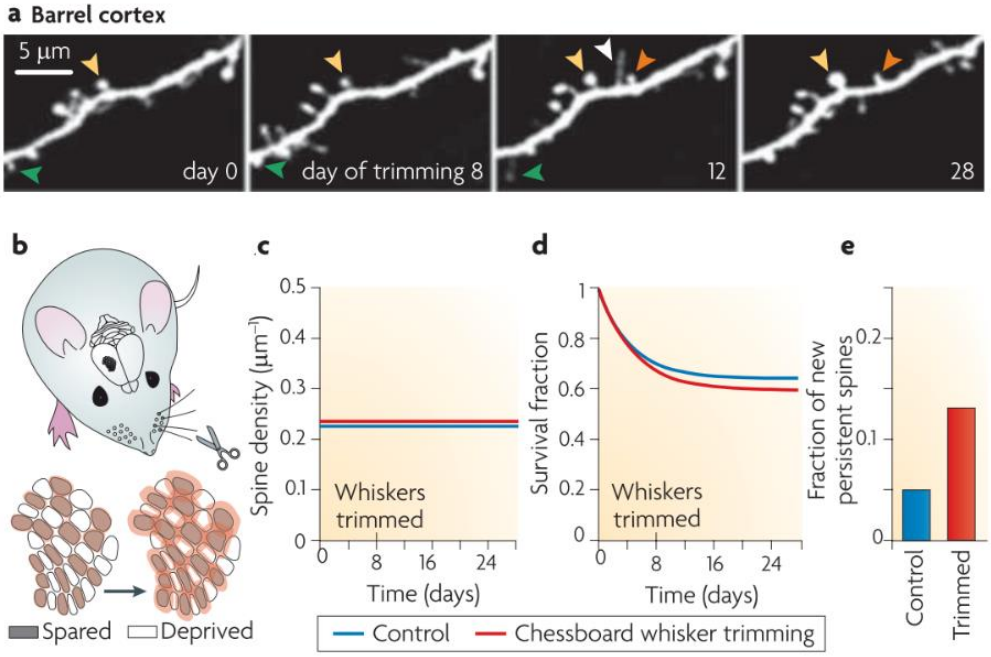

Fig. 15) Experience-dependent (postsynaptic) structural plasticity. A) Chronic *in vivo* 2-Photon imaging allows to image of the same population of dendritic spines across days. The advent of this imaging modality turn possible to determine how single spines evolve, from filopodia- to mushroom-like, before and **B)** after whisker trimming. **C)** Seminal work from Holtmaat and collaborators (2006 Nature) showed that even if whisker trimming does not change the overall spine density, **D)** it increases the survival rate of the newly formed spines, with the concomitant increase of the fraction of the new persistent spines. Figure reproduced from Holtmaat & Svoboda (2009) Nature Rev. Neurosci

3.6 Circuit and brain-wide mechanisms of cortical remapping

The section above discussed the synaptic and structural mechanisms that express whisker map plasticity at the cellular-level. Now we will provide an overview of the circuit and brain-wide mechanisms for cortical remapping. First, a description of the radial and layer-expression of trimming-induced map plasticity will be performed. Then, it will review some evidences defending an exclusive cortical locus for the expression of this mechanism. Neurovascular alterations induced by sensory experience will be briefly discussed to, once again, illustrate the incredible complexity of cortical remapping. Finally, it will drift from injury- to learning-related map plasticity by presenting how neuromodulation is well-placed to shape cortical representations on the behaving animal. This will be a good opportunity to discuss map plasticity as a whole-brain mechanism, depending on several different subcortical structures, and on animal behavior state.

SWE increases the functional representation of the spared input – a mechanism known as barrel expansion[9]. Extracellular recordings suggest that this expansion can range over an entire neighbor barrel column, with a radial distance up to 300 μm[183]. Interestingly, at the single-neuron level, response potentiation is higher in locations closer to the spared input. Conversely, decrease of deprived-whisker neuronal responses can also range over several neighboring barrels[9]. This implies that, upon whisker trimming, different barrel columns lose their surrounding-whisker representation and, by consequence, favoring re-wiring to the principal one. The degree of adult cortical plasticity is largely layer-specific[9]. While both L4 and L2/3 are profoundly affected by experience during the critical period of development, in the adulthood this plasticity is restricted to the superficial layers of the barrel cortex[166,188,191]. This implies that, on adult animals (about 6 months of age[9]), all the functional alterations induced by whisker trimming are restricted to the superficial layers of the barrel cortex. This is further confirmed with the nearly absence of experience-dependent plasticity in the thalamus[9]. As discussed by Professor Kevin Fox, there are three main arguments for an exclusive cortical locus for whisker map plasticity: (1) cortical remapping is absent if cortical activity is blocked (e.g., muscimol)[231]; (2) no alterations of VPM neurons responses are recorded followed whisker deprivation[231,232], and (3) small local injuries in the barrel cortex abolish cortical remodeling after whisker trimming[233]. A similar effect is also described for the visual cortex, where no plasticity is described on the visual thalamus after altered sensory experience[234]. Thus, whisker map plasticity during adulthood, is restricted to L2/3 pyramidal neurons, and has an essential intracortical origin.

The stereotyped cortical modification after SWE illustrates very-well an important hallmarks of map plasticity: the horizontal recruitment of neighboring barrels to the spared input (fig. 13). This horizontal spread was initially demonstrated to be important for map plasticity by injury-induced experiments. Local lesions induced on the septa between spared and deprived barrel, critically abolished barrel expansion during SWE[233]. How can the synaptic mechanisms aforementioned describe this horizontal spreading? One good possibility is a LTP-driven potentiation of the spared synapses of deprived pyramidal neurons on neighboring barrel columns. As mentioned on chapter 2, L2/3 axons and dendrites have an extensive branching across different barrels. Interestingly, these axons have continuous structural modifications even on FW animals – revealing the high intrinsic plasticity of these inputs[223]. This is corroborated by *in vivo* experiments, demonstrating a high probability of LTP induction on L2/3 pyramidal neurons by intracortical projections stimulation[180]. A similar idea can be extrapolated by the initial experiments of Glazewski and colleagues, demonstrating the dependence on LTP-like mechanisms for barrel expansion[169]. However, recent *in vivo* work indicate that this is not the only mechanism operating during map plasticity[208]. Accordingly, the induction of potentiation (STDP-LTP) between the spared whisker and deprived L2/3 neurons is only possible due to disinhibition. **These piece of work, raises three important questions: (1) does the described LTP and STDP-LTP share the same principles for the L2/3-L2/3 synaptic potentiation? (2) how can this potentiation be conciliated with the requirement for disinhibition? (3) and who comes first?**

Is disinhibition permitting potentiation? Or is potentiation driving disinhibition? Unfortunately, no answer to this "chicken or egg-like conundrum" is currently known.

Neurovascular alterations are also reported to occur after whisker trimming (reviewed elsewhere[35,235]). The barrel cortex has an extensive and complex pattern of vasculature[236]. The best example of how map plasticity influences neurovascular function in the barrel cortex is given by Lacoste and colleagues[237]. These authors elegantly proved that whisker deprivation decreased the neurovascular complexity, while whisker stimulation in the absence of deprivation increased. Therefore, a similar plasticity to neuronal cells is closely recapitulated by the complex neurovascular pattern in the barrel cortex. This suggests that map plasticity does not only rely on cellular, circuit, and whole-brain wiring alterations, but also on profound alterations in the tissue as a whole.

Map plasticity is not only induced by injury but also during natural behavior with all the sensory inputs preserved. The relationship between map plasticity and learning is complex, and likely results from a cooperation of different brain-wide mechanisms.

This is well-illustrated by the effects of behavioral-dependent neuromodulation on map plasticity (see for review[172,196,209,238]). Independently of the origin of the neuromodulators, they all regulate the excitatory-to-inhibitory balance to alter neocortical synaptic weights. In an oversimplified view, this is ultimately accomplished by a direct control of GABA release from inhibitory interneurons[238]. As a consequence, cortical representations are adjusted in a behavior-dependent manner, similarly to injury-related modification. A good example to start with are the cholinergic neurons in the basal forebrain. Acetylcholine-releasing neurons projecting to the cortex can efficiently signal reinforcement signals (i.e., reward or punishment)[239]. Associative learning induced by the pairing of nucleus basalis activation with auditory stimulation has been reported to occur in the auditory cortex[203]. This resulted in a fast reduction of synaptic inhibition, with the concomitant long-lasting alterations of cortical representations of the presented tone. Acetylcholine can additionally alter cortical maps during locomotion and arousal, as described to occur in the visual cortex[240].

Another neuromodulator, norepinephrine, can also regulate cortical activity by direct projections from locus coeruleus[241]. Activation of noradrenergic projection has been associated increase the signal-to-noise ratio of the evoked versus spontaneous activity in the auditory cortex in a long-lasting manner[242]. Experiments on the visual cortex suggest that this is due to a direct regulation of circuit inhibition[243]. New stimuli or unpredicted reward are reported to activate ventral tegmental area (VTA) dopaminergic neurons. An elegant study showed that VTA activation along with auditory stimulus presentation, increased the cortical area and neuronal selectivity to the presented tone[244]. This was due to dopamine release, and likely due to direct modulation of synaptic LTP on auditory neurons. Several other neuromodulators (e.g., serotonin, and oxytocin) have been directly or indirectly linked to long-lasting alterations on cortical representations[196].

The effect of neuromodulation on cortical representations is of great interest to understand how learning shapes cortical representations in the normal adult brain. However, it also indicates a degree of complexity not predicted by the synaptic and structural mechanisms described on section 3.2: how can learning, or brain state orchestrate injury-map plasticity? Does neuromodulation have a synergetic or a competitive effect on trimming-induced map plasticity?

Unfortunately, all the characterized synaptic and circuit-mechanisms are barrel-centric, and completely overlook brain-wide mechanisms engaged during behavior. At the time of writing only limited information describes the role of map plasticity during animal behavior. **How cortical remapping influences recovery of learned behaviors after injury? One can forecast two opposite possibilities: does cortical expansion compensates behavior by recruiting additional neurons to compute the spared input, compensating the absence of the trimmed ones? Or does this functional re-organization increase the computational noise and, consequently, decrease behavior performance? The answer to these questions requires a physiological manipulation of synaptic plasticity during map plasticity, in a system with a direct behavior readout.** Such requirements are not trivial and explains our current limited knowledge. The next section will overview data from sensory cortices to describe what is currently known and, more importantly, remains to be described about adaptive behaviors. This chapter will be closed by a description of a recent scientific developments that might help to solve a long-lasting question on the cortical plasticity field: how does synaptic changes underlie map plasticity and, ultimately, animal behavior?

3.7 Map plasticity and whisker-dependent adaptive behaviors

Studies determining how injury-induced map plasticity affects whisker perception are scarce. One study indicated that **altered sensory-experience early in life profoundly impacts whisker behavior** once in the adulthood[245]. Whisker clipping from birth to P45, followed by whisker regrowth, dramatically impaired whisker-dependent surface discrimination. Interestingly, animals with behavior deficits lacked normal whisker frequency (6-12 Hz), suggesting a profound alteration of the whisker sensorimotor integration. A similar effect is reported in another independent study[246]. Other study, using a different whisker trimming protocol, demonstrate that **early-life deprivation does not affect the gap-crossing performance, but does alter the behavioral strategy**[247]. Despite some differences on trimming or behavior protocols, all studies demonstrate **an early-life effect of sensory deprivation on the whisker-dependent behaviors during adulthood**. As they were performed during the critical period of development, where altered sensory experience profoundly alters cortical architecture, it makes it very hard to extrapolate to the adult condition. Barnéoud and collaborators provided one of the first evidences on how cortical remapping might be compensate animal behavior after injury[248]. They found that behavioral performance on the gap crossing task was strongly impaired after two weeks of barrel cortex lesion. However, ten weeks after injury, no deficits were longer seen on these animals. This led the authors to hypothesize that this recovery is due to a remodeling of the whisker-to-barrel neocortical circuitry[248]. Another example of a study addressing how adult map plasticity affects whisker perception was performed by Celikel and Sakmann (fig. 16A)[249]. These authors took

advantage of the **gap-crossing test to determine if SWE could alter whisker perception. They found that whisker trimming did not affect success rate (i.e., jump probability), but increased instead the time for the perception-mediated decision. This time differences can be explained by the advantage of multi-whisker sensory integration (i.e., input redundancy).** If the lack of differences on the success rate is due to map plasticity, it is hard to conclude. This is due to important limitations of the experimental design: (1) the lack of an internal control (training before/after whisker trimming) and (2) if existing, a compensatory mechanism should match the time-dependent evolution of cortical remapping. As all the data represented are averages across days, this subtle time-dependent evolution appears overlooked. **A better indication that map plasticity facilitates the recovery of learned behaviors comes from studies on stroke**[250]. In this study, motor impairments after ischemic stroke can be recovered by whisker trimming likely due to a LTP-like mechanism (fig. 16B). As whisker trimming opens a window for synaptic plasticity, it facilitates the remapping of the motor function and, as consequence, improves motor behavior. **The best proof-of-concept that LTP-driven cortical remapping compensates animal behavior was provided by Clem and collaborators (fig. 16C)**[190]**. LTP-driven increased neuronal excitability after SWE increases performance on an associative tactile conditions task (fig.16C). In agreement, blockage of synaptic LTP is accompanied by an important decrease on behavior performance.** Unfortunately, the experimental design of this study also has an important limitation: the usage of NMDAR antagonist (i.e., CPP)[251]. Even if it's true that CPP can efficiently impair the expression of synaptic LTP, it might also block basal synaptic transmission in the barrel cortex (detailed below). Therefore, it is difficult to conclude if the reported behavioral effects are due to plasticity mechanisms or a consequence of a reduction on the overall circuit activity.

Despite some technical limitations, the behavioral approach developed by Clem and collaborators can be decisive to describe how map plasticity translates into animal behavior[252]**. Approaches to specifically block synaptic LTP will be decisive to fill this important gap. A common theme on the field is, no matter by which mechanism, an enhancement of map plasticity is directly implicated on a recovery to both periphery or central injuries**[253,254]**. This illustrates very well the importance of studying synaptic LTP in the context of cortical remapping – not only for the understating of this cortical mechanism, but also to open new therapeutic avenues.**

To accomplish this *holy grail*, one has to be able to (1) accurately express and manipulate synaptic LTP in the alive animal; (2) easily induce map plasticity; (3) determine spatiotemporal evolution of the cortical alterations upon altered-sensory perception and (4) have a direct behavior readout. The next section will describe recent technical and theoretical developments that place the barrel cortex as the best alternative for these needs.

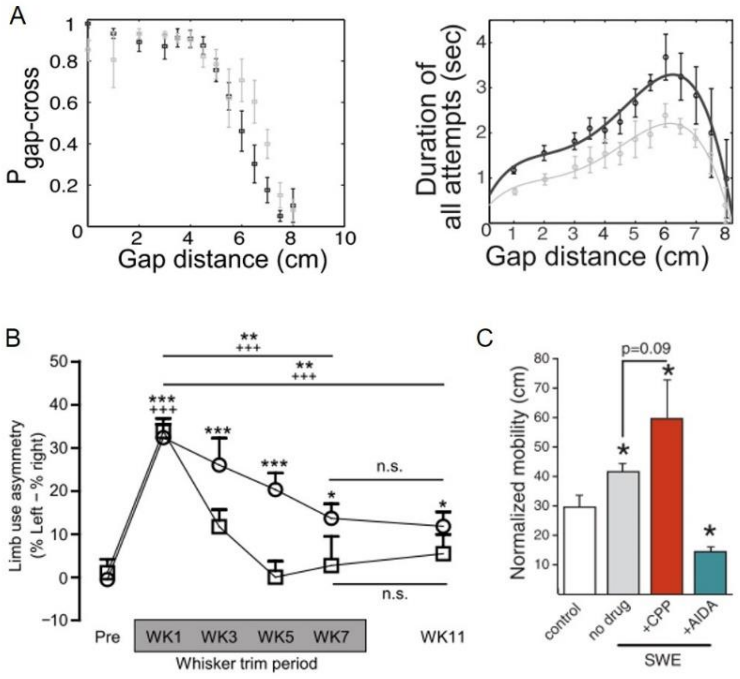

Fig. 16) Effects of whisker deprivation on whisker-related behaviors. A (left) Experiments using the gap-crossing apparatus revealed that SWE does not change the jump probability to any the gap distances. (right) Nevertheless, SWE mice require more time to jump. From these results, Celikel and Sakmann proposed that FW input redundancy improve the speed but not the accuracy of this whisker-related behavior. If the lack of differences for the jump probability is due to map plasticity is difficult to conclude. **B)** Whisker trimming improves behavioral performance on a motor-related task (limb use asymmetry). This is a proof-of-concept to the possible beneficial effect of map plasticity to recover performance on a learned behavior. Circles: control; Squares: whisker deprivation. **C)** This recovery of behaviors due to map plasticity might be dependent on synaptic LTP. In agreement, behavior performance on associative tactile conditioning can be dramatically affected by pharmacological manipulation of synaptic plasticity (mechanisms detailed on section 4). Figure A reproduced from Celikel & Sakmann (2007) PNAS; Figure B from Kraft, A. W. *et al.* (2018) Sci. Transl. Med and Figure C from Clem, R. L. (2008) Science.

3.8 Sensory-evoked synaptic plasticity

Almost fifty years have passed since the discovery of synaptic LTP by Bliss and Lømo[40]. In perspective, important advances were made regarding our knowledge on the molecular and cellular mechanisms of synaptic LTP (detailed on chapter 4). **Despite these heroic advances, the physiological meaning of LTP and its importance for animal behavior is still largely unknown**. Hippocampal LTP is currently the most studied form of synaptic plasticity and, as consequence, the best model to investigate the molecular basis for memory formation and retrieval[46]. However, it is worth nothing that most of the gathered evidences came from studies in brain slices or *in vivo* using non-physiological patterns of activity[255,256]. To understand how synaptic LTP induces activity-dependent circuit changes, and its importance for animal behavior, a physiological induction paradigm is required. Unfortunately, the intricate connectivity of the hippocampus with different cortical and subcortical structures, turns virtually impossible to achieve this requirement[257]. To tackle this fundamental limitation, a simpler model is required.

To study synaptic LTP in conditions of pure physiology, the archetypal model would: (1) compute natural stimuli; (2) transform stimulus into neuronal responses in a very simple, stereotyped, and invariant way; (3) have anatomical, physiological, developmental, and activity-dependent changes well-documented and (4) be relevant for animal behavior. The best models fulfilling these requirements are the different **sensory** cortices of rodents. Not surprisingly, successful attempts to induce highly-physiological sensory input-mediated LTP in the visual, auditory, and barrel cortex were reported[176,202,203]. We will focus our attention on the whisker-evoked synaptic LTP due to its interest for map plasticity and related adaptive behaviors.

Groundbreaking work from Hotlmaat's and collaborators described that rhythmic **whisker stimulation (RWS: 8Hz, 1 min) induces *bona fide* synaptic LTP on cortical synapses of L2/3 pyramidal neurons (defined as RWS-LTP)**[176]. **RWS-LTP is not driven by somatic action potentials but rather by NMDAR dendritic spikes: regenerative, local, and long-lasting (up to several hundred of milliseconds) dendritic depolarizations**[258]**.** Induction of NMDAR spikes is explained by a combination of synaptic, morphologic, and circuit factors (fig.17A). The synaptic-basis for NMDAR spikes generation is the activity of the receptor itself. NMDARs are ionotropic receptors permeable to calcium (Ca^{2+}), blocked by magnesium (Mg^{2+}) at the resting membrane potential, and responsible to drive strong postsynaptic depolarization in response to presynaptic activity[259]. The highest expression of NMDAR in the barrel cortex is on L2/3, where it participates on synaptic transmission from L4 inputs[87,260]. This explains why NMDAR antagonist can dramatically affect L2/3 circuitry basal synaptic transmission[260]. The membrane potential-dependent Mg^{2+} blockage, confers a non-linear computation to NMDARs: it can drive a continuous and sustained Ca^{2+} influx in the presence of high concentrations of glutamate[258]. The morphological origin for NMDAR spikes results from the extensive branching of L2/3 dendrites into L1. As they project away from the soma, distal dendrites become thinner, reducing their surface/volume ratio[49]. This create conditions where synaptic inputs can drive dendritic depolarization, similar to a somatic spike. **The presynaptic origin of these synaptic inputs is the last factor for the generation of NMDAR spikes. Indeed, Holtmaat's work demonstrate that, upon whisker deflection, there is a co-activation of both VPM (lemniscal) and POm inputs (paralemniscal) on the same L2/3 dendritic domain**[176]**. The synchronous activation of both pathways leads to a strong glutamate release, that is sensed by the large concentration of NMDARs on distal dendrites. As a consequence of the biophysical properties of both NMDARs and thin dendrites, each whisker deflection has the potential to evoke a NMDAR dendritic spike. Consequently, RWS can drive a prolonged NMDAR-dependent depolarization in defined dendritic domains (i.e., plateau), potentiating individual spines (LTP), independently of somatic activity (fig.17B). If recorded at the soma (e.g., *in vivo* patch clamp) this results in a sustained depolarization, reminiscent of a cortical UP state, defined by the authors as NMDAR plateaus.** Recent and elegant work from the same group came to elucidate the mechanisms regulating NMDAR dendritic spikes generation in the barrel cortex[92]. They found that, **in addition to the direct inputs to L2/3 pyramidal neurons, POm axons also innervate both PV and VIP interneurons. The activation of VIP cells drives an inhibitory**

input into SST interneurons targeting L2/3 distal dendrites[137]. As consequence, this feedforward disinhibitory microcircuit dictates "when" and "where" NMDAR spikes are generated. If this disinhibition is blocked, RWS-LTP is impaired *in vitro*[92]. This is not only important for the understanding of this synaptic mechanism, but also a possible point of regulation for map plasticity (i.e., disinhibition).

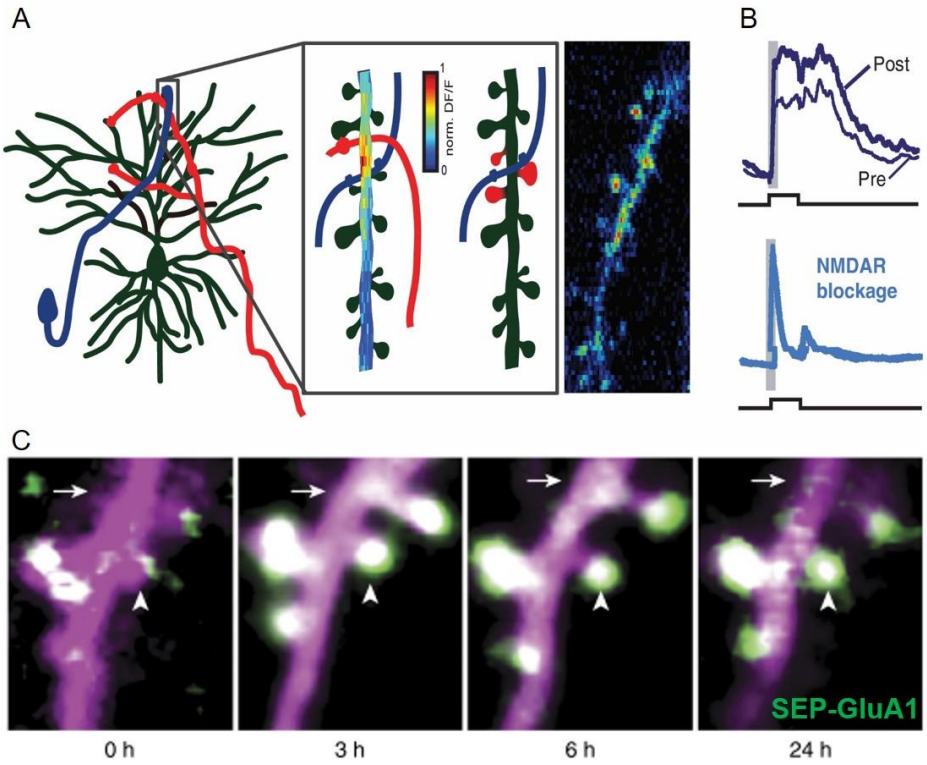

Fig. 17) Synaptic LTP evoked by rhythmic whisker stimulation. A) *(left)* NMDAR dendritic spikes are evoked by the synchronous activation of both the lemniscal (blue) and paralemniscal (red) inputs in distant dendrites of L2/3 pyramidal neurons (green). Distal dendrites have a low volume/surface ration and a high concentration of NMDARs in both synaptic and dendritic sites. (*right*, heatmap) In presence of high glutamate concentrations, NMDARs have a non-linear conductance, able to drive a strong postsynaptic depolarization. **B)** RWS induces a summation of NMDAR spikes in the same dendritic branch that is able to induce LTP without requiring backpropagating action potentials. This potentiation is abolished if NMDARs are pharmacologically blocked (e.g., DAP5). **C)** A similar protocol of whisker stimulation drives a long-lasting and NMDAR-dependent accumulation of postsynaptic AMPARs. This is a hallmark of synaptic LTP and its molecular mechanisms are discussed on chapter 4. Figure A and B adapted from Gambino, F. *et al.* (2014) Nature; Figure C reproduced from Zhang, Y *et al.* (2015) Nat. Neurosci.

The boundaries of our current knowledge on the molecular mechanisms for *in vivo* synaptic LTP have been recently expanded by an elegant work from Huganir's lab[177]. **These authors took advantage of *in vivo* 2-Photon imaging to demonstrate an AMPAR synaptic accumulation in L2/3 synapses after prolonged whisker stimulation** (fig. 17C)**.** This enrichment of AMPARs is NMDAR-dependent, and an important signature for synaptic LTP. To better understand the importance of this discovery, the next chapter will describe the molecular machinery at play to express and regulate the different forms of synaptic plasticity. It will shift from neuronal circuits

to the nanometric scale, and focus on individual excitatory synapses. There, it will review almost three decades of work using cellular models and *in vitro* preparations, with two major goals in mind: (1) to precisely determine the molecular machinery conveying presynaptic activity on postsynaptic plasticity, and (2) define a molecular target that could be used to manipulate synaptic plasticity *in vivo*. After this detour, we will change the scale back to animal-level, and review important work where impairment on synaptic proteins is associated with behavioral dysfunction. Finally, it will come back to the beginning, and review the molecular machinery underlying the different forms of synaptic plasticity described in the barrel cortex.

4. The Molecular Mechanisms of Synaptic Plasticity

4.1 The excitatory synaptic transmission

Most of excitatory synaptic transmission in the central nervous system (CNS) occurs at synapses formed between presynaptic boutons and postsynaptic dendritic spines[37]. **On the presynaptic site, vesicles filled with glutamate are released from a restricted section of the presynaptic terminal containing an electron-dense material, defined as the active zon**e (see for review[261]). There, a highly complex network of different proteins is responsible for precisely translating the electrical action potential (spike) into release of glutamate vesicles. This decoding is orchestrated by fluctuations of intracellular Ca^{2+} concentrations, driven by spike-dependent activation of presynaptic voltage-gated Ca^{2+} channels. Such transformation is not linear and can be adjusted at different timescales according to ongoing presynaptic activity: short-term plasticity by frequency-dependent alteration of glutamate release during spike trains or bursts, or long-lasting alterations of the presynaptic gain[262,263].

Glutamate released into the synaptic cleft is sensed by different ionotropic (iGluRs) or metabotropic (mGluRs) glutamate receptors accumulated in the pre- and postsynaptic membrane (see for review[264]). For sake of simplicity, I will focus this review to the postsynaptic role of these receptors. Glutamate signaling through **mGluRs (mGluR1-8)** can affect synaptic transmission due to pre- and/or postsynaptic effects (reviewed here[265]). All mGluRs convert glutamate binding into protein G activation, triggering the activation of complex signaling pathways largely dependent on the receptor subtype. They are implicated on both developmental and activity-dependent alterations of excitatory synapse function. While mGluRs modulate transmission, iGluRs mediate most of the direct excitatory currents. Glutamate binding to iGluRs drives conformational changes of the receptor that are propagated to the channel pore[264]. Pore opening allows diffusion of different ionic species, accordingly to their electrochemical gradients. iGluRs can be divided in four different groups based on their agonist pharmacology. **AMPAR (subunit GluA1-A4)** mediate sodium (Na^+)/potassium (K^+) currents and are responsible for mediating fast synaptic transmission to glutamate (detailed on section 4.2). The dynamic regulation of synaptic AMPARs controls both the fidelity of synaptic transmission and the expression of different plasticity mechanisms (see section 4.3). As aforementioned (section 3.5), **NMDAR** channel pore is blocked by Mg^{2+} at the resting membrane potential[259]. Their activation requires Mg^{2+} block relief by postsynaptic

depolarization, which allow Na^+ and Ca^{2+} influx in the presence of glutamate and co-agonists (either glycine or D-serine). As a consequence, NMDAR are coincident detectors of pre- and postsynaptic activity, without generally participating in basal synaptic transmission. Postsynaptic depolarization has different origins, such as AMPAR activation, dendritic spikes, or even backpropagating action potentials[255,258]. Importantly, NMDAR permeability to Ca^{2+} allows activation of different downstream pathways, responsible for engaging long-term alterations in the synaptic weights[255,266]. **Kainate receptors (KARs)** (subunits GluK1-K5) have both ionotropic (Na^+ permeability) and metabotropic functions (see for review[267]). Due to such unusual properties, KARs are responsible for (1) regulation of maturation of neuronal circuits along the neurodevelopment; (2) modulation of presynaptic neurotransmitter release and (3) mediation of postsynaptic currents at certain synapses (reviewed elsewhere[267]). The last iGluR is the δ receptors (subunits D1 and D2), the less characterized family of glutamate receptors[268].

These receptors are not randomly distributed in the plasma membrane, but rather accumulated in front of the presynaptic active zone (fig. 18A)[42,269]. This alignment is essential for a reliable and efficient synaptic transmission. The majority of excitatory transmission occurs at dendritic spines, defined as highly compartmentalized protrusions emerging from the dendritic shaft (fig. 18B)[270]. Each **individual spine has (1) a crowded disk-like proteinaceous structure known as postsynaptic density (PSD); (2) a rich meshwork of cytoskeletal elements[271]; (3) organelles forming a functional secretion pathway and (4) different endosomal compartments[272].** The PSD is built by an association of different proteins, including membrane receptors, transmembrane proteins, cytoplasmic scaffolding protein, signaling enzymes, and cytoskeletal proteins[273]. Scaffolding proteins orchestrate how these elements interact in the PSD and, by consequence, ensure a proper synaptic function. They belong to several families of proteins, accordingly to their relative position in the PSD: Homer, Shank, Guanylate-Kinase-Associated Protein (GKAP), and Membrane-Associated Guanylate Kinases (MAGUK)[274]. MAGUKs have protein-to-protein PDZ interaction domains, allowing to recruit and stabilize several other postsynaptic proteins[275]. PSD-95, the prototypal member of MAGUKs, is one of the best studied postsynaptic scaffolding proteins. The importance of PSD-95 is well-illustrated by studies linking its expression levels to spine morphology. As described on chapter 3.2, morphology of dendritic spines is rich, ranging from hair-like filopodia structures to mushroom-like with large head and narrow neck. A similar classification can be performed based on the expression levels of PSD-95: enrichment is well-correlated with the formation of mushroom-like spines, while spine shrinkage with a decrease[276,277]. Expression levels of PSD-95 are closely followed by other synaptic proteins, cytoskeleton volume, and plasma membrane surface – defining synaptic structure as a proxy to function[270–272]. This will be further discussed on section 4.3. In conclusion, synaptic scaffolding proteins are essential to organize postsynaptic receptors in front of presynaptic glutamate release sites, and in proximity to different postsynaptic signaling complexes. This guarantees an efficient and reliable activation of downstream signaling pathways upon glutamate binding, essential to express all the different forms of synaptic plasticity.

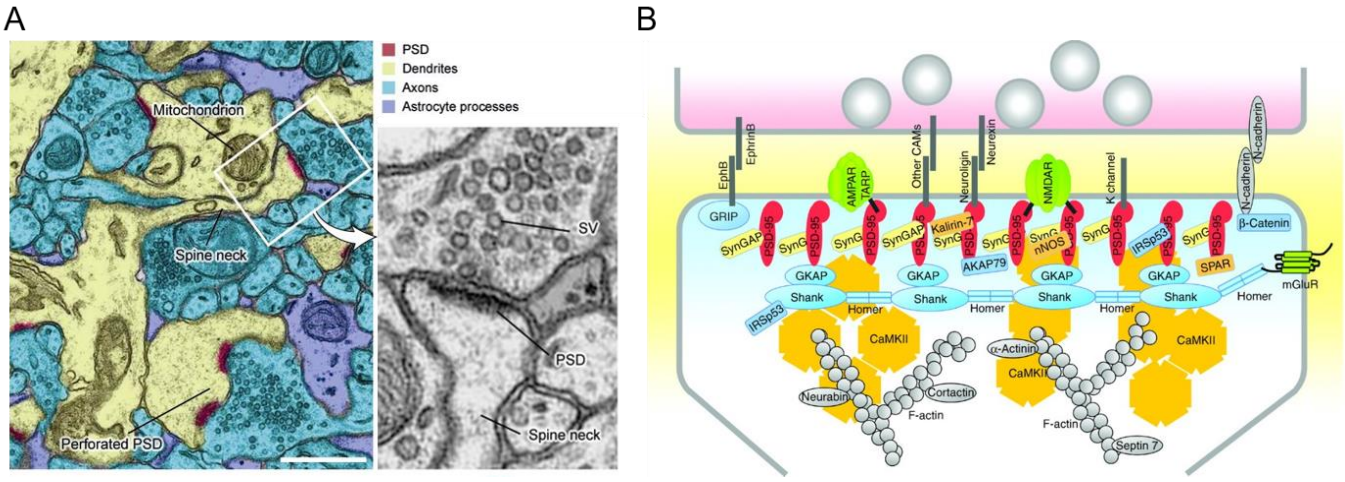

Fig. 18) Glutamatergic synaptic transmission. A) The excitatory synaptic transmission is performed between a presynaptic axon and a postsynaptic dendritic spine. Glutamate release in the active zone (vesicles represented as SV) are released into the synaptic cleft, and sensed by different glutamate receptors accumulated in the PSD. To ensure a proper synaptic transmission, receptors are believed to be accumulated in front of glutamate release sites. **B**) This precise organization is regulated in an activity-dependent manner by different proteins, including: transmembrane proteins, cytoplasmic scaffolding protein, signaling enzymes, and cytoskeletal proteins. Figure A adapted from Sheng & Hoogenraad (2007) Annu. Rev. Biochem. Figure B reproduced from Sheng & Kim (2011) Cold Spring Harb. Perspect. Biol.

The next section will describe in greater details AMPARs, also known as the workhorse of glutamatergic synaptic transmission. First, we will review fundamental concepts of AMPAR structure, gating, and function. Then, the notion of AMPAR proteome will be introduced by a non-exhaustive characterization of different AMPAR-related proteins. We will emphasize the current notion that the daily-life of AMPAR is under regulation of an extensive chain of different proteins that controls "how", "where", and "when" the receptor is activated. This will prepare the reader to AMPAR trafficking from intracellular organelles to synapses discussed in section 4.3.

4.2 AMPAR-mediated synaptic transmission

AMPARs mediate most of the fast excitatory transmission in the central nervous system (CNS). Due to their fast gating kinetics, **AMPARs mediate the primary postsynaptic depolarization in response to glutamate**[264]. This alleviates Mg^{2+} blockage from NMDARs, allowing the influx of additional cations (notably Ca^{2+}), to further amplify the initial AMPAR-mediated depolarization[255,278]. **The functional core of AMPARs is formed by tetrameric assemblies of the same (homotetramers) or different (heterotetramers) transmembrane subunits (GluA1-A4)** (fig. 19A). Each combination confers different trafficking, gating, and pharmacological properties to individual receptors[264,278,279]. This richness is further expanded by a decoration with subunit-specific protein binding partners and auxiliary proteins[280] (see below). **Each AMPAR subunit is differentially expressed throughout the brain, in a regional,**

developmental, and cell-specific manner[281]. The GluA1-A3 subunits are expressed all over the CNS, while GluA4 is preferentially expressed early in life, or during the adulthood in cerebellar granule cells, and certain inhibitory interneurons[279]. **The prototypal AMPAR subunit composition are the hippocampal GluA1/A2 and GluA2/A3.** The section 4.4 will review indirect evidences suggesting a similar composition in the barrel cortex. It is important to note that, besides the documented region-dependent expression[281], little is known about the precise AMPAR subunit composition throughout the brain.

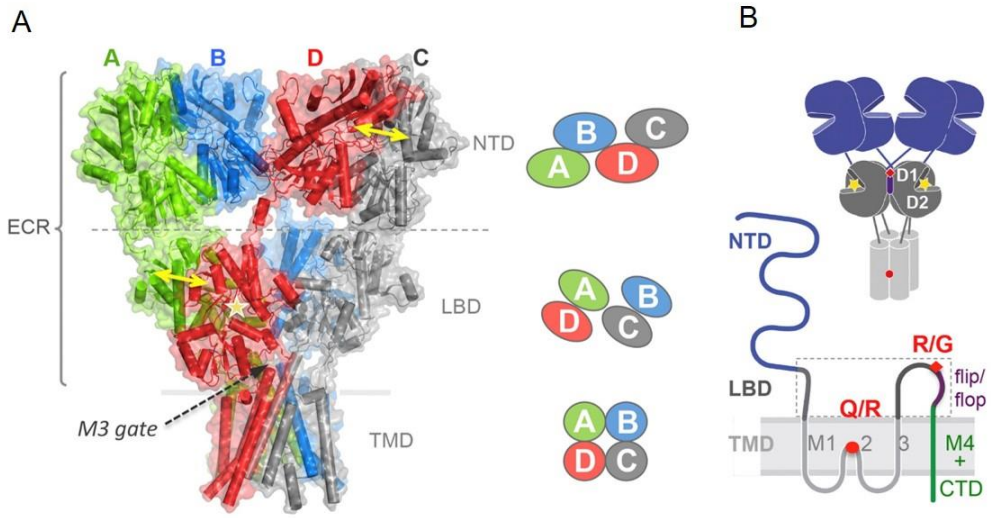

Fig. 19) The AMPAR-type glutamate receptor. A) AMPAR are tetrameric assemblies of different (heterotetramers) or the same (homotetramers) subunit. The different subunits are represented by different colors. **B)** Each subunit is composed by a highly conserved extracellular N-terminal domain (NTD), ligand-binding domain (LBD), and a membrane-embedded transmembrane domain (TMD) forming the ion channel. They also contain a highly divergent C-terminal domain (CTD), that differentially interact with cytoplasmic proteins to regulate AMPAR trafficking. Individual subunits are subjected to different post-translational modifications, such as phosphorylation or mRNA editing (detailed on text). Figure adapted from Greger *et al.* (2017) Neuron.

Each AMPAR subunit is a 900 amino acid long protein, with a molecular weight of approximately 100 kDa, encoded by four related but independent genes[282,283]**. Individual subunits are made of four different domains: an extracellular N-terminal domain (NTD), a ligand-binding domain (LBD), a membrane-embedded transmembrane domain (TMD) forming the ion channel, and a cytoplasmic C-terminal domain (CTD)** (fig.19B) [278]. All of them share a highly conserved LBD and TMD forming the channel pore and the domains for glutamate binding, but highly divergent CTD[279,283]. These differences on the CTD are proposed to be of critical importance to regulate AMPAR trafficking (see below). A crystallography study showed that, when complexed to form AMPAR core (i.e., ion channel), subunits are organized as a dimer of dimers[284]. As a result, there are four LBD in a tetrameric AMPAR, and a minimum of two have to be occupied to increase receptor conductance[278]. The TMD is built by four helical elements: M1-M4[278]. The M1, M3, and M4 cross the lipid bilayer, while the M2 is a reentering loop facing the cytosol, forming part of the channel pore. The M2 loop harbors a peculiar Q/R RNA editing in

almost all the GluA2 transcripts[279,283]. This quality-control editing converts a conserved glutamine into arginine, allowing GluA2 to leave the endoplasmic reticulum. As a result, GluA2-containing AMPARs are largely Ca^{2+} impermeable, have a low conductance, and a linear current-voltage (I-V) relationship. On the other hand, GluA2-lacking AMPAR are Ca^{2+} permeable, have higher conductance, fast decay kinetics, and inward rectification due to intracellular polyamines blockage at positive membrane potentials[255,279]. GluA2-lacking AMPAR can be alternatively designated as calcium permeable (CP-AMPARs) (see below). The LBD of all subunits have two isoforms due to alternative splicing – the flip and flop[278,283]. Alternative splicing of the exon 14 and 15 on the 1 dimer interface impacts AMPAR gating kinetics, subunit assembly, and trafficking from the ER. Interestingly, flip/flop splicing is directly regulated by ongoing neuronal activity and, as a consequence, is part of a homeostatic mechanism[285].

The behavior of AMPAR's gating is dictated by its conformation – structural interaction between domains of individual subunits forming the ion pore (see for review[278,286]). In an oversimplified view, AMPAR conformational states can be roughly divided in activated, deactivated, or desensitized. The first is due to glutamate-induced conformational changes in the LBD, responsible for opening the ion channel pore[287]. From different opened and highly-conductive states, AMPARs can be pushed to: (1) a non-conductive deactivated state, driven by glutamate dissociation from LBD or (2) non-conductive desensitized state[264,288]. AMPAR desensitization can occur upon prolonged or brief glutamate exposure, where the agonist remains bound to the receptor, even if the channel is closed. The recovery from this desensitized state occurs at variable timescales, and can impact AMPAR signaling at the millisecond scale (i.e., fast synaptic transmission)[289].

In the mature brain, the majority of AMPARs are heterotetramers, assembled in different combinations of GluA1-A4[278,279]. **As a consequence, the largest population of AMPARs contain the GluA2 subunit, that critically restricts Ca^{2+} permeability**. However, this does not rule-out the existence of CP-AMPARs, as will be discussed in section 4.4. **Formation of fully-mature AMPARs tetramers occurs in the endoplasmic reticulum (ER) in a stereotyped-manner** (reviewed here[278]). They are first stabilized as dimers due to NTD interactions, to then complex as tetramers by LBD and TMD interactions. Even if similar subunits tend to associate after translation, heterodimers are forced to form in the ER membrane due to affinities between NTDs, as the GluA1 NTD has an affinity for GluA2 NTD that is >200-fold higher than to another GluA1 NTD[290]. This partially explains why, in the hippocampus, synaptic AMPARs are composed of ~81% GluA2-GluA1 and ~16% GluA2-GluA3[291]. AMPAR biogenesis occurs mostly in the ER and Golgi close to the cell body, and are delivered to the plasma membrane either at the soma, or at the dendritic-level[283]. To be delivered far away from the soma, vesicles containing AMPARs are moved along a "microtubule highway" by different motor proteins[272,292]. Alternatively, AMPARs can be locally translated on the ER located just above the dendritic spines. This translation is highly-regulated, and is performed *on demand* accordingly to ongoing neuronal activity (see for review[293]).

The high heterogeneity of AMPAR's CTD has been proposed as an important mechanism to control receptor trafficking (see for review[279,283]). As described by Diering and Huganir, AMPARs can be divided in two groups accordingly to the size of their CTD: GluA1, GluA4, and a splice-variant of GluA2 (GluA2L) in the long-tail group, and the GluA2, GluA3, and a splice-variant of GluA4 in the short-tail group[279]. The consequence of this diversity is complex and, as proposed by the same authors, form an AMPAR code for synaptic plasticity (see section 4.4). AMPAR's CTDs hosts a panoply of different consensus amino acid sequences recognized by distinct intracellular proteins. These interactions are dynamically regulated by neuronal activity, due to complex patterns of post-translational modifications (e.g., phosphorylation, palmitoylation, etc…). These modifications orchestrate "how" and "when" an intracellular partners binds to the CTD, dictating its consequence on AMPAR trafficking. Good examples of these interactions are: (1) GluA1 interactions with SAP-97, and (2) GluA2/A3 interactions with GRIP1/GRIP2 and PICK1[294]. A complete description of AMPAR CTD interactors is beyond the scope of this thesis, and can be found here[279,283,294].

Besides these intracellular partners, native AMPARs are described as macromolecular complexes comprising different auxiliary proteins[280,281]. As proposed by Yan and Tomita, to be defined as an AMPAR auxiliary subunit, a protein has to (1) be a non-pore-forming subunit; (2) directly and stably interact with the pore-forming subunit; (3) impact receptor gating and/or trafficking properties, and (4) be required *in vivo* (i.e., synaptic phenotype)[295]. I further extended these requirements to incorporate transient interactions, that might occur at the different stages of AMPAR trafficking. The *social-network* of AMPARs has been expanded in the last ten years or so, comprising a large number of different proteins respecting these requirements.

The first AMPAR auxiliary subunit to be described was stargazin, a transmembrane AMPAR regulatory protein (TARP) γ-2[296]. Granule cells lacking this protein have a dramatic reduction of AMPARs at the cell surface[297]. This suggests an important role of stargazin in the trafficking and surface expression of AMPARs. Stargazin is a member of an extended family, including type I TARPs (γ-2, γ-3, γ-4, and γ-8), and type II TARPs (γ-5 and γ-7)[298]. These homologous proteins have a widespread and overlapping expression throughout the brain that differs across different cell types, and along neurodevelopment[299]. Moreover, TARPs are crucial regulators of AMPAR surface expression, and stabilization at the PSD through binding to PDZ-domain containing proteins (e.g., PSD-95)[300–302]. The importance of this interaction will be discussed on the next section. TARPs are also important modulators of AMPAR gating kinetics and pharmacology (reviewed elsewhere)[298,299,303]. This is well-illustrated by studies showing that stargazin increases the recovery from desensitization, deactivation, and potentiates AMPARs responses to glutamate[304,305].

Several other components of the AMPAR macromolecular complex have been identified. Some are already well-characterized: cornichon homologs 2 and 3 (CNIH2/3)[306]; Shisa family (CKAMP44/Shisa9, Shisa7, and Shisa6)[307–309] (see for review[299,310]), while several others have yet undetermined functions[280,281]. What is the physiological meaning of this extensive list of auxiliary

proteins? AMPAR are now believed to be under the regulation of a set of powerful biochemical reactions, involving a complex spatiotemporal interaction between a myriad of different proteins. As described, the expression of these proteins is regional, and cell-type specific. Consequently, their effects on AMPAR trafficking, and biophysical properties follow exactly the same rules. Therefore, this complexity might allow the required synaptic heterogeneity to support complex circuit function and regulation (e.g., plasticity), underlying different forms of behavior. Even if this idea of synapse-specific code for AMPAR properties is appealing, it also poses an important problem: studies on AMPAR physiology in a particular brain region, might not be generalized to others. This is especially true in the present study using the barrel cortex as a study model, to explore classical concepts coming from experiments in the hippocampus.

The next section will explore the daily-life of an AMPAR, from its trafficking across intracellular organelles, to its synaptic accumulation. It will take advantage of the structural and molecular mechanisms here described, to define how AMPAR trafficking underlies basal neurotransmission and synaptic plasticity.

4.3 The dynamic nano-synapse: a molecular machinery at play to regulate synaptic transmission and plasticity

AMPARs are continuously trafficking between intracellular compartments and the plasma membrane, in a constitutive and activity-dependent manner (fig. 20A)[269]. These "routes" are dictated by the AMPAR proteome that, in a complex chain of protein interactions, define the receptor "destination". Dendritic spines have fully-functional exocytic/endocytic pathways, where AMPAR traffic to and from the plasma membrane[272]. These organelles are the primary subcellular compartments where AMPARs can be mobilized or restricted accordingly to synaptic activity (see below). AMPAR insertion in the plasma membrane is believed to occur far away from the PSD, probably in the dendritic shaft[311]. It is worth it to mention that direct AMPAR exocytosis in spine heads has also been reported[312]. Similarly, AMPAR endocytosis is assumed to occur laterally to the PSD, in perisynaptic or extrasynaptic regions[313]. **As (1) AMPARs have a low affinity to glutamate, to be gated, they have to be placed in close proximity to the neurotransmitter release sites[314], and (2) receptor insertion/removal lies hundreds of nanometers away from the synapse, how can they reach and leave the PSD where they mediate neurotransmission?**

The solution to this conundrum was made in large part by the Choquet's laboratory over the last two decades. A series of elegant studies have demonstrated that upon insertion in the plasma membrane, AMPAR diffuse along it[301,315–317]. This mobility, also known as lateral diffusion, is Brownian in nature, meaning powered by the thermal molecular agitation (i.e., without active transport)[318]. During basal conditions, almost half of the AMPARs in the cell membrane are mobile, a percentage that is higher if only extrasynaptic regions are considered[316,319]. **This mobility allows AMPARs to explore the cell membrane, move inside synapses, scan the PSD surface, and eventually move out if not properly stabilized**[301,316,320]. It also implies that

extrasynaptic AMPARs can act as a reservoir pool of receptors to feed synaptic plasticity (see below). **Synaptic accumulation of AMPARs is mediated through a tripartite interaction between the receptor, its auxiliary proteins, and scaffolding proteins (i.e., MAGUKs), notably PSD-95**[301,302]**.** These interactions damp down lateral mobility, and accumulates AMPARs at synapses in clusters of less than <100 nm in diameter, and containing around 20-25 receptors[319]. This organization is closely matched to the presynaptic glutamate release sites, suggesting that excitatory transmission can be tuned at the nanoscale[321,322]. Therefore, **the number of synaptic AMPARs, which defines the synaptic weight, can be predicted by a dynamic equilibrium between intracellular, extrasynaptic, and synaptic compartments**[269]**. By extension, altered synaptic transmission during different forms of plasticity can ultimately be explained by a perturbation of this equilibrium.**

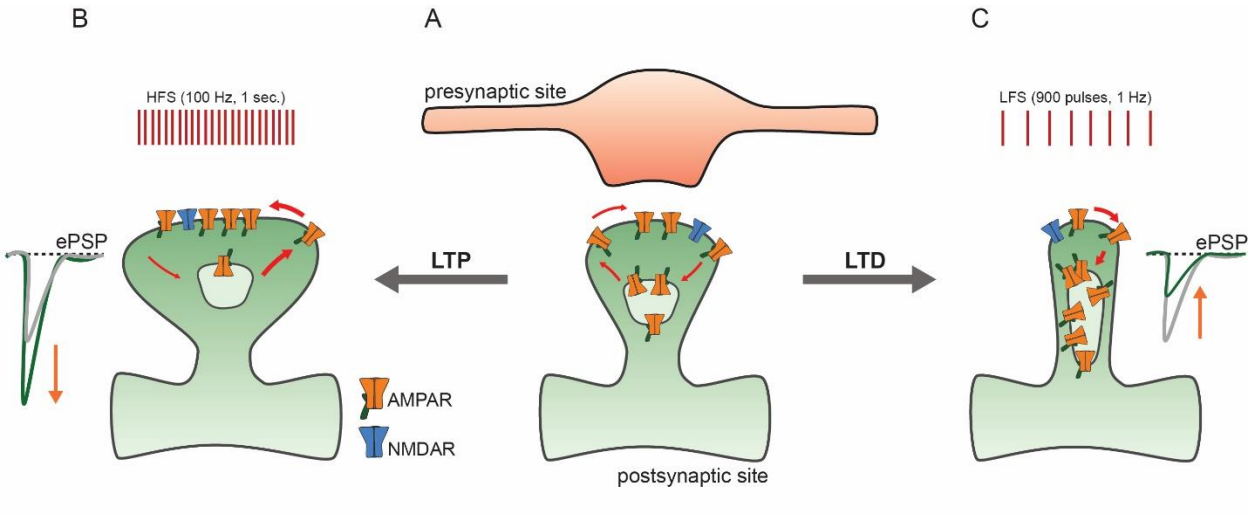

Fig. 20) A three-step recruitment of AMPARs to the synapse. A) During basal synaptic transmission, AMPARs (orange) are constitutively recycling between the plasma membrane and intracellular organelles (red arrows). The balance between endo/exocytosis, AMPAR lateral mobility, and synaptic trapping defines the number of synaptic AMPARs. **B)** Synaptic LTP can be explained by an increased receptor accumulation recruited by AMPAR lateral mobility (early phase), and AMPAR exocytosis (late phase). This shifts the recycling balance towards AMPAR synaptic accumulation. **C)** The opposite is true for LTD, where a destabilization of synaptic AMPARs, followed by endocytosis might explain the reduction of synaptic AMPARs. LTP and LTD are induced by different electrically-induced protocols (HFS and LFS, respectively). These protocols drive a different NMDAR signaling (blue) that engage the molecular mechanisms to shift the route of AMPAR trafficking.

Several different evidences have implicated **an increased number of synaptic AMPARs as a mechanism for NMDAR-LTP expression** (reviewed elsewhere[42,269]). A good example of these seminal studies are experiments using glutamate uncaging[323]. Matsuzaki and colleagues have demonstrated that repetitive activation of NDMAR, leads to long-lasting and spine-specific increase of AMPAR responses. These alterations were not due to alterations on the unstimulated presynaptic terminal. This is in agreement with a preceding study demonstrating a synaptic accumulation of exogenously expressed green fluorescent protein (GFP)-tagged AMPARs, after NMDAR-LTP induction[324]. Conversely**, NMDAR-LTD has been reported to be associated to**

a decrease in the number of surface AMPARs by endocytosis leading to a depletion in synaptic AMPAR[325]. How can the bidirectional regulation of synaptic strength by NMDAR-LTP/LTD be explained at the molecular level?

The most parsimonious explanation to this question lies on a differential NMDAR signaling[255,266]. NMDAR gating drives Ca^{2+} influx in the dendritic spine during synaptic activity[259]. Variation in intracellular Ca^{2+} is activity-dependent, with high frequency activation of NMDARs during LTP driving a high increase, whereas low frequency during LTD drives a smaller increase[42,255]. This subtle variation of Ca^{2+} flowing though NDMARs recruits different downstream signaling pathways that explains the bidirectional effect during NMDAR-LTP/LTD[255]. High levels of Ca^{2+} during LTP activates low-affinity kinases able to phosphorylate a broad range of proteins, culminating into an enhanced synaptic transmission. This is well-illustrated by the **activation of a major synaptic protein, CaMKII**[326]. In the presence of Ca^{2+}, this kinase is autophosphorylated at T286, and becomes a molecular switch: its activity is persistent and Ca^{2}-independent. Once active**, CaMKII can phosphorylate different synaptic substrates, such as: (1) GluA1 S831, enhancing channel conductance**[327]**; (2) AMPAR CTDs, to regulate receptor intracellular trafficking**[294]**, and (3) AMPAR auxiliary proteins, increasing their affinity to PSD-95**[301,320]**.** Interestingly, CaMKII activation promotes the synaptic recruitment of SAP97, and likely their interaction with GluA1 CTD during LTP[294,328]. However, the requirement of this interaction during synaptic plasticity is not clear, since conditional *knockout* for SAP97 have normal LTP[329]. Other kinases, such as protein kinase C (PKC) or cAMP-dependent protein kinase (PKA), can also be activated during LTP (see for example[311]). PKC phosphorylation at S818 increases interaction with protein 4.1N, and increases receptor exocytosis during NMDAR-LTP[311]. Other prominent CTD interaction during LTP is the GluA2/A3 interaction with GRIP1/GRIP2 and PICK1[294,330].

The interaction between AMPAR auxiliary proteins and PSD-95 provides an alternative model to explain the synaptic accumulation of AMPARs after NMDAR-LTP induction. As discussed, auxiliary proteins anchor AMPARs to PSD-95, accumulating receptors at the PSD[301]. Upon induction of NMDAR-LTP, CaMKII phosphorylates auxiliary proteins (e.g., stargazin), and increases their affinity to PSD-95[320]. As a consequence, highly mobile AMPARs are accumulated in the PSD, where the rate-limiting step for this accumulation are the available number of PSD-95 slots. Thus, independently of its complexity, the signaling cascade underlying LTP expression culminates in a shift of AMPAR trafficking equilibrium, towards receptor synaptic accumulation (fig. 20B). This can be ultimately explained by a three-step model proposed by Opazo and Choquet, where NMDAR-LTP induction requires (1) increase AMPAR exocytosis far from the PSD; (2) lateral diffusion along the membrane plane and (3) AMPAR synaptic accumulation due to PDZ-PDZ interaction between auxiliary and scaffolding proteins[331]. However, groundbreaking work from the same laboratory, came to reveal that this is an incomplete view[332]. **Penn and collaborators took advantage of an elegant AMPAR cross-linking approach, where receptor lateral mobility is blocked by extracellular antibody application, to demonstrate how**

AMPAR surface trafficking is mandatory for NMDAR-LTP (fig. 21). The authors found that if *in vitro* slices were pre-treated with AMPAR cross-linking agents, followed by washout, the early phase of LTP induction is abolished (fig. 21B). However, a late potentiation is seen, likely due to AMPAR exocytosis, and the recruitment on new receptors to the synapse by lateral mobility. Conversely, if AMPAR exocytosis is blocked by tetanus toxin (TeTx), an initial potentiation is seen (fig. 21C). This is in agreement with a previous study, where a similar effect is reported[333]. This is proposed to result from a pool of pre-existing extrasynaptic AMPARs that, upon NMDAR-LTP induction, are recruited to the synapse by lateral mobility, and accumulated in the PSD as aforementioned[320]. The only way to completely abolish NMDAR-LTP expression was in the continuous presence of AMPAR cross-linking, or by pre-treatment along with TeTx application (fig. 21D).

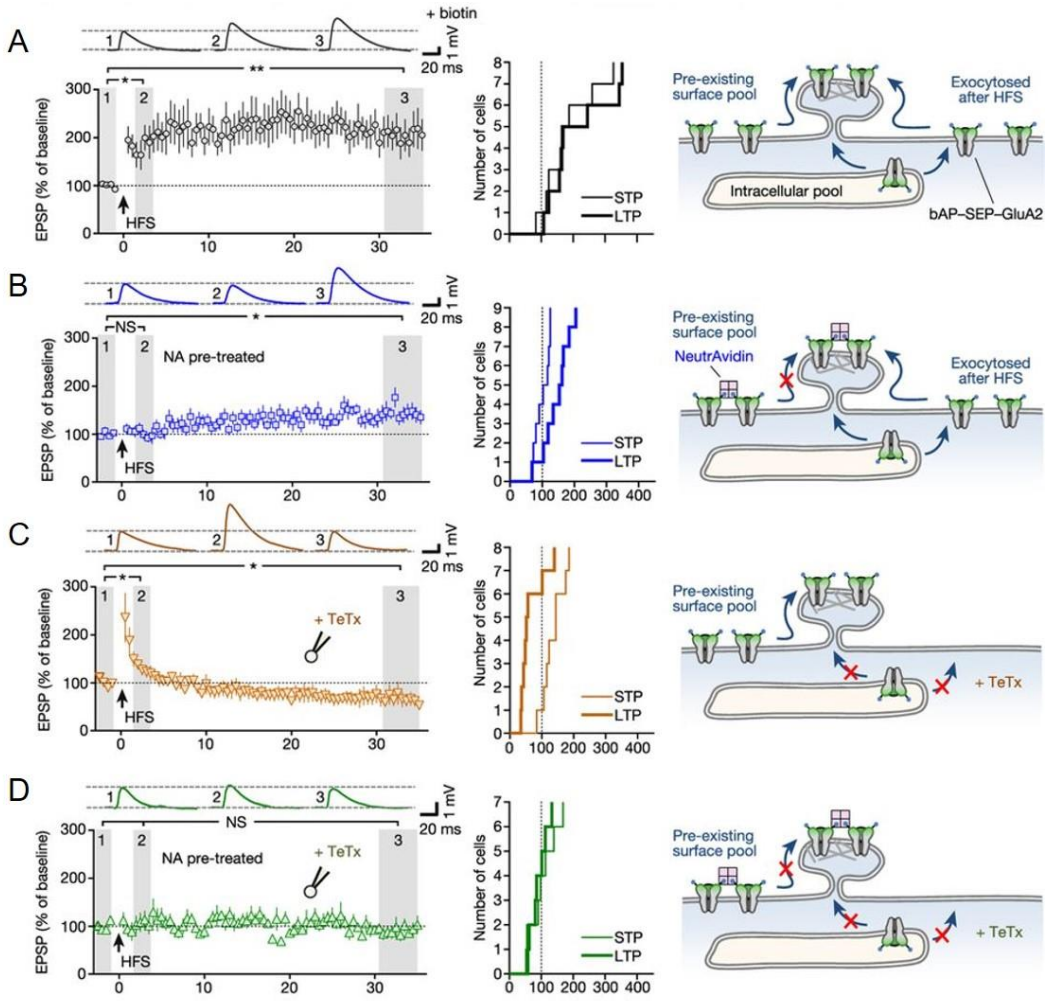

Fig. 21) The interplay between AMPAR lateral mobility and exocytosis during NMDAR-LTP. A) Hippocampal high-frequency stimulation (HFS) drives NMDAR-LTP due to an increase of synaptic AMPARs. **B)** If AMPAR lateral mobility is blocked before HFS, a late component of LTP is seen. **C)** Conversely, if postsynaptic exocytosis is blocked by TeTx in the recording solution, an initial potentiation is seen, but decaying soon after HFS. **D)** NMDAR-LTP is completely blocked by the pre-treatment with AMPAR cross-linkers, and exocytosis blockage by TeTx. This clearly demonstrates the complex relationship between AMPAR lateral mobility and exocytosis to increase receptor synaptic content during NMDAR-LTP. Figure reproduced from Penn, A. *et al.*, (2017) Nature.

Conversely, the precise molecular mechanisms for the expression of NMDAR-LTD are still somewhat enigmatic. Classically, it has been though that transient Ca^{2+} signaling recruits high-affinity phosphatases, with the concomitant dephosphorylation of proteins, and decreased synaptic transmission[255]. However, this view has been recently challenged by experiments showing that CaMKII activation is necessary to induce NMDAR-LTD[334]. Even less clear is the precise sequence of molecular events translating NMDAR-LTD induction to decreased number of synaptic AMPARs. Opazo and Choquet have hypothesized a reverse mechanism as seen during LTP, with: (1) destabilization of synaptic anchored AMPARs; (2) increased population of mobile AMPARs; (3) increase AMPAR endocytosis (fig. 20C)[331]. However, it is currently unknown if either AMPAR unbinding from PSD or its increased internalization by endocytic mechanisms is the primary mechanism for NMDAR-LTD expression.

One interesting debate in the glutamatergic field is the AMPAR subunit-dependent rules for the expression of synaptic plasticity. It has been classically proposed that GluA1 is required for LTP, while GluA2 endocytosis is necessary for LTD[42,279,283]. By extension, CP-AMPARs have been reported in a few studies to be compulsory to prime the initial phase of hippocampal NMDAR-LTP[335–338]. This is highly debatable, since other studies have reported that GluA2-containing AMPARs are involved in NMDAR-LTP as well[339,340]. This picture gets even more complicated with other studies showing that LTP can be sustained by all subunits of AMPARs, or even exogenous KARs[341]. The only requirement that these authors demonstrated is of a reserve pool of membrane receptors, to potentiate synapses after NMDAR-LTP induction. The concept raised by the authors is important to be here discussed. Regardless or the presence or not of a subunit-specific rule, LTP expression can be ultimately explained by AMPARs synaptic accumulation. This illustrates very well why methods manipulating AMPAR trafficking, are very good approaches to manipulate synaptic LTP.

The ultimate goal since the discovery of synaptic LTP, is to understand whether and how its expression underlies modifications in neuronal circuit activity, and consequent behavioral adaptations. Unfortunately, a direct link between synaptic LTP and animal behavior has not yet been directly experimentally established. This lack of knowledge is partially explained by the absence of tools to block LTP without affecting basal synaptic transmission**. However, a new generation of tools to directly or indirectly manipulate AMPAR trafficking might finally allow to overcome this limitation.** This is well-illustrated by the chromophore-assisted light inactivation (CALI) approach, where monoclonal antibody targeting anti-GluA1 are coupled to a photosensitive molecule to inactivate synaptic AMPARs upon green light application[342]. CALI-GluA1 is reported to drive important impairments on hippocampal NMDAR-LTP, and on animal behavior (see below). The synaptic optoprobe AS-PaRac1 might also allow control LTP *in vivo*, by destabilizing behavioral-relevant potentiated synapses[343]. Additionally, lightsensitive inhibitors of CaMKII are also available[344]. Once again, these tools block NMDAR-LTP expression, by interfering with its downstream signaling pathways. Alternatively, light-sensitive botulinum toxin

was recently described[345]. This approach might be of valuable interest to blocking LTP, by modulating AMPAR exocytosis with a notable spatiotemporal resolution. Unfortunately, the existence of a membrane pool of mobile AMPARs might still express LTP (at least, an early-phase) under these conditions. Lastly, the Choquet lab described an efficient way to block LTP by interfering with AMPAR trafficking using extracellular antibody-crosslinkers[332]. Depending when and how this cross-linking approach is used, one can dissect different properties of LTP (see above). Indeed, one can completely block LTP expression, by impairing lateral diffusion of pre-existing, and recently exocytosed AMPARs. Importantly, AMPAR cross-linking turns possible to manipulate trafficking of endogenous receptors, without affecting basal synaptic transmission[332]. These properties define this tool as a good and straightforward approach to study LTP *in vivo.*

In the present study, we aimed to understand how synaptic LTP underlies cortical remapping, and related adaptive behavior (see next chapter). For this, we developed a novel AMPAR cross-linking approach to manipulate LTP *in vivo* based on the knowledge here presented. We combined this molecular framework with recordings in the barrel cortex, due to its circuit simplicity, facility to induce map plasticity, and possibility of a straightforward behavior readout. To better understand our experimental rationale, the next section will describe the limited knowledge on barrel cortex's AMPAR proteome. Then, we will review the state-of-art of the molecular mechanisms underlying synaptic plasticity in this cortical region. This chapter will finish with a description of how AMPAR trafficking in different brain regions underlies different components of animal behavior. With this, we aim to support why our *in vivo* AMPAR cross-linking approach is a valuable tool to link synapses, circuits, and animal behavior.

4.4 Towards the barrel cortex's AMPAR proteome

A high-throughput proteomic study in native tissue have identified the major components of the AMPAR proteome in the neocortex[281]. The major AMPAR subunit is GluA2 (~45%), roughly equal amounts of GluA1/GluA3 (around 21% and 27%), and GluA4 with a residual expression (~6%). Similar results were obtained by an independent study[344]. Moreover, TARP γ-8, and CNIH2 are the AMPAR auxiliary subunits with higher protein abundancy associated to neocortical AMPARs complexes. As this study did not perform a detailed region-analysis of all neocortical structures, it is difficult to extrapolate if the same stands true in the barrel cortex. Some variations might exist, as indicated by a study demonstrating stargazin as an important regulator of AMPAR expression in this cortical region[346]. A barrel-specific transcriptomic and proteomic of AMPARs has been performed in older studies, with an important limitation: despite the high spatial resolution, the techniques used by these studies might not be sensitive enough to quantify slight variations in AMPAR expression. Indications defining GluA2 as the main subunit in the barrel cortex comes from Condo and collaborators[347]. This study reported that around 70% of putative pyramidal neurons in the adult rat barrel cortex expressed GluA2 but not GluA1 (measured as mRNA and protein levels). The other percentage of the population was either GluA2/GluA1-expressing or GluA1-expressing/GluA2-lacking cells. The enrichment in GluA2-expressing cells was obvious in all cortical layers, notably L2/3. Most of GluA1-

expressing/GluA2-lacking cells were also immunoreactive to parvalbumin and, therefore, putative interneurons. A similar observation of an intense GluA2 staining (i.e., immunohistochemistry) on rat barrel cortex pyramidal neurons was demonstrated by an independent work[348]. Unfortunately, the levels of GluA3 and GluA4 subunits were overlooked by these two studies. A more recent study, using electrophysiological approaches, has demonstrated that in L2/3 of the rat barrel cortex GluA2-containing AMPARs are predominant[349]. Brill and Huguenard showed that before P12, L2/3 pyramidal neurons have a pronounced expression of CP-AMPARs. However, due to a developmental switch between P14 and P16, GluA2-containing AMPARS are predominant in the adult animal. This is in agreement with experiments on the hippocampus, showing that CP-AMPARs are a residual portion of receptor's population[291,350]. Therefore, one can hypothesize that in the adult barrel cortex, GluA2-containg AMPARs (~70% of GluA2/A3 and ~30% of GluA2/A1 or GluA1/A3) are predominant (figure 22). As described in chapter 3.2, whisker trimming alters the genetic and proteomic landscape of cells in the barrel cortex. Not surprisingly, altered expression of AMPARs in the barrel cortex is reported to occur after whisker trimming[351]. Sparing row C of whiskers increased mRNA levels of the GluA2 subunit on the spared but not on the deafferented cortex. On the contrary, a study in adult raccoons demonstrated an increase in GluA2 protein levels in synaptoneurossomes prepared from the deafferented cortex, after single-digit amputation[352].

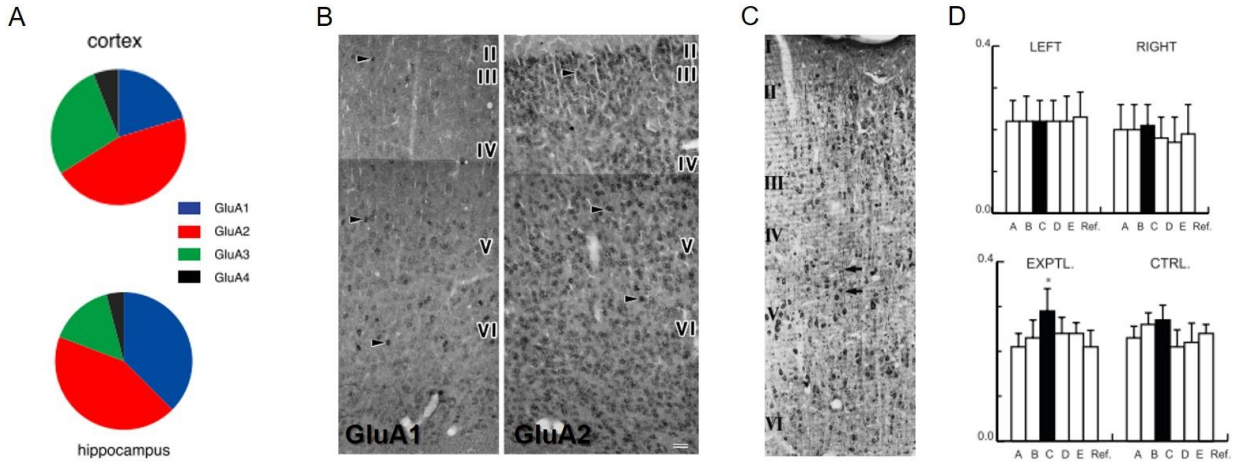

Fig. 22) The AMPAR proteome in the barrel cortex. A) A recent high-resolution proteomic revealed that AMPAR composition in the neocortex remarkably differs from the hippocampus. Indeed, neocortical regions have a preferential expression of the GluA2 subunit, followed by GluA3, and GluA1 subunits. **B)** Laminar and cellular distribution of GluA1, and GluA2 mRNA in the barrel cortex. Note the notably accumulation of GluA2 mRNA on L2/3. **C)** This enrichment is confirmed at the protein-level, as indicated by immunohistochemistry. Once again, the GluA2 subunit of AMPARs is expressed across all the barrel cortex's layers. **D)** Trimming-induced map plasticity increases the levels of GluA2 mRNA. Figure A adapted from Schwenk, J. *et al.,* (2014) Neuron. Figure B adapted from Kondor, M. *et al.,* (1997) Journal of Neurosci; Figure C adapted from Vissavajjhala, P. *et al.,* (1996) Exper. Neuro.; Gierdalski, M. *et al.,* (1999) Molecular Brain Research.

While the synaptic mechanisms in the barrel cortex are fairly well-described, their molecular underpinnings are still unknown. As described, the bulk of our knowledge on the circuit expression of synaptic proteins, and their alterations by sensorial experience, is restricted to a

handful of studies. The emergence of the barrel cortex as the model to study LTP in a physiological context will raise the interest in studies using modern and highly-sensitive proteomic approaches. This will be decisive to better understand how the AMPAR proteome shapes barrel cortex plasticity. The next pargraph will describe in detail the current knowledge on the molecular underpinnings of barrel cortex LTP induced by normal sensorial experience, or by whisker trimming.

4.5 Molecular mechanisms of barrel cortex synaptic LTP

As discussed in chapter 3, NMDAR signaling is critical for L2/3-L2/3 circuit transmission. **As a consequence, the molecular machinery expressing LTP on L2/3 synapses might share some similarities with the one described for hippocampal NMDAR-LTP.** In agreement, LTP on L2/3 pyramidal neurons is abolished *in vitro* by mutations on CaMKII[181]. Bearing in mind the importance of CaMKII and downstream targets, one could also expect an accumulation of synaptic AMPARs in the same synapses. The first observation supporting this hypothesizes came from a pioneer study performed by Takahashi and collaborators[178]. By overexpressing GFP-GluA1 by Syndbis virus injection in the barrel cortex, these authors showed an increased AMPAR insertion in L2/3 synapses by normal sensory experience. This insertion could be abolished by overexpressing GluA1 CTD, suggesting similar mechanisms for receptor trafficking than the ones reported in the hippocampus (see above). However, as AMPARs were virally-expressed, this enrichment can result from overexpression artifacts. A similar result was obtained in a more recent *in vitro* study, reporting an accumulation of SEP-GluA1 after sensory experience[179]. The authors also reported that SEP-GluA2 synaptic enrichment only occurred when all the whisker were trimmed, likely due to homeostatic mechanisms. **The definitive proof that *in vivo* LTP requires AMPAR recruitment, came from an elegant study from Huganir's laboratory[177]. Zhang and collaborators reported a NMDAR-dependent accumulation of SEP-GluA1 in L2/3 pyramidal neurons synapses after prolonged whisker stimulation.** As the authors used *in utero* co-electroporation of SEP-GluA1 along with non-fluorescent myc-GluA2, the findings are likely not due to overexpression artifacts. Furthermore, a similar whisker stimulation protocol is described to induce LTP on the same synapses, supporting that AMPAR synaptic recruitment might also occur *in vivo*[176]. **Therefore, is tempting to assume that similar AMPAR trafficking rules to the one described in the hippocampus, might also stand true for sensory-evoked LTP**. It remains to be determined if this SEP-GluA1 accumulation is driven by GluA1 homomers or GluA1/A2 heteromers. It is worth to mention that important differences to the hippocampal NMDAR-LTP might also exist. Indeed, an important presynaptic component for L2/3 synaptic LTP is reported to occur in the barrel cortex[186]. In agreement, nitric oxide synthase (NOS1) null-mutants drastically reduced the degree of L4-L2/3 potentiation *in vivo*.

4.6 Molecular mechanisms of barrel cortex map plasticity

Synaptic LTP is also hypothesized to be the main mechanism driving cortical remapping after whisker trimming (section 3.2). The first evidence that map plasticity shares some similarities with hippocampal NMDAR-LTP came from studies with CaMKII mutants[169,181,183]. In the absence of a functional CaMKII, essential for LTP induction, SWE-induced barrel expansion is abolished. Once again, if similar rules to the hippocampus are applied, one should expect AMPAR synaptic accumulation during map plasticity. Indeed, Clem and Barth demonstrated *in vitro* a SWE-induced increase AMPAR/NMDAR ratio in the spared barrel[189]. This is in agreement with a LTP-like mechanism, and demonstrated to require a synaptic insertion of CP-AMPARs. Unfortunately, two technical limitations are associated with these findings: (1) evoked neuronal responses are obtained by electrical stimulation, and likely potentiating synapses not used *in vivo*, and (2) stimulation was restricted to L4 barrel and, as a consequence, not recruited POm projections. Therefore, it is hard to predict if indeed CP-AMPARs are essential to express map plasticity during physiological conditions. **Even if some similarities exist to hippocampal NMDAR-LTP, LTP-driven cortical remapping has some interesting particularities.** The most remarkable was described by Clem and collaborators[252]. They demonstrated that **NMDAR-LTP drives the initial potentiation of the neuronal responses to the spared input, along with a slower mGluR-dependent component.** After 24h after SWE, spared synapses were potentiated due to recruitment of CP-AMPARs in an NMDAR-dependent manner, as indicated by occlusion of *in vitro* LTP induction. Remarkably, if the same experiments were performed in the presence of a NMDAR blocker (e.g., CPP), a strong and mGluR-dependent LTP was recorded. Interestingly, mGluR blockade during an associative tactile conditioning task impaired animal behavior. This led the authors to propose that NMDAR-dependent LTP drives the initial cortical remodeling, while cumulative experience (i.e., learning) is driven by mGluR-LTP. Such metaplastic effect might allow to store behaviorally-relevant formation on synapses potentiated by map plasticity. Interestingly, a presynaptic role for the LTP-driven potentiation during map plasticity has been reported[185]. In agreement, SWE-driven barrel expansion was impaired in a NOS1 *KO* mice. Altogether, these results reinforce the idea that cortical remapping is a compound phenomenon, involving different cell types and circuit structures, orchestrated by a complex molecular machinery. A summary of the major findings linking AMPAR trafficking to LTP-driven map plasticity is found on figure 23.

One of the biggest challenges of modern neurosciences is to understand how experience shapes synapses, and neuronal circuits, to optimize subject-environment interaction. While it appears clear that synaptic LTP allows to store information at the single-cell level and to critically regulate animal behavior, the molecular, and circuit mechanism underlying such process remains elusive. Studies altering AMPAR trafficking rules have provided good indications of its significance *in vivo*. The last section of this chapter will review studies linking AMPAR trafficking, synaptic plasticity, and different aspects of animal behavior. With this, we aim to

convince the reader that *tools* blocking normal AMPAR trafficking, notably lateral mobility, induce strong phenotype at the behavior level.

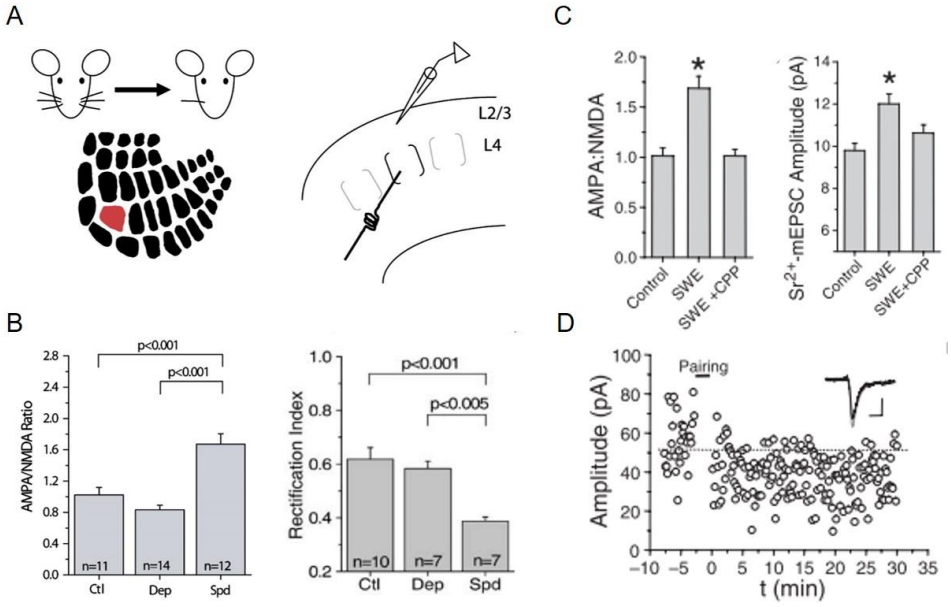

Fig. 23) Map plasticity increases AMPAR synaptic content. A) *In vitro* slice electrophysiology after *in vivo* altered sensory experience (i.e., SWE) has provided valuable information about the synaptic mechanism underlying map plasticity. **B**) SWE increases AMPAR/NMDAR ratio due to a synaptic accumulation of CP-AMPARs. **C)** This postulate is confirmed by an independent study, showing an increase of AMPAR/NMDAR ratio, and the amplitude of quantal AMPAR-EPSPs. **D)** In agreement, LTP induction induced *in vitro* is occluded after 2 days of SWE. Altogether, these data provides strong evidences for a LTP-driven increase of synaptic AMPARs after trimming-induced map plasticity. Figure A and B adapted from Clem, R. L. & Barth, A (2006) Neuron; Figure C and D adapted from Clem, R. L. *et al.*, (2008) Science.

4.7 Is there any link between AMPAR, synaptic plasticity, and animal behavior?

The first evidences that synaptic LTP stores behavioral-relevant information came from *in vivo* pharmacological experiments[353,354]. By inhibiting NMDAR and CaMKII signaling, these studies demonstrated strong memory impairments on different behavioral tests. However, the first experimental link between behavioral learning and synaptic LTP came from a notable occlusion experiment in the hippocampus[355]. Here, these authors showed that one-trial inhibitory avoidance learning in rats, occluded RWS-LTP in the hippocampal CA1 region. However, to the time of writing, the strongest evidence that LTP is required for mammalian associative learning comes from cued-fear memory behavioral experiments[356]. This task is an associative memory encoded by the temporal association between a foot shock, and a conditioned stimulus (e.g., sound)[357]. After pairing, condition stimulus presentation by itself, drives a freezing behavior similar to the foot shock presentation (i.e., associative memory). It has been shown that optogenetically-induced LTP in the auditory inputs in the amygdala is sufficient to reactive the previously learned associative memory[356].

In agreement with its importance for LTP expression, circuit-dependent manipulations of AMPAR trafficking has been reported to drive different behavioral deficits (see for review[358]). For example, genetic ablation of AMPAR subunits has been described to impair hippocampal-dependent spatial working memory, amygdala-dependent fear conditioning, or even the biology of addiction[359–362]. Behavior deficits are not restricted to genetic manipulations of AMPARs *per se* but also to their auxiliary proteins. The behavior phenotype is dependent of the mutated protein, due to their highly regional-specificity. For instance, while Shisa 7 *KO* have specific deficits in contextual fear conditioning, stargazin *KO* drives a strong "stargazer" phenotype, ranging from absence seizures to ataxia[309,363]. Independently of where the AMPAR proteome is affected, they all alter animal behavior due to impairments on synaptic plasticity, notably NMDAR-LTP. The resulting phenotype is complex, depending on which cell-type, and circuit is affected by the protein mutation. It is important to note that the majority of the studies take advantage of chronic genetic manipulations of the AMPAR proteome (e.g., AMPAR subunit *KO*). This makes it hard to know if some of the reported deficits are caused by the lack of protein, or due to long-lasting circuit- and brain-wide adaptations to these manipulations.

This important limitation is now possible to be tackled due to the development of new tools to acutely block AMPAR trafficking *in vivo* (see above). In agreement, CALI-GluA1 has been successfully used to block hippocampal-dependent fear memories in mice[342]. Alternatively, cross-linking of endogenous AMPARs is also reported to be an efficient approach to affect hippocampal-related contextual learning during a fear conditioning task[332] (fig. 24). I believe that new generation of approaches to block AMPAR trafficking will pave the way to understand the physiological meaning of synaptic LTP. In combination with their usage in simpler working models (e.g., sensorial modalities), while allow to bridge LTP, circuit dynamics (i.e., engram formation), and related animal behavior.

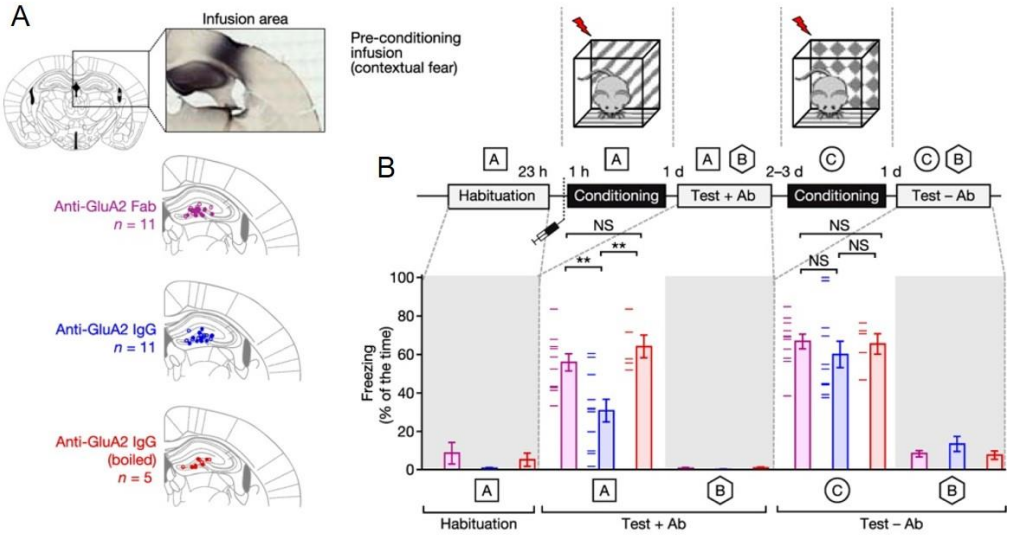

Fig. 24) *In vivo* AMPAR cross-linking blocks LTP and impairs animal behavior. A) In vivo AMPAR cross-linking by stereotaxic injection of an anti-GluA2 antibody. Other antibodies can be injected in different cohorts of animals to provide important controls of non-specific effects of IgG injection. **B)** The blockage of AMPAR lateral mobility in the dorsal hippocampus blocks NMDAR-LTP. As a consequence, contextual fear-conditioning is impaired by AMPAR cross-linking. Figures reproduced from Penn, A. *et al.*, (2017) Nature.

Executive summary

This thesis aimed to demonstrate a direct link between synaptic plasticity, cortical remapping, and adaptive behavior following peripheral injury. For this, we developed a novel approach to block *in vivo* LTP by AMPAR cross-linking, without affecting circuit function. We performed chronic *in vivo* AMPAR cross-linking during SWE-induced cortical remapping, to understand if it could be reversed by synaptic LTP blockade. We then applied this approach during a whisker-dependent behavior to understand how the LTP-driven map plasticity is translated in sensory perception. We aimed to determine if map plasticity is a compensatory mechanism, where the cortical representation is increased in order to enhance the computational efficacy of the spared whisker.

It has been recently described that RWS can potentiate cortical synapses *in vivo* with the support of NMDAR-dependent dendritic plateau potentials[208]. Pioneer work from Huganir's lab reported an accumulation of AMPARs *in vivo* during a similar sensory stimulation in a long-lasting and NMDAR-dependent manner[177]. This inspirational work led us to hypothesize that changes in the number of synaptic AMPARs powered by lateral diffusion might be a key process during *in vivo* LTP as well. The major evidences for the contribution of AMPAR lateral mobility during LTP comes from a study in the hippocampus[332]. We questioned if upon RWS, a recruitment of AMPARs by lateral mobility is also required to support potentiation of L2/3 cortical synapses. If this would be true, AMPAR cross-linking might be a good candidate to block LTP *in vivo*, without affecting circuit basal transmission: an essential requirement to study how this synaptic mechanism underlies map plasticity.

A common theme for the re-organization of functional sensory maps in the cerebral cortex after peripheral injury, is the gaining of cortical space by the active modalities[3,13]. This functional expansion occurs at the expense of deafferented regions. While map plasticity has been hypothesized to promote learning and to recover learned behaviors, its circuit and synaptic underpinnings remains to be elucidated[364–366]. This work took advantage of the mouse whisker-to-barrel cortical system to explore the relation between the synaptic mechanisms of map plasticity, and correlated adaptive behaviors[74]. Trimming some whiskers causes L2/3 pyramidal neurons located in the deprived and spared-related columns to shift their responses to the spared whiskers[169,173,191]. This results in a strengthening and expansion of the spared whiskers representation within the map[54]. Synaptic LTP has long been postulated as the mechanism for neuronal response strengthening during normal sensory use (i.e., learning) and trimming-induced plasticity[54,169,187,189,191,252]. A large body evidence reported that NMDARs, AMPARs, and α-CaMKII are all involved in response potentiation in spared L2/3[185,189,252]. These evidences provide consistent, yet indirect indications that LTP underlies whisker map plasticity. While sensory experience facilitates learning and recovery from injury, and despite successful attempts to induce sensory-evoked LTP *in vivo*, a direct link between synaptic plasticity, cortical remapping, and adaptive behaviors following altered sensory experience has not yet been demonstrated[176,202,203,250,252].

Here, by manipulating AMPAR lateral mobility *in vivo*, we demonstrated that diffusion of GluA2 is required for increasing synaptic AMPAR content during LTP induced by physiological and behaviorally relevant stimuli. To our knowledge, in combination with Zhang and colleagues, this study is the first to demonstrate that some of the basic properties of AMPAR trafficking reported *in vitro*, are also recapitulated *in vivo*. We believe that these results will inspire further studies, aiming to understand the complete molecular machinery at play during sensory-evoked forms of LTP. Moreover, this NMDAR-dependent form of LTP is required during the early phases of SWE with improvements in behavioral recovery. This data suggests that that sensory-evoked LTP occurs shortly after sensory deafferentation, proving new important processing resources for spared inputs. Supporting this, training-related increases in cortical representations correlate with perceptual learning, suggesting that deafferentiation could improve behavior by promoting cortical remapping[364–366]. To our knowledge, this is the first proof-of-concept that synaptic LTP is the mechanism driving map plasticity in L2/3 pyramidal cells. I hope that this study will be incentive to many others to precisely determine how LTP is interacting with other synaptic mechanisms, to drive the circuit-wide alterations during map plasticity. Moreover, we also showed that LTP is much more than a simple memory storage mechanism, and can participate in any other brain mechanisms, like perception. We also confirmed the work performed by Penn and collaborators, by corroborating AMPAR crosslinking as a tool to dissect the complex interplay between synaptic LTP and animal behavior[332]. Our results are of great importance for clinical applications as briefs periods of sensory deprivation have been proposed as therapeutic venues to promote recovery of lost function after injury (e.g., stroke)[250].

Materials and Methods

Animals

All experiments were performed in accordance with the Guide for the Care and Use of Laboratory Animals (National Research Council Committee (2011): Guide for the Care and Use of Laboratory Animals, 8th ed. Washington, DC: The National Academic Press.) and the European Communities Council Directive of September 22th 2010 (2010/63/EU, 74). Experimental protocols were approved by the institutional ethical committee guidelines for animal research (N°50DIR_15-A) and by the French Ministry of Research (N°02169.01). We used male C57BL6/J 5- and 6-weeks old mice from Charles River that were housed with littermates (3 mice per cage) in a 12-h light-dark cycle. Cages were enriched and food and water were provided *ad libitum*, except during behavioral experiments (see below).

Cranial window implantation and virus injection

Anesthesia. Anesthesia was induced using isoflurane (4% containing ~0.5 l min^{-1} O2) and then continued using an intraperitoneal (i.p.) injection of a MB mixture (MB) (5 µl/g) composed of medetomidine (0.2 $mg.kg^{-1}$), and buprenorphine (0.2 $mg.kg^{-1}$). A heating-pad was positioned underneath the animal to keep the body temperature at 37°C. Eye dehydration was prevented by topical application of ophthalmic gel. Analgesia was achieved by local application of 100 µL of lidocaine (lurocaine, 1 %) and subcutaneous (s.c.) injection of buprenorphine (buprécare, 0.05 $mg.kg^{-1}$). To prevent risks of inflammation and brain swelling 40 µL of dexamethasone (dexadreson, 0.1 $mg.mL^{-1}$) were injected intramuscularly (i.m.) before the surgery. After disinfection of the skin (with modified ethanol 70% and betadine), the skull was exposed and a ~5mm plastic chamber was attached to it above the relative stereotaxic location of the C2 barrel column (-1.5 mm from bregma, + 3.3 mm mideline) using a combination of super glue (Loctite) and dental cement (Jet Repair Acrylic, Lang Dental Manufacturing). The chamber was filled with saline (0.9% NaCl) and sealed with a glass coverslip.

Intrinsic Optical Imaging (IOI) for barrel column targeting. To locate the cortical barrel column computing the whisker C2 (wC2), intrinsic optical signals (IOS) were imaged as previously described, through the intact skull using a light guide system with a 700 nm (bandwidth of 20 nm) interference filter and stable 100-W halogen light source (fig. 25A)[208,367,368]. Briefly, the head of the animal was stabilized using a small stereotaxic frame and the body temperature kept constant with a heating pad. An image of the surface vascular pattern was taken using a green light (546 nm- interference filter) at the end of each imaging session. Images were acquired using the Imager 3001F (Optical Imaging, Mountainside, NJ) equipped with a large spatial 602 × 804 array, fast readout, and low read noise charge-coupled device (CCD) camera. The size of the imaged area was adjusted by using a combination of two lenses with different focal distances (upper lens: Nikon 135 mm, f2.0; bottom lens: Nikon 50 mm, f1.2). The CCD camera was focused on a plane 300 µm below the skull surface. Images were recorded at 10 Hz for 5 sec., with a spatial resolution of 4.65

µm/pixel comprising a total area of 2.9 x 3.7 mm^2. wC2 was deflected back and forth (8 Hz, 1 sec.) using a glass-capillary attached to a piezoelectric actuator (PL-140.11 bender controlled by an E-650 driver; Physik Instrumente) triggered by a pulse stimulator (Master-8, A.M.P.I.). Each trial consisted of a 1 sec. baseline period (frames 1-10), followed by a response period (frames 11-22) and a post-stimulus period (frames 23-50). Intertrial intervals lasted 20 sec. to avoid contamination of the current IOS by prior stimulations. IOS were computed by subtracting each individual frame of the response period by the average baseline signal (fig. 25B). The obtained IOS was overlapped with the vasculature image using ImageJ software to precisely identify the cortical region computing wC2.

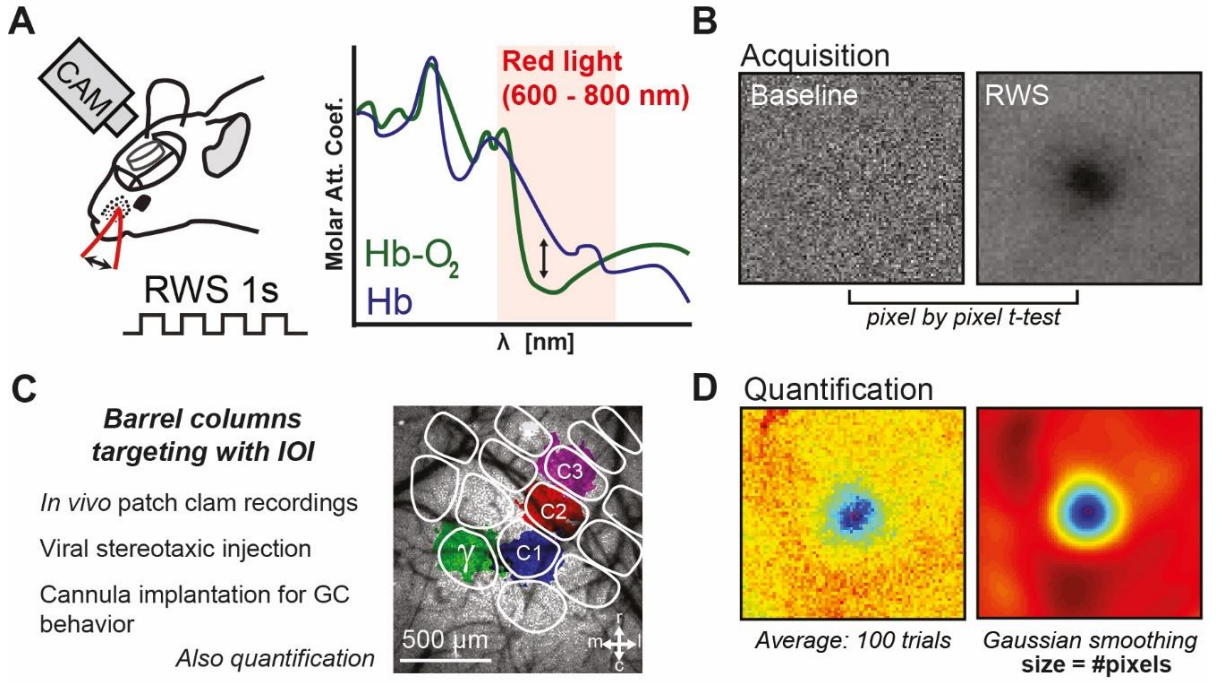

Fig. 25) Intrinsic optical imaging (IOI) to target and size quantification of the barrel columns. A) Neuronal activity increases local metabolism, translated into oxygen consumption, and increase in deoxyhemoglobin. Hemoglobin has a different absorption when imaged with a stable red light source and is, as consequence, an indirect measure for neuronal activity. **B**) The subtraction of IOS of each individual frame during whisker stimulation by the average baseline signal (no stimulation), turns possible to precisely determine the cortical area responding to the whisker stimulation. **C)** This targeting is central to all the experiments performed in the current thesis, including: (1) *in vivo* whole cell patch clamp recordings, where a defined whisker is stimulated and neuronal activity in the principal barrel is recorded; (2) viral stereotaxic injection and (3) cannula implantation for chronic antibody injection during GC. This allows to target stereotaxic injections in the cortical column associated to the whisker that will be spared. **D)** A precise quantification for the size of the barre column was performed as described in Schubert, V. *et al.* (2013) Journal of Neurosci. Briefly, averages of epochs without (baseline) or with stimulation of at least 100 trials were subtracted. Responding pixels were determined by a pixel-to-pixel analysis between baseline and stimulation epoch. As whisker stimulation drives neuronal activity in the same cortical region, responding pixels are statistically significant (represented in blue). On the other hand, background noise is random and, with low statistical significance (represented in red). A gaussian smooting is finally applied to average t-values of neighboring pixels and further increase the statistical significance of the responding pixels. The final barrel area is then calculated by quantifying the number of pixels with a t-value<-2.0 (i.e., highly significant). See Zepeda, A. *et al.*,(2004) Journal of Neurosci. Methods for further information on IOI principles and applications.

Craniotomy and viral injection. After IOI, adequate anaesthesia was assessed (absence of toe pinch reflexes, corneal reflexes, and vibrissae movement) and prolonged using supplementary isoflurane if necessary. Dehydration was prevented by injecting sterile saline by s.c. injection. A ~3*3mm craniotomy was then made over the maximum IOS using a pneumatic dental drill. Stereotaxic injections were then targeted to the layer 2/3 and 200 nL of virus were injected at a maximum rate of 60 nL/min, using a glass pipette (Wiretrol, Drummond) attached to an oil hydraulic manipulator (MO-10, Narishige). The following viruses were used depending on the experiment: (1) AAV-GCaMP6f (AAV1.Syn.GCaMP6f.WPRE.SV40, Penn Vector Core) to perform *in vivo* somatic calcium imaging and (2) AAV-GCaMP6s-Flex (AAV9.Syn.Flex.GCaMP6s.WPRE.SV40, Penn Vector Core) combined with AAV-Cre (AAV1.hSyn.Cre.WPRE.hGH, Penn Vector Core), diluted 1/10 000 with sterile saline to perform *in vivo* dendritic calcium imaging. After injections, the viruses were allowed to diffuse for at least 10 min before the pipette was withdrawn.

Cranial Window (C.W.) implantation. After stereotaxic injection, the craniotomy was covered with sterile saline and sealed with a 3 mm glass coverslip. The coverslip was sealed to the skull using dental acrylic and dental cement (Jet Repair Acrylic, Lang Dental Manufacturing). Mice were then waked-up by a sub-cutaneous injection of an AB mixture (AB) containing atipamezole (Revertor, 2.5 $mg.kg^{-1}$), and buprenorphine (Buprécare, 0.1$mg.kg^{-1}$). A delay of 2-3 weeks for surgery recovery was respected before all imaging experiments, during which the body weight of mice was daily checked. Animals used for chronic IOI had C.W. implanted following the same protocol without stereotaxic injection of any viruses (see below).

Chronic Intrinsic Optical Imaging

Imaging protocol. MB-anaesthetized mice were daily-imaged during 1 session with all their whiskers (baseline), followed by 2 sessions (SWE 1-2) with all their whiskers trimmed except wC2. A cohort group was additionally recorded for 3 days with all their whiskers (FW 1 -3) as a control for barrel expansion. During each session, wC2 was deflected back and forth (8Hz, 1 sec) and IOS recorded through a C.W.

Spatiotemporal analysis of IOS. An average of 200 trials were recorded per sessions to quantify IOS as previously described[368]. The IOS of different sessions from the same animal were spatially aligned using the animal's brain surface vasculature and spatially binned (6*6, final resolution: 27.9 µm/pixel or 3*3, final resolution: 13.95 µm/pixel). A high pass-filter was then applied by subtracting from each image-frame the same image-frame that was convolved using a 1270 µm full-width at half maximum (FWHM) Gaussian kernel. The whisker-evoked IOS were then simulated using a pixel-by-pixel paired t-test, comparing the baseline period and the response period of all trials within a session (fig. 25D). The t maps for each individual trial were low pass-filtered with a 340 µm FWHM Gaussian kernel and averaged into a final t map response. A threshold was set to $t<-2.0$ and any signal below this value was considered to belong to the

stimulus-evoked response area. If the pixel value was $t \geq -2.0$ it was considered background noise and discarded for barrel are quantification. This usually resulted in an image with a clear minimum, representing the response maximum and the barrel's center of mass. Changes on IOS pixel area caused by whisker trimming were computed as the ratio between the whisker-evoked IOS response of the baseline and SWE sessions. All data analysis was performed using a custom software written in MATLAB (MathWorks).

2-Photon laser-scanning microscope (2PSLM)-based calcium imaging

In vivo calcium imaging. Two weeks after C.W. implantation, period to enable mice to fully recover from surgery and effective viral expression, a custom-made stainless steel head stage was attached to the previous implant using dental acrylic and dental cement. Animals used for somatic calcium imaging were anaesthetized for imaging three days after using isoflurane (4% for induction, then 1.5% for recordings with ~0.5 l min−1 O2). Anaesthesia of animals used for dendritic calcium imaging was induced using isoflurane (4% with 0.5 l min-1 O2) and then continue using an i.p. injection of urethane (1.5 g kg-1, in lactated ringer solution containing (in mM) 102 NaCL, 28 Na-L-lactate, 4 KCl, 1.5 CaCl2). Spontaneous vibrissae movements were controlled using an infra-red camera and avoided using supplementary isoflurane if necessary. Calcium images were acquired through a C.W. using an *in vivo* nondescanned FemtoSmart two-photon laser-scanning microscope (2PLSM, Femtonics) equipped with a x15 objective (0.8 NA, Nikon) was used (fig. 26A and 27A). The microscope, acquisition parameters and the TTL-driven synchronization between acquisition and whisker stimulation were controlled by the MES software (MES v4.6, Femtonics, Budapest, Hungary). The GCaMP were excited using a Ti:sapphire laser operating at λ=910 nm (Mai Tai DeepSee, Spectra-Physics) with an average excitation power at the focal point lower than 50 mW. For each animal, time-series images were acquired within a field-of-view of 300 X 300 μm (for somas and dendrites, 256 lines, 1 ms/line) corresponding to the cortical region with maximum IOS. The somatic recording protocol lasted 6 minutes: a first baseline minute without whisker stimulation followed by 5 minutes of wC2 stimulation (0,1 Hz) to obtain whisker-evoked calcium events (fig. 26G). The dendritic recording protocol lasted 6 seconds and was repeated 10 times before and after antibody injection: first 3 seconds without whisker deflection followed by 3 seconds with whisker stimulation (8 Hz) (fig. 27A). wC2 was deflected as aforementioned and synchronized with imaging acquisition using a TTL output from the E-650 driver. L2/3 somatic imaged mice were first imaged during three baseline sessions (one per day, B1 to B3) will all their whiskers targeting (fig. 26B). Then, all the whisker except C2 were trimmed and mice imaged for two additional sessions (one per day, SWE1 and SWE2). A fixed position of the animal holder ensured consistent orientation of focal planes across different sessions. Dendritic imaged mice where imaged before and after stereotaxic injection of an anti-GluA2 antibody (monoclonal IgG1-K, gift from E. Gouaux, Portland, OR) (fig. 27B) A 30 nL solution containing antibody (0.05 mg/mL), Alexa 568 (50 μM, A10437, Thermofisher), and saline was injected at a maximum rate of 15 nL/min in three injection sites (-0.1 to 0.3 mm dorsoventral, 30 sec. injection interval) using a glass pipette attached to an oil hydraulic

manipulator. A small whole in the glass C.W. was made with the help of a dental driller to perform antibody stereotaxic injection.

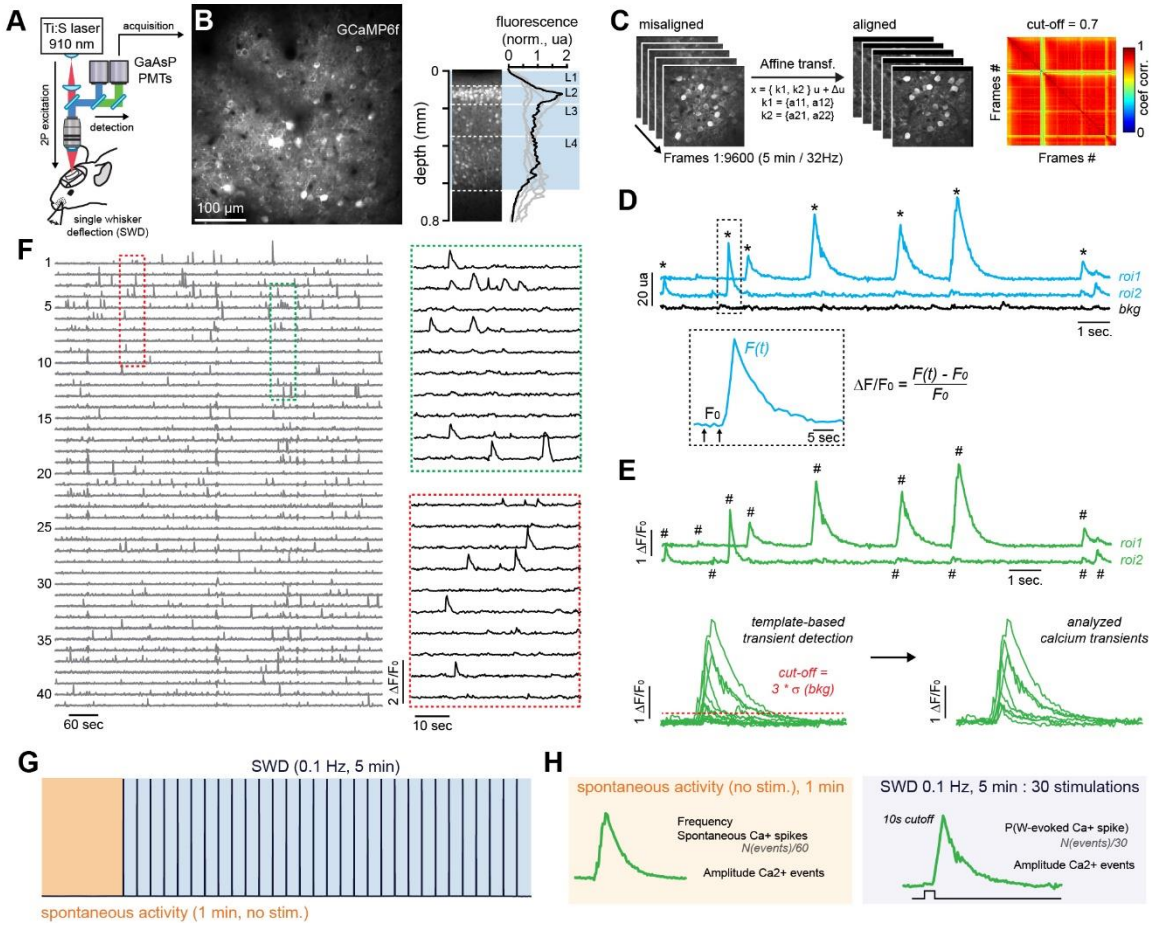

Fig. 26) Pipeline of *in vivo* 2-Photon dendritic imaging. A) Somatic Ca^{2+} images acquired through a C.W. using a 2-Photon microscope. **B)** L2/3 pyramidal neurons expressing GCaM6f were imaged before and after whisker trimming. **C)** Motion correction was performed as detailed on the main text. **D)** Individual neurons were manually segmented and peak of fluorescence detected for normalization (ΔFt/F0). **E)** To be considered as a neuronal spike, fluorescence transient had to be three fold higher than the background noise. **F)** Example of normalized Ca^{2+} transients for all the neurons in a given recording session. **G)** Stimulation protocol comprising 1 minute without stimulation to record baseline activity and 5 minutes of single-whisker deflection (SWD, 0. Hz). **H)** The TTL-driven inputs from the whisker stimulator allows to synchronize recordings with stimulation events. This allows to extract spontaneous and whisker-evoked neuronal spikes (i.e., Ca^{2+} transients). Analysis of both spontaneous and evoked activity were performed as described in the figure.

Analysis of the in vivo calcium images. Images were analyzed as previously described using custom routines written in ImageJ and MatLab[176]. Images were registered over time and XY motion artifacts corrected within a single imaging session by using cross-correlation based on rigid body translation (Stack Aligner, Image J, NIH, USA) (fig. 26C). Regions of interest (ROIs) for somas of pyramidal neurons were selected and drawn manually. All pixels within each ROI were averaged providing a single time-series of raw fluorescence. Peaks of fluorescence were detected,

and the baseline fluorescence (F0) was calculated as the mean of the lower 50% of previous 3 sec (fig. 26D). fluorescence values to limit the effect of fluorescence drift over time. Normalized changes in fluorescence ($\Delta F_t/F_0$) was defined as $(F_t\text{-}F_0)/F_0$, where F_t is the fluorescence intensity at time t (time of the first pixel in each frame). Calcium transients whose peak amplitude reached a 3 X background standard deviation threshold were detected as events and considered for analysis (fig. 26E). Each detected event was inspected visually and analysis was restricted to detected events rather than on raw fluorescence (fig. 26F). Calcium events recording during baseline were used to compute spontaneous averaged firing rate (frequency, Hz) and the averaged peak amplitude ($\Delta F_t/F_0$) (fig. 26H). This allowed to control alterations on neuronal activity induced by anaesthesia across sessions. Whisker-evoked calcium events where defined as calcium transients locked to passive whisker stimulation (10 sec. cutoff) (fig. 26H). Probability was determined as the number of whisker-evoked calcium events divided by the total number of stimulations. The estimated number of spikes was computed by multiplying this probability by averaged peak amplitude of the calcium events. Spontaneous analysis was plotted as non-normalized data while each session of whisker-evoked data was normalized to the average of the 3 baseline recordings. For extracting dendritic calcium events, dendrites were segmented in small ROIs of 2 X 2 pixels using a custom routine in ImageJ (fig. 27B). Normalized changes in fluorescence for each individual ROI was computed as described before. Trials were defined as responding or non-responding using a t-test comparing the averaged $\Delta F/F_0$ (all ROIs considered) before and after whisker stimulation (fig. 27C). Responding trials where considered the ones with statistical significance to then extract the spatial spread of calcium events by calculating the FWHM (expressed as % of total dendritic length) of the normalized Gaussian corresponding to the maximal averaged $\Delta F/F_0$. This allowed to calculate the size of the Ca^{2+} event in µm while the response probability was computed as the number of responding trials divided by the number of stimulations (fig. 27C).

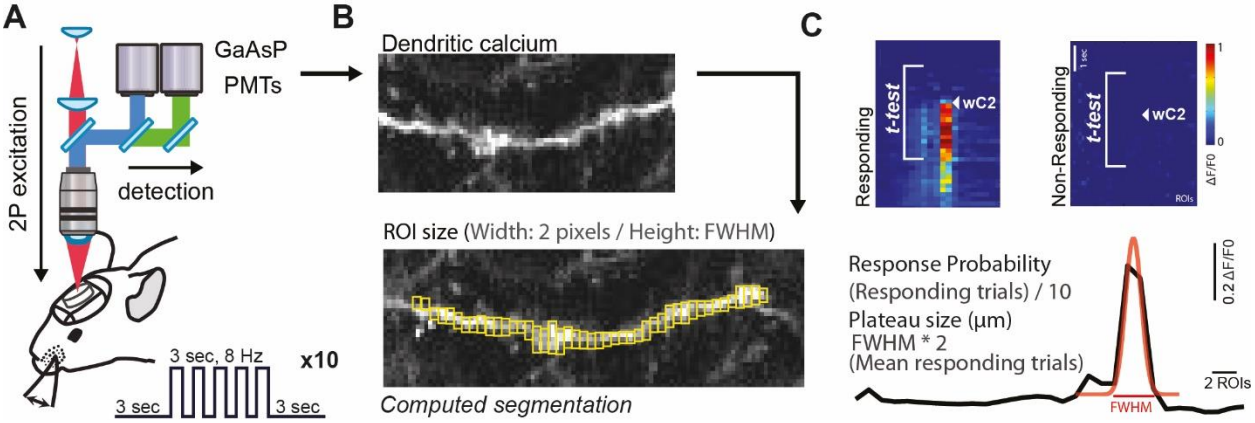

Fig. 27) Pipeline of *in vivo* 2-Photon dendritic imaging. A) Superficial L2/3 dendrites were imaged through a C.W. using a 2-Photon microscope. The expression of GCaMP6s permitted determine NMDAR spikes evoked by whisker deflection. Protocol of whisker stimulation is detailed on the figure. The ten times cycle of stimulation allowed us to determine the probability of whisker-evoked NMDAR spike. **B)** Recorded images were segmented in a custom made ImageJ script. **C)** After extraction and normalization of Ca^{2+} transients, trials were divided into responding or non-responding by t-test (all extracted ROI's, before and after whisker stimulation). The spatial spread of the calcium transients was calculated as detailed on the main text.

In vivo whole-cell recordings

Acute AMPAR X-linking surgery. Anaesthesia was induced using isoflurane (4% with 0.5 l min^{-1} O2) and then continue using i.p. injection of urethane (1.5 g kg^{-1}). Surgery preparation and IOI were performed as aforementioned. After imaging, adequate anesthesia was assessed and prolonged by supplementary urethane (0.15 g kg^{-1}) if necessary. A small ~1 × 1 mm craniotomy (centered above the C2 whisker maximum IOS response) was made using a pneumatic dental drill. Thee injections of either an anti-GluA2 antibody or a monoclonal anti-GFP IgG1-K (Roche, 11814460001) were targeted to the L2/3 of S1 (-0.1 to 0.3 mm dorsoventral). A 30 nL solution containing antibody diluted in sterile saline (0.05 mg/mL) was injected at maximum rate of 15nl/min, with 30 sec intervals between injection sites as described before. All the experiments were performed blind for the antibody injected.

Chronic AMPAR X-linking surgery. Anesthesia was induced using isoflurane (4% containing ~0.5 l min^{-1} O2) and continued using an i.p. injection of MB to perform IOI targeting of the wC2 cortical barrel. Adequate anaesthesia was assessed and prolonged using isoflurane if necessary. Dehydration was also prevented by s.c. injection of sterile saline. A small ~1 × 1 mm craniotomy above the maximum IOS was made using a pneumatic dental drill. The dura was left intact to then perform stereotaxic injection of either an anti-GluA2 or anti-GFP antibody. The same protocol of injection than the acute surgery was used. After stereotaxic injection, the craniotomy was covered with sterile saline and protected with a 3 mm polydimethylsiloxane (PDMS) coverslip. PDMS was attached to the skull using an ultra-violet (U.V.) curing optical adhesive (NOA61, Norland) cured with a 50 mW U.V. laser (3755B-150-ELL-PP, Oxxius). Before wakening the animals using AB, all the whisker except C2 were trimmed (SWE1). Antibodies were re-injected twice on the day after (SWE2), with a 12h interval between injections using isoflurane anaesthesia (4% for induction, then 2% for injection with ~0.5 l min−1 O^2). Stereotaxic injections were performed through the PDMS CW with the same injection protocol than before. After 12h of antibody washout (SWE3), mice were finally anesthetized with isoflurane (4% with 0.5 l min-1 O2) and an i.p. injection of urethane (1.5 g.kg^{-1}). Before the patch-clamp recordings, the PDMS C.W. was removed and the cortex protected with saline. All the experiments were performed blind for the antibody injected.

Recordings. Whole-cell patch-clamp recordings of L2/3 pyramidal neurons were obtained as describes previously[176]. Current-clamp recordings were made using a potassium-based internal solution in mM: 135 potassium gluconate, 4 KCl, 10 HEPES, 10 Na2-phosphocreatine, 4 Mg-ATP and 0.3 Na-GTP), pH adjusted to 7.25 with KOH, 285 mOsM). High positive pressure (200–300 mbar) was applied to the pipette (5–8 MΩ) to prevent tip occlusion. After passing the pia the positive pressure was immediately reduced to prevent cortical damage. The pipette was then advanced in 1-µm steps, and pipette resistance was monitored in the conventional voltage clamp configuration. When the pipette resistance suddenly increased, positive pressure was relieved to obtain a 3–5-GΩ seal. After break-in, membrane potential (Vm) was measured, and dialysis could occur for at least 5 min before deflecting the whisker. Spiking pattern of patched cells was analyzed

to identify pyramidal neurons. Action potentials were obtained by a step-increment of injected current and the number or the minimum threshold for spike represented. Spontaneous slow-have fluctuations of the resting membrane potentials were recorded as previously described[369]. PSPs were evoked by back and forth deflection of the whisker (100 ms, 0.133 Hz) as previously described[176]. The voltage applied to the actuator was set to evoke a displacement of 0.6 mm with a ramp of 7-8 ms of the wC2. Different frequencies of stimulation were used accordingly to the experiment (RWS-LTP: 8Hz, 1 min; cumulative PSPs: 8Hz, 2.5 sec). Series and input resistance were monitored with a 100-ms long-lasting hyperpolarizing square pulse 400 ms before each single-deflection and extracted offline by using a double-exponential fit. Recordings were discarded if the change in these parameters were larger than 30%. The bridge was usually not balanced, and liquid junction potential not corrected. All the data were acquired using a Multiclamp 700B Amplifier (Molecular Devices) and digitized at 10 kHz (National Instruments) using software. Offline analysis was performed using custom routines written in IGOR Pro (WaveMetrics).

Behavior

Gap crossing apparatus. The custom-made gap crossing (G.C.) apparatus (Imetronic, France) consists of two individual moveable platforms made of transparent Plexiglas: (1) a starting platform containing an automated door to precisely control the start of a trial; (2) a reward platform containing a pellet distributor to deliver a calibrated food reward (fig. 28A). Both platforms (10x20 cm) were elevated 37.4 cm from the surface and surrounded on the three sides with a 20-cm-high Plexiglas walls. The two platforms were placed end-to-end, facing each other with a high-speed 300 frames per second (fps) camera at the top and an infra-red pad at the bottom. This allowed us to precisely track mice behavior and whisker motion with high spatiotemporal resolution. The edges of the platforms close to the gap (10x10 cm) were made of a metal grid to allow a better grip when the animals are performing the decision to jump. A ruler placed in between the platforms was used to precisely define the gap distances (G.D.) at a given trial. The maze was placed into a light- and soundproof cage containing ventilation, surrounding speakers with a continuous white noise, infra-red light source and an infra-red control camera. This ensures that mice do not have visual nor auditory clues regarding the reward platform. Food pellet odor was saturated inside the box to avoid any olfactory-related clue.

Behavioral protocol. At least 5 days before starting behavior, mice were food restricted and handled to decrease stress (fig. 28B). After a 15 – 10 % reduction of the initial body weight, habituation was performed during 3 days: (1 – Maze Habituation) Mice were placed on the G.C. apparatus with a GD = 0 cm for 10 min. where the pellet distributor was randomly presented for multiple times without food reward; (2 – Jump Habituation) mice where trained for 3 blocks (16 trials each block, GD = 0 cm) to the distribution of a food pellet in the reward platform. A given trial was defined as success if the animal reached the reward platform and ate the food pellet or as a failure if it took more than 2 min to do so. At the end of a trial, the animal was placed back in the starting platform to beginning the next one; (3 – Jump Habituation) The same protocol than (2)

but using a GD = 3 cm to habituate the animal for a distance between platforms. Habituation is considered successful and the test sessions started if the success rate was >95%. FW mice were initially used to optimize the test sessions. The optimized protocol had 1 session per day during 4 days where each session was composed of 16 trials containing GD = 4, 5, 6, and 6.5 cm. Individual blocks started with the minimal GD, had random GD sequences, and finished with a catch trial (GD: 100 cm) where the reward platform was removed (fig. 28C). This allowed to rule out any motor habituation during jumping decision. When addressing the effect of whisker trimming on expert mice, test sessions were performed before and after whisker trimming.

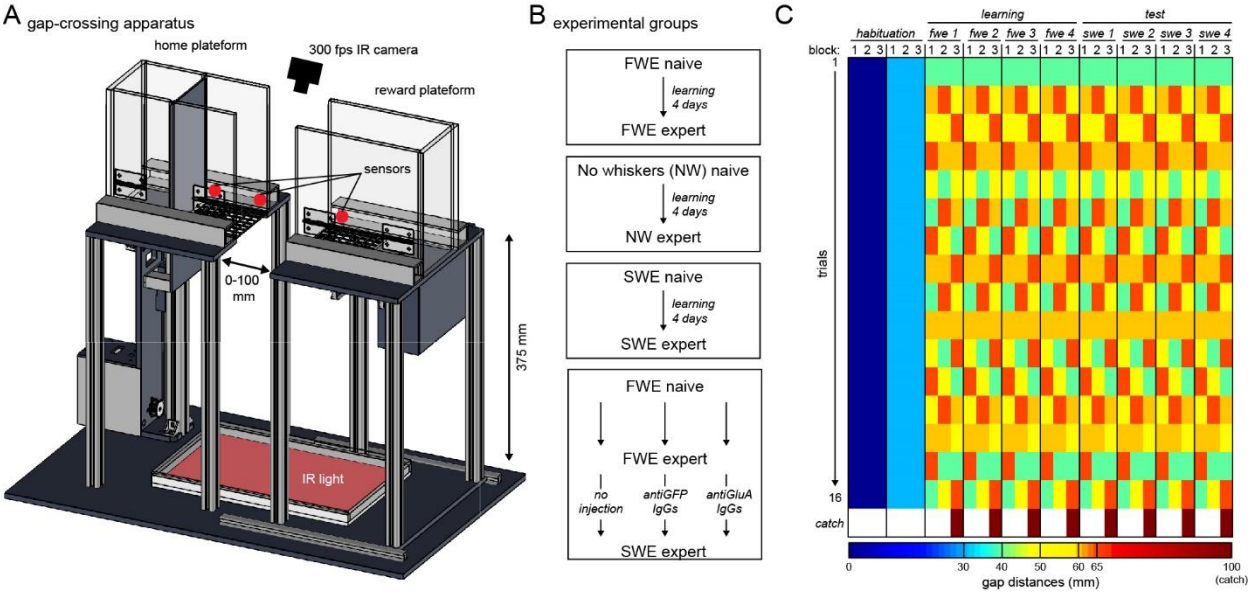

Fig. 28) Pipeline of *in vivo* 2-Photon dendritic imaging. A) Overview of the gap-crossing apparatus. It consists of two individual moveable platforms made of transparent Plexiglas: (i) a starting platform containing an automated door to precisely control the start of a trial; (ii) a reward platform containing a pellet distributor to deliver a calibrated food reward. Both platforms are elevated 374 mm from the surface and surrounded with 20-cm-high Plexiglas walls. The two platforms face each other with a high-speed 300 fps camera at the top and an infra-red pad at the bottom. This allows us to precisely track mice behavior and whisker motion with high spatiotemporal resolution. The edges of the platforms close to the gap (10x10 cm) are made of a metal grid to allow a better grip during jump. A ruler placed in between the platforms is used to precisely define the gap distances (GD) at a given trial. **B)** The behavior protocol for all the experiments performed in this thesis. **C)** Food-restricted mice are first habituated to the apparatus. During test, each session consists of 3 blocks of 16 trials with pseudo-randomized GD (40, 50, 60, and 65 mm). A given trial is defined as success if mice reach the reward platform and eat the food pellet or as a failure if it takes more than 2 min to do so. At the end each trial, the animal is placed back in the home platform to start the next one. Each session ends with a catch trial where the reward platform is removed. This allows to rule out any motor habituation during jumping decision.

Cannula implantation for chronic AMPAR X-linking. Anaesthesia was induced using isoflurane and continued by an i.p. injection of MB to perform IOI targeting of the wC2 cortical barrel as aforementioned. A small craniotomy above the maximum IOS was made using a pneumatic dental drill, preventing any cortical damage. After drilling, a guide cannula (62001, RWD Life Science Co., LTD) was guided and stereotaxically inserted in the brain using a cannula holder through the craniotomy previously made. The size of the cannula (0.6 mm) was adjusted to target L1 of the somatosensory cortex. The guide cannula was fixed to the skull using two stainless

steel screws and a mix of super glue (Loctite), dental acrylic and dental cement. Anaesthesia was reverted by a s.c. injection of AB and mice left to recover over 2 weeks before starting food restriction. During food restriction, mice were additionally habituated to be restrained by a different experiment to avoid stress during antibody injection. Mice were tested during 4 sessions with FW followed 4 SWE sessions where either an anti-GluA2 or an anti-GFP antibody (0.05 mg/mL) was injected. Antibodies were injected twice per day, before and after each test session, using a pump (D404, RWD Life Science CO.) with an injection speed of 6nL/min for the first 120nL and 3nL/min for the remaining 30nL of antibody. Mice were freely moving in their home cage during injection. An additional test session (washout) was performed in the G.C. 3 days after the last antibody injection where the mice were kept in SWE but without any injection. All the experiments were performed blind for the antibody injected.

Histology

To evaluate the antibody injection profiles in S1, animals were intracardially perfused with PBS (1%) and PFA (4%). Fixed brains were sliced with a vibratome and sections posteriorly incubated with PBS.H202 (0.3%) during 30 min to block endogenous peroxide. Brain slices were then incubated with a secondary anti-mouse biotinylated antibody from donkey (1/200), during 2h at room temperature (RT). To finally reveal the injected primary antibody, slices were first incubated with an avidin-biotin complex (1/200 in PBS (1x) – Triton 0.1%), and then with DAB (ab64259, Abcam). Brain slices were finally mounted between slide and coverslip and imaged post-hoc using a Nanozoomer (S360, Hamamatsu). To evaluate the viral expression profiles in the barrel cortex, fixed brain slices were directly imaged post-hoc on the same microscope. Illumination was set such that the full dynamic range of the 16-bit images was utilized. A two-dimensional graph of the intensities of pixel was then plotted using a Fiji Software. 16-bit image's brightness was processed and a mask were registered to the corresponding coronal plates (ranging from -0.26 to -1.94 mm) of the mouse brain atlas using Illustrator (Adobe), at the various distances posterior to the bregma.

Statistics.

Detailed statistics are described below. For all tests, statistical difference was considered at $p<0.05$.

Figure 29

Fig.	Variable	Group	N	Normality	Mean	Std Dev	Test	p-value
E	Responding Area (normalized to first session)	SWE0	6	Passed P=0.673	1	0.149	One-way anova Repeated measures	p=0.012
		SWE1	6		1.25	0.246		SWE0/SWE1, p=0.246
		SWE2	6		1.756	0.69		SWE0/SWE2, p=0.004
		FWE0	7		1	0.0658		p=0.306
		FWE1	7		0.854	0.11		
		FWE2	7		0.97	0.304		

Figure 30 (preliminary data, *statistics represented in the figure.*)

Figure 31

Fig.	Variable	Group	N	Median	25%	75%	Test	p-value
B	Fraction spiking cells Non spiking (-) / Spiking (+)	FWE-	16				Chi test	p<0.001
		FWE+	16					
		SWE-	9					
		SWE+	9					
	Spiking probability	FWE	20	0	0	0	*Mann-Whitney rank sum test*	p<0.001
		SWE	13	0.56	0.125	0.785		
D	PSP peak (mV)	FWE	20	9.209	7.093	12.041	*Mann-Whitney rank sum test*	p<0.001
		SWE	13	16.414	12.64	21.27		
	Plateau strength (mV*sec)	FWE	20	0.812	0.514	1.325	*Mann-Whitney rank sum test*	p=0.311
		SWE	13	1.13	0.709	1.409		

Figure 32

Fig	Variable	Group	N	Normality	Mean	Std Dev	Test	p-value
B	LTP (%) nor. to baseline	FWE	7	Passed p=0.218	8.18	3.119	*Two-tailed paired t-test*	p=0.002
		SWE	7		9.771	2.984		
D	PSPpeak (mV) FWE	Baseline	7	Passed p=0.965	20.45	5.987	*Two-tailed paired t-test*	P=0.264
		RWS	7		19.91	5.627		
	PSPpeak (mV) SWE	Baseline	7	Failed p<0.05	123.5	15.59	*Mann-Whitney rank sum test*	p<0.001
		RWS	7		97.64	5.58		

Figure 33

Fig.	Variable	Group	N	Normality	Mean	Std Dev	Test	p-value
A	Rheobase (pA)	FWE	24	Failed p<0.05	370.4	96.33	t-test *Mann-Whitney rank sum test*	p=0.42 p=0.29
		SWE	27		308.3	115.78		
E	8Hz-cumulative PSP (mV*sec)	FWE	10	Passed p=0.075	4.637	2.63	t-test *Mann-Whitney rank sum test*	p=0.004 p=0.005
		SWE	10		9.185	3.40		

Figure 34

Fig.	Variable	Group	N	Normality	Mean	Std Dev	Test	p-value
D	10 sec. Cumulative Vm mV*sec	AntiGFP	14	Failed p<0.05	27.4	16.095	t-test *Mann-Whitney rank sum test*	p=0.83 p=0.74
		AntiGluA2	20		26.08	18.08		

Figure 35

Fig.	Variable	Group	N	Normality	Mean	Std Dev	Test	p-value
B	1/τ (ms-1)	AntiGFP	18	passed p=0.478	0.32	0.156	t-test	p=0.615
		AntiGluA2	25		0.32	0.198	*Mann-Whitney rank sum test*	p=0.610
C	up-state amplitude (mV)	AntiGFP	18	passed p=0.504	10.72	3.32	t-test	p=0.396
		AntiGluA2	25		11.51	2.67	*Mann-Whitney rank sum test*	p=0.675
	IV curve	AntiGFP	4	failed p<0.05	0.815	0.0357	two-way anova repeated measures	p=0.238
		AntiGluA2	2		0.751	0.0456		
D	PSPpeak Amplitude (mV)	AntiGFP	34	failed p<0.05	8.874	4.474	t-test	p=0.895
		AntiGluA2	31		8.732	4.07	*Mann-Whitney rank sum test*	p=0.974
	PSP integral (mV*sec)	AntiGFP	34	failed p<0.05	0.642	0.319	t-test	p=0.596
		AntiGluA2	31		0.684	0.306	*Mann-Whitney rank sum test*	p=0.614
E	PSP onset (ms)	AntiGFP	34	passed p=0.063	11.87	2.229	t-test	p=0.621
		AntiGluA2	31		12.22	3.029	*Mann-Whitney rank sum test*	p=0.865
	Onset jitter (ms)	AntiGFP	34	failed p<0.05	1.876	1.07	t-test	p=0.178
		AntiGluA2	31		2.444	1.77	*Mann-Whitney rank sum test*	p=0.992

Figure 36 (preliminary data, *statistics represented in the figure.*)

Figure 37

Fig.	Variable	Group	N	Normality	Mean	Std Dev	Test	p-value
B	PSP peak (mV) anti-GFP	Baseline	9	passed p=0.703	7.987	5.62	two-tailed paired t-test	p=0.002
		RWS+	9		9.721	6.252		
D	PSP peak (mV) anti-GFP	Baseline	8	passed p=0.750	10.82	6.046	two-tailed paired t-test	p=0.205
		RWS-	8		11.15	6.535		
C	PSP peak (mV) anti-GluA2	Baseline	8	passed p=0.750	10.59	3.531	two-tailed paired t-test	p=0.102
		RWS+	8		11.33	3.804		
E	PSP peak (mV) anti-GluA2	Baseline	8	passed p=0.603	8.899	4.072	two-tailed paired t-test	p=0.145
		RWS-	8		8.526	3.714		
F	LTP (% of baseline)	AntiGFP RWS+	9	passed p=0.154	123.9	15.331	one-way anova All pairwise multiple comparisons (Holm-Sidak method)	p<0.001 p<0.001; antiGFP, RWS+ vs. RWS- p=0.085; antiGluA2, RWS+ vs. RWS- p=0.003; RWS+, antiGFP vs. antiGluA2 p=0.449; RWS-, antiGFP vs. antiGluA2
		AntiGFP RWS-	8		101.6	5.673		
		AntiGluA2 RWS+	8		107.1	10.187		
		AntiGluA2 RWS-	8		97.48	9.1		

Figure 38

Fig.	Variable	Group	N	Normality	Mean	Std Dev	Test	p-value
A	plateau potentials onset (ms)	AntiGFP	26	failed p<0.05	31.4	6.0878	*Mann-Whitney rank sum test*	p=0.420
		AntiGluA2	24		30.03	6.2541		
	probability	AntiGFP	26	failed p<0.05	0.702	0.2301	*Mann-Whitney rank sum test*	p=0.770
		AntiGluA2	24		0.685	0.2341		
	strength (mV*sec)	AntiGFP	26	failed p<0.05	0.717	0.4797	*Mann-Whitney rank sum test*	p=0.828
		AntiGluA2	24		0.775	0.551		
B	LTP (% of baseline) plateau strength>0.5	AntiGFP	4	passed p=0.087	138.6	10.123	*t-test*	p<0.001
		AntiGluA2	7		108	10.679		

Figure 40

Fig.	Variable	Group	N	Normality	Mean	Std Dev	Test	p-value
B	PSPpeak (mV)	FWE	20	failed p<0.05	9.883	3.883	*one-way anova All pairwise multiple comparisons (Holm-Sidak method)*	p<0.001 p<0.001; FWE. vs SWE p<0.001; Xswe GFP vs. FWE p<0.001; Xswe GluA2 vs. SWE p=0.003; Xswe, GluA2 vs. GFP p=0.375; Xswe-GluA2 vs FWE p=0.792; Xswe-GFP vs. SWE
		SWE	13		17.98	8.163		
		XSWE	6		14.5	5.207		
		XGFP	9		7.978	3.845		
D	Spiking Probability	FWE	20	failed p<0.05	0	0	*one-way anova All pairwise multiple comparisons (Holm-Sidak method)*	p<0.001 p<0.001; FWE. vs SWE p<0.001; Xswe GluA2 vs. SWE p=0.03; Xswe, GluA2 vs. GFP p=0.07; Xswe GFP vs. FWE p=0.395; Xswe-GluA2 vs FWE p=0.208; Xswe-GFP vs. SWE
		SWE	13		0.487	0.331		
		XSWE	6		0.458	0.398		
		XGFP	9		0.081	0.112		

Figure 41

Fig.	Variable	Group	N	Normality	Mean	Std Dev	Test	p-value
A	LTP (% of baseline)	X-SWE	6	failed p<0.05	12.9	21.778	one-way anova All pairwise multiple comparisons (Holm-Sidak method)	p<0.001 p<0.001; Xswe, GluA2 vs. GFP p<0.001; Xswe GluA2 vs. SWE p<0.001; Xswe GFP vs. FWE p<0.001; FWE. vs SWE p=0.551; Xswe-GluA2 vs FWE p=0.945; Xswe-GFP vs. SWE
		X-GFP	8		98.09	5.906		
		FWE	7		123.85	15.599		
		SWE	7		97.64	5.58		
B	PSP peak (mV) anti-GluA2	Baseline	5	Passed p=0.503	8.679	3.722	*Paired t-test*	p=0.039
		RWS+	5		11.89	5.765		
	PSP peak (mV) anti-GFP	Baseline	8	Ongoing experiment				
		RWS+	8					

Figure 42

Fig.	Variable	Group	N	Normality	Mean	Std Dev	Test	p-value
A	LTP (% of baseline)	FWE	7	passed p=0.643	123.5	15.599	one-way anova repeated measures multiple comparisons vs. fwe (Holm-Sidak method)	p<0.001 FWE vs. FWE anti-GFP, p=0.951 FWE vs. FWE anti-GluA2, p=0.023 fwe vs. swe, p<0.001 fwe vs. swe antiGFP, p<0.001 fwe vs. swe antiGluA2, p=0.558
		FWE antiGFP	9		123.9	15.331		
		FWE antiGluA	8		107.1	10.187		
		SWE	7		97.64	5.58		
		X-GFP	6		98.09	5.906		
		X-GluA2	6		127.9	21.778		
B	plateau strength (mV*sec)	FWE	20	failed p<0.05	0.994	0.705	one-way anova	p=0.149
		FWE antiGFP	34		0.693	0.449		
		FWE antiGluA	31		0.85	0.524		
		SWE	13		1.347	1.057		
		X-GFP	6		0.959	0.617		
		X-GluA2	9		0.754	0.577		

Figure 43

Fig.	Variable	Group	N	Normality	Mean	Std Dev	Test	p-value
F	Fraction of success 65 mm	FWE	15	failed p<0.05	0.89	0.213	Two-way anova repeated measures multiple comparison (Holm-Sidak method)	FWEvsSWE, p=0.005 FWEvsNW, p=0.014
		SWE	8		0.567	0.667		
		NW	4		0.604	0.35		
G	GD exploration (sec.) 65mm	FWE	15	passed p=0.129	25.33	25.02	Two-way anova repeated measures multiple comparison (Holm-Sidak method)	NWvsFWE, p=0.05 SWEvsFWE, p=0.01
		SWE	8		40.89	26.60		
		NW	4		46.03	32.65		
H	Decision latency (sec.) 65mm	FWE	15	failed p<0.05	4.563	1.95	Two-way anova repeated measures multiple comparison (Holm-Sidak method)	FWEvSWE, p=0.01 S1, p=0.004
		SWE	8		6.63	2.59		
		NW	4		5.27	2.63		

Figure 44

Fig.	Variable	Group	N	Normality	Mean	Std Dev	Test	p-value
A	fraction of success 65mm	FWE4	6	passed p=0.797	0.958	0.120	*one-way anova repeated measures multiple comparisons vs. FWE session 4 (Holm-Sidak method)*	swe5 vs fwe4, p=0.034 swe6 vs fwe4, p=0.006 swe7 vs fwe4, p=0.372 swe8 vs fwe4, p=0.653
		SWE5	6		0.681	0.322		
		SWE6	6		0.875	0.234		
		SWE7	6		0.917	0.105		
		SWE8	6		0.958	0.069		
B	fraction of success normalized session8/session4		6	passed p=0.681	1.014	0.17	*t-test*	p=0.503
			5		0.934	0.211		
C	Latency of decision 60mm	FWE4	6	Passed p=0.791	2.056	0.889	*one-way anova repeated measures multiple comparisons vs. FWE session 4 (Holm-Sidak method)*	FWE4vsSWE5, p<0.001
		SWE5			4.357	1.667		
		SWE6	6		3.237	1.532		
		SWE7	6		3.353	1.727		
		SWE8	6		3.112	1.783		
	Latency of decision 65mm	SWE4	6	Passed p=0.597	3.948	1.695	*one-way anova repeated measures multiple comparisons vs. FWE session 4 (Holm-Sidak method)*	p=0.615
		SWE5	6		4.512	0.831		
		SWE6	6		5.004	1.255		
		SWE7	6		4.524	1.2		
		SWE8	6		4.262	1.051		
D	Total GD exploration (sec.)	FWE4	6	Passed p=0.140	10.727	14.37	*one-way anova repeated measures multiple comparisons vs. FWE session 4 (Holm-Sidak method)*	FWE4vsSWE5, p<0.001 SWE5vsSWE8, p<0.001
		SWE5	6		34.773	17.23		
		SWE6	6		20.735	15.35		
		SWE7	6		18.53	14.12		
		SWE8	6		11.198	7.41		

Figure 45

Fig.	Variable	Group	N	Normality	Mean	Std Dev	Test	p-value
B	fraction of success anti-GFP 65mm	FWE session 4	7	failed p<0.05	1	0	one-way anova repeated measures multiple comparisons vs. FWE session 4 (Holm-Sidak method)	p=0.025 SWE5 vs FWE4, p=0.015 SWE6 vs FWE4, p=0.250 SWE7 vs FWE4, p=0.125 SWE8 vs FWE4, p=0.5
		FWE session 5	7		0.774	0.178		
		FWE session 6	7		0.905	0.183		
		FWE session 7	7		0.826	0.252		
		FWE session 8	7		0.917	0.16		
	fraction of success anti-GluA2 65mm	FWE session 4	7	passed p=0.734	1	0	one-way anova repeated measures multiple comparisons vs. FWE session 4 (Holm-Sidak method)	p<0.001 SWE5 vs FWE4, p<0.001 SWE6 vs FWE4, p<0.001 SWE7 vs FWE4, p=0.031 SWE8 vs FWE4, p=0.059
		FWE session 5	7		0.382	0.325		
		FWE session 6	7		0.512	0.374		
		FWE session 7	7		0.726	0.384		
		FWE session 8	7		0.739	0.396		
D	fraction of success 65mm Session 5	Anti-GFP	7	passed p=0.111	0.774	0.178	t-test Mann-Whitney rank sum test	p=0.0016 p=0.0026
		Anti-GluA2	7		0.382	0.325		
	fraction of success 65mm Session 6	Anti-GFP	7	passed p=0.388	0.905	0.183	t-test Mann-Whitney rank sum test	p=0.028 p=0.038
		Anti-GluA2	7		0.512	0.374		
	fraction of success 65mm Session 7	Anti-GFP	7	failed p<0.05	0.826	0.252	t-test Mann-Whitney rank sum test	p=0.577 p=0.805
		Anti-GluA2	7		0.726	0.384		
	fraction of success 65mm Session 8	Anti-GFP	7	failed p<0.05	0.917	0.16	t-test Mann-Whitney rank sum test	p=0.293 p=0.535
		Anti-GluA2	7		0.739	0.396		

Figure 46

Fig.	Variable	Group	N	Normality	Mean	Std Dev	Test	p-value
B	Decision latency (sec) 65mm	Anti-GluA2	7	failed p<0.05	5.513	2.56	Two-way anova repeated measures multiple comparison (Holm-Sidak method)	p=0.83
		Anti-GFP	7		4.868	2.03		
		FWE/SWE	6		4.51	1.24		
C	Dec. Lat. 65mm Session 5	Anti-Glu2	7	passed p=0.074	1.801	1.23	t-test Mann-Whitney rank sum test	p=0.84
		Anti-GFP	7		1.907	0.59		
	Dec. Lat. 65mm Session 6	Anti-Glu2	7	passed p=0.074	1.950	0.79	t-test Mann-Whitney rank sum test	p=0.27
		Anti-GFP	7		1.506	0.57		
	Dec. Lat. 65mm Session 7	Anti-Glu2	7	passed p=0.91	1.694	0.37	t-test Mann-Whitney rank sum test	p=0.15
		Anti-GFP	7		1.391	0.29		
E	Total GD exploration (sec.)	Anti-GluA2	7	failed p<0.05	23.36	19.69	Two-way anova repeated measures multiple comparison (Holm-Sidak method)	p=0.31
		Anti-GFP	7		16.45	12.62		
		FWE/SWE	6		20.56	18.25		
D	GD Expl. 65mm Session 5	Anti-Glu2	7	passed p=0.22	41.197	19.54	t-test Mann-Whitney rank sum test	p=0.29
		Anti-GFP	7		31.78	12.17		
	GD Expl. 65mm Session 6	Anti-Glu2	7	passed p=0.53	25.47	19.47	t-test Mann-Whitney rank sum test	p=0.26
		Anti-GFP	7		15.42	8.16		
	GD Expl. 65mm Session 7	Anti-Glu2	7	failed p<0.05	14.74	9.076	t-test Mann-Whitney rank sum test	p=0.66
		Anti-GFP	7		11.49	5.349		

Results

A. SWE increases and expands the spared whisker cortical representation

Single-whisker experience (SWE) is a good model to study the synaptic mechanisms of sensory-driven neuronal responses potentiation *in vivo*[166,168,169,189]. LTP has long been postulated as the synaptic mechanism for such response strengthening during learning and deprivation-induced plasticity[54,169,189,191,252]. Here, we took advantage of SWE as a model to study the synaptic, and circuit mechanisms of cortical remapping *in vivo*. Mice were exposed to a brief period of SWE (2-4 days) by clipping all except the C2 whisker (wC2). We applied intrinsic optical imaging (IOI) to roughly quantify the circuit-wide effects of SWE. As described, IOI is an imaging modality that extrapolates indirect neuronal activity from local variations on hemoglobin concentration (see fig. 24A for details). Intrinsic optical signals (IOS) driven by wC2 stimulation on both FWE (**fig. 29A and B**) and SWE (**fig. 29C and D**) were consecutively imaged for three days. Spared whisker evoked IOS increased upon SWE within and outside of the wC2 barrel column (SWE0: 1 ± 0.15, SWE2: 1.76 ± 0.7) (**fig. 29E**). As FWE IOS were stable across imaging sessions (FWE0: 1 ± 0.06, FWE2: 0.97 ± 0.304), the reported SWE-induced barrel expansion does not result from alterations on the anesthesia levels. Moreover, it also occurred at a time which no alterations in activity of L4 neurons have been observed[188,191]. Therefore, we hypothesize that IOS variations after SWE might originate primarily from changes in neuronal activity within L2/3 circuits[169,188,191]. This is supported by previous studies reporting increased whisker representation due to increase level of neuronal spiking, and occlusion of electrically-induced LTP *in vitro*[168,169,191].

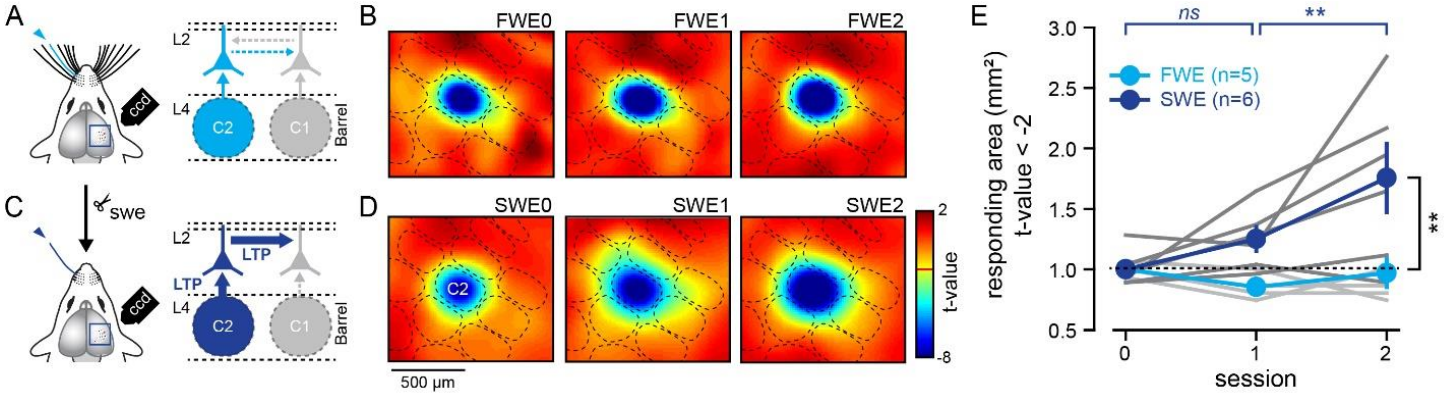

Fig. 29) SWE drives map plasticity in the barrel cortex. A) A) IOI was performed on FWE mice. **B)** Due to the one-to-one relationship between whiskers and barrels, the wC2-evoked IOS are restricted to the C2 barrel. **C)** SWE is reported to increase functional representation of the spared whisker by LTP-like mechanisms. **D)** In agreement, C2-evoked IOS are increased after two days of SWE. Figure B and D are processed IOS where pixel color represented accordingly to significant differences (t-test) before and after wC2 stimulation (blue: highly significant; red: non-significant). **E)** Quantification of the responding area (t-value threshold = -2) per session for both FWE and SWE. Dark and light blue average IOS across session (with sem). Gray lines are individual contribution of each recorded animal. SWE increases functional representation of the spared whisker. All the values and statistics represented in Table 1.

B. Chronic *in vivo* 2-Photon calcium imaging revealed that SWE alters whisker computation

IOI is a mesoscale approach to indirectly quantify neuronal activity across the entire rodent brain[370]. This comes at expense of reduced temporal and spatial resolution. To precisely determine the circuit effect of SWE, one has to chronically record a well-defined neuronal population with higher spatiotemporal resolution. These requirements are fulfilled by *in vivo* 2-Photon Ca^{2+} imaging[371,372]. This approach not only allows to image hundreds of individual cells at once, but also subcellular structures, such as dendrites or spines, with a millisecond resolution. We performed somatic calcium imaging in isoflurane-anaesthetized mice while passively stimulating wC2 (**fig. 30A**). Virus expressing GCaMP6f in the IOI-targeted C2 barrel column were stereotaxically injected followed by a C.W. implantation. GCaMP6f is a genetically-encoded Ca^{2+} indicator composed of an enhanced GFP (eGFP), flanked by the calcium-binding protein calmodulin, and the calmodulin-binding peptide M13[372,373]. In the absence of Ca^{2+}, the conformational state of this protein quenches eGFP, preventing fluorescence emission. However, calmodulin-M13 domains are able to interact upon raise of intracellular Ca^{2+} (e.g., somatic spike), and the resulting conformational changes increase eGFP fluorescence[372]. Therefore, the quantification of the normalized fluorescence transients ($\Delta F/F0$) in the cell bodies are a good readout of the neuronal firing rate. This allowed us to record the same population of L2/3 neurons for three days on full-whisker naïve animals (FWE), and SWE-induced alterations on their firing rate (**fig. 30B**). A previous study using single-units recordings has reported increased spiking activity in L2/3 pyramidal neurons of the barrel cortex after SWE[188]. However, due to technical limitations, it is hard to predict if this is caused by a higher spiking probability, or if due to the recruitment of additional spiking neurons. We found increased wC2-evoked Ca^{2+} events in the spared barrel after SWE (paired t-test, p=0.01) (fig. 29C). The product of spiking probability and the average peak amplitude of evoked Ca^{2+} events is a good estimation of the number of whisker-evoked somatic spikes. This value is augmented after SWE (paired-test, p=0.03) (**fig. 30C**), revealing an increased L2/3 neuronal excitability by spared whisker stimulation. Importantly, neither the amplitude (one-way anova, p=0.69) nor the frequency (one-way anova, p=0.71) of the spontaneous calcium transients are changed across the imaging sessions (**fig. 30D**). Therefore, the increased neuronal excitability after SWE is specifically induced by whisker trimming and not caused by variations of the animal's anesthesia depth. We then asked ourselves about the synaptic origin of this increased neuronal excitability.

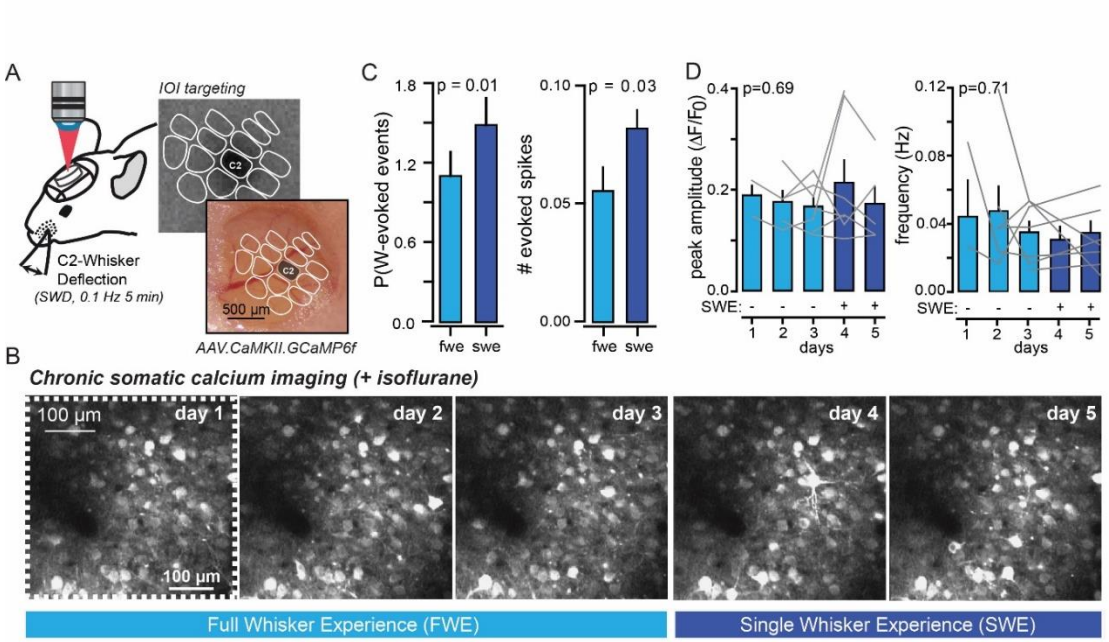

Fig. 30) SWE alters circuit-wide whisker computation (preliminary data). A) Virus expressing GCaMP6f were targeted by IOI to the C2 barrel column, followed by a C.W. implantation. After surgery recovery, animals were imaged though the C.W. using a 2-Photon microscope. **B)** This allowed to image the spiking activity of the same population of L2/3 pyramidal neurons for three days in full-whisker naive animals, followed by two days of SWE. **C**) SWE increases the probability and the number of whisker-evoked Ca2+ events. **D)** The amplitude nor the frequency of spontaneous activity are changed across the imaging sessions. Altogether, these data indicate that SWE shifts whisker computation from sub- to suprathreshold. Dark and light blue are mean (± sem) before (FWE) and after SWE. Error bars, sem. Grey lines are individual FOV contribution.

C. SWE increased whisker-evoked somatic spikes and altered whisker-evoked PSPs

To determine the synaptic underpins of this SWE-induced circuit-wide alterations, one has to record neuronal activity at the single-cell level. To do so, we took advantage of *in vivo* whole-cell patch clamp recordings of L2/3 pyramidal neurons, while deflecting back and forth wC2 on FWE or SWE mice (**fig. 31A**). Current-clam recordings were targeted to the principal barrel column by IOI targeting prior to surgery. Whisker deflection on FWE mice evoked a complex PSP containing a short- and a long-component (see below) (**fig. 31B**). This is in line with previous evidences in favor of a subthreshold computation of whisker-evoked PSPs, through NMDARs-dependent plateau potentials driven by the coordinated activation of segregated thalamo-cortical circuits[176]. The same stimulation protocol on SWE mice consistently generated PSPs with somatic action potentials. In agreement, SWE increased the fraction of spiking neurons (FWE: 0/20; SWE: 11/13; χ^2=25.4, p<0.001) and the number of spikes per whisker deflection (spiking probability; FWE: 0; SWE: 0.48 ± 0.09; p<0.001) (fig. 30B). This corroborates the results of section B, suggesting that SWE shifts whisker computation from sub- to suprathreshold. To better understand the source of the SWE-driven whisker-evoked somatic spikes, we analyzed in great detail the different components of the recorded PSPs[176]. In urethane-anesthetized mice, whisker-evoked

PSPs can be divided in two different clusters accordingly to their properties (**fig. 31C**). The first cluster containing a fast and AMPAR-mediated early-phase (i.e., PSPpeak). The second cluster where the PSPpeak is followed by a long-lasting, plateau-like, and NMDAR-dependent late phase[176]. This late phase is the somatic reminiscence of the dendritic spikes evoked by VPM and POm co-activation[176]. The NMDAR plateau strength is then calculated by the product of a probability of recording a PSP belonging to cluster two and the subtracted integral of late-phase. As defined by Holtmaat's work, this measure is a good approximation of how likely the recorded cell is of being potentiated upon rhythmic whisker stimulation (RWS)[176]. This relationship is predicted by the following rule: the higher the plateau strength, more dendritic spikes occurred, the higher the NMDAR drive was, and the greater a neuron should potentiate. We found that SWE increases whisker-evoked PSPpeak (PSP; FWE: 9.88 ± 0.86 mV; SWE: 17.98 ± 2.26 mV; p<0.001), without changing NMDAR plateau strength (plateau; FWE: 0.81 ± 0.51; SWE: 1.11 ± 0.70) (**fig. 31D**). As the PSPpeak is likely mediated by synaptic AMPAR, we hypothesize that the increased fraction of whisker-evoked somatic spikes after SWE might be driven by synaptic LTP[176].

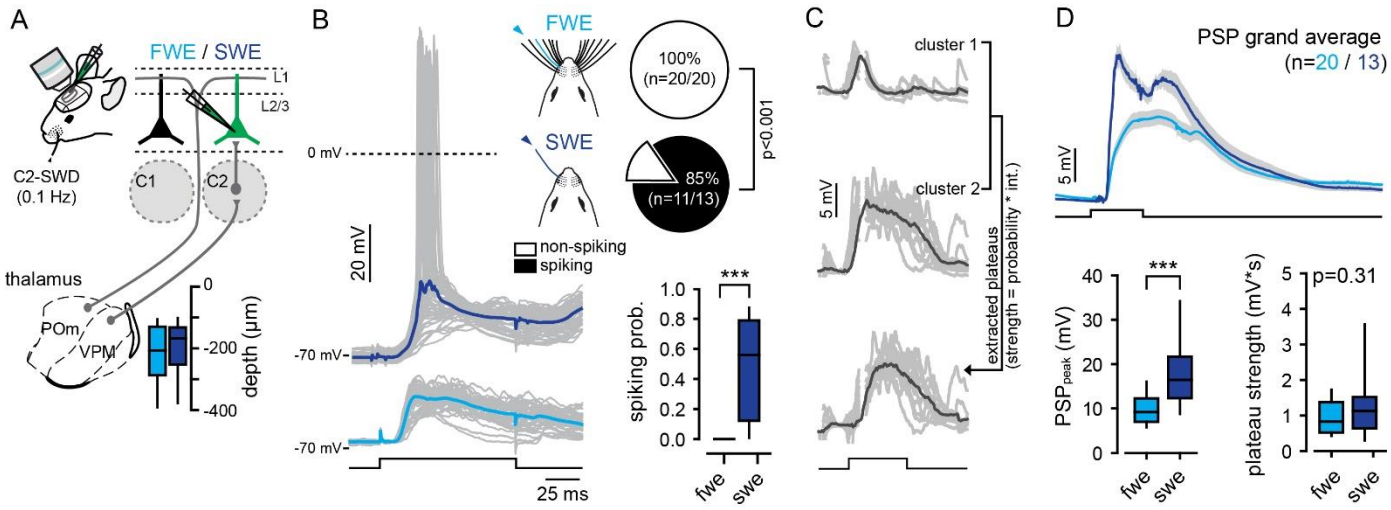

Fig. 31) SWE increased whisker-evoked somatic spikes and altered whisker-evoked PSPs. A) Schematic of recordings in L2/3 cells in full-experience experience (FWE) and single-whisker experience (SWE) mice. C2 barrel column was targeted by IOI prior to electrophysiological recordings. PSPs are evoked by single-whisker deflection (SWD) of wC2 at 0.1 Hz. This recruits both POm and VPM inputs into the recorded L2/3 neurons. **B)** Left, Single-cell examples of whisker-evoked responses (grey, single trials; dark and light blue, averaged traces from SWE and FWE mice). Square pulse lines, whisker deflections (100 ms). Right, fraction of spiking neurons (top) and number of spikes per whisker deflection (spiking probability; median ± interquartile range). SWE increases the fraction of spiking neurons and the number of spikes evoked by whisker deflection. **C)** Whisker-evoked PSPs are divided in two different clusters: (*type 1*) containing only a AMPAR-mediated early-phase, defined as PSPpeak, (*type 2*) with the same early-phase, followed by a long-lasting, plateau-like, and NMDAR-dependent late phase. NMDAR plateau strength can be then calculated my multiplying the probability of a PSP with late-phase by the subtracted integral of late-phase. Importantly, the higher the NMDAR plateau strength, the more a neuron should potentiate after RWS. **D)** (*top*) wC2-evoked PSP grand average (all recorded cells averaged) ± sem. Square pulse lines, whisker deflections (100 ms). (*bottom*) Median (± interquartile range) PSP amplitude and plateau strength. SWE increases AMPAR-mediated PSPpeak without affecting NMDAR plateau strength. All the values and statistics represented in Table 1.

D. SWE occludes sensory-evoked LTP

To test this, we rhythmically stimulated wC2 for 1 min at 8 Hz (RWS) (**fig. 32A**), a frequency naturally used by rodents to explore their environment[55]. RWS has been shown to induce LTP (RWS-LTP) through NMDARs-dependent plateau potentials[176]. RWS evoked an UP-state-like depolarization recorded in the soma, resulting from the temporal summation of dendritic spikes allover L2/3 dendritic tree. We confirmed that RWS drives a significant potentiation of subsequent whisker-evoked PSPs in FWE mice (baseline: 8.18 ± 1.17 mV, RWS: 9.77 ± 1.11 mV; n=7; p=0.002) (**fig.32B**). Conversely, RWS failed to strength whisker-evoke PSPs after 48 hours of SWE (baseline: 20.45 ± 2.26 mV, RWS: 19.9 ± 2.12 mV; n=7; p=0.264). This difference is well-illustrated on figure **32C**. We believe that this is an occlusion of RWS-LTP, because: (1) SWE has no effect on plateau potentials evoked by SWD (**fig. 31D**); (2) whisker-evoked PSPpeak are higher on SWE as compared to FWE animals before RWS (FWE: 8.18 ± 3.11 mV, SWE: 20.45 ± 5.99 mV) (**fig. 32D**). This suggests that L2/3 synapses are already saturated, and no further potentiation after RWS is possible (FWE, baseline: 8.18 ± 3.11 mV, RWS: 9.77 ± 2.95 mV, p=0.002; SWE, baseline: 20.45 ± 5.99 mV, RWS: 19.91 ± 5.63 mV, p=0.26) (**fig. 32E**), and (3) SWE alters the linear relationship between LTP (%) and plateau strength (**fig. 32F**), with neurons with high plateau strength failing to potentiate. These results indicate that NMDAR-dependent induction of RWS-LTP is not suppressed during SWE. Instead, the occlusion of RWS-LTP might be caused by an increased synaptic gain, a state that cannot be further potentiated (FWE: 123.5 ± 5.9 %, n=7; SWE: 97.6 ± 2.1 %, n=7; p=0.001).

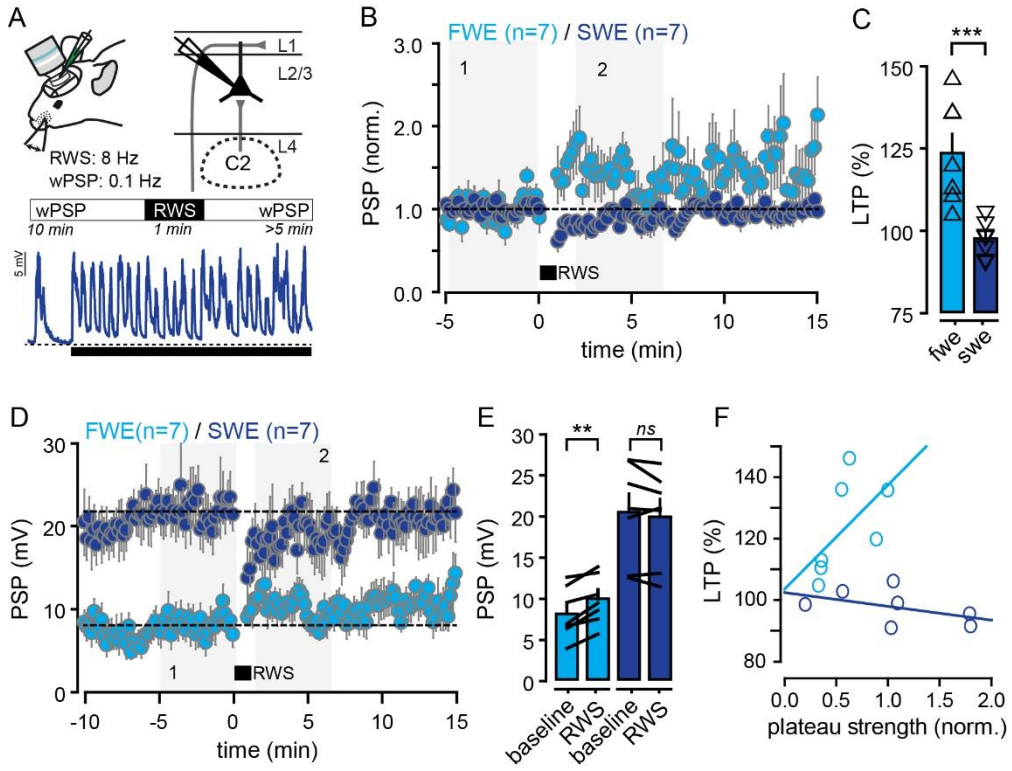

Fig. 32) SWE occludes sensory-evoked LTP (legend on the next page)

Fig. 32) SWE occludes sensory-evoked LTP. A) (*top*) Schematic representation of RWS recordings in L2/3 pyramidal neurons. Bona fide LTP (RWS-LTP) was evaluated by recording wC2-evoked PSPs before and after RWS. LTP (%) is expressed as difference on PSPpeak induced by RWS. (*bottom*) RWS evoked an UP-state-like long-lasting depolarization in the cell body. **B)** Single-cell examples of whisker-evoked responses (grey, single trials; dark and light blue, averaged traces from SWE and FWE mice). Square pulse lines, whisker deflections (100 ms). RWS increased wC2-evoked PSPs on FWE, but not on SWE mice. **C)** Fraction of spiking neurons (top) and number of spikes per whisker deflection (spiking probability; median ± interquartile range). **D)** Time-course of averaged PSP amplitude before and after RWS, in FWE and SWE mice. Note that whisker-evoked PSPpeak on SWE mice are higher compared to FWE. **E)** Mean (± sem) amplitude before (baseline) and after RWS. Error bars, sem; grey lines between bars, pairs. This illustrates that the increased synaptic gain after SWE occludes a further potentiation by RWS. **F)** Plot of normalized plateau strength as a function of LTP (%) (differences on PSPpeak before/after RWS). Circles are individual cells, lines the fitting of the plotted data. There is a positive correlation between these two properties on FWE: the higher the NMDAR plateau strength, the higher the recorded cell potentiate. This is not seen on cells recorded from SWE mice, because cells with NMDAR strength fail to potentiate. All the values and statistics represented in Table 1.

E. Effect of SWE on L2/3 pyramidal neurons excitability and RWS-evoked cumulative depolarization

We next asked if, besides an increased synaptic gain, SWE has additional effects at the synaptic and cellular-level. We determined the input-output function between somatic injected current and the number of evoked spikes, as a metric for cellular excitability. We found that SWE alters this relationship, as indicated by the reduction of spike threshold (rheobase, FWE: 370.4 ± 96.3 pA, SWE: 308.3 ± 115.78, p=0.04) (**fig. 33A**). We also determined the effect of SWE on the membrane depolarization during RWS by stimulating wC2 at 8 Hz during 2.5 sec (sRWS) (**fig. 33B**). The duration of this protocol of whisker stimulation is not enough to drive RWS-LTP (data not shown). We found that RWS-induced depolarization is increased after SWE (8Hz-cumulative PSP, FWE: 4.63 ± 2.63 mV, SWE: 9.19 ± 3.4 mV, p=0.004) (**fig. 33C**). Since SWE does not alter single-whisker plateau potentials (fig. 31D), this enhanced depolarization might be related to increased AMPAR-mediated responses or a frequency-dependent disinhibitory mechanism (see discussion).

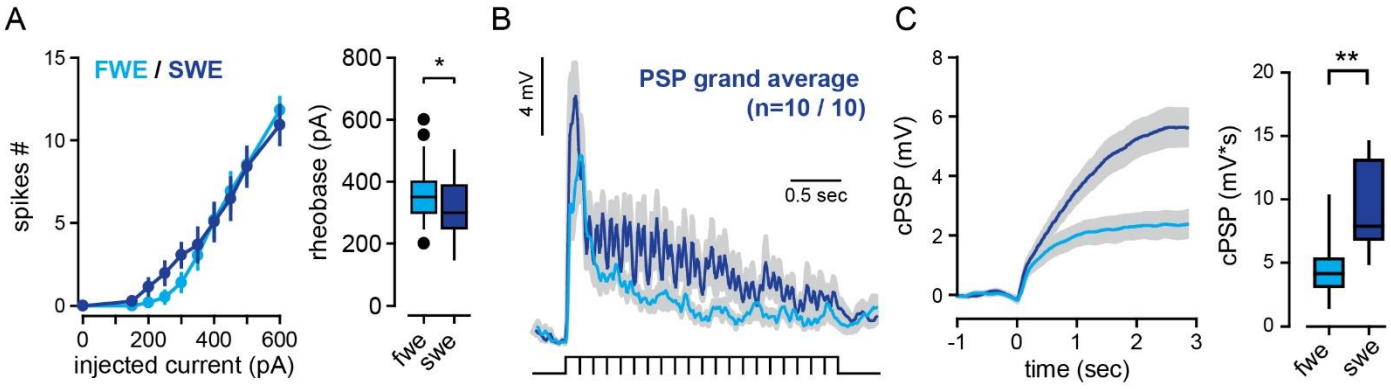

Fig. 33) SWE alters pyramidal neurons excitability and RWS-evoked cumulative depolarization. A) (*left*) average (± sem) number of action potentials (APs) triggered by incremental current injections in FWE (light blue) and SWE (dark blue) mice. (*right*) Median (± interquartile range) minimal current amplitude (pA) triggering action potentials (rheobase). **B)** Grand average (all recorded cells averaged, ± sem) of membrane depolarization upon rhythmic whisker stimulation (20 stimuli at 8 Hz). **C)** *(left)* cumulative RWS-induced depolarization. *(right)* Median (± interquartile range) cumulative depolarization measured at the end of the stimulation. All the values and statistics represented in Table 1.

F. *In vivo* AMPAR cross-linking in the barrel cortex

Next, we asked if we could prevent experience-driven response potentiation by interfering with the mechanisms of RWS-LTP during SWE. If indeed LTP is driving map plasticity, its manipulation should prevent trimming-induced increased synaptic gain, and revert RWS-LTP occlusion. If this is true, then LTP is the synaptic substrate underlying circuit functional alterations during SWE. While blocking the induction of LTP with NMDARs antagonists provided the most indirect evidences that synaptic plasticity in L2/3 synapses is required for both potentiation of spared whisker responses, it might obstruct normal sensory transmission *in vivo*, which relies on NMDARs conductances[374]. Instead, we aimed to develop a novel approach to specifically manipulate the expression but not the induction of LTP *in vivo*. For this, we took inspiration from *in vitro* work developed by the Choquet's lab, describing extracellular AMPAR cross-linking as an effective tool to block synaptic LTP[332]. To do so, we first targeted a craniotomy above the C2 barrel using IOI. Then, one of two different antibodies (IgGs) were stereotaxically injected: (1) an anti-GluA2 antibody for extracellular AMPAR cross-linking, or (2) a control anti-GFP antibody, with a similar IgG, but recognizing a different epitope (**fig. 34A**). The injection protocol was optimized to concentrate antibody in L2/3, without affecting L4 microcircuit, and reduce spread to adjacent barrels. We choose to targeted the GluA2 subunit of AMPARs because is predominantly expressed in the barrel cortex, its expression is increased upon partial sensory deafferentation, and has been successfully performed *in vivo* by Penn and collaborators[281,332,347,351,352]. After antibody injection, *in vivo* whole-cells recording of L2/3 pyramidal neurons in the principal C2 barrel was performed. At the end of the experiment, animals were perfused for *post hoc* revealing of the antibody injection. Only cells recorded from samples with DAB staining were considered for analysis (**fig. 34A**). To determine if antibody application *per se* has cytotoxic effects, we recorded cell-intrinsic and circuit-wide electrophysiological properties. No differences between the two IgGs in the number of spikes as a function of injected somatic current was seen, suggesting no alteration on cell intrinsic excitability (**fig. 34B**). We then recorded circuit spontaneous activity to quantify the effects of antibody application at the circuit level (**fig. 34C**). Under our experimental conditions, the resting membrane potential (Vm) oscillates between UP and DOWN states in a low-frequency manner. These fluctuations correspond to waves of local and synchronous activity in the L2/3 circuitry (UP state), intercalated by quiescent periods of activity (DOWN state)[369]. We found that neither the anti-GluA2 nor the anti-GFP IgGs change the cumulative distribution of UP states, nor UP state probability (anti-GFP: 0.192 ± 0.06, anti-GluA2: 0.173 ± 0.08, p=0.45) (**fig. 34D**). Thus, AMPAR cross-linking does not alter basic cellular and circuit electrophysiological properties. We then asked ourselves if the same is true for whisker-evoked neuronal activity.

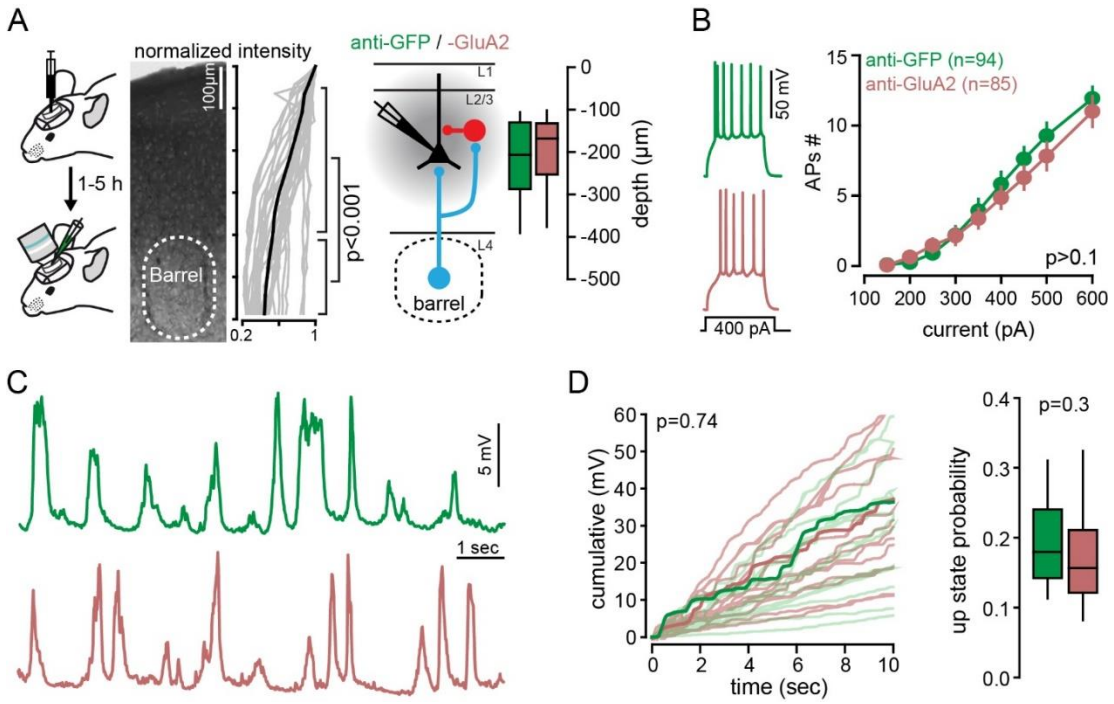

Fig. 34) ***In vivo*** **AMPAR cross-linking in the barrel cortex. A)** Schematic representation of *in vivo* stereotaxic injection of antibody, followed by whole-cell patch clamp recordings. Example of a DAB-revealed sample after electrophysiological recordings. Note the antibody accumulation in L2/3, without enrichment in L4. L2/3 pyramidal neurons (black) were targeted for recording. Inhibitory drive into this cells (red) was indirectly measured, and is presented on section G. **B)** We recorded the number of evoked spikes by increased intensity of somatic current injection. (*left*) Example of somatic spikes on current-clamp in the presence of both anti-GFP and anti-GluA2 antibodies. (*right*) Average values of the number of spikes per injected current with sem represented. No differences between the two IgGs were seen, suggesting that GluA2 antibody injection does not alter cell intrinsic excitability. **C)** Example traces of spontaneous UP and DOWN fluctuations of the resting membrane potential for both anti-GluA2 and anti-GFP antibody injection. **D)** (left) Cumulative sum of all the UP states as a time function. Dark red and green average values, light traces of all the individual recorded cells per condition. (right) Median (± interquartile range) probability of spontaneous up-states. Anti-GluA2 antibody application does not alter spontaneous activity in the barrel cortex. All the values and statistics represented in Table 1.

G. AMPAR cross-linking does not alter excitatory nor inhibitory components of whisker-evoked PSPs

The effect of whisker deflection on neuron's Vm is largely dependent on the resting membrane potential (**fig. 35A**)[369]. If a stimulation occurs during a DOWN state, the result is a complex PSP belonging either to cluster one or two (**fig. 31C**). However, if a deflection is made during a UP state, the result is a sharp decrease on the Vm, likely due to the recruitment of inhibitory drive[369]. We fitted PSPs evoked during UP states to extrapolate if AMPAR cross-linking can affect inhibitory inputs made into the recorded excitatory neuron (**red cell, fig. 34A**). We found that the exponential fitting was not different between both antibody injections (1/τ (ms-1), anti-GFP: 0.32 ± 0.16, anti-GluA2: 0.35 ± 0.2, p=0.6) (**fig. 35B**). This indirectly suggest that our cross-linking approach does not impair local L2/3 inhibition. To have another readout of the inhibitory drive into L2/3 pyramidal neurons, we extrapolated the reverse potential for inhibition by recording whisker-evoked PSPs at different holding

membrane potentials (fig. 35C). As the inhibitory drive is not contaminated by the excitatory one at 0 mV, the fitting of all the normalized PSPs is a good approximation of the inhibition recruited by whisker deflection. No differences between fittings of the different conditions were seen (IV curve, anti-GFP: 0.815 ± 0.04, anti-GluA2: 0.75 ± 0.05, 2-way ANOVA), indicating no effect of AMPAR cross-linking on inhibitory networks. We then focused our attention in the basic properties of the excitatory whisker-evoked PSPs (fig. 35D). Neither the PSPpeak (anti-GFP: 8.87 ± 4.4 mV, anti-GluA2: 8.732 ± 4.07 mV, p=0.9), nor the late-phase integral were affected by anti-GluA2 antibody application (anti-GFP: 0.64 ± 0.32 mV*sec, anti-GluA2: 0.68 ± 0.3 mV*sec, p=0.0.6). In agreement, the reliability of whisker-evoked neuronal responses, measured as the jitter (anti-GFP: 1.88 ± 1.07 ms, anti-GluA2: 2.44 ± 1.77 ms, p=0.6) and onset (anti-GFP: 11.87 ± 2.22 ms, anti-GluA2: 12.22 ± 3.02 ms, p=0.6), were also not affected by AMPAR cross-linking (fig. 34E). Altogether, these data suggest that AMPAR cross-linking does not affect excitatory, and inhibitory conductances, nor L2/3 basal synaptic transmission. These findings are supported by a previous *in vitro* study, demonstrating that the same approach does not impact hippocampal basic circuit properties[332].

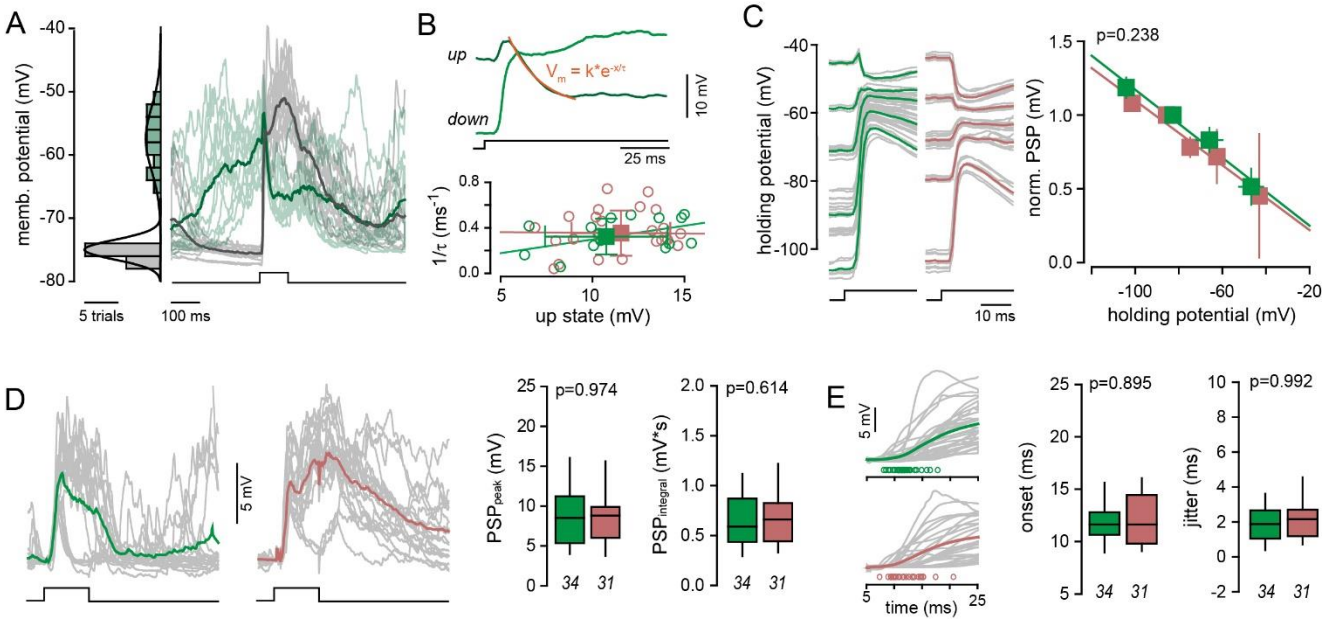

Fig. 35) AMPAR cross-linking does not alter excitatory nor inhibitory components of whisker-evoked PSPs. A) (*left*) membrane potential histogram showing the average (30 ms) membrane potential before each wC2 stimulation. Down (grey) and up (green) states follow separated Gaussian distributions. (*right*) wC2-evoked PSPs during down (green) and up (dark green) states. Individual trials are represented with light lines. **B)** (*top*) single-cell examples of wC2-evoked PSP in down and up states. The decay of membrane potential during up states is fitted with an exponential, which is indicative of the degree of wC2-evoked inhibition. *(bottom)* Relation between the amplitude of up states and the exponential tau, in anti-GFP (green) and anti-GluA2 (magenta) IgGs injected mice. Circles, individual cells; squares, mean (± s.e.m.). **C)** (*left*) Single-cells examples of wC2-evoked PSPs at different holding potentials. (*rigt*) Relation between holding potential and the amplitude of wC2-PSPs (normalized to the amplitude at resting membrane potential). **D)** (*left*) Whisker-evoked PSPs of an example cell in the presence of either anti-GluA2 or anti-GFP antibody. Colored traces are averages, gray traces are individual trials contribution. *(right)* Median (± interquartile range) of PSPpeak and PSPintegral. No differences are seen between conditions. **E)** (*left*) single-cells examples of PW-evoked PSPs illustrating the onset of PSP. Circles, individual cells. (*right*) Median (± interquartile range) PSP onset and onset jitter. Square pulse line, whisker deflections (100 ms). All the values and statistics represented Table 1.

H. 2-Photon dendritic calcium imaging indicates that AMPAR cross-linking does not alter NMDAR-dependent dendritic spikes

Due to its importance as the induction mechanism of RWS-LTP, we decided to directly image NMDAR dendritic calcium spikes before and after AMPAR cross-linking. To do so, we are currently performing *in vivo* 2-Photon Ca^{2+} imaging of mice sparsely expressing GCaMP6f (**fig. 36A**). This allow us to image isolated distal L2/3 dendrites, and record localized dendritic calcium transients evoked by wC2 stimulation in urethane-anesthetized mice. The anesthesia does not only allow to recapitulate a brain state similar to the electrophysiological recordings, but also to avoid dendritic evens evoked by spontaneous whisking that could occur during awake conditions. Preliminary data suggests that acute anti-GluA2 application does not alter the size, nor the probability of evoking a calcium event (over ten cycles of whisker stimulation) (**fig.36B**). This further supports the previous electrophysiological findings (**fig. 35D**), showing no differences after antibody application on the NMDAR component of the evoked PSPs.

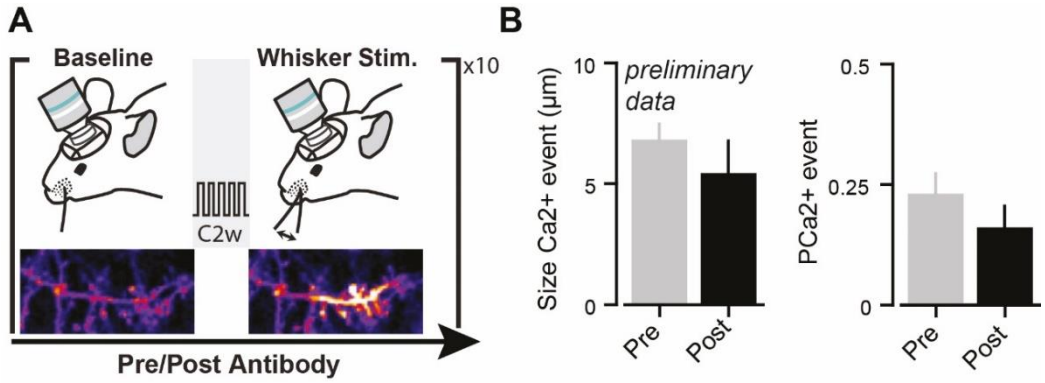

Fig. 36) ***In vivo*** **2-Photon dendritic calcium imaging with AMPAR cross-linking. A)** *In vivo* 2-Photon dendritic Ca^{2+} imaging in urethane-anesthetized mice. L2/3 pyramidal neurons sparsely infected with GCaMP6s were imaged through a C.W. before and after antiGluA2 stereotaxic injection. Distal dendritic spikes were evoked by passive stimulation of wC2 by cycles of ten stimulations. This allowed us to extract both the size, and the probability of whisker-evoked Ca^{2+} transients. **B)** Preliminary data suggest that these properties are not affected by *in vivo* AMPAR cross-linking.

I. AMPAR cross-linking blocks RWS-LTP expression

Next, we asked if we could prevent RWS-LTP by interfering with AMPAR trafficking *in vivo*. For this, we performed RWS while patching L2/3 pyramidal neurons after anti-GluA2 IgGs stereotaxic injections (**fig.37A**). RWS induced a significant LTP of wC2-evoked PSPs in the presence of the anti-GFP IgGs (RWS+ vs. RWS-: 123.9 ± 1.7 % vs. 101.6 ± 0.71 %, $p<0.001$) (**fig. 37B**). In contrast, cross-linking mediated suppression of GluA2 diffusion completely blocked RWS-LTP (RWS+ vs. RWS-: 107.1 ± 3.6 % vs. 97.5 ± 3.1 %, $p>0.05$) (**fig. 37C**). This impairment was not caused by alterations of response baseline, since no differences on PSPpeak between conditions are seen if RWS is not performed (anti-GFP, baseline: 10.82 ± 6.05, RWS-: 9.72 ± 6.25, p:0.2; anti-GluA2: 8.89 ± 4.07, RWS: 8.53 ± 3.7) (fig. 36D and 36E). **Figure 37F** summarizes all the effects of the different IgGs injections on RWS-LTP and baseline PSPs. Therefore, similar to

large body of evidences gathered *in vitro*, changes in the number of synaptic AMPARs powered by lateral mobility is a key process during *in vivo* LTP as well.

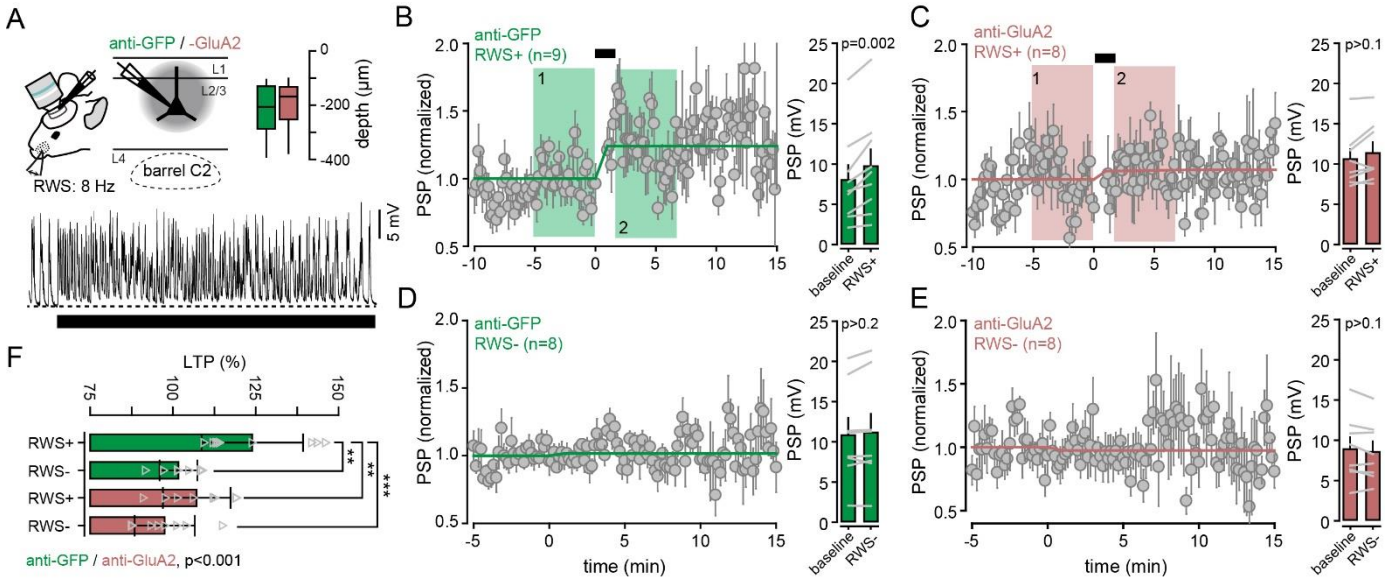

Fig. 37) AMPAR cross-linking blocks RWS-LTP expression. A) (*top*) Recordings schematic of L2/3 pyramidal neurons in the presence of anti-GluA2 or anti-GFP IgGs. Depth of recorded cells is indicated. (*bottom*) Example trace of sustained depolarization induced by RWS (8 Hz for 1 min; black bar). **B)** Time-course of averaged PSP amplitude upon (RWS+), **(D)** and in the absence of RWS (RWS-) of anti-GFP injected animals. (*Right*) Mean (± sem) amplitude before (baseline) and after RWS+ (B) or RWS-. Error bars, s.e.m; grey lines between bars, pairs. Color box, analysis time point. **C and E)** Same as in (B) and (D) but for the anti-GluA2 condition. **F)** Mean (± sem) amplitude normalized to baseline (% of LTP). Triangles, individual cells. AMPAR cross-linking blocks the expression of RWS-LTP. All the values and statistics represented in Table 1.

J. AMPAR cross-linking does not alter the induction of RWS-LTP

To re-ensure that AMPAR cross-linking does not alter NMDAR signaling on L2/3 synaptic transmission, we extracted NMDAR plateau potentials of all the neurons in which we performed RWS (**fig. 38A**). We found no differences between conditions on both the onset (anti-GFP: 31.4 ± 6.08 ms, anti-GluA2: 30.03 ± 6.3 ms, p=0.4), probability (anti-GFP: 0.7 ± 0.23, anti-GluA2: 0.69 ± 0.23 ms, p=0.77), nor strength (anti-GFP: 0.72 ± 0.48 mV*sec, anti-GluA2: 0.78 ± 0.55 mV*sec, p=0.8) of NMDAR plateaus. Normalized plateau strength predicted the level of RWS-induced LTP in anti-GFP, but not in anti-GluA2 IgGs injected mice (**fig. 38B**). Indeed, anti-GFP with high plateau strength, strongly potentiated, whereas anti-GluA2 cells show high NMDAR drive did not. Altogether, these results demonstrate that our cross-linking approach specifically block RWS-LTP expression, without changing its NMDAR-dependent induction mechanisms. This is in line with the results obtained on section G (**fig.35D**) and H (**fig. 36B**). In conclusion, our results indicate that, in addition to GluA1, the recruitment of diffusive GluA2-containing AMPARs to the synapse is required for the expression of RWS-LTP *in vivo*[177].

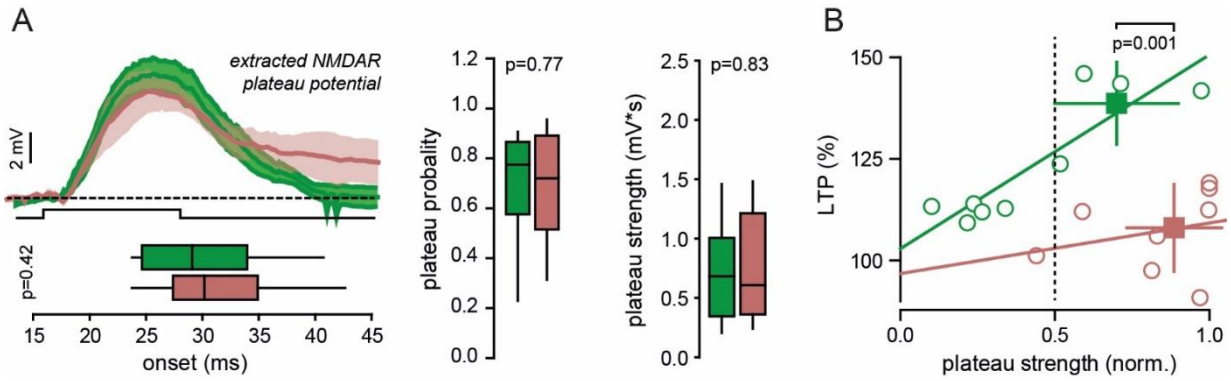

Fig. 38) AMPAR cross-linking does not alter the induction of RWS-LTP. A) *(left top)*, grand average of wC2-evoked extracted plateau potential (all recorded cells averaged) ± sem. Square pulse lines, whisker deflections (100 ms). *(left)* bottom, Median (± interquartile range) onset of plateau potentials. *(right)* Median (± interquartile range) plateau probability and strength. **B)** Normalized plateau strength predicts the level of RWS-induced LTP in anti-GFP, but not anti-GluA2 IgGs injected mice. AMPAR cross-linking impairs the expression but no the induction of RWS-LTP. All the values and statistics represented in table 1.

K. Chronic AMPAR cross-linking during SWE reduces whisker-evoked somatic spikes and reverts RWS-LTP occlusion

We showed that AMPAR cross-linking is an efficient tool to block sensory-evoked synaptic potentiation without affecting circuit's basal transmission. This made us wonder if the chronic injection of IgGs (X-SWE) to suppress GluA2 surface diffusion during SWE reverts the potentiation of the neuronal responses to the spared whisker. If indeed LTP during map plasticity drives the increased gain on "spared synapses", then this potentiation should be reverted after X-SWE. As a consequence, we should be able to induce RWS-LTP on SWE mice, and re-potentiate L2/3 synapses after map plasticity. If this is true, then LTP-driven map plasticity is indeed the synaptic mechanisms re-shaping neuronal responses, likely L2/3 microcircuits, to increase spared whisker cortical representation. To test this hypothesizes, anti-GluA2 (or anti-GFP as a control) IgGs were injected in the barrel cortex for two consecutive days while trimming all but the contra-lateral wC2 (**fig. 39A**). L2/3 pyramidal neurons were recorded after a 12h clearance period, to allow antibody washout (**fig. 39B**). With this we hoped to block LTP during SWE-induced cortical remapping, and re-evaluate the state of L2/3 synapses after washout. We expected to record cells with decreased synaptic gain (i.e., PSPpeak), and sensitive to RWS-LTP induction.

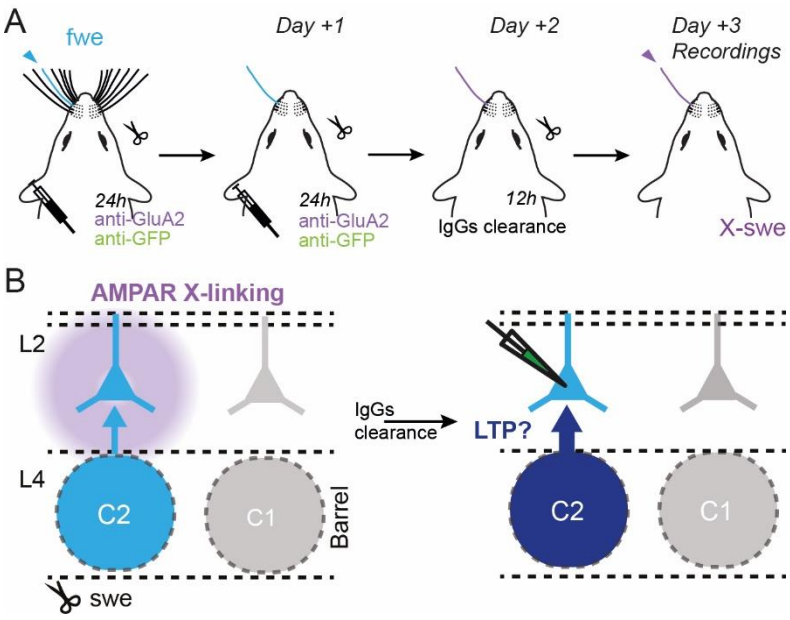

Fig. 39) Chronic AMPAR cross-linking during SWE. A) Schematic of experimental strategy. IgGs are injected during SWE then washed-out for recordings. **B)** We aimed to block synaptic LTP in L2/3 pyramidal neurons in the principal barrel during map plasticity. If cortical remapping is driven by LTP, our chronic AMPAR cross-linking should revert RWS-LTP occlusion, and increased neuronal excitability. If this is true, we should be able to induce RWS-LTP on X-SWE mice after antibody washout. This reduced synaptic gain, should be accompanied by a decreased neuronal excitability, to similar levels than FWE mice.

To determine if X-SWE reduces spared whisker response potentiation in L2/3 pyramidal neurons, we recorded whisker-evoked PSPs (**fig. 40A**). We found a smaller PSP in neurons exposed to chronic GluA2 for two days as compared to the anti-GFP control (PSPpeak X-SWE, anti-GFP: 14.5 ± 5.2 mV, anti-GluA2: 7.97 ± 3.85, p=0.03) (**fig. 40B**). Indeed, X-SWE anti-GluA2 average PSPpeak is similar to FWE-subjected mice (X-SWE anti-GluA2: 7.97 ± 3.85, FWE: 9.88 ± 3.89 mV, p=0.4). On the other hand, the control X-SWE anti-GFP where LTP was allowed to occur, is not different from SWE-subjected mice (X-SWE anti-GFP: 14.5 ± 5.2 mV, SWE: 17.98 ± 8.2 mV, p= 0.2). If an increased synaptic gain increases spared whisker-evoked somatic spikes, then this increased excitability should be reduced after X-SWE anti-GluA2. Although X-SWE anti-GluA2 did not modify the fraction of spiking neurons (X-SWE anti-GluA2: 6/9; SWE: 11/13; p>0.05) (**Fig. 40C**), it significantly decreased the average number of spikes per PW deflection (X-SWE anti-GluA2: 0.08 ± 0.03; n=9; X-SWE anti-GFP: 0.45 ± 0.16, n=7; p=0.003) (**Fig. 40C, D**). Thus, a relationship between increased synaptic gain and somatic spikes does exist. We thus questioned if this is a consequence of synaptic LTP.

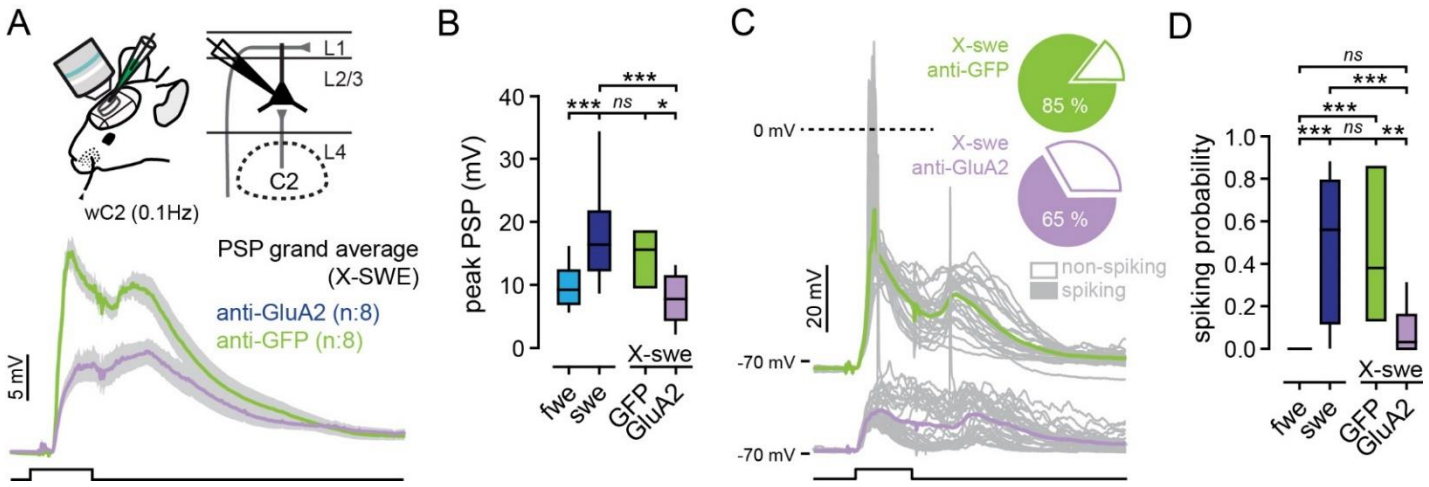

Fig. 40) Chronic AMPAR-crosslinking reduces SWE-induced neuronal response potentiation of the spared whisker. A) *(top)* Schematic representation of recordings of whisker evoked-PSPs before chronic antibody injection. *(bottom)* wC2-evoked PSP grand average (all recorded cells averaged) ± sem. Square pulse lines, whisker deflections (100 ms). **B)** Median (± interquartile range) PSP amplitude. Note that X-SWE PSPpeak amplitude are similar to FWE, while GFP to SWE. **C)** (*left*) Single-cell examples of whisker-evoked responses (grey, single trials; green and purple, averaged traces from anti-GFP and antiGluA2 injected mice). Square pulse lines, whisker deflections (100 ms). (*right*) Fraction of spiking neurons. Number of spikes per whisker deflection (spiking probability; median ± interquartile range). X-SWE does not reduce the number of spiking neurons, but decreased the probability of whisker-evoked spikes. All the values and statistics represented in Table 1.

We hypothesize that increased gain of spared synapses drives the higher fraction of neurons spiking upon spared whisker deflection. If this is true, and as our X-SWE anti-GluA2 approach reduced the fraction of spiking neurons, then we should be able to re-induce RWS-LTP on this condition. RWS potentiated wC2-evoked PSPs after washout of X-SWE anti-GluA2 antibody (baseline: 8.7 ± 1.6 mV, RWS: 11.9 ± 2.5 mV; n=6; p=0.03) but not anti-GFP (baseline: 19.1 ± 1.9 mV, RWS: 18.8 ± 1.8 mV; n=9; p=0.4) (fig. 41A). We believe that this is caused by a reversion of RWS-LTP occlusion, because wC2-evoked PSPpeak amplitude in X-SWE anti-GluA2 before RWS are smaller compared to anti-GFP (fig. 41B). While RWS increased the amplitude of evoked-PSPpeak on anti-GluA2, it failed on anti-GFP mice, where synapses are already saturated due to LTP-driven map plasticity (X-SWE anti-GluA2, baseline: 8.67 ± 3.7, RWS+: 11.89 ± 5.8 mV, p=0.04). This confirms the relationship between LTP, increased synaptic gain, and response potentiation to the spared whisker. If this core synaptic mechanism is blocked, then all of this "neuronal phenotypes" are reverted, with a concomitant decrease of somatic spikes, and spared whisker cortical representation.

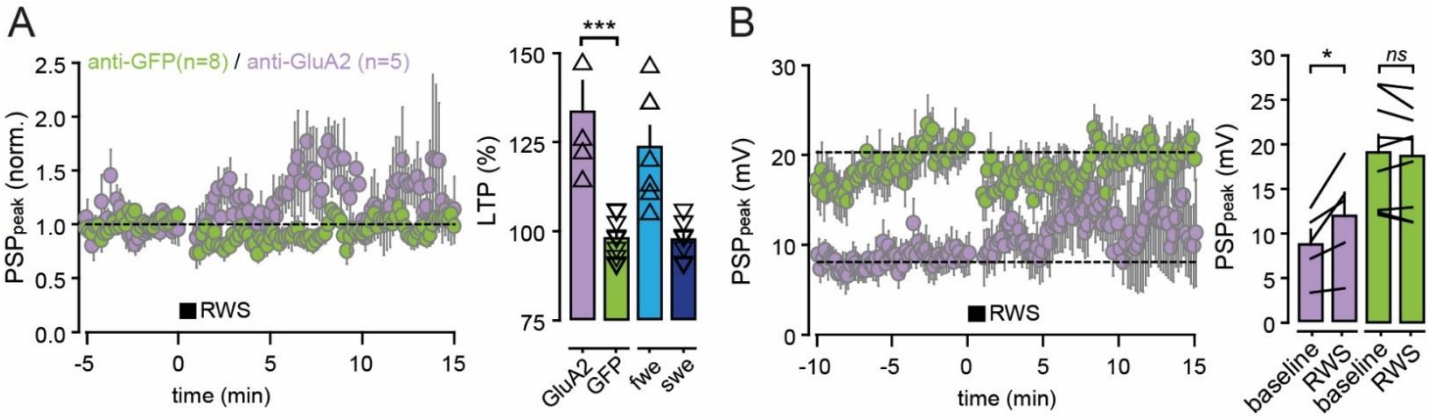

Fig. 41) Chronic AMPAR-crosslinking reverts RWS-LTP occlusion after SWE. A) (*left*) Time-course of averaged PSP amplitude upon RWS in anti-GFP and anti-GluA2 injected mice (after wash-out). (*right*) Mean (± sem) amplitude before (baseline) and after RWS. Error bars, sem; grey lines between bars, pairs. **B) (***left*) time-course of averaged PSP amplitude normalized to baseline. (*right*) Mean (± sem) amplitude normalized to baseline (% of LTP). Triangles, individual cells. Note that X-SWE reverts RWS-LTP occlusion. In agreement, the evoked PSPpeak amplitude before RWS is smaller than the GFP condition, where RWS-LTP is occluded. All the values and statistics represented in Table 1.

Figure 42 describes how the different conditions used throughout this work influenced RWS-LTP. The degree of potentiation of X-SWE anti-GluA2 animals is comparable to FWE or acute anti-GFP mice (fig. 42A), suggesting an efficient reversion by chronic AMPAR cross-linking and wash-out of LTP occlusion by SWE. Conversely, chronic anti-GFP during SWE had impairments on LTP similar to SWE and acute AMPAR cross-linking conditions. We analyzed the plateau potentials to all the conditions, to determine if the reduction of synaptic LTP of X-SWE anti-GluA2 mice is due to impairments in NMDAR signaling (fig. 42B). We found no differences across conditions, suggesting that neither acute, nor chronic AMPAR cross-linking affect NMDAR plateau potentials (see table of statistics). Therefore, the effects reported for X-SWE anti-GluA2 are likely specific for a blockage of LTP, and not caused by impairments in basal synaptic transmission. We also plotted LTP (%) as a function of NMDAR plateau strength (fig. 42C). As expected, we found a positive correlation for FWE, acute anti-GFP antibody injections, and X-SWE anti-GluA2 conditions. On the other hand, SWE and acute AMPAR cross-linking had cells with high NMDAR plateau strength that failed to potentiate. This results from different synaptic effects between both conditions, as: (acute AMPAR-cross-linking) surface mobility of AMPARs is blocked, receptors cannot be recruited to the synapses, and no potentiation is recorded; (SWE) LTP-driven synapses potentiation during SWE increases the synaptic gain to a saturation level, no further potentiation is possible. The latter, underlies spared whisker neuronal response potentiation, and map plasticity-induced augmentation of neuronal spikes in the spare barrel. It remains to be determine if this spared whisker response potentiation is then propagated to the neighboring barrels, causing the functional "barrel expansion" after SWE (see discussion).

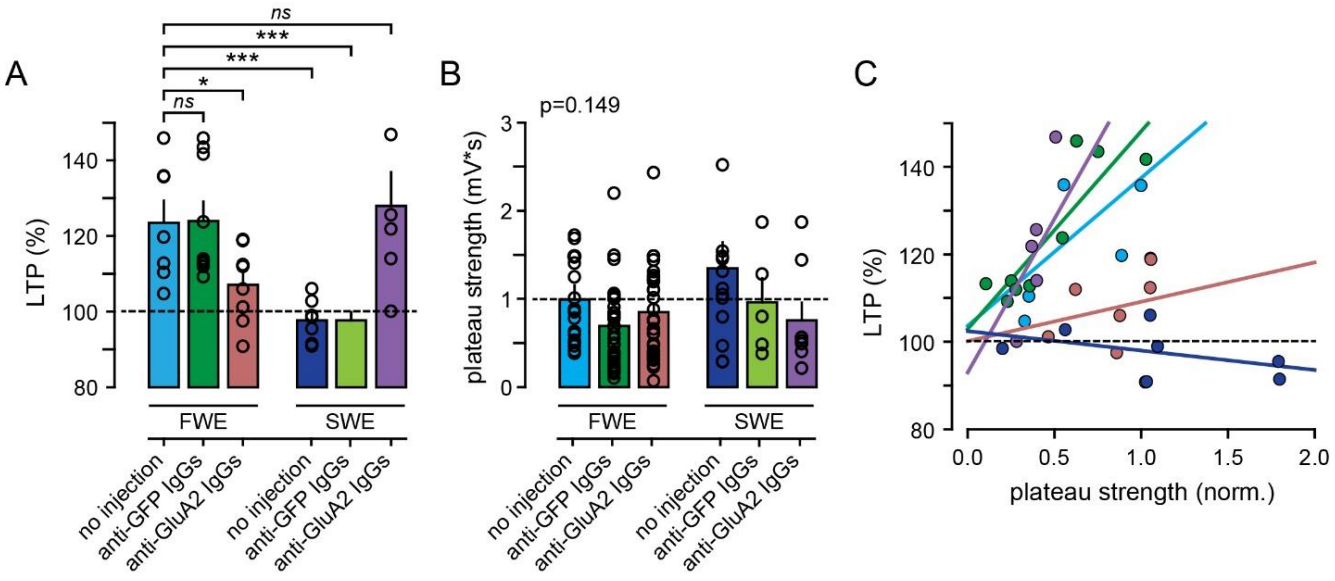

Fig. 42) Resume of all the RWS-LTP experiments. A) Mean (± sem) LTP (%) (difference of PSPpeak before/after RWS-LTP). Circles represent individual cells. **B)** Same than (A) but plotting NMDAR plateau strength. **C)** Normalized plateau strength predicts the level of RWS-induced LTP in acute GFP, FWE, and X-SWE. This positive correlation is abolished for SWE and acute anti-GluA2 IgG injected mice. This clearly illustrates the effect of blocking LTP (by different mechanisms), in both conditions without affecting NMDAR-dependent induction mechanisms. All the values and statistics represented in Table 1.

L. Gap Crossing as a whisker-dependent behavior protocol

SWE alters various whisker-mediated behavioral tasks[248,249,252]. Here, we demonstrated that SWE drives cortical remapping and neuronal responses potentiation of the spared whisker. At the cellular level, this is driven by synaptic LTP, as indicated by our RWS-LTP experiments. Thus, if cortical remapping compensates tactile perception when sensory inputs are lost, then whisker-dependent behavioral performance should be affected by our X-SWE approach. We decided to test this possibility by taking advantage of a classical gap-crossing (GC) behavioral task. Mice were trained to reach a suspended reward platform separated by a gap distance (GD) ranging from 40 to 65 mm. As GDs are randomly presented, and the behavioral task is performed in the absence of auditory, olfactory, and visual clues, the perception of the reward platform should be whisker-mediated. To ensure this, we first performed the GC task on animals with all their whisker trimmed (NW, no whiskers), FWE-subjected, and SWE-subjected mice. Whisker trimming was performed after behavioral habituation, one day before the first recording session (S). We focused our analysis in three different parameters: (1) success rate, defined as the probability of jumping to the reward platform; (2) decision latency, a measure of the time exploring the GD in the moment of jump (successful trial) (**fig. 43A**), and (3) exploration time, calculated as the sum of the total time spent in the jump area (independently of success) (**fig. 43B**). We found that all these parameters are whisker-dependent (**fig. 43C-E**). For non-challenging GDs (40 and 50 mm), behavioral performance was not affected by whisker trimming, remaining stable across the four recording sessions. The GD=65mm had the biggest discrepancies and, consequently, we focused our analysis

to this GD. This is in agreement with previous studies showing that at this distances, mice use preferentially their whisker to located the target platform and jump onto it to receive reward platform[248,249]. While FWE-subjected mice reached expertise (i.e., success=1) by S2, NW-subjected, and SWE-subjected animals never accomplished this performance (**fig. 43F**). As consequence, differences on the success rate are seen by the last days of recordings between trimming protocols (fraction of success, FWE: 0.89 ± 0.213, SWE: 0.567 ± 0.667, NW: 0.604 ± 0.35). SWE-subjected mice appear to recover progressively their success rate, while NW-subjected mice drastically improved at S2, remaining relatively stable until S4. At this distance, important differences on exploration time across whisker trimming protocols are seen (**fig. 43G**). Indeed, NW-subjected mice spent more time exploring the jump area, followed by SWE-subjected, and FWE-subjected ones (exploration FWE: 25.33 ± 25.02 sec., SWE: 40.89 ± 26.20 sec., NW: 46.03 ± 32.65 sec.). Interestingly, exploration time in FWE- and SWE-subjected mice progressively decreases along the recording sessions (**fig. 43C2 and E2**). Conversely, NW-subjected mice had a drop on exploration time at S2, remaining constant across sessions (**fig. 43D2**). Decision latency was remarkably stable across whisker trimming and recording sessions (**fig. 43 C3-E3**). Except in S1, we found no differences on this parameter for a GD = 65 mm (FWE: 4.56 ± 1.95 sec; NW: 5.27 ± 2.63 sec.; SWE: 6.63 ± 2.59 sec., p=0.01) (**fig. 43H**). The analyze of both parameters suggest that, once the platform is detected (GD exploration), the latency to jump is not whisker-dependent. Altogether, these results confirm that the classical GC behavioral task, under our experimental conditions, is whisker-dependent.

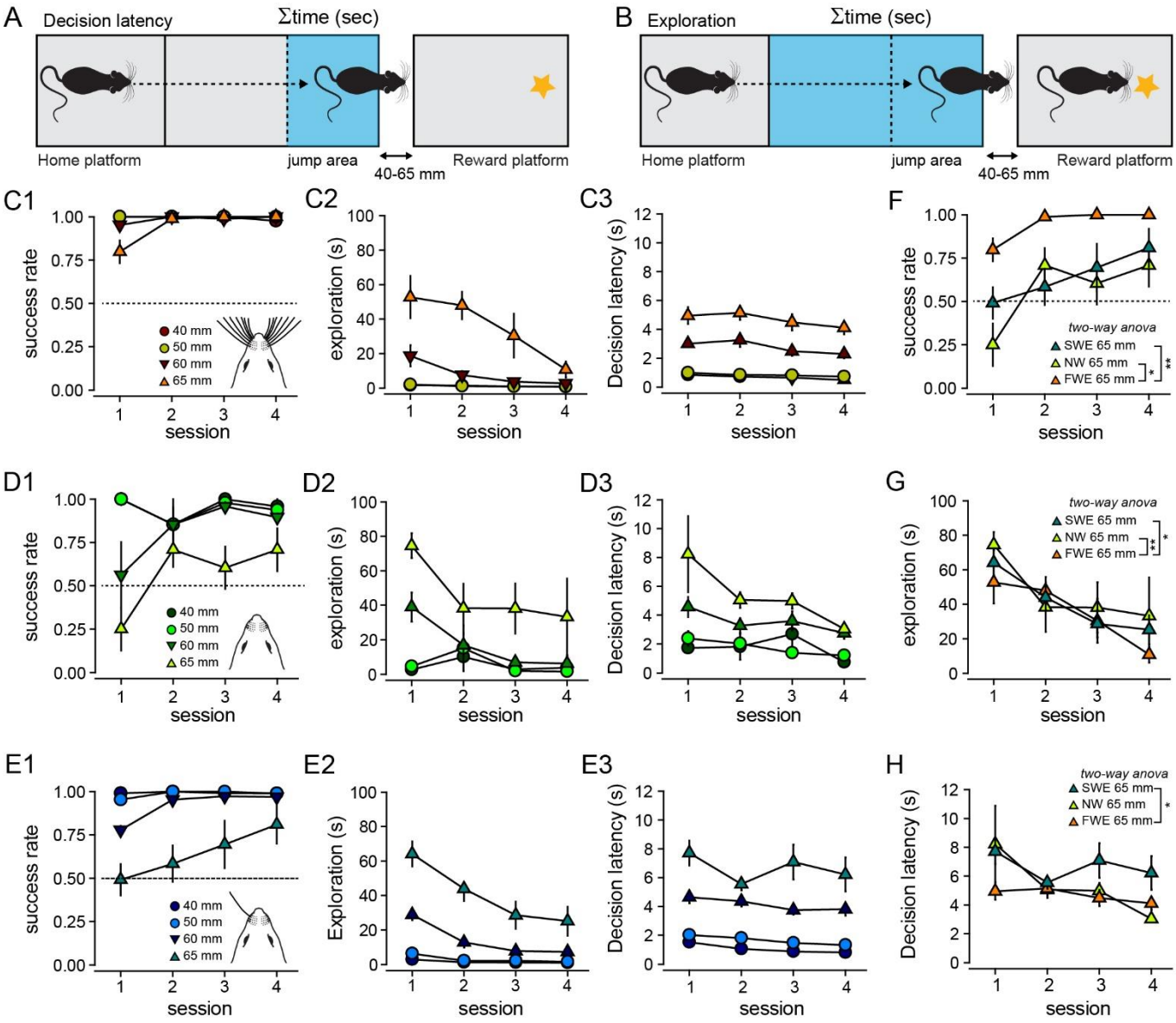

Fig. 43) Gap Crossing as a whisker-dependent behavioral task. A) Overview of the gap-crossing task (see material and methods for details). Here, we extract either the success rate (probability of jump to the reward platform), the latency of decision in the GD exploration preceding the jump and **B)** sum of the time spent exploring the jump area of both successful and unsuccessful trials. **C1)** Average (± sem) fraction of success, **C2)** Average (± sem) GD exploration, and **C3)** Average (± sem) decision latency for all the GDs on FWE-subjected mice. **D1-D3)** Same than C1-C3 for NW (no whisker)-subjected mice and **E1-E3)** SWE-subjected mice. **F)** Averaged (± sem) fraction of gap-crossing success at a distance of 65 mm, in FWE (orange), NW (green) and SWE (cyan) mice. **G)** Same than (F) but for total GD exploration, and **(H)** decision latency. All the values and statistics represented in table 1.

M. Map plasticity compensates a learned whisker-dependent behavior

We then asked ourselves if map plasticity impacts a learned whisker-dependent behavior task. While the previous approach provides good information on whiskers mediate tactile information, it gives limited information on the behavioral correlates of map plasticity. To have a causal link between map plasticity and whisker-tactile performance, we trained FWE mice until reaching expertise (S1-S4), followed by four additional sessions on SWE (S5-S8). We hypothesized that this would permit to determine how map plasticity influences spared whisker perception, independently of the task learning. GC performance decreased immediately after SWE (GD=65 mm, session 4: 0.96 ± 0.04; session 5: 0.68 ± 13; n=6; p=0.006) but recovered quickly after 2 days of SWE (session 6: 0.87 ± 0.09; p=0.372), a time scale at which RWS-LTP has been fully saturated (**fig. 44A**). Importantly, mice that were not tested during SWE (sessions 5 to 7) had similar final success rate (session 8 training; 0.95 ± 0.03, n=6; session 8 no-training, 0.89 ± 0.08, n=5; p>0.05), suggesting that behavioral recovery was likely not caused by a new learning phase (**fig. 44B**). We found no differences in the decision latency at this GD (values here) (**fig. 44C**). However, for a GD=60 mm, decision latency was impaired by whisker trimming, recovering fast at S6. Nevertheless, exploration time is strongly affected by SWE, and has a similar recovery than all the other parameters (exploration, FWE4: 10.227 ± 14.37 sec., SWE5: 34.773 ± 17.23 sec., p<0.001) (**fig. 44D**). Collectively, our data suggest that SWE-mediated cortical remapping is associated with the recovery of a whisker-dependent task.

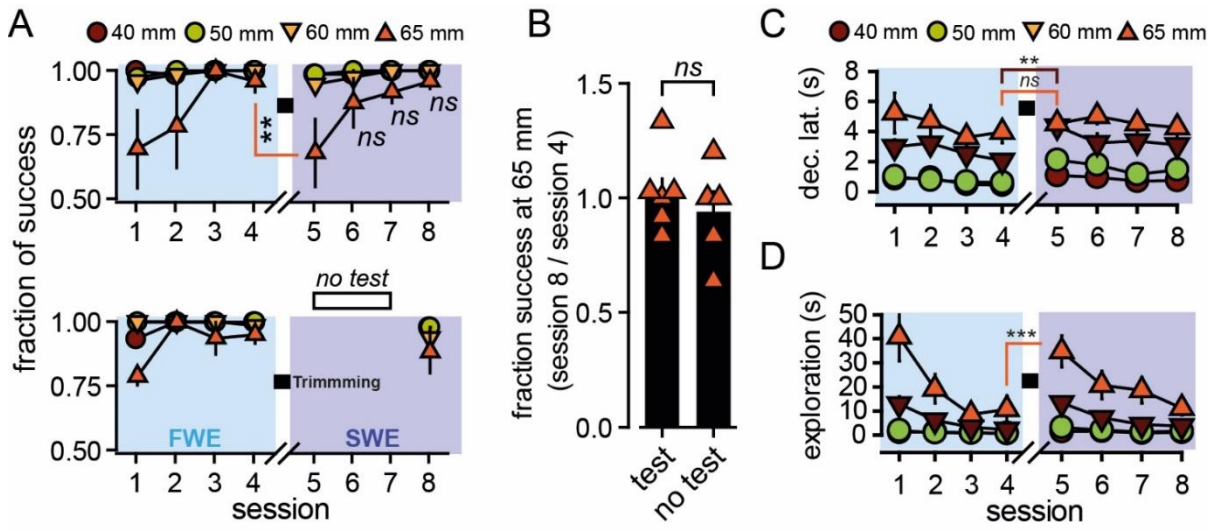

Fig. 44) Map plasticity compensates a learned whisker-dependent behavior. (A) (*top*), Averaged (± sem) fraction of gap-crossing success for different gap distances, in non-injected mice. Bottom, tests in session 5 to 7 were omitted to assess the role of learning during SWE. **B)** Mean (± sem) fraction of success in the final session (normalized to session 4 before SWE) at a distance of 65 mm for mice that are tested every day (test) and for mice that are not tested in sessions 5 to 7 (no test). Triangles, individual mice. **C)** Same than (A) but for decision latency (in seconds) and **(D)** total GD exploration time. All the values and statistics represented in table 1.

N. LTP-driven cortical remapping facilitates the recovery of a learned behavior

If indeed LTP is the driving force for the SWE-mediated recovery of tactile perception, then behavioral performance should be affected by our chronic AMPAR cross-linking. To test this hypothesizes, we trained FWE until reaching expertise, followed by SWE while chronically inject either anti-GluA2 or anti-GFP (**fig. 45A**). We aimed to block synaptic LTP throughout all the recording sessions, and determine if this impair behavioral recovery after SWE. In parallel with the effects of IgGs on synaptic strength and RWS-LTP in SWE mice (**Fig. 41A**), gap-crossing performance of anti-GluA2 IgGs-injected mice decreased more (session5: -61.8 ± 12% vs. -22.6 ± 6.7%, p=0.016) and recovered significantly slower as compared to anti-GFP injected mice (**Fig. 45B-D**). Nevertheless, final success rates were similar between both groups (0.82 ± 0.09 vs. 0.72 ± 0.14; p=0.805) (Fig. 46D), which might reflect barrel cortex-independent behavioral strategies and/or the existence of additional synaptic mechanisms that preserve a minimal but slow capacity for cortical remapping[248,249]. We also quantified the chronic IgGs effect on both the decision latency (**fig. 46A**), and total exploration time (**fig. 46B**). Both parameters were affected by SWE in a similar way than control subjects (no injection, **fig.46C and D**). However, no differences were found between chronic anti-GluA2 and anti-GFP injection (**fig.46B-C** and **46E-F**). Nevertheless, it should be noted a trend towards increased explorations times for anti-GluA2 condition (**fig. 46F**). This suggest that the effect of LTP blockage is due to alterations on whisker perception, and not caused by impairments on animal's decision making. Additionally, as all the recorded parameters at GD=40 and 50 mm are not affected by antibody injection, the reported effect on success rate are not caused by non-related effects (e.g., impaired locomotion). Altogether, these data revealed an unexpected and complex relationship between synaptic LTP, map plasticity, and recovery of tactile perception after whisker trimming. While LTP is undeniably associated with the initial recovery phases after SWE, their action is not exclusive, and can be compensated by other synaptic mechanisms (see discussion). Additionally, this work also demonstrates that perturbations of AMPAR trafficking are associated with impairments on whisker perception.

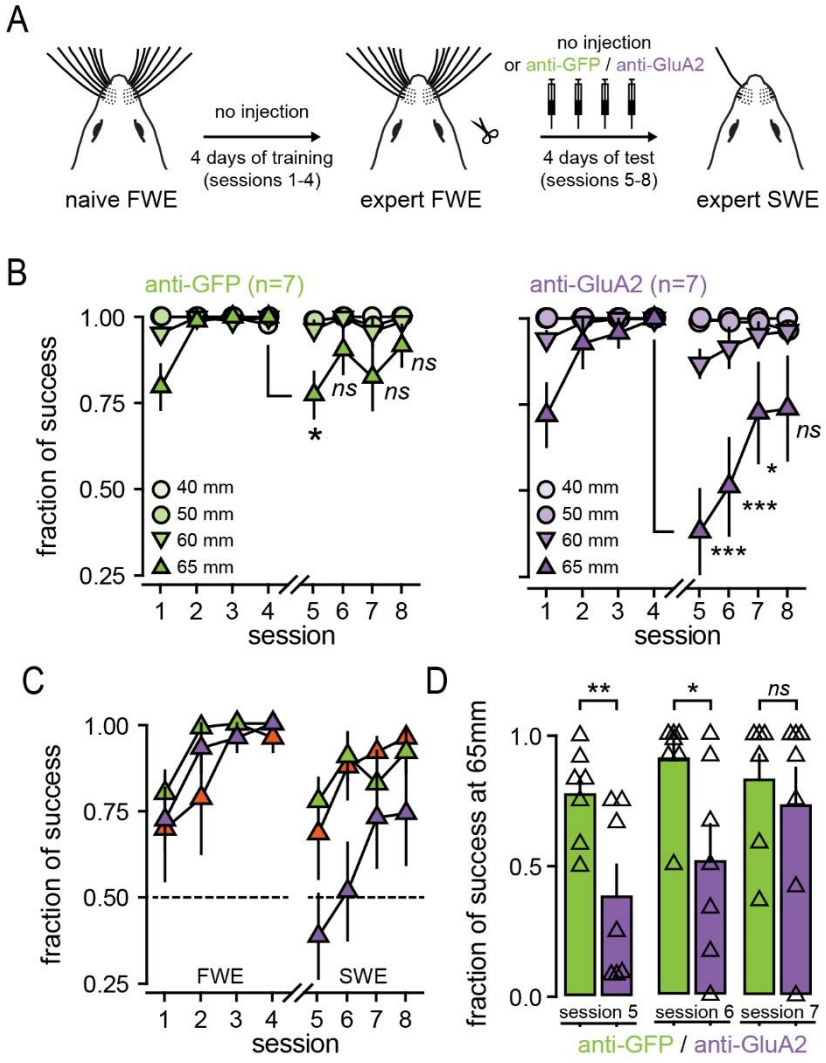

Fig. 45) LTP facilitates the recovery of altered whisker-dependent behaviors during the early phases of SWE. A) Schematic of the time-course regarding the behavior, the trimming of the whiskers and IgGs injections. Mice learn to reach the rewarding platform (4 consecutive days) before SWE is induced during which anti-GFP or anti-GluA2 IgGs are injected through implanted cannula twice a day (before and after each behavioral session). **B)** Averaged (± sem) fraction of gap-crossing success for different gap distances, in anti-GFP (left) and anti-GLuA2 (right) injected mice. **C)** Averaged (± sem) fraction of gap-crossing success at a distance of 65 mm, in non-injected (orange), anti-GFP (green) and anti-GLuA2 (purple) injected mice. **D)** Mean (± sem) fraction of success at a distance of 65 mm after expertise in FWE mice and during SWE. Triangles, individual mice. All the values and statistics represented in Table 1.

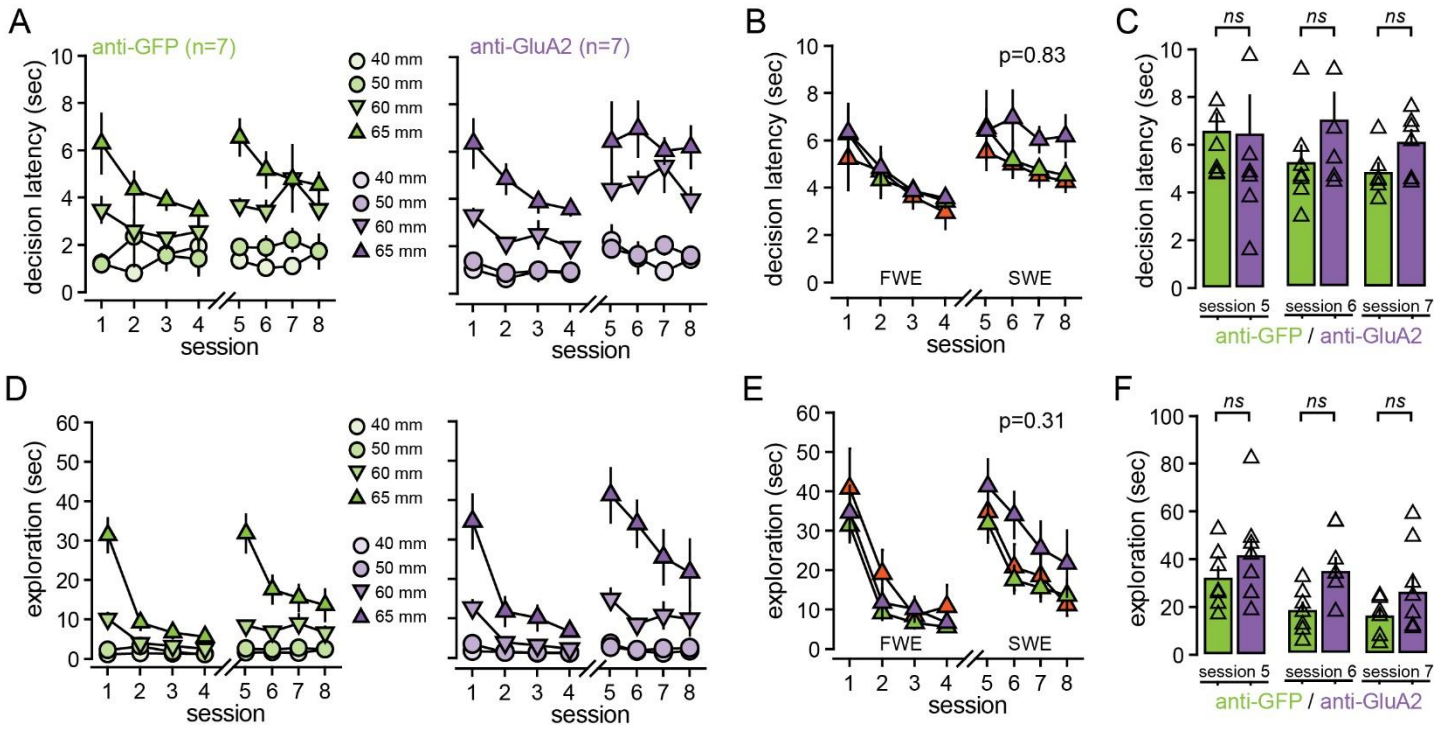

Fig. 46) LTP-driven map plasticity does not alter the decision latency, neither GD exploration. A) Averaged (± sem) fraction of gap-crossing decision latencies for different gap distances, in anti-GFP (*left*) and anti-GLuA2 (*right*) injected mice. **B)** Averaged (± sem) time of decision latency (in seconds) at a distance of 65 mm, in non-injected (orange), anti-GFP (green) and anti-GLuA2 (purple) injected mice. **C)** Mean (± sem) decision latency at a distance of 65 mm after expertise in fwe mice and during swe. Triangles, individual mice. **D and E)** Same than (A B) but for total GD exploration time (in seconds). **F)** Same than (C) but for total GD exploration time (in sec). All the values and statistics represented in Table 1.

Discussion

Neuronal receptive fields in the cerebral cortex change throughout life due to sensory experience or after brain injury[54]. The single-whisker experience (SWE) paradigm in rodents helped to better understand the synaptic mechanisms underlying this experience-dependent plasticity. Indirect evidences suggest that cortical remapping might rely on the activity-dependent alterations of pre-existing excitatory synapses[54,169,174,183,187,252,375]. Here, we combined *in vivo* whole-cell recordings with 2-Photon imaging on the mouse somatosensory cortex to demonstrate a direct implication of LTP in SWE. It has been described that rhythmic whisker stimulation potentiates cortical synapses (RWS-LTP) *in vivo*[176]. Our data demonstrates that this potentiation is occluded by SWE, suggesting that cortical synapses are already potentiated after this trimming protocol. This is translated into an augmented fraction of whisker-evoked spiking neurons in the spared barrel. To better understand the implications of LTP in cortical remapping, we developed a tool to block AMPAR synaptic recruitment *in vivo* using extracellular antibodies. Hippocampal NMDAR-LTP has been extensively studied in *ex vivo* preparations, and cellular models, over the last three decades[42]. Despite successful attempts to induce sensory input-mediated LTP *in vivo,* we currently know very little about their molecular mechanisms of expression[176,202,203]. Elegant work from Huganir's lab raised the possibility that a similar dependence of an increased content of synaptic AMPARs might also underlie these physiological forms of LTP. Here, we demonstrated that the synaptic recruitment of AMPARs is indeed required for RWS-LTP expression. In agreement, our AMPAR cross-linking approach efficiently blocked the expression of this LTP, without affecting the NMDAR-dependent induction mechanism, neither the cellular, nor the circuitry fundamental properties. This defines AMPAR cross-linking as a good tool to manipulate synaptic plasticity in alive, behaving animals. As a consequence, we decided to use it in a chronic way, blocking LTP during SWE (X-SWE anti-GluA2), to understand the relationship between this synaptic mechanism, and map plasticity. We found that X-SWE anti-GluA2 efficiently reverts the increased fraction of whisker-evoked somatic spikes seen after cortical remapping. This is translated into a reversion of RWS-LTP occlusion in SWE-subjected mice, suggesting that LTP occurs nearly-immediately following partial sensory deafferentation, shifting neuronal responses tuning to the spared input. If this compensatory mechanism is blocked by X-SWE anti-GluA2, important behavioral impairments in a whisker-dependent task are seen in the initial phases of SWE. This revealed an unexpected role for synaptic LTP in injury-induced circuit remapping, and recovery of sensorial perception after loss of sensorial inputs. To better discuss the major findings of this work, I will divide this section in three major parts, from a synaptic, circuit, and behavioral standpoint.

I. AMPAR cross-linking blocks the expression, but not the induction of RWS-LTP, without affecting inhibitory microcircuits

This work provides a major breakthrough by manipulating LTP *in vivo*, induced by sensory relevant stimuli, with implications for cortical remapping and whisker-mediated perception. With this, we aimed to bridge synapses, circuits, and animal behavior, to define a physiological meaning for LTP. This was allowed by the blockage of AMPAR lateral mobility by extracellular antibodies cross-linking. We did so, by stereotaxic injections of anti-GluA2 antibodies in the barrel cortex, preferentially targeting L2/3 pyramidal neurons. We discern excitatory from inhibitory interneurons based on cell-intrinsic electrophysiological signatures (e.g., spiking patterns). Antibody application by itself had a limited (if existent) cytotoxic effects, as indicated by unaltered cell-intrinsic excitability (fig. 34B), and circuitry spontaneous activity (fig. 34D). Additionally, AMPAR cross-linking did not altered whisker-evoked PSPs, as supported by an unchanged inhibitory drive (fig. 35B and C), and basal excitatory neurotransmission (fig.35D, 37D and 37E). The only reported effect for the acute (fig. 37C), and chronic *(see below)* AMPAR cross-linking, was a remarkable blockage of LTP expression. Therefore, our cross-linking approach is specifically blocking LTP *in vivo*, without affecting its NMDAR-dependent induction mechanisms. This is supported by unchanged NMDAR dendritic plateau potentials, recorded either by electrophysiological (fig. 38), and imaging approaches (fig. 36). The effect on RWS-LTP is likely due to postsynaptic AMPARs, as revealed by increased frequency-dependent short-term depression in L2/3 synapses (see section XVIII).These results are supported by previous imaging data (see[177]), and *in vitro* electrophysiological recordings (see[187]), indicating an AMPAR-driven LTP-mediated potentiation on L2/3 synapses after sensorial experience. In the next sections, I will discuss some of the limitations, and open-questions raised by the use of antibody-based GluA2 cross-linking to manipulate LTP *in vivo*.

II. Nonspecific effects of the use of antibodies for AMPAR cross-linking *in vivo*

Virtually all the experiments performed in this work exploited the use of an anti-GluA2 antibody to block AMPAR lateral mobility *in vivo*. Unfortunately, this approach might have other impairments on AMPAR signaling, more complex than blocking receptor lateral mobility. For instance, pathogenic human anti-GluA2 auto-antibodies are reported to strongly alter the organization of synaptic AMPARs on mice dissociated neuronal cultures[376]. Chronic incubation with this pathogenic IgGs, resulted in a subunit exchange of synaptic AMPARs, as seen by antibody-induced increase expression of CP-AMPARs. Importantly, this effect might be restricted to the pathogenic antibodies, since no alteration on AMPAR trafficking or signaling are described to occur upon incubation with commercially available AMPAR antibodies[377]. It is worth to mention that the antibodies used in our study are non-pathogenic and likely do not alter normal AMPAR function. As discussed, this is supported by a lack of IgGs effects on both basal synaptic transmission, and whisker-evoked neuronal responses. Nevertheless, the existing evidences for side-effects induced by IgGs application, raise the necessity of performing additional experiments

to further support our main-findings. It would be of great interest to determine if, under our experimental conditions, anti-GluA2 antibody application increases CP-AMPARs in L2/3 synapses of the barrel cortex. This could be evaluated by recording changes on rectification indexes before/after receptor cross-linking (as performed here[332]), without any whisker manipulation. Unfortunately, the spatial attenuation of voltage clamp *in vivo,* and the polysynaptic nature of whisker-evoked PSPs, do not allow to efficiently record CP-AMPARs-induced changes of rectification indexes in distal L2/3 synapses. This limitation could be solved by injecting anti-GluA2 antibodies *in vivo,* and record rectification indexes of L2/3 pyramidal neurons *in vitro,* in a similar experimental set-up than the one described by Williams and Holtmaat[92]. Additionally, it would be important to perform immunohistochemistry experiments, in order to detect signs of inflammation (e.g., TNFα) induced by our acute or chronic antibody injection protocols. This would allow us to rule-out any no-specfic effect on L2/3 plasticity mechanisms caused by neuroinflammation. As we can induce RWS-LTP on X-SWE anti-GluA2 to similar levels than FWE-subjected mice, this is likely not the case (fig. 42A).

III. Towards a novel AMPAR cross-linking approach *in vivo*

Despite the important information provided by the use of extracellular antibodies for AMPAR cross-linking, it is important to mention that this tool has important limitations to study synaptic plasticity *in vivo*. The first drawback is the lack of cellular resolution for the cross-linking effect. Indeed, the anti-GluA2 antibody here applied, recognizes, and cross-links all the endogenous GluA2-containing AMPARs, independently of the cell-type. Consequently, indirect, and unspecific effects than the blockage of synaptic LTP might co-exist. For instance, RWS-LTP expression is believed to strongly depend on a disinhibitory microcircuit, where inhibitory drive into SST-expressing interneurons permits the formation of NMDAR dendritic spikes in L2/3 dendrites[92]. This explains why we made an important effort to determine if AMPAR cross-linking alters inhibitory, and basal excitatory neurotransmission. Again, the only effect found was a selective impairment of RWS-LTP expression. Nevertheless, it is important to bear in mind that this is the first generation of this tool, and improvements are required to better fit the needs of an *in vivo* application. For this reason, Choquet's lab is making significant efforts in developing new tools for AMPAR cross-linking, with better spatiotemporal resolution. Possibly one of the most exciting, and more advanced approach is the development of an AP-GluA2 *KI* mice (data not shown). This will allow to manipulate synaptic LTP in well-defined cell types, by cross-linking AP-AMPARs with exogenous NeutrAvidin (see reference for methodological details[332]). In a more preliminary phase of development are the light-sensitive cross-linkers. They explore protein domains (e.g., DRONPA) that, under illumination with the proper wavelength, are able to cross-link AMPARs. Such technique will allow to define when, and where (at a barrel-resolution) AMPARs are cross-linked, and to control which synapses are potentiated. This spatiotemporal resolution will be essential to better understand how LTP underlies cortical remapping, in a time-and-barrel specific manner.

Despite the aforementioned limitations, it is incontestable that AMPAR cross-linking provided important information about the molecular mechanisms of *in vivo* LTP. In the next sections, I will discuss the main-findings obtained with this approach.

IV. AMPAR synaptic recruitment after sensory-evoked LTP

Zhang and collaborators demonstrated that prolonged whisker stimulation drives the insertion of SEP-GluA1 in L2/3 synapses of the barrel cortex[177]. Here, by combining *in vivo* AMPAR cross-linking with whole-cell patch clamp recordings, we confirmed a similar accumulation of AMPARs after RWS. However, under our experimental conditions, we efficiently blocked RWS-LTP by impairing GluA2 subunit lateral mobility. How can both findings be conciliated? Is there any subunit-specificity for the synaptic recruitment of AMPARs during RWS-LTP?

A pertinent point raised by Zhang's work is whether the reported synaptic accumulation of SEP-GluA1, results from the recruitment of GluA2/A1 heteromers or GluA1/A1 homomers (CP-AMPARs)[177]. The traditional view of AMPAR trafficking during synaptic plasticity states that GluA1 is required for LTP, while GluA2 endocytosis is necessary for LTD[42,279,283]. When different subunits are assembled in heteromers, the trafficking rules are dictated by the long-tailed subunits. As an extension, NMDAR-LTP in the adult hippocampus is classically described to depend on the synaptic incorporation of GluA2/GluA1 heteromers, whereas GluA2/A3-containing AMPARs are recruited in a constitutive manner. In a more extreme, and highly-debated model, CP-AMPARs have been described to be recruited transiently upon LTP induction, to prime this mechanism due to their Ca^{2+} permeability[337]. The idea of an obligational recruitment of CP-AMPARs during hippocampal NMDAR-LTP has been supported by several different studies[335–338]. However, these findings are questionable, since several other evidences suggest that this requirement is not compulsory[339,340].

Does RWS-LTP require CP-AMPARs synaptic accumulation? This is a pertinent question not only for the complete understanding of the molecular mechanisms governing LTP *in vivo*, but also for its role during map plasticity (see section IX). The initial *in vitro* study exploring how AMPARs underlie LTP in L2/3 of the barrel cortex, defined an important contribution of CP-AMPARs[178]. However, our and Zhang's work in more physiological conditions, came to question these findings[177]. As Zhang and collaborators overexpressed SEP-GuA1 along with non-tagged GluA2, there's a strong possibility that the reported results underlie SEP-GluA1/GluA2 synaptic accumulation[177]. Unfortunately, as this elegant work took advantage of overexpressed receptors, it makes it hard to clearly define any subunit-specific dependence for RWS-LTP. Our findings indicate that the blockage of endogenous GluA2-containing AMPARs is sufficient to block the induction of this form of LTP. This is in agreement with the transcriptomic and proteomic analyzes in the barrel cortex, defining GluA2/A1 and GluA2/A3 as the major subunits composition (see section 4.4). As a consequence, it is likely that both studies, by exploring different approaches, report an accumulation of GluA2/A1 synaptic accumulation during RWS-LTP. However, based

on the available evidences, we cannot rule out the recruitment of CP-AMPARs as well, particularly if it is transient. One could test this, by recapitulating the whole-cell patch clamp recordings here performed, while acutely cross-linking the GluA1 subunit. It is worth it to mention that, as this would block lateral mobility of both GluA2/A1-containing and CP-AMPARs, it would make it difficult to interpret the obtained results. Another possibility, and likely more straightforward, would be to induce RWS in the presence of specific antagonists of CP-AMPARs (e.g., IEM 1925), and record if RWS-LTP occurs under this conditions[378]. Alternatively, we could also record *in vitro* rectification indexes after *in vivo* RWS, in a similar way than the one described on section II. Independently of this debate, our study places AMPAR synaptic recruitment as a central mechanism for *in vivo* LTP. As discussed, if this mechanism is destabilized by our AMPAR cross-linking approach, important impairments at the synaptic, circuit, and behavioral level are seen. We hope that our work will inspire several others that, by manipulating AMPAR trafficking at different levels, will describe the precise sequence of events driving AMPARs to synapses after sensorial stimulation. In the next section, I will speculate some possibilities on how this might occur, and put forward some experimental approaches to test them.

V. Defining the route: which molecular mechanisms orchestrate AMPAR trafficking to L2/3 synapses during RWS-LTP?

The relationship between AMPAR lateral mobility and LTP expression is complex (see section 4.3). While lateral diffusion *per se* supports the early phase of hippocampal NMDAR-LTP, its late component importantly requires AMPAR exocytosis[332]. Are the same requirements applied in the barrel cortex, during sensory-evoked LTP? Unfortunately, our approach does not allow to answer this question in a conclusive manner. Antibody stereotaxic injection impregnates the brain tissue with anti-GluA2 IgGs throughout the electrophysiological recordings area (fig. 34A). As a consequence, the lateral mobility of both pre-existing membrane AMPARs, and of newly exocytosed receptors after RWS, is impaired. This makes it hard to know if, similarly to hippocampal RWS-LTP, AMPAR synaptic accumulation during RWS-LTP requires both AMPAR lateral diffusion and exocytosis. As illustrated in fig. 42, neurons where RWS induced synaptic LTP, have a difference in PSPpeak amplitude of around 20%. This is in contrast with what is normally reported in the hippocampus where, electrically high-frequency stimulation, induces a stronger potentiation (50-100%, depending on the protocol)[255,332,379]. Therefore, it is plausible that these conditions have different requirements, and rules to accumulate synaptic AMPARs after LTP induction. This possibility makes even more sense if considering the computational requirements of both brain regions. While in the hippocampus NMDAR-LTP is required to encode stable and long-lasting memories, plasticity in the barrel cortex, is likely more labile, to adapt the moment-to-moment variations on sensorial experience. Therefore, it is conceivable that a pool of pre-existing extrasynaptic receptors might fuel entirely RWS-LTP, without requiring exocytosis. On the other hand, imaging evidences from Zhang's work, describe an enrichment of SEP-GluA1 in L2/3 distal dendrites 1/2h after whisker stimulation[177]. This is in agreement with AMPAR exocytosis occurring in extrasynaptic regions, from where it can diffuse

to synaptic regions, and further potentiate whisker-evoked PSPs. Does a similar dendritic enrichment of AMPARs also occur during our experimental conditions? It is difficult to know, due to two major reasons. First, while Zhang and collaborators used a single-whisker stimulation at 10 Hz for one hour, we exploited a similar frequency but for one minute. This variation on the protocol of whisker stimulation, might induce different plasticity mechanisms in L2/3 synapses (see section 3.1). Second, while chronic 2-Photon imaging used on Zhang's work allowed to image the same dendritic segment up to 48h after RWS, we are restricted by technical limitations to a 15-minutes time window. This makes it very hard to conciliate, and extrapolate results between studies. To determine if RWS-LTP, under our experimental conditions, depends on AMPAR exocytosis, would require to record L2/3 pyramidal neurons with an intracellular solution containing tetanus toxin (TeTx) (as performed here[332]). This neurotoxin blocks specifically synaptic vesicles exocytosis, and when restricted to the postsynaptic membrane, impairs NMDAR-LTP without affecting presynaptic glutamate release[255,332,380]. This would provide a definitive proof-of-concept that RWS-LTP requires a multi-step trafficking mechanism, from the recruitment of pre-existing AMPARs by lateral mobility, to the exocytosis of new receptors.

We are just now appreciating the advantage of using the barrel cortex as a model to study the molecular mechanisms of synaptic LTP in physiological conditions. As a consequence, the current knowledge on how RWS-LTP is expressed at the single-cell level is still unknown. More studies are thus required to understand this form of sensory-evoked LTP. I believe that modern proteomic approaches will be fundamental to precise describe the AMPAR proteome with an unprecedented layer- and cellular-resolution. This information, coupled with the revolution of the CRISP-Cas9 technology, will allow to dissect piece-by-piece the complex biochemical chain of proteins, regulating the different steps of AMPAR trafficking (see[381]). For example, NMDAR-dependent activation of CamKII has been reported to trigger phosphorylation of stargazin, which in turn traps AMPARs in hippocampal synapses through increased interactions with PSD-95[302,320]. It would be of great interest to express phosphorylation mutants of the major AMPAR auxiliary subunit in the barrel cortex, and further test its impact on dendritic plateau potentials, and RWS-LTP. Such technological development will permit more physiological approaches, aiming to better understand the importance of LTP at the synaptic, circuit, and behavior level. Hopefully, these advances will overcome some important limitations of our work, and eventually recapitulate some of our findings. I consider that the next decade of the AMPAR-centric research will be exciting, and profoundly alter our current definition of synaptic LTP, with a special focus of studies at the circuit-level.

VI. SWE-mediated increase in whisker-evoked somatic spikes is driven by synaptic LTP

We exploited chronic AMPAR cross-linking to block synaptic LTP during SWE (X-SWE anti-GluA2). If indeed this mechanism increases synaptic gains, and whisker-evoked somatic spikes during map plasticity, then these phenotypes should be reverted by X-SWE. If this is true, then we should be able to induce RWS-LTP on SWE, after GluA2 IgGs washout. We found that

X-SWE anti-GluA2 reduces the AMPAR-mediated component of whisker-evoked responses to similiar levels than FWE (fig. 36B). This reduction on the synapse gain, is accompanied by a reduction of the averaged number of spikes per whisker-defletion (fig. 40D). As a consequence, there is a reverstion of RWS-LTP occlusion after X-SWE (fig. 41A). We believe that this is a desoclussion, since the AMPAR-component of whisker-evoked PSPs are smaller on X-SWE compared to control conditions before RWS (fig. 41B). These findings confirms that LTP-driven map plasticity is indeed one of the synaptic mechanisms re-tunning neuronal responses, and increased spared whisker representation after SWE.

Interestingly, our X-SWE approach did not alter the fraction of spiking neurons (fig. 39C). This suggests that other mechanisms than synaptic LTP might be recruited to the circuit-wide alterations during cortical remapping (see below). None of these effects are due to deleterious effect of the chronic antibody injections, since no alterations on NMDAR plateau strengths are seen across conditions (fig. 41B). This suggests that basic circuit, and cellular properties are preserved after X-SWE. To further confirm this, we are currently performing experiments to record whisker-evoked excitatory and inhibitory conductances after chronic antibody applicaton (data not shown).

In the next sections, I will describe the hypothetical mechanisms and order of events that translate whisker-trimming, into increased neuronal responses to the spared whisker. This ultimately culminates with an increased number of spiking cells, and shifting whisker computation from sub- to suprathreshold. I will also propose alternative mechanisms than synaptic LTP, that might well co-exist to efficiently drive cortical alterations after SWE.

VII. The “chicken-egg” conundrum of the mechanisms underlying SWE-driven map plasticity in the spared barrel

In this study we confirmed a long-lasting hypothesis, by demonstrating a causal relationship between synaptic LTP, and cortical remapping. This was extrapolated from the occlusion of RWS-LTP, suggesting that L2/3 synapses are somehow potentiated after SWE. This is translated into response potentiation of the spared whisker, and increased whisker-evoked somatic spikes. It is worth it to mention that we exploited RWS-LTP as a readout for the synaptic gain of L2/3, after two/three days of SWE. Therefore, we cannot conclude if LTP is either a cause or a consequence of cortical remapping. It is important to bear in mind that a three-days interval between whisker trimming and recordings is important, since alterations on L2/3 firing rates are seen 24h after SWE[188]. It is conceivable that during this time window, multiple synaptic mechanisms do occur, in a complex temporal progression, across different cell types, to saturate L2/3 synaptic gains. Therefore, the ultimate question is to understand the precise sequence of events translating whisker trimming in the increased neuronal excitability, and RWS-LTP.

Here, I will focus my attention on the mechanisms occurring soon after SWE in the spared barrel. How these cortical alterations are propagated to the neighboring barrels is hypothesized on

section XI. During FWE, L2/3 circuits are organized in a way that the stronger responses are evoked by the principal whisker (see section 2.5). As elegantly described in Holtmaat's work, synapses responding to the principal whisker are selected from a background of "surrounding ones", by NMDAR-dependent LTP mechanisms[176]. However, surrounding-whisker responses and RWS-LTP can also co-exist in the principal barrel[176,208]. This surrounding-potentiation occurs in a different subset of synapses, and has a smaller magnitude, and higher latencies that principal-whisker evoked ones[121,122,176]. These differences are dictated by circuit-wiring properties (e.g., VPM and POm inputs), and is essential to preserve whisker-to-barrels somatotopy. During FWE, both types of synapses are sensitive to RWS-LTP, as indicated by our (section I) and Holtmaat's work[176]. At the structural level, this is accompanied by a remarkable stability of L2/3 dendritic spines[53]. Which mechanism underlies such stability, by keeping synaptic weights stable, and far from saturation? I believe that the response to this question lies on the inhibitory microcircuits. As elegantly described by Williams and Holtmaat, RWS-LTP is under the tight-regulation of a feedforward disinhibitory microcircuit[92]. It is possible that this dendritic inhibitory drive sets how" and "where" RWS-LTP occurs, fixing synaptic weights to a steady-state level. In combination with a strong somatic inhibition, these mechanisms renders L2/3 firing rates during FWE incredible sparse[91]. This explains why inhibition is defined as a key mechanism to regulate the integration of excitatory inputs at the dendritic level, and to sharpen the neuronal receptive fields (see section 3.2).

Not surprisingly, the tight balance between excitation and inhibition is seriously compromised after whisker trimming[208,210,211]. Alterations on dendritic and somatic inhibition are also reported to occur in the visual cortex during map plasticity[214,218,219]. It is likely that disinhibition exacerbates spared whisker representation, and increases the number of spiking neurons in the barrel cortex. Below, I propose two independent, but related mechanisms for the increased spared whisker neuronal responses on its principal barrel:

Excitatory-centric. Likely the most straightforward hypothesis lies on the excitatory networks itself. SWE imposes to the animal a complete environmental exploration by the remaining, spared-whisker. Here, I consider environmental exploration as a normal sensory experience, without environmental enrichment (see[171]). Under this conditions, animals overuse the spared whisker, causing a persistent potentiation of L2/3 synapses. This can be paralleled, to some extent, to the stimulation protocol used by Zhang and collaborators, where they reported an accumulation of AMPARs in the same synapses[177]. However, a similar protocol of passive whisker stimulation, with all the sensorial inputs preserved, drives a different form of map plasticity than the one reported in our work[170]. Therefore, some other mechanism might exist to explain the spared column alterations after SWE.

Inhibitory-centric. Besides the occlusion of RWS-LTP, we also reported alteration of cell excitability upon SWE. After whisker-trimming, the input/output function of individual neurons is changed, as indicated by the reduced threshold for spiking generation (fig. 33A). These alterations can certainly be explained by cell-intrinsic mechanisms (see[200], and discussion below),

but also by a reduction in the inhibitory drive. In agreement, perisomatic-inhibitory drive on PV-positive basket cells into L2/3 pyramidal neurons has been described to decrease after whisker trimming[210]. This reduction of somatic inhibitory drive can be a good explanation for the alteration of spiking threshold, and increased somatic firing rate (fig. 30 and fig. 31B) (see below). Additionally, we also found possible evidences that SWE reduced inhibitory gating in L2/3 distal dendrites, as indicated by the increased membrane depolarization by sRWS (fig. 33C) (see VII). Therefore, it is plausible that disinhibition in the spared barrel, creates permissive conditions where L2/3 pyramidal synapses can be potentiated to a saturation level. It is tempting to hypothesize that this is mediated by alterations of the inhibitory gating reported by Williams and Holtmaat[92]. Indeed, a strong reduction of SST interneurons inputs into L2/3 distal dendrites, might explain very-well the increased whisker-evoked depolarization reported on fig. 33E. This might create conditions where whisker-evoked NMDAR-spikes are stronger and likely more reliable. In combination with a reduction of inhibitory inputs at the synaptic level (see[217]), this might explain the occlusion of RWS-LTP during SWE. This is in agreement with studies in the visual cortex, where reduction in dendritic inhibition has been reported to occur after monocular deprivation[218,219]. This reduction was fast, and occurred before than any change on dendritic spines, suggesting that disinhibition might precede any alteration in excitatory neurons.

Both models assume that synaptic LTP and alterations of inhibitory inputs into L2/3 pyramidal neurons are the major driving forces for SWE-induced cortical remapping. However, Mahon and Charpier have reported increased firing probability on whisker-evoked PSPs, without alterations on L5 synaptic strength[200]. They proposed that cell intrinsic excitability changes the efficacy of sensory processing (i.e., increased firing rates), without depending on any synaptic modifications. This is not supported by our data, where we demonstrated that SWE drives RWS-LTP occlusion (section D). However, we cannot rule-out that under our experimental conditions, alterations of cell-intrinsic excitability might also co-exist with the LTP-driven saturation of L2/3 synaptic gains. Indeed, the decreased spiking threshold after SWE, that I interpreted as a result of decreased inhibition, can also be explained by increased cellular excitability (as reported here[200]). It would be interesting to directly record different populations of interneurons during SWE (as performed here[90]), to determine which mechanism alters the input/output function of L2/3 pyramidal neurons. We are also currently refining the analysis of our electrophysiological data recorded from SWE-subjected mice (e.g., spiking probability during UP state) to determine if increased cellular excitability occurs under our experimental conditions. Even if this might-well be the case, this cell intrinsic mechanism does not explain all the synaptic phenotypes that we recorded throughout our experiments. As we can revert SWE-induced saturations of L2/3 synapses by our chronic AMPAR cross-linking, these alterations are likely preferentially driven by synaptic plasticity mechanisms.

The collaborative effect of these models, is an appealing possibility to explain the increased neuronal responses to spared whisker-deflection. Indeed, the shift of whisker-computation can be explained by local disinhibition, accompanied by a whisker-overuse induced LTP in the “spared

synapses". However, long-lasting structural effect of SWE might also co-exist. Indeed, increased whisker-evoked somatic spikes might dependent on the formation of additional synapses computing the spared input. We are currently analyzing whisker-evoked PSPs during SWE to determine if indeed this is the case. Nevertheless, this possibility fits very-well with the recruitment and stabilization of new spines, described to occur after whisker trimming[53]. These alterations are accompanied by a retraction of inhibitory axons, that possibly facilitate the formation of new synapses in L2/3 dendrites (see also fig. 14)[226]. These recently-formed synapses can eventually be recruited to compute the spared whisker by Hebbian-like mechanisms[54]. I believe that the combination of saturation of pre-existing synapses, and the recruitment of additional ones, reduces the threshold for whisking-evoke spike generation, with the concomitant increase of spared whisker cortical representation. Important to bear in mind that, this LTP-driven increased neuronal responses to the spared whisker only occur possibly due to local disinhibition. It would be of great interest to determine whether our AMPAR cross-linking approach can block the recruitment, and stabilization of new "spared synapses". If indeed this is the case, then LTP is the mechanism stabilizing the new synapses formed during cortical remapping.

In the same way that two are needed for tango, the recruitment of additional synapses after SWE should be accompanied by alterations on presynaptic structures. As a consequence, SWE should alter axonal dynamics of both intracortical, and thalamocortical projections. While the fist is described to occur (see[225]), the latter is still completely enigmatic. Classically, in adult animals it is defined that the effects of SWE at this time-scale is restricted to L2/3 microcircuit, with no effects in subcortical structures[231,232]. However, these studies were based on the average population analysis, likely overlooking subtle effect of map plasticity on VPM or POm projections into the barrel cortex. POm projections are of great importance, since they are well-place to propagate the effect of the spared whisker to the entire barrel field[166]. Moreover, it can also have important implication on animal behavior, during whisker-mediated tactile perception. Therefore, it would be valuable to perform *in vivo* 2-Photon calcium imaging of VPM or POm boutons before and after SWE. This approach would provide decisive information to fill one of the biggest gap of knowledge on the cortical remapping field.

In conclusion, cortical remapping during SWE might require the complex spatiotemporal interplay between different synaptic mechanisms occurring in distinct cell types. This is likely mediated by early-modifications of pre-existing excitatory, and inhibitory synapses, followed by long-lasting recruitment of additional synapses. In combination, these mechanisms built-up an exacerbation of synapses computing the spared whisker in L2/3 synapses. This results in a potentiation of the spared whisker neuronal responses, with the concomitant increase of L2/3 pyramidal neurons firing rates. This ultimately explains the shift on whisker computation in the spared barrel, from sub- to suprathreshold. In the next section, I will discuss the possibility for the co-existence of other excitatory postsynaptic mechanisms than LTP. Indeed, the proposed LTP-driven theory for cortical remapping during SWE might be an oversimplified view of the complete mechanism.

VIII. Is synaptic LTP the sole mechanisms shaping L2/3 microcircuits in the spared barrel after SWE?

AMPAR lateral mobility not only underlies synaptic LTP, but all other synaptic mechanisms requiring alterations of AMPAR synaptic content. This includes its counteracting force, LTD, but also homeostatic plasticity (see chapter 4). Thus, the AMPAR cross-linking approach used in this study, is not RWS-LTP specific, affecting several other mechanisms. In a classical perspective, LTD is believed to drive a rapid depression of neuronal responses to the deprived input, while LTP slowly potentiates spared-input responses in both deprived and spared barrel column[54]. However, their action might not be mutual exclusive, and LTD might also participate in the potentiation of neuronal responses to the spared whisker. For instances, it has been showed in the auditory cortex that LTP induced by a well-defined pitch is matched by a heterosynaptic form of LTD of the neuronal responses to the original best frequency[195]. As barrel cortex L2/3 pyramidal neurons respond to both principal- and surrounding-whiskers, a similar mechanism might also exist during SWE. Indeed, LTP-driven potentiation of the spared whisker synapses, might be accompanied by a heterosynaptic LTD on "trimmed whisker synapses". If this is true, this would further differentiate spared whisker responses from the neighboring ones, helping to shift neuronal receptive fields. If this is true, then this form of LTD is also blocked by our AMPAR cross-linking approach. Alternatively, professor Feldman proposed a role for homeostatic plasticity on the potentiation of the neuronal responses to the spared input[54]. This might be a feedforward mechanism to further increase the initial LTP-driven alterations. Additionally, results on the GC behavioral task, also raised the existence of metaplasticity effects co-existing with synaptic LTP (in agreement with[252]). How can we confirm that indeed our results are LTP-specific, and not due to any other synaptic mechanism? We could record surrounding-whisker evoked PSPs after SWE to understand if they are reduced as compared to FWE. If this is true, then synaptic LTD likely co-exists to RWS-LTP in the spared barrel to remodel L2/3 responses. Alternatively, we could address the efficacy of inducing STD-LTD before and after whisker trimming. To address if homeostatic mechanisms are also involved, one could recapitulate the experiments performed by Makino and Malinow but in the alive animal[179]. We could image the AP-GluA2 *KI* mice with *in vivo* 2-Photon imaging to determine if AMPAR accumulation after SWE is either input-specific and LTP-mediated, or global homeostatic-like. These complementary approaches would refine, and complement the main finding of this study, where we reported LTP-driven GluA2-mediated cortical remapping during SWE. In the next section, I will discuss some of existing bibliography, refuting this GluA2-dependece for map plasticity, by describing CP-AMPARs accumulation in L2/3 synapses.

IX. Does SWE depend on the synaptic expression of CP-AMPARs?

Different studies have reported an obligatory recruitment of CP-AMPARs to L2/3 synapse, as a hallmark of the LTP-driven cortical remapping[178,189,252]. All of them took advantage of *in vitro* recordings in the barrel cortex, reporting alterations of rectification indexes after *in vivo* whisker trimming. Here, by chronically blocking lateral mobility of GluA2-containing AMPARs, we were able to block SWE-induced cortical remapping. The importance of GluA2 during map plasticity is corroborated by a study demonstrating increased mRNA levels of this subunit in the spared barrel[351]. How can we conciliate these discrepancies, and define a subunit-specific rule for AMPAR expression during map plasticity? I believe that this is explained by differences in the experimental pipeline. All the aforementioned studies used *ex vivo* preparations to record electrically-evoked L2/3 synaptic conductances. Here, we performed *in vivo* recordings, under more physiological conditions, evoking neuronal responses by passive whisker deflection. It is possible that the *ex vivo* slice preparation creates artificial conditions (e.g., altered oxygen conditions), that are permissive for an aberrant recruitment of CP-AMPARs. Considering the increased neuronal excitability after SWE, and the pathological expression of CP-AMPARs during traumatic brain injury, or seizures, it is possible that this is the case[382]. Alternatively, evoking neuronal responses by electrical stimulation might recruit synapses that are not normally used *in vivo*. Moreover, it is also likely that all the anatomical pathways recruited by whisker deflection, are not stimulated during *in vitro* recordings (see for example[189]).). Hence, it is required to elucidate if CP-AMPARs are indeed recruited to L2/3 spared synapses *in vivo*. In my opinion, due to their Ca^{2+} permeability, and possible cytotoxic effects, their expression must be regulated in a restricted manner. Therefore, I believe that is unlikely that there is a continuous expression of CP-AMPARs for several days, to sustain the synaptic effects of map plasticity. Unfortunately, due to technical reasons, we cannot record the alterations of rectification indexes in our *in vivo* whole-cell recordings. However, we could induce SWE, microdissect the spared barrel, and quantify the protein levels of all the GluA subunits (as performed here[383]). Alternatively, we could perform SWE while chronically image GluA2-containing AMPARs synaptic accumulation using *in vivo* 2-Photon imaging (e.g., on AP-GluA2 *KI* mice). An increased GluA2 content on L2/3 synapses after SWE would support our X-SWE anti-GluA2 data, and help to rule-out he role of CP-AMPARs during map plasticity.

In the next section, I will shift my attention away from synapses, and focus in the dendritic branch as the basic computational unit. I will discuss the exciting possibility that SWE, besides changing L2/3 synaptic gain, it also alters dendritic integration in the same neurons.

X. SWE increases synaptic gains, and changes dendritic computation

Throughout this project, we focused our attention on the synaptic underpinnings of map plasticity. However, we gathered some evidences that SWE might also alters the fundamental dendritic computation of whisker-evoked neuronal responses. For instance, RWS drives a strong postsynaptic depolarization, resulting from the temporal summation of NMDAR dendritic spikes all over the dendritic tree (fig. 33D). This depolarization is strongly increased after SWE (fig. 33E), without altering the average NMDAR plateau strength (fig.31D). While this can be explained by increased AMPAR-mediated responses, one can also suspect that a frequency-dependent disinhibitory mechanisms might also occur. The latter is supported by (1) the large variability of all recorded plateaus (sem, fig. 31D), and (2) the fact that the strongest plateau strength recorded for all the conditions, belongs to SWE-subjected mice (fig. 42C). This suggests that either the reliability, or the size of NMDAR dendritic spikes might also be increased after SWE. Even without any other experimental data, I would like to discuss the possible cause and consequence of this enhancement.

Inhibitory inputs can be directly made on dendrites, or even directly in dendritic spines[216,217]. SST-inhibitory inputs in L2/3 dendrites of the barrel cortex has been directly implicated in the orchestration of NMDAR-dendritic spikes[92]. Therefore, there are high chances that the disinhibition assumed to occur during SWE, also potentiates this dendritic mechanism. Importantly, enhanced NMDAR-drive can alternatively explain RWS-LTP occlusion after whisker trimming. Indeed, if the likelihood of driving, and the size of NMDAR spikes are increased, then surrounding synapses should be strongly potentiated. This can collaborate with the mechanisms discussed on section VII to alter L2/3 pyramidal neurons response tuning. Another striking possibility is that a global dendritic disinhibition might underlie the increased spikes recorded in the soma (fig. 30 and 31B). By definition, NMDAR dendritic spikes are a strong and localized depolarization, occurring in thin distal dendrites[49,258]. It is possible that, upon SWE, this dendritic depolarization can be pronounced to the point that it recruits other dendritic mechanisms (e.g. Ca^{2+} spike), and is propagated to the principal dendritic branch[384]. This could perfectly result in an electrophysiological signature very similar to a *bona fide* somatic spike, when recorded in the cell body. This raises the urgency to take advantage of *in vivo* 2-Photon dendritic calcium imaging to determine if indeed SWE dendritic integration of L2/3 pyramidal neurons.

XI. Is LTP-driven increased spared whisker representation in the principal barrel driving barrel expansion during SWE?

Throughout this work, we restricted our attention on how map plasticity alters spared whisker cortical representation on its principal barrel. However, SWE is characterized by a stereotyped barrel expansion, where neurons localized in surrounding barrels shift their responses towards the spared input[166]. How is this functional expansion mediated? Is the increased spared whisker representation in the principal barrel propagated to the surrounding ones? Is this responsible to shift deprived neurons responses towards the spared whisker? Unfortunately, a clear response to this important question still remains to be determined. However, I will discuss some anatomical and physiological evidences, and put forward a hypothesizes for SWE-driven barrel expansion.

Axonal projections and dendritic morphologies of L2/3 pyramidal neurons are remarkably complex[83,95]. These structures project several millimeters away from the soma, invading cortical domains of the surrounding barrels. Even during FWE, intracortical L2/3 axons are remarkably dynamic, with continuous structural modifications[223]. This suggests that L2/3 intracortical projections have a strong potential to be modulated by experience-dependent cortical plasticity. Not surprisingly, the density of horizontal projections from the spared pyramidal neurons into the deprived columns is increased after whisker trimming[225]. This is also accompanied by a retraction of inhibitory axons in the deprived barrel, likely disinhibiting excitatory cells as described in the visual cortex[218].This is agreement with previous studies demonstrating the extent of lateral inhibition is reduced by whisker deprivation[211]. Are these structural re-arrangements associated with alterations in L2/3 excitatory synaptic properties? During FWE, induction of STDP-LTP is restricted to the principal whisker-stimulation, as predicted by the one-to-one relationship between whiskers and barrels[208]. However, upon whisker trimming, there is a strong disinhibitory component that renders the circuit promiscuous, with STDP-LTP induced in the principal-barrel by surrounding-whisker stimulation. This suggests that horizontal excitatory projections between barrels, along with intra- and interbarrel inhibitory inputs are likely altered upon trimming-induced map plasticity. In agreement, local injuries on intracortical projections (e.g., septal regions) are able to dramatically impair SWE-induced barrel expansion[233]. How can we conciliate our main-findings with this barrel expansion?

As proposed by professor Feldman, injury-induced map plasticity implies a rapid depression of neuronal responses to the deprived input by NMDAR-LTD, followed by a slower potentiation of spared-input responses in both deprived and spared barrel column[54]. Here, we defined that the latter is indeed LTP-mediated, as evidences by RWS-LTP occlusion in the spared barrel after SWE. This was importantly accompanied by increased number of L2/3 spiking neurons in the same barrel column, as supported by several other studies[169,183,188]. At the same time, the trimmed-whisker responses in the principal (deprived)-barrel are reduced by LTD-like mechanisms[192,193]. I believe that the combination of different synaptic mechanisms, occurring in a different spatiotemporal manner, drives the shift of neuronal responses in the deprived barrel.

The first one, is a LTP-driven recruitment of spared whisker responding neurons in the main barrel. As discussed on chapter two, L2/3 axons can project directly to the adjacent barrel columns, and other cortical regions. I believe that the combination of these two factors is the substrate for the horizontal spreading of spared whisker information during barrel expansion. If indeed axons of spared neurons with increased whisker-evoked spikes are directly projecting to deprived L2/3 dendrites, then deprived neurons responses might be shifted by a STDP-like mechanism. Here, as the spared axon fires first than the postsynaptic NMDAR spike, "spared synapses" on the deprived will be potentiated. This is likely true, and dependent of local disinhibition, as supported by previous evidences[208]. At the same time, LTD-like mechanisms operate in deprived synapses, decreasing their synaptic gain. These results in an unbalance of synaptic weights, increasing the saliency of the spared synapses, shifting response tuning towards the spared whisker. This is in agreement with a study demonstrating that increased whisker representation is due to a shift to the spared neurons responses[173]. It also fits very-well the model of Sammons and Keck for the shift of response tuning after injury in the visual cortex (fig. 14)[215]. It is important to mention that this is purely speculative, since no direct experimental evidences are supporting this sequence of synaptic events.

We are currently performing a series of experiments to test the possibility that LTP-driven spared whisker response potentiation is indeed mandatory for SWE-induced barrel expansion. The most obvious approach is to exploit chronic IOI while performing X-SWE anti-GluA2 in the spared barrel. If indeed LTP-driven excitability in the spared barrel drives an increased spared whisker representation, then X-SWE anti-GluA2 should prevent increased IOS after whisker trimming. To do so, I am trying to implement IOI through a PDMS CW, to allow chronic imaging with IgGs injections in a barrel-specific manner[385]. We are also improving the experimental pipeline of section B, by recording L2/3 pyramidal neurons in the spared and deprived barrel (similar to what performed here[173]). This approach has the spatiotemporal resolution necessary to determine if the whisker-evoked response potentiation in the spared barrel here reported, is followed by a similar enhancement in the deprived one. This is very likely considering the existent set of evidences[169,183]. We are also testing the same hypothesizes but using single-unit recordings (see section XVII). Even if these approaches provide good indications on the circuit correlates of barrel expansion, they have limited information regarding its synaptic mechanisms. To tackle this limitation, we are aiming to perform *in vivo* whole-cell recordings of deprived neurons responses during SWE, while stimulating the spared whisker. At the early moments of SWE (1-2 days), spared whisker response potentiation should be restricted to the spared barrel. As a consequence, we should be able to induce RWS-LTP in the deprived barrel by spared whisker stimulation. If indeed STDP-like mechanisms from the spared to deprived columns are driving shift on response tuning, then RWS-LTP should be progressively occluded with SWE progression. If this is true, then we would have the horizontal spreading is indeed the driving force for SWE-induced barrel expansion. This should be dependent of an increased excitability of interbarrel projecting neurons, disinhibition, and likely accompanied by LTD in the deprived barrel.

XII. Impact of cortical remapping in a learned whisker-dependent behavior

Here, we exploited the whisker-to-barrel system to study the relationship between synaptic mechanisms of sensory map plasticity and correlated adaptive behaviors. Rodents use their whiskers to explore their immediate tactile environment (see chapter 2). During FWE, neurons in each barrel-column have receptive fields that are strongly tuned towards the principal whisker[83,166]. However, SWE causes L2/3 pyramidal neurons in the deprived and spared-related columns to respond stronger to the spared whisker, increasing the cortical representation of the spared whisker[54,169,173,183]. In the previous sections, I have discussed all the evidences placing synaptic LTP as one the major mechanisms underlying SWE-induced map plasticity. As we developed an efficient way to block RWS-LTP, and by consequence map plasticity, we decided to test its consequence at the behavioral level. We hypothesized that, by recruiting additional neurons, cortical remapping decreases the perceptual threshold of the spared whisker, and compensates the absence of the other whiskers. If this is true, then the recovery of a learned whisker-dependent behavior should be also LTP-dependent. To test this appealing possibility, we decided to monitor freely behaving mice in a whisker-dependent gap-crossing task. Here, food deprived mice were trained to reach a reward platform separated by randomly presented GDs. We hypothesized that the decision to jump onto the reward platform requires the strict usage of whiskers, and therefore, a good readout for animal's tactile perception.

To test that under our experimental conditions, if the classical GC task is indeed whisker-dependent, we subjected mice to different whisker trimming protocols (fig. 43). We found that all the recorded behavioral parameters were affected by whisker trimming, especially for a GD=65 mm. While FWE-subjected mice reached the expertise after two-recording sessions, SWE never reached this performance (fig. 43F). This was associated with a slight increase on the exploration time (fig. 43G), and no differences on the decision latency (at S4) (fig. 43H). These results can be partially conciliated with the ones reported by Celikel and Sakmann[249]. While we found the same observation for the time to detect a reward platform, we could not recapitulate the same results on the animal's success rate. Contrary to Celikel's work, our SWE-subjected mice never reached success values similar to the FWE-subjected ones. I believe that these discrepancies might be caused by differences on the construction of both gap crossing apparatus. Interestingly, while the total exploration time of the jump area decreased across the recording sessions (fig. 43C2 and E2), no differences are seen for the decision latency (fig. 43C3 and E3). In a first analysis, this might indicate that training improves task learning (less time to target the platform), but not the time for the whisker-mediated tactile perception. Unfortunately, we do not have a concrete way to discern if reduced GD exploration are due to faster trials (learning-induced), or if resulted from decreased number of GD explorations (sensory-mediated). Against what expected, no differences on performance between NW-subjected and SWE-subjected mice are seen (fig. 43F). How can we conciliate these results? I believe that the high success rate recorded on NW-subjected mice are explained by alterations on the behavioral strategy to detect the reward platform. Supporting this

notion, we found that (1) their behavioral performance steadily increased between S1-S2, remaining stable above the chance level across all the recording sessions (GD=65 mm, fig. 43E1); (2) this is accompanied by a drop on GD exploration time (fig. 43E2) and (3) a large variability on the decision latency at S1 (fig. 43E3). It is conceivable that at S1, NW-subjected mice adopt another behavioral strategy than their whiskers to detect the reward platform. This makes sense, since at this GD distance whiskers improve, but are not necessary for platform detection[248]. This is supported by the fact that, besides no differences on success, SWE-subjected mice explored less time than NW-subjected mice to perform the jump. Therefore, the presence of whiskers can be a seen as a slight advantage for tactile detection, not imperative (at least SWE), but that decreases the exploration needed to detect the reward platform. It would be of great interest to increase the GD's to a point where whiskers are strictly required to determine if SWE-subjected mice can have higher success rates than NW-subjected ones. We are also currently developing tools to analyze the high-frequency whisker motion videos (see section XVIII), to determine if indeed there are a change of behavioral strategy induced by whisker trimming. Altogether, these data clearly demonstrated that the time and success performance on the GC task are indeed whisker-dependent.

We then asked ourselves if map plasticity can affect the whisker-dependence of the GC task. The rationale behind this experiments is that, upon task learning, SWE-subjected mice should improve behavioral performance on a LTP-dependent manner. Unfortunately, analyzing the trimming effect on naïve animals, makes it very difficult to address this possibility. To do so, we decided to induce cortical remapping after FWE animals reached expertise (S5-S8). Gap-crossing performance decreased immediately after SWE, but recovered quickly after two days of SWE (fig. 44A). Remarkably, this corresponds to a time-point where RWS-LTP is occluded in L2/3, and independent of a new learning phase (fig. 44B). Interestingly, the improvement of behavioral success rate is higher on FWEexpert/SWE-subjected mice than one SWE naïve ones (fig. 43E1 vs 44A). This suggest that, even if the animals do not have to learn how to navigate the maze with just one whisker, training *per se* can strongly alter sensorial performance. This might be further catalyzed by a strong component of food-reward imprinted during FWE expertise, that somehow might help map plasticity during SWE (see section XIV). Interestingly, we found no differences on decision latency for the GD= 65 mm, but strong impairments on shorter GDs (fig. 44C). I believe that this is explained by an analysis bias, since the decision latency is restricted to the successful trials. As for GD=65mm, these animals had a low success rate, the calculation of this time variable might lead to a biased readout of the decision latency. In agreement with this, strong differences on the total exploration (where both successful and unsuccessful trials are considered) at a GD=65 mm can be seen (fig. 44D). It remains to be determined if this is caused by an increased attempt to investigate the GD. Interestingly, and contrary to what seen in SWE naïve mice, an improve on the decision latency at GD=60 mm is reported (fig. 44C). Once again, this might well-indicate that the behavioral readout between naïve and expert animals might be remarkably different. Independently of these details, it is clear that SWE strongly impairs the success rate, and increased the exploration time to reach the reward platform. Interestingly, the recovery of behavioral performance matches the one predicted by LTP-like mechanisms. It could have been

interesting to perform IOI recording on these animals, and determine if there is a correlation between barrel expansion and behavioral recovery. If indeed, this is a LTP-dependence mechanism, then it should be strongly modulated by our X-SWE anti-GluA2 approach.

XIII. LTP-driven map plasticity improves whisker-tactile perception during the early phases of LTP

We decided to test our last hypothesizes by chronically injecting anti-GluA2 antibodies during SWE on expert FWE mice. In parallel with the effect of IgGs on synaptic weights and RWS-LTP, we found that GC performance of X-SWE anti-GluA2 is predominantly impaired when compared to anti-GFP control subjects (fig. 45B). Interestingly, these impairments were reverted across the recording session, and at S4 no differences between groups is seen. This recovery can be explained by different reasons. First, due to problems with the chronic injections of antibody in one of the recording sessions. As LTP-driven cortical alterations after SWE can occur as 24h after SWE, it is possible that a missed injection can drive a strong map plasticity, that might explain the recovery on animal's behavior. Then, in a similar way than NW-subjected mice, a different behavioral strategy might be adopted by X-SWE anti-GluA2. Indeed, it is conceivable that in the absence of a proper usage of the remaining whisker, animals can sense the reward platform using their nose or even paws. To rule out this possibility, we have to analyze the high-frequency recordings of the whisker motion (see section XVIII). Finally, and the more likely, other forms of plasticity might underlie trimming-induced map plasticity. Clem and collaborators reported a slower mGluR-dependent form of plasticity, occurring in parallel to a faster NMDAR-dependent form of LTP[252]. Interestingly, mGluR blockage during an associative tactile conditioning task, the behavior of SWE-subjected mice is dramatically impaired. This fits very-well with the recovery of performance reported in our study. Additionally, considering the importance of map plasticity as a fundamental brain mechanism, it makes sense to be supported by redundant mechanisms for its expression. This can be, somehow, parallel to large amount of protein controlling AMPAR synaptic accumulation, where a redundancy of protein function is seen. It would be interesting to co-inject mGluR blockers (e.g., CPP) with anti-GluA2 antibodies, to block both forms of plasticity, and see if we can abolish this behavioral recovery.

XIV. Is map plasticity different between GC trained and naïve mice?

We took advantage of whole-cell patch clamp recordings in anesthetized mice to demonstrate that SWE potentiates spared whisker neuronal responses, and occludes RWS-LTP. Then, by performing chronic AMPAR cross-linking, we reverted this occlusion, suggesting that LTP-driven map plasticity explains the increased spared whisker cortical representation after whisker trimming. If the same approach is performed on behaving mice, during the GC task, we impaired behavior recovery during the initial phases of SWE. Are these different evidences directly related? It is important to mention that the GC is a complex form of behavior. Indeed, it not only involves the sensorial perception of whisker *per se*, but also a strong component of food reward, and motivation. This of critical importance, since map plasticity is reported to be

modulated by neuromodulation, in a brain state-dependent manner[172,196,209,238]. For instance, VTA activation along with auditory stimulus presentation, increased the cortical area and neuronal selectivity to the presented tone[244].This was due to dopamine release in the auditory cortex, and likely due to a direct modulation of synaptic LTP on auditory neurons. Can the same occur during food-reward on SWE-subjected mice? Can this recruit additional synaptic mechanisms than the ones reported on our anesthetized experiments? Importantly, these brain state-dependent forms of map plasticity, might perfectly explain the recovery on GC behavioral performance of X-SWE anti-GluA2. A similar mechanism might also explain the discrepancies on the behavioral performance between naïve SWE and FWEexpert/SWE mice (see above). Would be interesting to recapitulate the whole-cell recordings but on animals subjected to the GC task. By comparing to the existing data on the non-trained mice, we would be able to answer this question. Additionally, we could also perform the GC behavior with a probabilistic distribution of the food reward (i.e., some successful trials without food presentation). If the manipulation of reward drives a differential performance on SWE-subjected mice, then we would confirm that indeed SWE map plasticity is dependent on animal's brain state. Despite this complexity, it is likely that synaptic LTP mediates the core mechanism of trimming-induced map plasticity. Our results are supported by a myriad of different others. If any other form of plasticity co-exist (e.g., mGluR, neuromodulatory-dependent), they will likely act at the top of the LTP-driven mechanisms. This notion is supported by our GC behavioral data, and Clem's associative tactile conditioning task[252]. Importantly, no differences were found between X-SWE anti-GluA2 and anti-GFP injections on both decision latency, and total exploration time (fig.46B-C and 46E-F). This effect suggests that the impairment on the success rate, are not related to impairments on the decision making by the animal. However, it also raises the need to improve our behavioral analysis (see below), since other time-related parameter should explain the impairments on the behavioral performance. Importantly, no differences to any of the recorded parameters are seen for shorter, and non-challenging (likely not whisker-mediated) GDs. This supports that the reported behavioral deficits are not caused by side-effects caused by chronic antibody injection (e.g., locomotion). It would be interesting to complement this data, with an open field analysis after antibody injection, to see if this is indeed the case. Moreover, it is also important to mention that the gap crossing task here performed is a simplified, two-dimensional measure for whisker perception. It would be interesting to determine the effect of map plasticity, and the X-SWE anti-GluA2 in more complex whisker-dependent task (e.g., texture detection[143]). Altogether, these data revealed an unexpected and complex relationship between synaptic LTP, lap plasticity, and recovery of tactile perception after whisker trimming. While LTP is undeniably associated with the initial recovery phases after SWE, their action is not exclusive, and can be compensated by all the other synaptic mechanisms discussed throughout this section.

XV. Is LTP-driven map plasticity in the barrel cortex propagated to other brain regions during SWE?

Here, we have focused our attention in the map plasticity effects exclusively on L2/3 microcircuits. However, L2/3 pyramidal neurons can project directly to S2 and M1 cortices, and indirectly to several other subcortical regions[83,95,110]. This intricate connectivity is required for an efficient somatosensation, where the core sensorial processing and the motor control of whiskers and full-body motion are continuously updating each other. It has been described that L2/3 neuronal spiking is incredible sparse, with a spatial intermingled activity that largely depends of the whisker behavior[91,145]. This segregated distribution likely represents different populations of pyramidal neurons within L2/3 circuits that mutually projects to S2 ("BC-S2 neurons") or to M1 ("BC-M1 neurons")[146]. As discussed on chapter 2, the functionality is greatly dependent on their behavioral functionality, since: (1) whisking, and object location were respectively encoded by BC-S2, and BC-M1 neurons, and (2) BC-M1 had a higher discrimination for object location, while S1-S2 for texture discrimination. Unfortunately, our approach (fig. 30) do not have the cellular-resolution to determine which of the L2/3 neurons subtype has enhanced spiking activity after SWE. Would be of great interest to perform a similar approach than Chen and colleagues, and determine if they are exclusively M1, S2, or intracortical projecting neurons[146]. In my opinion, is very likely that barrel cortex map plasticity is not restricted to the cortical columns itself. For example, it is highly likely that spared barrel information is conveyed to M1, in order to adapt the spared whisker motion (or in the barrel cortex itself[68]). This would update the whisker sensorimotor behavior, and maximizing the environmental exploration by the remaining input, compensating all the trimmed whiskers. We are currently developing whisker motion analysis on SWE-subjected mice to determine if this is indeed the case (see section XVIII).

Further approaches

In this section, I will present all the ongoing projects that we launched based on the information gathered throughout my PhD project. I will start to introduce the exciting possibility that, besides underlying *in vivo* LTP, AMPAR lateral mobility can also control L2/3 synaptic transmission at the millisecond scale. Then, I will discuss an important project, where we aim to describe neuronal correlates of whisker dependent behaviors in the GC task, and their SWE-induced alteration. Finally, I will overview our collaborative efforts to develop an unsupervised, machine-learning approach to extract whisker and whole-body motion during the GC task. I believe that all of these projects will be determinant to refine, and support the previously discussed postulates.

XVI. The millisecond effect of RWS on Layer 2/3 synapses of the barrel cortex

Besides being an important mechanism to adjust synaptic weights in an activity-dependent manner, it is also proposed that AMPAR lateral mobility can tune synaptic transmission at the millisecond timescale[316,386]. Prior synaptic activity can either increase (paired-pulse facilitation) or decrease (paired-pulse depression, PPD) a subsequent postsynaptic response, if both stimulus occurs within less than a couple hundred milliseconds (e.g., brief trains of action potentials)[387,388]. These mechanisms are collectively known as short-term synaptic plasticity, and its expression locus has been a topic of intense debate. Classically, this phenomenon is described to have a restricted presynaptic expression (see for review[388]). However, Choquet's lab has shown that, under certain conditions, the postsynaptic side can also largely influence the dynamics of short-term plasticity[316,386]. Even inside the PSD, not all the AMPARs are stabilized, and around half of the receptors are constantly diffusing within the membrane plane[315,389]. The distances travelled by mobile AMPARs within a couple of milliseconds are theoretically enough to allow receptors to move across large sections of the entire PSD[390]. This mobility is critical to exchange desensitized non-conductive AMPARs by naïve ones upon fast glutamate release, maintaining postsynaptic response fidelity during high-frequency neurotransmission[316,386]. This is believed to reduce the extent of postsynaptic PPD, since: (1) immobilization of AMPARs through cross-linking increases PPD[316]; (2) facilitating AMPAR lateral mobility by degrading the extracellular matrix enhanced recovery from PPD[390] and (3) AMPAR stabilization by increased interaction between auxiliary proteins and PSD-95 drives synaptic depression upon high-frequency stimulation[331,386].

We are currently determining if a similar mechanism occurs *in vivo* in L2/3 synapses of the barrel cortex, while stimulating animal's whiskers a short RWS (sRWS, 8Hz 2.5 sec.). This is a physiological frequency used by rodents, and not enough to induce RWS-LTP in L2/3 synapses (data not shown). This is not a trivial question, due to circuit, and cellular-related experimental challenges. The first difficulty is imposed by the complex pathways, involving hundreds of different synapses, conveying whisker-related information to L2/3 synapses[83]. If during sRWS,

other subcortical, and intracortical synapses have PPD, they will low-pass filter the frequency effect. As a consequence, L2/3 synapses will be insensitive to sRWS-induced PPD, as this effect gets diluted in downstream synapses. It has been described that passive whisker stimulation at 5Hz in anesthetized rats, facilitates L4 responses during the whisker train, while L2/3 usually depressed[391]. This is in agreement with other studies, showing that L4-L2/3 and L2/3 synapses have mixed short-term dynamics[9,186,392]. Thus, if sRWS can induce PPD, there is a fairly good possibility to record it in L2/3 synapses (but see[393]). The second problem is the synaptic integration of whisker-evoked neuronal activity. As discussed, the large part of L4-L2/3 synaptic transmission is NMDAR-mediated[374]. Single whisker deflection drives NMDAR dendritic spikes in L2/3 distal dendrites, events that are recorded in the soma as long-lasting (up to 300 msec.) depolarization[176]. This is highly incompatible with the time window where the postsynaptic AMPAR-mediated component can influence synaptic PPD (50-100 msec.)[316]. As a consequence, if postsynaptic PPD exists in L2/3 synapses, it gets diluted by the strong NMDAR drive evoked by whisker stimulation. This makes it virtually impossible to extract AMPAR-mediated PPD from PSPs evoked after sRWS.

To tackle this limitation, we decided to perform *in vivo* whole-cell patch clamp recordings, while blocking synaptic NMDARs. To do so, we used an intracellular solution containing MK801, avoiding a presynaptic effect. Importantly, MK801 is a non-competitive NMDAR antagonist with an activity-dependent blockage of channel conductance[394]. This implies that just after break-in, one can easily identify the strong NMDAR-mediated depolarization evoked by sRWS (black trace, fig. 47A). However, after the progressive build-up of the MK801 effect, this depolarization is abolished. The result PSP is a frequency-evoked depolarization that is purely AMPAR-mediated (blue trace, **fig. 47A**). This is translated into a strong decrease of the evoked cumulative Vm depolarization, due to the absence of the major NMDAR drive (**fig. 47B**). If indeed, L2/3 synapses show postsynaptic short-term plasticity, the rate their PPD can be increased by our AMPAR cross-linking approach. To test this hypothesizes, we recorded cells in the presence of either an anti-GluA2, or anti-GFP IgGs, while blocking NMDAR signaling with MK801. The sRWS protocol evoked a remarkably different PSP between these two conditions (**fig. 48A**). The recorded PSPpeaks after sRWS in control conditions has a slower decay than in the presence of AMPAR cross-linking (**fig. 48B**). While the first PSPpeak is not different between conditions, the subsequent stimulations are significantly reduced in the presence of the anti-GluA2 antibody (**fig. 48C**). Importantly, as (1) the first PSPpeak is identical between conditions, and (2) no differences are seen at a frequency that should not induce PPD (2 Hz, **fig. 48D**), the effect of AMPAR cross-linking should be specific to short-term dynamics of L2/3 synapses. This preliminary data suggests that likely a similar mechanism to the one reported by Heine and collaborators might also exist *in vivo*, induced by a physiological pattern of whisker stimulation[316] (**fig. 49**).

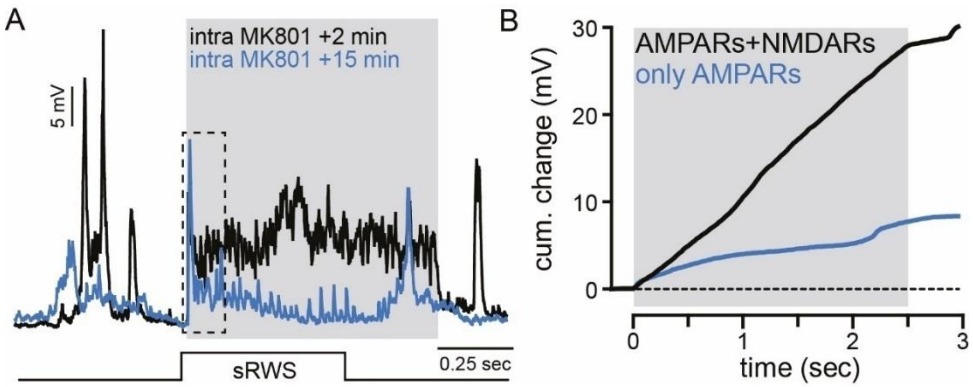

Fig. 47) MK801 intracellular application abolishes NMDAR-mediated plateau potentials and reveals a high-frequency AMPAR component. A) Example traces of sRWS-evoked postsynaptic depolarization of the same cell 2 minutes after breaking-in (black trace), and after 15 minutes. Note the blockage of NMDAR-dependent long-lasting depolarization. **B)** Average cumulative Vm changes induced by sRWS (grey) before and after MK801 effect. NMDAR blockage, abolish the strong dendritic depolarization, with the concomitant decrease on the cumulative Vm changes. The remaining depolarization is purely AMPAR-mediated.

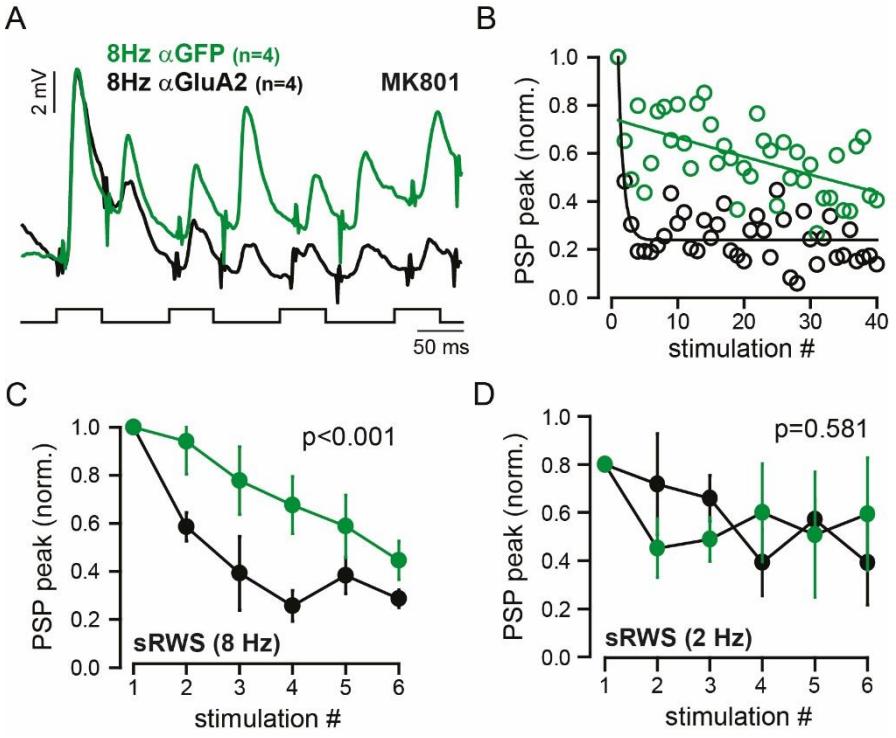

Fig. 48) AMPAR cross-linking reveals a postsynaptic short-term depression induced by sRWS. A) Example traces of sRWS-evoked PSPs in the presence of MK801 in the presence of anti-GluA2 (black), or anti-GFP (green) IgGs. Zoom-in in the four initial ON/OFF stimulations. **B)** Circles, PSPpeaks (AMPAR-mediated) to all the stimulations within the 8Hz 2.5 sec. of an example anti-GluA2 or anti-GFP cell. **C)** PSP peak of the six initial stimulations (8Hz, 2.5 sec). Circles are averages, with sem represented. Note that anti-GluA2 cells have a strong depression of PSPpeaks. **D)** Same but for a 2 Hz stimulation (during 25 sec.). For a low-frequency stimulation, no difference between conditions is seen.

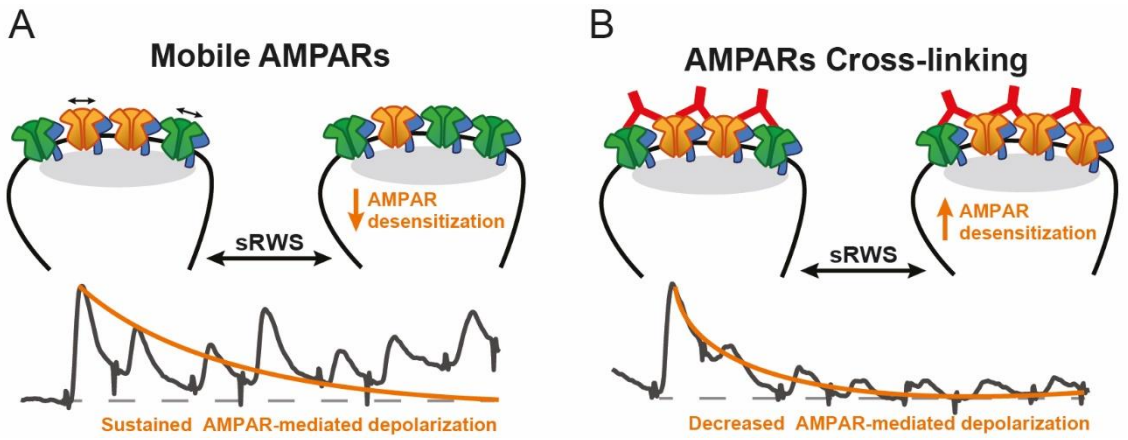

Fig. 49) Proposed model for sRWS-evoked short-term plasticity on L2/3 synapses. A) In the absence of NMDAR-depolarization, a frequency-dependent depolarization is seen. As described by Heine, M. *et al.* (2008) Science, this depression is likely mediated by AMPAR desensitization (remains to be tested). **B)** In agreement, if lateral diffusion is blocked by AMPAR cross-linking, the extent of synaptic depression is increased. It is likely that, similar to *in vitro*, lateral mobility of naïve AMPARs is critical to keep synaptic fidelity during high-frequency transmission (e.g., 8 Hz) in L2/3 synapses of the barrel cortex.

XVII. Neuronal correlates of whisker dependent behaviors in the GC task

To better characterize the whisker-dependence of the GC behavior, we are currently performing single-unit recordings in the barrel cortex (**fig. 50A**). We aim to chronically record activity of a population of L2/3 pyramidal neurons, while animal performing this form of whisker-dependent behavior. To do so, we are recording putative excitatory neurons from both L2/3 and L4 of two independent barrel columns. Our preliminary data suggest that, during the most challenging GDs, there is an increased firing rate of L2/3 locked to the moment that the animal jumps onto the reward platform (t=0, **fig. 50B**). As this corresponds to the epoch where animals have to use their whiskers to detect the reward platform, we believe that this is the neuronal correlate for the tactile perception. Currently, we are trying to understand how this sensory mediated perception is propagated to other cortical, and subcortical structures, to mediate a complex goal-directed sensorimotor transformation. Additionally, we are also trying to determine if decision can be encoded within the barrel cortex, or if propagated from other brain region. To do so, we are planning to manipulate circuits involved in decision (e.g., mPFC) by optogenetical meanings, to determine this exciting relationship between perception and decision making.

We are also exploiting the same technique to study if SWE differentially alters L2/3 spiking properties on both spared and deprived barrel column (data not shown). In agreement with previous studies, our preliminary data confirms that SWE increases neuronal excitability in the spared barrel column[188]. This also supports the data obtained from *in vivo* 2-Photon and whole-cell recordings during SWE. Remarkably, the firing properties of deprived L2/3 pyramidal neurons are steadily decreased soon after whiskers are trimmed. However, by the forth recording session of SWE, it

increases once again, in response to spared whisker motion. This fits very-well the model proposed on section XI, where spared barrel excitability is propagated to the deprived ones. It will be interesting to determine if this preliminary data is indeed true, and to better understand the mechanisms of horizontal spreading underling SWE-induced barrel expansion.

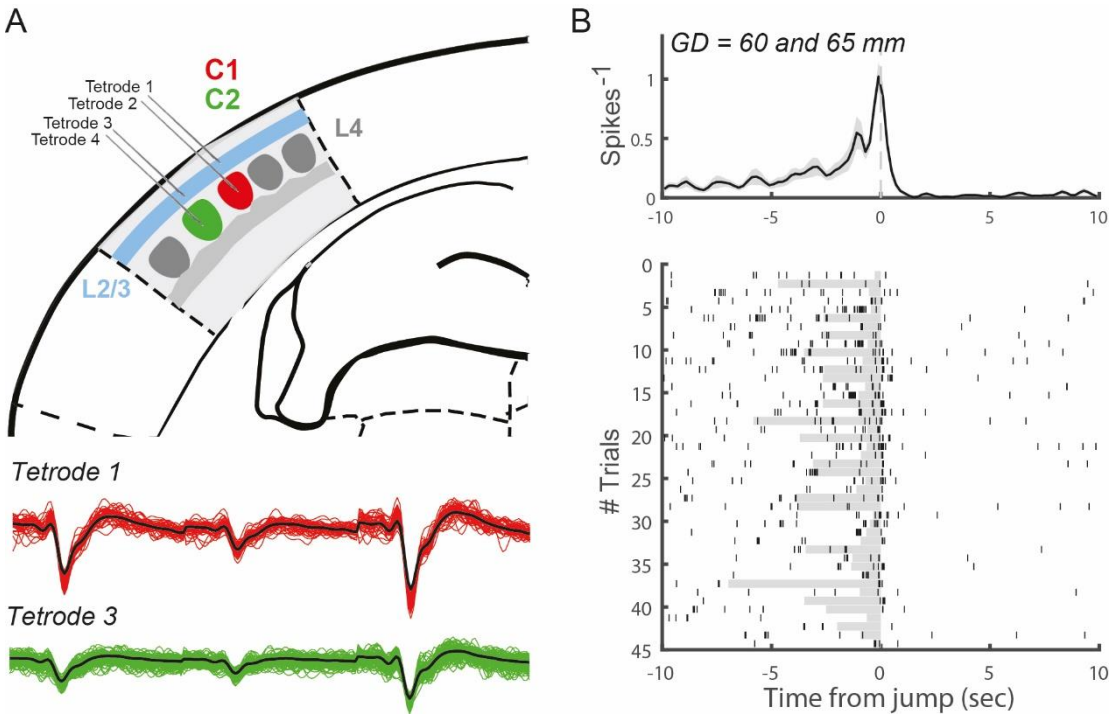

Fig. 50) Single-unit recordings in the barrel cortex to explore the neuronal correlates of SWE and GC behavior. A) (*top*) Representation of the recording pipeline, with tetrodes targeting both L2/3 and L4 of two independent barrel columns. (*bottom*) Recording examples of two putative pyramidal neurons on freely behaving mice performing the GC task. **B)** (*top*) Average spike frequency of all the trials recorded at GD = 60 and 65 mm, and aligned to the moment of the jump (t=0). (*bottom*) Individual trial contribution. Note the preferential firing rate of putative pyramidal neurons in the moment of GD exploration (preceding the jump).

XVIII. Toward an unsupervised analysis of whisker motion during GC behavior

All the experiments on the Gap Crossing task are accompanied by a high-frequency recording (300 fps) of the whisker behavior during animal's gap exploration. This information is rich, containing whisking properties *per se*, head orientation, and paw movements as an attempt to reach the rewarding platform. This is of critical importance since SWE, and our X-SWE might importantly alter the full-body transformation of the whisker-related information. If this is true, then it might be completely overlooked by the simple analysis performed in the result section, derived from the time stamps of the animal along the maze. We are currently developing a video analysis method inspired in DeepLabCut, to extract the maximal behavior relevant information from all the high-frequency videos[395]. We are aiming to record whisking properties, such as

deflection, angle, and amplitude, as an attempt to have a readout of the animal's brain state (fig. 51A). We are also recording animal's snout, and pow to understand if indeed a different behavioral strategy might be engaged on NW-subjected mice to detect the reward platform (fig. 51B). Importantly, this will allow us to determine if SWE alter sensibility and reliability of the spared whisker, indicated by a putative increase of failed attempts to grab the reward platform. These developments will be essential to refine the results obtained during our GC experiments, and to better dissect how SWE alters whisker-tactile perception.

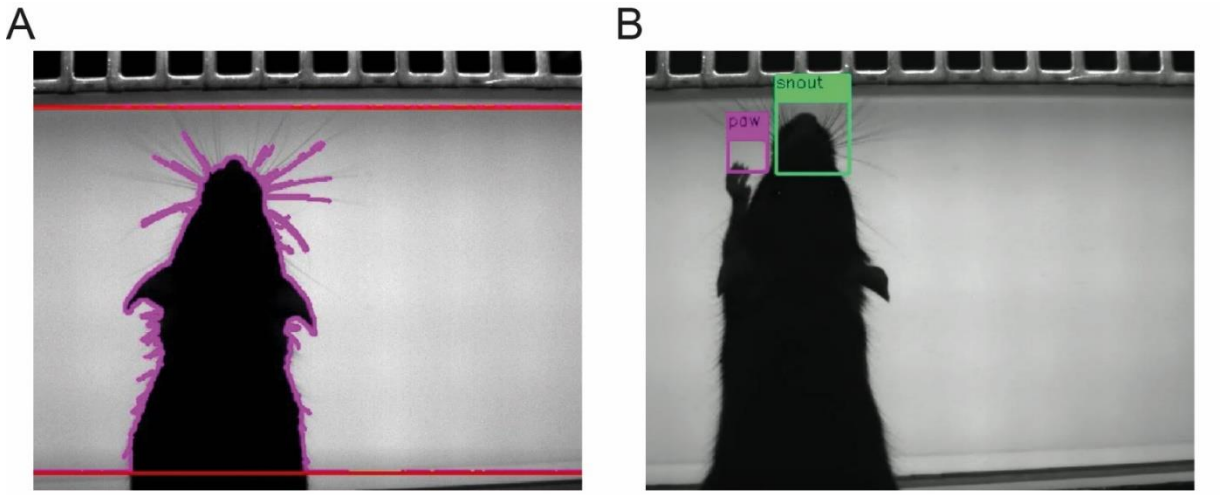

Fig. 51) Towards an unsupervised analysis of whisker motion during GC behavior. We are currently developing an unsupervised machine-learning approach to analyze whisking behavior, and GD exploration in all the behavior performed in this work. **A)** We aim to extract components of the whisker motion (e.g., frequency), as a brain state readout, and **B)** other behavioral-relevant information (snout) to rule-out any whisker-independent behavioral strategy of gap crossing.

Conclusion

At the beginning of my PhD, we started an ambitious collaboration to determine the relationship between synaptic LTP, map plasticity, and adaptive behaviors. To do so, we had to develop a novel methodology to specifically block LTP *in vivo*, without affecting basic circuit function. We inspired ourselves from the theoretical framework developed by the Choquet's lab in the last decade to implement an *in vivo* AMPAR cross-linking in the barrel cortex. We demonstrated that AMPAR synaptic recruitment, powered by lateral mobility, is required to express a sensory-evoked form of synaptic LTP. To my knowledge, our and Zhang's work, are the first to define an important role of AMPAR trafficking as a hallmark for LTP *in vivo*[177]. This corroborates decades of *in vitro* work, where the molecular machinery at play during hippocampal NMDAR-LTP has been extensively described[42,279]. It also suggests that the AMPAR-dependence, as workhorses for the activity-dependent alterations of the excitatory neurotransmission, is ubiquitous across brain regions, as seen in the hippocampus and neocortex. I hope that the experimental approach here developed will inspire other studies to determine how AMPAR trafficking underlies synaptic LTP in several other brain regions. In previous works, controlling synaptic plasticity in rodents has been used to alter memories they have formed[332,356]. We extended this behavioral meaning, by showing that this NMDAR-dependent form of LTP induced by whisker stimulation is associated with behavioral recovery in the early phases of SWE. This is accompanied by an increased neuronal excitability to the spared whisker, and occlusion of RWS-LTP after two days of SWE. Importantly, if synaptic LTP is blocked during SWE by chronic AMPAR cross-linking, a reduction of neuronal excitability, and increased sensitivity to RWS-LTP is seen. This is associated with strong impairments on behavior performance in a whisker-dependent gap crossing task. Therefore, LTP is mechanistically not only required for memory formation, but also to injury-induced circuit remodeling and, ultimately, sensorial perception. After whisker trimming, LTP shifts neuronal response tuning towards the spared input, increasing the number of responding neurons in the spared barrel. We hypothesize that this increased excitability is propagated, by unknown mechanisms, to the deprived barrel column. At the circuit-level, this is translated into a recruitment of additional neurons to compute the spared whisker. This functional barrel expansion, likely decreases the perceptual threshold of the spared whisker, compensating the absence of the trimmed inputs. Our results are of great importance for clinicians and patients as brief periods of sensory deprivation have been proposed as therapeutic ways to promote recovery of lost functions after peripheral injury or stroke[250]. The identification of synaptic LTP as the core mechanism for cortical remapping, paves the way to new therapeutic targets aiming to improve patient's symptomatology.

Bibliography

1. Silver, M. A. & Kastner, S. Topographic maps in human frontal and parietal cortex. *Trends Cogn. Sci.* **13**, 488–495 (2009).

2. Murphy, T. H. & Corbett, D. Plasticity during stroke recovery: From synapse to behaviour. *Nat. Rev. Neurosci.* **10**, 861–872 (2009).

3. Harding-Forrester, S. & Feldman, D. E. Somatosensory maps. in *The Parietal Lobe* (eds. Vallar, G. & Coslett, H. B.) **151**, 73–102 (Elsevier, 2018).

4. Jackson, J. H. On the anatomical and physiologival localisation of movements in the brain. *Lancet* **101**, 84–85 (1873).

5. Leyton, A. S. F. & Sherrington, C. S. Observations on the Excitable Cortex of the Chimpanzee, Orang-Utan, and Gorilla. *Q. J. Exp. Physiol.* **11**, 135–222 (1917).

6. Penfield, W. & Boldrey, E. Somatic motor and sensory representation in the cerebral cortex of man as studied by electrical stimulation. *Brain* **60**, 389–443 (1937).

7. Marshall, W. H., Woolsey, C. N. & Bard, P. Cortical representation of tactile sensibility as indicated by cortical potentials. *Science (80-.).* **85**, 388–390 (1937).

8. Woolsey, T. A. & Van der Loos, H. The structural organization of layer IV in the somatosensory region (S I) of mouse cerebral cortex. The description of a cortical field composed of discrete cytoarchitectonic units. *Brain Res.* **17**, 205–242 (1970).

9. Fox, K. & Woolsey, T. *Barrel cortex*. (Cambridge University Press, 2008). doi:10.1017/CBO9780511541636

10. Krubitzer, L. A. & Seelke, A. M. H. Cortical evolution in mammals: The bane and beauty of phenotypic variability. *Proc. Natl. Acad. Sci.* **109**, 10647–10654 (2012).

11. Wiesel, T. & Hubel, D. The Period of Susceptibility to the Physiological Effects of Unilateral Eye Closure in Kittens. *J. Physiol.* **89**, 419–436 (1970).

12. Hübener, M. & Bonhoeffer, T. Neuronal plasticity: Beyond the critical period. *Cell* **159**, 727–737 (2014).

13. Merzenich, M. M. *et al.* Somatosensory cortical map changes following digit amputation in adult monkeys. *Journal of Comparative Neurology* **224**, 591–605 (1984).

14. Clark, S. A., Allard, T., Jenkins, W. M. & Merzenich, M. M. Receptive fields in the body-surface map in adult cortex defined by temporally correlated inputs. *Nature* **332**, 444–445 (1988).

15. Gilbert, C. D. & Wiesel, T. N. Receptive field dynamics in adult primary visual cortex. *Nature* **356**, 150–152 (1992).

16. Recanzone, G. H., Schreiner, C. E. & Merzenich, M. M. Plasticity in the frequency representation of primary auditory cortex following discrimination training in adult owl monkeys. *J. Neurosci.* **13**, 87–103 (1993).

17. Gilbert, C. D. Horizontal integration and cortical dynamics. *Neuron* **9**, 1–13 (1992).

18. Jenkins, W. M. & Merzenich, M. M. Reorganization of neocortical representations after brain injury: a neurophysiological model of the bases of recovery from stroke. in *Neural Regeneration* (eds. Seil, F. J., Herbert, E. & Carlson, B. M.) **71**, 249–266 (Elsevier, 1987).

19. Xerri, C. Imprinting of idyosyncratic experience in cortical sensory maps: Neural substrates of representational remodeling and correlative perceptual changes. *Behav. Brain Res.* **192**, 26–41 (2008).

20. Jenkins, W. M., Merzenich, M. M., Ochs, M. T., Allard, T. & Guíc-Robles, E. Functional reorganization of primary somatosensory cortex in adult owl monkeys after behaviorally controlled tactile stimulation. *J. Neurophysiol.* **63**, 82–104 (1990).

21. Vidyasagar, R., Folger, S. E. & Parkes, L. M. Re-wiring the brain: Increased functional connectivity within primary somatosensory cortex following synchronous co-activation. *Neuroimage* **92**, 19–26 (2014).

22. Sterr, A. *et al.* Perceptual correlates of changes in cortical representation of fingers in blind multifinger Braille readers. *J. Neurosci.* **18**, 4417–23 (1998).

23. Elbert, T., Pantev, C., Wienbruch, C., Rockstroh, B. & Taub, E. Increased use of the left hand in string players associated with increased cortical representation of the fingers. *Science (80-.).* **220**, 21–23 (1995).

24. Pantev, C. *et al.* Increased auditory cortical representation in musicians. *Nature* **392**, 811–814 (2002).

25. Butterworth, S. *et al.* Abnormal cortical sensory activation in dystonia: An fMRI study. *Mov. Disord.* **18**, 673–682 (2003).

26. Mogilner, A. *et al.* Somatosensory cortical plasticity in adult humans revealed by magnetoencephalography. *Proc. Natl. Acad. Sci.* **90**, 3593–3597 (2006).

27. Cramer, S. C. Repairing the human brain after stroke: I. Mechanisms of spontaneous recovery. *Ann. Neurol.* **63**, 272–287 (2008).

28. Jones, T. A. & Adkins, D. L. Motor System Reorganization After Stroke: Stimulating and Training Toward Perfection. *Physiology* **30**, 358–370 (2015).

29. N., T. & S.-I., I. Rehabilitation with poststroke motor recovery: A review with a focus on neural plasticity. *Stroke Research and Treatment* (2013).

30. Sengpiel, F. Plasticity of the visual cortex and treatment of amblyopia. *Curr. Biol.* **24**, R936–R940 (2014).

31. Li, R. W., Ngo, C., Nguyen, J. & Levi, D. M. Video-game play induces plasticity in the visual system of adults with amblyopia. *PLoS Biol.* **9**, (2011).

32. Flor, H., Nikolajsen, L. & Jensen, T. S. Phantom limb pain: A case of maladaptive CNS plasticity? *Nat. Rev. Neurosci.* **7**, 873–881 (2006).

33. Yang, T. T. *et al.* Sensory maps in the human brain. *Nature* **368**, 592–593 (1994).

34. Jutzeler, C. R., Curt, A. & Kramer, J. L. K. Relationship between chronic pain and brain reorganization after deafferentation: A systematic review of functional MRI findings. *NeuroImage Clin.* **9**, 599–606 (2015).

35. Kole, K., Scheenen, W., Tiesinga, P. & Celikel, T. Cellular diversity of the somatosensory cortical map plasticity. *Neurosci. Biobehav. Rev.* **84**, 100–115 (2018).

36. Squire, L. *et al. Fundamental Neuroscience*. (Elsevier Science, 2013).

37. Kandel, E. R., Jessell, T. M., Schwartz, J. H., Siegelbaum, S. A. & Hudspeth, A. J. *Principles of Neural Science*. (McGraw-Hill Education, 2013).

38. Connors, B. W. & Long, M. A. Electrical Synapses in the Mammalian Brain. *Annu. Rev. Neurosci.* **27**, 393–418 (2004).

39. Hebb, D. O. *The organization of behavior; a neuropsychological theory. John Wiley & Sons, Inc* (Wiley, 1949). doi:10.1364/OL.24.000954

40. Bliss, T. V. P. & Lømo, T. Long-lasting potentiation of synaptic transmission in the dentate area of the unanaesthetized rabbit following stimulation of the perforant path. *J. Physiol.* **232**, 357–374 (1973).

41. Artola, A. & Singer, W. Long-term potentiation and NMDA receptors in rat visual cortex. *Nature* **330**, 649–652 (1987).

42. Huganir, R. L. & Nicoll, R. AMPARs and synaptic plasticity: the last 25 years. *Neuron* **80**, 704–717 (2013).

43. Bliss, T. V. P. & Collingridge, G. L. A synaptic model of memory: long-term potentiation in the hippocampus.pdf. *Nature* **361**, 31–39 (1993).

44. Citri, A. & Malenka, R. C. Synaptic plasticity: Multiple forms, functions, and mechanisms. *Neuropsychopharmacology* **33**, 18–41 (2008).

45. Malenka, R. C. & Bear, M. F. LTP and LTD: an embarrassment of riches. *Neuron* **44**, 5–21 (2004).

46. Collingridge, G. L., Peineau, S., Howland, J. G. & Wang, Y. T. Long-term depression in the CNS. *Nat. Rev. Neurosci.* **11**, 459–473 (2010).

47. Feldman, D. E. The spike-timing dependence of plasticity. *Neuron* **75**, 556–71 (2012).

48. Lisman, J. & Spruston, N. Postsynaptic depolarization requirements for LTP and LTD: a critique of spike timing-dependent plasticity. *Nat. Neurosci.* **8**, 839–841 (2005).

49. Sjöström, P. J., Rancz, E. A., Roth, A. & Häusser, M. Dendritic Excitability and Synaptic Plasticity. *Physiol. Rev.* **88**, 769–840 (2008).

50. Turrigiano, G., Kenneth R. Leslie, Niraj S. Desai, L. C. R. & S. B. N. Activity-dependent scaling of quantal amplitude in neocortical neurons. *Nature* **391**, 892–896 (2002).

51. Turrigiano, G. Homeostatic synaptic plasticity: local and global mechanisms for stabilizing neuronal function. *Cold Spring Harb. Perspect. Biol.* **4**, a005736 (2012).

52. Turrigiano, G. The Self-Tuning Neuron: Synaptic Scaling of Excitatory Synapses. *Cell* **135**, 422–435 (2008).

53. Holtmaat, A. & Svoboda, K. Experience-dependent structural synaptic plasticity in the mammalian brain. *Nat. Rev. Neurosci.* **10**, 647–658 (2009).

54. Feldman, D. E. Synaptic Mechanisms for Plasticity in Neocortex. *Annu. Rev. Neurosci.* **32**, 33–55 (2009).

55. Diamond, M. E., von Heimendahl, M., Knutsen, P. M., Kleinfeld, D. & Ahissar, E. 'Where' and 'what' in the whisker sensorimotor system. *Nat. Rev. Neurosci.* **9**, 601–612 (2008).

56. Welker, E. & Van der Loos, H. Quantitative correlation between barrel-field size and the sensory innervation of the whiskerpad: a comparative study in six strains of mice bred for different patterns of mystacial vibrissae. *J. Neurosci.* **6**, 3355–73 (1986).

57. Brecht, M., Preilowski, B., Merzenich, M. M. & Keck, W. M. Functional architecture of the mystacial vibrissae. *Behav. Brain Res.* **84**, 81–97 (1997).

58. Ritt, J. T., Andermann, M. L. & Moore, C. I. Embodied Information Processing: Vibrissa Mechanics and Texture Features Shape Micromotions in Actively Sensing Rats. *Neuron* **57**, 599–613 (2008).

59. Arabzadeh, E., Zorzin, E. & Diamond, M. E. Neuronal encoding of texture in the whisker sensory pathway. *PLoS Biol.* **3**, (2005).

60. Jadhav, S. P., Wolfe, J. & Feldman, D. E. Sparse temporal coding of elementary tactile features during active whisker sensation. *Nat. Neurosci.* **12**, 792–800 (2009).

61. Lenschow, C. & Brecht, M. Barrel Cortex Membrane Potential Dynamics in Social Touch. *Neuron* **85**, 718–725 (2015).

62. Diamond, M. E. & Arabzadeh, E. Whisker sensory system - from receptor to decision. *Prog. Neurobiol.* **103**, 28–40 (2013).

63. Berg, R. W. & Kleinfeld, D. Rhythmic Whisking by Rat: Retraction as Well as Protraction of the Vibrissae Is Under Active Muscular Control. *J. Neurophysiol.* **89**, 104–117 (2003).

64. Schroeder, J. B. & Ritt, J. T. Selection of head and whisker coordination strategies during goal-oriented active touch. *J. Neurophysiol.* **115**, 1797–1809 (2016).

65. Deschênes, M., Moore, J. & Kleinfeld, D. Sniffing and whisking in rodents. *Curr. Opin. Neurobiol.* **22**, 243–250 (2012).

66. Arkley, K., Grant, R. A., Mitchinson, B. & Prescott, T. J. Strategy change in vibrissal active sensing during rat locomotion. *Curr. Biol.* **24**, 1507–1512 (2014).

67. Lee, L. J. & Erzurumlu, R. S. Altered parcellation of neocortical somatosensory maps in N-methyl-D-aspartate receptor-deficient mice. *J. Comp. Neurol.* **485**, 57–63 (2005).

68. Petersen, C. C. H. Cortical Control of Whisker Movement. *Annu. Rev. Neurosci.* **37**, 183–203 (2014).

69. Bosman, L. W. J. *et al.* Anatomical Pathways Involved in Generating and Sensing Rhythmic Whisker Movements. *Front. Integr. Neurosci.* **5**, 1–28 (2011).

70. Herfst, L. J. & Brecht, M. Whisker Movements Evoked by Stimulation of Single Motor Neurons in the Facial Nucleus of the Rat. *J. Neurophysiol.* **99**, 2821–2832 (2008).

71. Takatoh, J. *et al.* New Modules Are Added to Vibrissal Premotor Circuitry with the Emergence of Exploratory Whisking. *Neuron* **77**, 346–360 (2013).

72. Rice, F. L., Kinnman, E., Aldskogius, H., Johansson, O. & Arvidsson, J. The innervation of the mystacial pad of the rat as revealed by PGP 9.5 immunofluorescence. *J. Comp. Neurol.* **337**, 366–385 (1993).

73. Ebara, S., Kumamoto, K., Matsuura, T., Mazurkiewicz, J. E. & Rice, F. L. Similarities and differences in the innervation of mystacial vibrissal follicle-sinus complexes in the rat and cat: A confocal microscopic study. *J. Comp. Neurol.* **449**, 103–119 (2002).

74. Petersen, C. C. H. H. The functional organization of the barrel cortex. *Neuron* **56**, 339–355 (2007).

75. Feldmeyer, D. *et al.* Barrel cortex function. *Prog. Neurobiol.* **103**, 3–27 (2013).

76. Ma, P. M. Barrelettes—architectonic vibrissal representations in the brainstem trigeminal complex of the mouse. II. Normal post-natal development. *J. Comp. Neurol.* **327**, 376–397 (1993).

77. Erzurumlu, R. S., Murakami, Y. & Rijli, F. M. Mapping the face in the somatosensory brainstem. *Nat. Rev. Neurosci.* **11**, 252–263 (2010).

78. Lo, F.-S., Guido, W. & Erzurumlu, R. S. Electrophysiological Properties and Synaptic Responses of Cells in the Trigeminal Principal Sensory Nucleus of Postnatal Rats. *J. Neurophysiol.* **82**, 2765–2775 (2017).

79. Woolston, D. C., La Londe, J. R. & Gibson, J. M. Comparison of response properties of cerebellar- and thalamic-projecting interpolaris neurons. *J. Neurophysiol.* **48**, 160–173 (2017).

80. Minnery, B. S. & Simons, D. J. Response Properties of Whisker-Associated Trigeminothalamic Neurons in Rat Nucleus Principalis. *J. Neurophysiol.* **89**, 40–56 (2006).

81. Van Der Loos, H. Barreloids in mouse somatosensory thalamus. *Neurosci. Lett.* **2**, 1–6 (1976).

82. Haidarliu, S. & Ahissar, E. Size Gradients of Barreloids. *J. Comp. Neurol.* **387**, 372–387 (2001).

83. Feldmeyer, D. Excitatory neuronal connectivity in the barrel cortex. *Front. Neuroanat.* **6**, 1–22 (2012).

84. Brecht, M. & Sakmann, B. Whisker maps of neuronal subclasses of the rat ventral posterior medial thalamus, identified by whole-cell voltage recording and morphological reconstruction. *J. Physiol.* **538**, 495–515 (2002).

85. Lefort, S., Tomm, C., Floyd Sarria, J. C. & Petersen, C. C. H. The Excitatory Neuronal Network of the C2 Barrel Column in Mouse Primary Somatosensory Cortex. *Neuron* **61**, 301–316 (2009).

86. Staiger, J. F. *et al.* Functional diversity of layer IV spiny neurons in rat somatosensory cortex: Quantitative morphology of electrophysiologically characterized and biocytin labeled cells. *Cereb. Cortex* **14**, 690–701 (2004).

87. Feldmeyer, D., Lubke, J. & Silver, R. A. Synaptic connections between layer 4 spiny neurone-layer 2/3 pyramidal cell pairs in juvenile rat barrel cortex: physiology and anatomy of interlaminar signalling within a cortical column. *J. Physiol.* 803–822 (2002). doi:10.1013/jphysiol.2001.012959

88. Petersen, C. C. H. Cell-type specific function of GABAergic neurons in layers 2 and 3 of mouse barrel cortex. *Curr. Opin. Neurobiol.* **26**, 1–6 (2014).

89. Petersen, C. C. H. & Crochet, S. Synaptic Computation and Sensory Processing in Neocortical Layer 2/3. *Neuron* **78**, 28–48 (2013).

90. Gentet, L. J., Avermann, M., Matyas, F., Staiger, J. F. & Petersen, C. C. H. Membrane potential dynamics of GABAergic neurons in the barrel cortex of behaving mice. *Neuron* **65**, 422–35 (2010).

91. O'Connor, D. H., Peron, S. P., Huber, D. & Svoboda, K. Neural activity in barrel cortex underlying vibrissa-based object localization in mice. *Neuron* **67**, 1048–1061 (2010).

92. Williams, L. E. & Holtmaat, A. Higher-Order Thalamocortical Inputs Gate Synaptic Long-Term Potentiation via Disinhibition. *Neuron* **101**, 91–102.e4 (2019).

93. Alloway, K. D. Information processing streams in rodent barrel cortex: The differential functions of barrel and septal circuits. *Cereb. Cortex* **18**, 979–989 (2008).

94. Simons, D. J. Response properties of vibrissa units in rat SI somatosensory neocortex. *J. Neurophysiol.* **41**, 798–820 (1978).

95. Fox, K. Deconstructing the cortical column in the barrel cortex. *Neuroscience* **368**, 17–28 (2018).

96. Oberlaender, M. *et al.* Cell type-specific three-dimensional structure of thalamocortical circuits in a column of rat vibrissal cortex. *Cereb. Cortex* **22**, 2375–2391 (2012).

97. Bureau, I., Von Paul, F. Saint & Svoboda, K. Interdigitated paralemniscal and lemniscal pathways in the mouse barrel cortex. *PLoS Biol.* **4**, 2361–2371 (2006).

98. Urbain, N. & Deschenes, M. A New Thalamic Pathway of Vibrissal Information Modulated by the Motor Cortex. *J. Neurosci.* **27**, 12407–12412 (2007).

99. Furuta, T., Kaneko, T. & Deschenes, M. Septal Neurons in Barrel Cortex Derive Their Receptive Field Input from the Lemniscal Pathway. *J. Neurosci.* **29**, 4089–4095 (2009).

100. Yu, C., Derdikman, D., Haidarliu, S. & Ahissar, E. Parallel Thalamic Pathways for Whisking and Touch Signals in the Rat. *PLoS Biol.* **4**, (2006).

101. Pierret, T., Lavallée, P. & Deschênes, M. Parallel streams for the relay of vibrissal information through thalamic barreloids. *J. Neurosci.* **20**, 7455–62 (2000).

102. Hutson, K. A. & Masterton, R. B. The sensory contribution of a single vibrissa's cortical barrel. *J. Neurophysiol.* **56**, 1196–223 (1986).

103. Miyashita, T. & Feldman, D. E. Behavioral detection of passive whisker stimuli requires somatosensory cortex. *Cereb. Cortex* **23**, 1655–1662 (2013).

104. Bruno, R. M. & Sakmann, B. Cortex Is Driven by Weak but Synchronously Active Thalamocortical Synapses. *Science (80-.).* **312**, 1622–1627 (2006).

105. Lübke, J., Roth, A., Feldmeyer, D. & Sakmann, B. Morphometric analysis of the columnar innervation domain of neurons connecting layer 4 and layer 2/3 of juvenile rat barrel cortex. *Cereb. Cortex* **13**, 1051–1063 (2003).

106. Feldmeyer, D., Lübke, J. & Sakmann, B. Efficacy and connectivity of intracolumnar pairs of layer 2/3 pyramidal cells in the barrel cortex of juvenile rats. *J. Physiol.* **575**, 583–602 (2006).

107. Takahashi, N., Oertner, T. G., Hegemann, P. & Larkum, M. E. Active Cortical Dendrites Modulate Perception. *Science* **354**, 1159–1165 (2016).

108. Killackey, H. P. & Sherman, S. M. Corticothalamic Projections from the Rat Primary Somatosensory Cortex. *J. Neurosci.* **23**, 7381–7384 (2018).

109. Zhang, Z. W. & Deschênes, M. Intracortical axonal projections of lamina VI cells of the primary somatosensory cortex in the rat: a single-cell labeling study. *J. Neurosci.* **17**, 6365–79 (1997).

110. Aronoff, R. *et al.* Long-range connectivity of mouse primary somatosensory barrel cortex. *Eur. J. Neurosci.* **31**, 2221–2233 (2010).

111. Kwegyir-Afful, E. E. Response Properties of Whisker-Related Neurons in Rat Second Somatosensory Cortex. *J. Neurophysiol.* **92**, 2083–2092 (2004).

112. Matyas, F. *et al.* Motor Control by Sensory Cortex. *Science (80-.).* **330**, 1240–1243 (2010).

113. Sato, T. R. & Svoboda, K. The Functional Properties of Barrel Cortex Neurons Projecting to the Primary Motor Cortex. *J. Neurosci.* **30**, 4256–4260 (2010).

114. Mao, T. *et al.* Long-Range Neuronal Circuits Underlying the Interaction between Sensory and Motor Cortex. *Neuron* **72**, 111–123 (2011).

115. Ferezou, I. *et al.* Spatiotemporal Dynamics of Cortical Sensorimotor Integration in Behaving Mice. *Neuron* **56**, 907–923 (2007).

116. Petreanu, L., Mao, T., Sternson, S. M. & Svoboda, K. The subcellular organization of neocortical excitatory connections. *Nature* **457**, 1142–1145 (2009).

117. Smith, J. B. & Alloway, K. D. Functional Specificity of Claustrum Connections in the Rat: Interhemispheric Communication between Specific Parts of Motor Cortex. *J. Neurosci.* **30**, 16832–16844 (2010).

118. Gao, P., Hattox, A. M., Jones, L. M., Keller, A. & Zeigler, H. P. Whisker motor cortex ablation and whisker movement patterns. *Somatosens. Mot. Res.* **20**, 191–198 (2003).

119. Wilent, W. B. Synaptic Responses to Whisker Deflections in Rat Barrel Cortex as a Function of Cortical Layer and Stimulus Intensity. *J. Neurosci.* **24**, 3985–3998 (2004).

120. Frostig, R. D., Xiong, Y., Chen-Bee, C. H., Kvasnak, E. & Stehberg, J. Large-Scale Organization of Rat Sensorimotor Cortex Based on a Motif of Large Activation Spreads. *J. Neurosci.* **28**, 13274–13284 (2008).

121. Brecht, M., Roth, A. & Sakmann, B. Dynamic receptive fields of reconstructed pyramidal cells in layers 3 and 2 of rat somatosensory barrel cortex. *J. Physiol.* **553**, 243–265 (2003).

122. Armstrong-James, M. & Fox, K. Spatiotemporal convergence and divergence in the rat S1 'barrel' cortex. *J. Comp. Neurol.* **263**, 265–281 (1987).

123. Armstrong-James, M., Fox, K. & Das-Gupta, A. Flow of excitation within rat barrel cortex on striking a single vibrissa. *J. Neurophysiol.* **68**, 1345–1358 (1992).

124. Khatri, V. & Simons, D. J. Angularly nonspecific response suppression in rat barrel cortex. *Cereb. Cortex* **17**, 599–609 (2007).

125. Drew, P. J. & Feldman, D. E. Representation of Moving Wavefronts of Whisker Deflection in Rat Somatosensory Cortex. *J. Neurophysiol.* **98**, 1566–1580 (2007).

126. Armstrong-James, M. & Callahan, C. A. Thalamo-cortical processing of vibrissal information in the rat. II. Spatiotemporal convergence in the thalamic ventroposterior medial nucleus (VPm) and its relevance to generation of receptive fields of S1 cortical "Barrel" neurones. *J. Comp. Neurol.* **303**, 211–224 (1991).

127. Mountcastle, V. B. Modality and Topographic Properties of Single Neurons of Cat'S Somatic Sensory Cortex. *J. Neurophysiol.* **20**, 408–434 (1957).

128. Pluta, S. R., Lyall, E. H., Telian, G. I., Ryapolova-Webb, E. & Adesnik, H. Surround Integration Organizes a Spatial Map during Active Sensation. *Neuron* **94**, 1220–1233.e5 (2017).

129. Jacob, V., Le Cam, J., Ego-Stengel, V. & Shulz, D. E. Emergent Properties of Tactile Scenes Selectively Activate Barrel Cortex Neurons. *Neuron* **60**, 1112–1125 (2008).

130. Shimegi, S., Ichikawa, T., Akasaki, T. & Sato, H. Temporal characteristics of response integration evoked by multiple whisker stimulations in the barrel cortex of rats. *J. Neurosci.* **19**, 10164–75 (1999).

131. Petersen, C. C. H., Grinvald, A. & Sakmann, B. Spatiotemporal dynamics of sensory responses in layer 2/3 of rat barrel cortex measured in vivo by voltage-sensitive dye imaging combined with whole-cell voltage recordings and neuron reconstructions. *J. Neurosci.* **23**, 1298–309 (2003).

132. Clancy, K. B., Schnepel, P., Rao, A. T. & Feldman, D. E. Structure of a single whisker representation in layer 2 of mouse somatosensory cortex. *J. Neurosci.* **35**, 3946–58 (2015).

133. Sato, T. R., Gray, N. W., Mainen, Z. F. & Svoboda, K. The functional microarchitecture of the mouse barrel cortex. *PLoS Biol.* **5**, 1440–1452 (2007).

134. Kerr, J. N. D. *et al.* Spatial Organization of Neuronal Population Responses in Layer 2/3 of Rat Barrel Cortex. *J. Neurosci.* **27**, 13316–13328 (2007).

135. Gentet, L. J. Functional diversity of supragranular GABAergic neurons in the barrel cortex. *Front. Neural Circuits* **6**, 52 (2012).

136. Griffen, T. C. GABAergic synapses: their plasticity and role in sensory cortex. *Front. Cell. Neurosci.* **8**, 1–22 (2014).

137. Gentet, L. J. *et al.* Unique functional properties of somatostatin-expressing GABAergic neurons in mouse barrel cortex. *Nat. Neurosci.* **15**, 607–612 (2012).

138. Mateo, C. *et al.* In vivo optogenetic stimulation of neocortical excitatory neurons drives brain-state-dependent inhibition. *Curr. Biol.* **21**, 1593–1602 (2011).

139. Avermann, M., Tomm, C., Mateo, C., Gerstner, W. & Petersen, C. C. H. Microcircuits of excitatory and inhibitory neurons in layer 2/3 of mouse barrel cortex. *J. Neurophysiol.* **107**, 3116–3134 (2012).

140. Petersen, C. C. H. & Sakmann, B. Functionally Independent Columns of Rat Somatosensory Barrel Cortex Revealed with Voltage-Sensitive Dye Imaging. *J. Neurosci.* **21**, 8435–8446 (2018).

141. Ego-Stengel, V., Le Cam, J. & Shulz, D. E. Coding of Apparent Motion in the Thalamic Nucleus of the Rat Vibrissal Somatosensory System. *J. Neurosci.* **32**, 3339–3351 (2012).

142. Estebanez, L., Férézou, I., Ego-Stengel, V. & Shulz, D. E. Representation of tactile scenes in the rodent barrel cortex. *Neuroscience* **368**, 81–94 (2018).

143. Helmchen, F., Gilad, A. & Chen, J. L. Neocortical dynamics during whisker-based sensory discrimination in head-restrained mice. *Neuroscience* **368**, 57–69 (2018).

144. Crochet, S., Lee, S. H. & Petersen, C. C. H. Neural Circuits for Goal-Directed Sensorimotor Transformations. *Trends Neurosci.* **42**, 66–77 (2019).

145. Peron, S. P., Freeman, J., Iyer, V., Guo, C. & Svoboda, K. A Cellular Resolution Map of Barrel Cortex Activity during Tactile Behavior. *Neuron* **86**, 783–799 (2015).

146. Chen, J. L., Carta, S., Soldado-Magraner, J., Schneider, B. L. & Helmchen, F. Behaviour-dependent recruitment of long-range projection neurons in somatosensory cortex. *Nature* **499**, 336–340 (2013).

147. Schubert, D., Kötter, R., Luhmann, H. J. & Staiger, J. F. Morphology, electrophysiology and functional input connectivity of pyramidal neurons characterizes a genuine layer Va in the primary somatosensory cortex. *Cereb. Cortex* **16**, 223–236 (2006).

148. Schubert, D. *et al.* Layer-specific intracolumnar and transcolumnar functional connectivity of layer V pyramidal cells in rat barrel cortex. *J. Neurosci.* **21**, 3580–92 (2001).

149. Chen, J. L. *et al.* Pathway-specific reorganization of projection neurons in somatosensory cortex during learning. *Nat. Neurosci.* **18**, 1101–1108 (2015).

150. Huber, D. *et al.* Multiple dynamic representations in the motor cortex during sensorimotor learning. *Nature* **484**, 473–8 (2012).

151. Petreanu, L. *et al.* Activity in motor-sensory projections reveals distributed coding in somatosensation. *Nature* **489**, 299–303 (2012).

152. Chen, J. L., Voigt, F. F., Javadzadeh, M., Krueppel, R. & Helmchen, F. Long-range population dynamics of anatomically defined neocortical networks. *Elife* **5**, 1–26 (2016).

153. Kwon, S. E., Yang, H., Minamisawa, G. & O'Connor, D. H. Sensory and decision-related activity propagate in a cortical feedback loop during touch perception. *Nat. Neurosci.* **19**, 1243–1249 (2016).

154. Alloway, K. D., Lou, L., Nwabueze-Ogno, F. & Chackrabarti, S. Topography of Cortical Projections to the Dorsolateral Neostriatum in Rats: Multiple Overlapping Sensorimotor Pathways. *J. Comp. Neurol.* **499**, 33–48 (2006).

155. Hoover, J. E., Hoffer, Z. S. & Alloway, K. D. Projections From Primary Somatosensory Cortex to the Neostriatum: The Role of Somatotopic Continuity in Corticostriatal Convergence. *J. Neurophysiol.* **89**, 1576–1587 (2003).

156. Cohen, J. D., Hirata, A. & Castro-Alamancos, M. A. Vibrissa Sensation in Superior Colliculus: Wide-Field Sensitivity and State-Dependent Cortical Feedback. *J. Neurosci.* **28**, 11205–11220 (2008).

157. Cohen, J. D. & Castro-Alamancos, M. A. Detection of Low Salience Whisker Stimuli Requires Synergy of Tectal and Thalamic Sensory Relays. *J. Neurosci.* **30**, 2245–2256 (2010).

158. Hemelt, M. E. & Keller, A. Superior Colliculus Control of Vibrissa Movements. *J. Neurophysiol.* **100**, 1245–1254 (2008).

159. Benedetti, F. Orienting Behaviour and Superior Colliculus Sensory Representations in Mice with the Vibrissae Bent into the Contralateral Hemispace. *Eur. J. Neurosci.* **7**, 1512–1519 (1995).

160. Jenkinson, E. W. & Glickstein, M. Whiskers, Barrels, and Cortical Efferent Pathways in Gap Crossing by Rats. *J. Neurophysiol.* **84**, 1781–1789 (2017).

161. Le Merre, P. *et al.* Reward-Based Learning Drives Rapid Sensory Signals in Medial Prefrontal Cortex and Dorsal Hippocampus Necessary for Goal-Directed Behavior. *Neuron* **97**, 83–91.e5 (2018).

162. Lacefield, C. O., Pnevmatikakis, E. A., Paninski, L. & Bruno, R. M. Reinforcement Learning Recruits Somata and Apical Dendrites across Layers of Primary Sensory Cortex. *Cell Rep.* **26**, 2000–2008.e2 (2019).

163. Bieler, M., Xu, X., Marquardt, A. & Hanganu-Opatz, I. L. Multisensory integration in rodent tactile but not visual thalamus. *Sci. Rep.* **8**, 1–18 (2018).

164. Maruyama, A. T. & Komai, S. Auditory-induced response in the primary sensory cortex of rodents. *PLoS One* **13**, 1–18 (2018).

165. Hong, Y. K., Lacefield, C. O., Rodgers, C. C. & Bruno, R. M. Sensation, movement and learning in the absence of barrel cortex. *Nature* **561**, 542–546 (2018).

166. Fox, K. *A critical period for experience-dependent synaptic plasticity in rat barrel cortex*. *The Journal of neuroscience : the official journal of the Society for Neuroscience* **12**, (1992).

167. Diamond, M. E., Huang, W. & Ebner, F. F. Laminar comparison of somatosensory cortical plasticity. *Science (80-.).* **265**, 1885–1888 (1994).

168. Barth, A. L. *et al.* Upregulation of cAMP response element-mediated gene expression during experience-dependent plasticity in adult neocortex. *J. Neurosci.* **20**, 4206–16 (2000).

169. Glazewski, S., Chen, C. M., Silva, A. & Fox, K. Requirement for α-CaMKII in experience-dependent plasticity of the barrel cortex. *Science (80-.).* **272**, 421–423 (1996).

170. Welker, E., Rao, S. B., Dörfl, J., Melzer, P. & van der Loos, H. Plasticity in the barrel cortex of the adult mouse: effects of chronic stimulation upon deoxyglucose uptake in the behaving animal. *J. Neurosci.* **12**, 153–70 (1992).

171. Polley, D. B., Kvašňák, E. & Frostig, R. D. Naturalistic experience transforms sensory maps in the adult cortex of caged animals. *Nature* **429**, 67–71 (2004).

172. Carcea, I. & Froemke, R. C. *Cortical plasticity, excitatory-inhibitory balance, and sensory perception*. *Progress in Brain Research* **207**, (Elsevier B.V., 2013).

173. Margolis, D. J. *et al.* Reorganization of cortical population activity imaged throughout long-term sensory deprivation. *Nat. Neurosci.* **15**, 1539–1546 (2012).

174. Fox, K. Anatomical pathays and molecular mechanisms for plasticity in the barrel cortex. *Neuroscience* **111**, 1–16 (2002).

175. Roth, R. H., Zhang, Y. & Huganir, R. L. Dynamic imaging of AMPA receptor trafficking in vitro and in vivo. *Curr. Opin. Neurobiol.* **45**, 51–58 (2017).

176. Gambino, F. *et al.* Sensory-evoked LTP driven by dendritic plateau potentials in vivo. *Nature* **515**, 116–119 (2014).

177. Zhang, Y., Cudmore, R. H., Lin, D.-T., Linden, D. J. & Huganir, R. L. Visualization of NMDA receptor–dependent AMPA receptor synaptic plasticity in vivo. *Nat. Neurosci.* **18**, 402–407 (2015).

178. Takahashi, T., Svoboda, K. & Malinow, R. Experience Strengthening Transmission by Driving AMPA Receptors into Synapses. *Science (80-.).* **1585**, 1585–1589 (2003).

179. Makino, H. & Malinow, R. Compartmentalized versus global synaptic plasticity on dendrites controlled by experience. *Neuron* **72**, 1001–1011 (2011).

180. Glazewski, S., Herman, C., McKenna, M., Chapman, P. F. & Fox, K. Long-term potentiation in vivo in layers II/III of rat barrel cortex. *Neuropharmacology* **37**, 581–592 (1998).

181. Hardingham, N. *et al.* Neocortical Long-Term Potentiation and Experience-Dependent Synaptic Plasticity Require α-Calcium/Calmodulin-Dependent Protein Kinase II Autophosphorylation. *J. Neurosci.* **23**, 4428–4436 (2003).

182. Castro-Alamancos, M., Donoghue, J. & Connors, B. Different forms of synaptic plasticity in somatosensory and motor areas of the neocortex. *J. Neurosci.* **15**, 5324–5333 (1995).

183. Glazewski, S., Giese, K. P., Silva, A. & Fox, K. The role of α-CaMKII autophosphorylation in neocortical experience-dependent plasticity. *Nat. Neurosci.* **3**, 911–918 (2000).

184. Daniel E, F. Timing-Based LTP and LTD at Vertical Inputs to Layer II/III Pyramidal Cells in Rat Barrel Cortex. *Neuron* **27**, 45–56 (2000).

185. Dachtler, J. *et al.* Experience-Dependent Plasticity Acts via GluR1 and a Novel Neuronal Nitric Oxide Synthase-Dependent Synaptic Mechanism in Adult Cortex. *J. Neurosci.* **31**, 11220–11230 (2011).

186. Hardingham, N. & Fox, K. The Role of Nitric Oxide and GluR1 in Presynaptic and Postsynaptic Components of Neocortical Potentiation. *J. Neurosci.* **26**, 7395–7404 (2006).

187. Finnerty, G. T., Roberts, L. S. E. & Connors, B. W. Sensory experience modifies the short-term dynamics of neocortical synapses. *Nature* **400**, 367–371 (1999).

188. Benedetti, B. L., Glazewski, S. & Barth, A. L. Reliable and Precise Neuronal Firing during Sensory Plasticity in Superficial Layers of Primary Somatosensory Cortex. *J. Neurosci.* **29**, 11817–11827 (2009).

189. Clem, R. L. & Barth, A. Pathway-specific trafficking of native AMPARs by in vivo experience. *Neuron* **49**, 663–670 (2006).

190. Clem, R. L. Ongoing in Vivo Experience in the Neocortex. *Science (80-.).* **101**, 101–104 (2008).

191. Glazewski, S. & Fox, K. Time course of experience-dependent synaptic potentiation and depression in barrel cortex of adolescent rats. *J. Neurophysiol.* **75**, 1714–1729 (1996).

192. Allen, C. B., Celikel, T. & Feldman, D. E. Long-term depression induced by sensory deprivation during cortical map plasticity in vivo. *Nat. Neurosci.* **6**, 291–299 (2003).

193. Bender, V. A. Two Coincidence Detectors for Spike Timing-Dependent Plasticity in Somatosensory Cortex. *J. Neurosci.* **26**, 4166–4177 (2006).

194. Heynen, A. J. *et al.* Molecular mechanism for loss of visual cortical responsiveness following brief monocular deprivation. *Nat. Neurosci.* **6**, 854–862 (2003).

195. Froemke, R. C. *et al.* Long-term modification of cortical synapses improves sensory perception. *Nat. Neurosci.* **16**, 79–88 (2013).

196. Froemke, R. C. Plasticity of Cortical Excitatory-Inhibitory Balance. *Annu. Rev. Neurosci.* **38**, 195–219 (2015).

197. Mrsic-Flogel, T. D. *et al.* Homeostatic Regulation of Eye-Specific Responses in Visual Cortex during Ocular Dominance Plasticity. *Neuron* **54**, 961–972 (2007).

198. Daoubal Gael, & D. D. Long-Term Plasticity of Intrinsic Excitability: Learning Rules and Mechanisms. *Learn. Mem.* 456–465 (2003). doi:10.1101/lm.64103.shown

199. Marder, E. & Prinz, A. A. Modeling stability in neuron and network function: The role of activity in homeostasis. *BioEssays* **24**, 1145–1154 (2002).

200. Mahon, S. & Charpier, S. Bidirectional Plasticity of Intrinsic Excitability Controls Sensory Inputs Efficiency in Layer 5 Barrel Cortex Neurons in Vivo. *J. Neurosci.* **32**, 11377–11389 (2012).

201. Barth, A. L. Alteration of Neuronal Firing Properties after In Vivo Experience in a FosGFP Transgenic Mouse. *J. Neurosci.* **24**, 6466–6475 (2004).

202. Meliza, C. D. & Dan, Y. Receptive-field modification in rat visual cortex induced by paired visual stimulation and single-cell spiking. *Neuron* **49**, 183–189 (2006).

203. Froemke, R. C., Merzenich, M. M. & Schreiner, C. E. A synaptic memory trace for cortical receptive field plasticity. *Nature* **450**, 425–9 (2007).

204. Li, Y., Van Hooser, S. D., Mazurek, M., White, L. E. & Fitzpatrick, D. Experience with moving visual stimuli drives the early development of cortical direction selectivity. *Nature* **456**, 952–956 (2008).

205. Foeller, E., Celikel, T. & Feldman, D. E. Inhibitory Sharpening of Receptive Fields Contributes to Whisker Map Plasticity in Rat Somatosensory Cortex. *J. Neurophysiol.* **94**, 4387–4400 (2005).

206. Celikel, T., Szostak, V. A. & Feldman, D. E. Modulation of spike timing by sensory deprivation during induction of cortical map plasticity. *Nat. Neurosci.* **7**, 534–541 (2004).

207. Jacob, V., Brasier, D. J., Erchova, I., Feldman, D. & Shulz, D. E. Spike Timing-Dependent Synaptic Depression in the In Vivo Barrel Cortex of the Rat. *J. Neurosci.* **27**, 1271–1284 (2007).

208. Gambino, F. & Holtmaat, A. Spike-timing-dependent potentiation of sensory surround in the somatosensory cortex is facilitated by deprivation-mediated disinhibition. *Neuron* **75**, 490–502 (2012).

209. Kripkee, B. & Froemke, R. C. *Organization and Plasticity of Cortical Inhibition. The Oxford Handbook of Developmental Neural Plasticity* (2017). doi:10.1093/oxfordhb/9780190635374.013.14

210. Yuanyuan Jiao, Zhang, C., Yanagawa, Y. & Sun, Q.-Q. Major Effects of Sensory Experiences on the Neocortical Inhibitory Circuits. *J. Neurosci.* **26**, 8691–8701 (2006).

211. Kelly, M. K., Carvell, G. E., Kodger, J. M. & Simons, D. J. Sensory Loss by Selected Whisker Removal

Produces Immediate Disinhibition in the Somatosensory Cortex of Behaving Rats. *J. Neurosci.* **19**, 9117–9125 (1999).

212. Li, L., Gainey, M. A., Goldbeck, J. E. & Feldman, D. E. Rapid homeostasis by disinhibition during whisker map plasticity. *Proc. Natl. Acad. Sci.* **111**, 1616–1621 (2014).

213. House, D. R. C., Elstrott, J., Koh, E., Chung, J. & Feldman, D. E. Parallel regulation of feedforward inhibition and excitation during whisker map plasticity. *Neuron* **72**, 819–831 (2011).

214. Keck, T. *et al.* Loss of sensory input causes rapid structural changes of inhibitory neurons in adult mouse visual cortex. *Neuron* **71**, 869–882 (2011).

215. Sammons, R. P. & Keck, T. Adult plasticity and cortical reorganization after peripheral lesions. *Curr. Opin. Neurobiol.* **35**, 136–141 (2015).

216. Villa, K. L. *et al.* Inhibitory Synapses Are Repeatedly Assembled and Removed at Persistent Sites In Vivo. *Neuron* **89**, 756–769 (2016).

217. Boomsma, D. I. *et al.* Compartmentalization of GABAergic inhibition by dendritic spines. *Science (80-.).* **340**, 759–762 (2013).

218. van Versendaal, D. *et al.* Elimination of Inhibitory Synapses Is a Major Component of Adult Ocular Dominance Plasticity. *Neuron* **74**, 374–383 (2012).

219. Chen, J. L. *et al.* Clustered Dynamics of Inhibitory Synapses and Dendritic Spines in the Adult Neocortex. *Neuron* **74**, 361–373 (2012).

220. Rasband, M. N. Glial Contributions to Neural Function and Disease. *Mol. Cell. Proteomics* **15**, 355–361 (2016).

221. Mizrahi, A. & Katz, L. C. Dendritic stability in the adult olfactory bulb. *Nat. Neurosci.* **6**, 1201–1207 (2003).

222. Holtmaat, A. J. G. D. *et al.* Transient and persistent dendritic spines in the neocortex in vivo. *Neuron* **45**, 279–291 (2005).

223. De Paola, V. *et al.* Cell type-specific structural plasticity of axonal branches and boutons in the adult neocortex. *Neuron* **49**, 861–875 (2006).

224. Zuo, Y., Yang, G., Kwon, E. & Gan, W. B. Long-term sensory deprivation prevents dendritic spine loss in primary somatosensory cortex. *Nature* **436**, 261–265 (2005).

225. Marik, S. A., Yamahachi, H., McManus, J. N. J., Szabo, G. & Gilbert, C. D. Axonal dynamics of excitatory and inhibitory neurons in somatosensory cortex. *PLoS Biol.* **8**, (2010).

226. Villa, K. L. & Nedivi, E. Excitatory and Inhibitory Synaptic Placement and Functional Implications. in *Dendrites: Development and Disease* (eds. Emoto, K., Wong, R., Huang, E. & Hoogenraad, C.) 467–487 (Springer Japan, 2016). doi:10.1007/978-4-431-56050-0_18

227. Bisler, S. *et al.* Expression of c-Fos, ICER, Krox-24 and JunB in the whisker-to-barrel pathway of rats: Time course of induction upon whisker stimulation by tactile exploration of an enriched environment. *J. Chem. Neuroanat.* **23**, 187–198 (2002).

228. Santos, A. R., Comprido, D. & Duarte, C. B. Regulation of local translation at the synapse by BDNF. *Prog. Neurobiol.* **92**, 505–516 (2010).

229. Rocamora, N., Welker, E., Pascual, M. & Soriano, E. Upregulation of BDNF mRNA Expression in the Barrel Cortex of Adult Mice after Sensory Stimulation. *J. Neurosci.* **16**, 4411–4419 (1996).

230. Kowiański, P. *et al.* BDNF: A Key Factor with Multipotent Impact on Brain Signaling and Synaptic Plasticity. *Cell. Mol. Neurobiol.* **38**, 579–593 (2018).

231. Wallace, H., Glazewski, S., Liming, K. & Fox, K. The Role of Cortical Activity in Experience-Dependent

Potentiation and Depression of Sensory Responses in Rat Barrel Cortex. *J. Neurosci.* **21**, 3881–3894 (2001).

232. Glazewski, S., McKenna, M., Jacquin, M. & Fox, K. Experience-dependent depression of vibrissae responses in adolescent rat barrel cortex. *Eur. J. Neurosci.* **10**, 2107–2116 (1998).

233. Fox, K. The cortical component of experience-dependent synaptic plasticity in the rat barrel cortex. *J. Neurosci.* **14**, 7665 LP-7679 (1994).

234. Darian-Smith, C. & Gilbert, C. D. Topographic reorganization in the striate cortex of the adult cat and monkey is cortically mediated. *J. Neurosci.* **15**, 1631 LP-1647 (1995).

235. Kole, K. Experience-dependent plasticity of neurovascularization. *J. Neurophysiol.* **114**, 2077–2079 (2015).

236. Stewart, R. S., Huang, C., Arnett, M. T. & Celikel, T. Spontaneous oscillations in intrinsic signals reveal the structure of cerebral vasculature. *J. Neurophysiol.* **109**, 3094–3104 (2013).

237. Lacoste, B. *et al.* Sensory-Related Neural Activity Regulates the Structure of Vascular Networks in the Cerebral Cortex. *Neuron* **83**, 1117–1130 (2014).

238. Hattori, R., Kuchibhotla, K. V, Froemke, R. C. & Komiyama, T. Functions and dysfunctions of neocortical inhibitory neuron subtypes. *Nat. Neurosci.* **20**, 1199–1208 (2017).

239. Hangya, B., Ranade, S. P., Lorenc, M. & Kepecs, A. Central Cholinergic Neurons Are Rapidly Recruited by Reinforcement Feedback. *Cell* **162**, 1155–1168 (2015).

240. Niell, C. M. & Stryker, M. P. Modulation of Visual Responses by Behavioral State in Mouse Visual Cortex. *Neuron* **65**, 472–479 (2010).

241. Sara, S. J. The locus coeruleus and noradrenergic modulation of cognition. *Nat. Rev. Neurosci.* **10**, 211–223 (2009).

242. Martins, A. R. O. & Froemke, R. C. Coordinated forms of noradrenergic plasticity in the locus coeruleus and primary auditory cortex. *Nat. Neurosci.* **18**, 1483–1492 (2015).

243. Paspalas, C. D. & Papadopoulos, G. C. Noradrenergic Innervation of Peptidergic Interneurons in the Rat Visual Cortex. *Cereb. Cortex* **9**, 844–853 (1999).

244. Bao, S., Chan, V. T. & Merzenic, M. M. Cortical remodelling induced by activity of ventral tegmental dopamine neurons. *Nature* **412**, 79–83 (2001).

245. Carvell, G. & Simons, D. Abnormal tactile experience early in life disrupts active touch. *J. Neurosci.* **16**, 2750–2757 (2018).

246. Chu, Y. F., Yen, C. T. & Lee, L. J. Neonatal whisker clipping alters behavior, neuronal structure and neural activity in adult rats. *Behav. Brain Res.* **238**, 124–133 (2013).

247. Papaioannou, S., Brigham, L. & Krieger, P. Sensory deprivation during early development causes an increased exploratory behavior in a whisker-dependent decision task. *Brain Behav.* **3**, 24–34 (2013).

248. Barnéoud, P., Gyger, M., Andrés, F. & van der Loos, H. Vibrissa-related behavior in mice: transient effect of ablation of the barrel cortex. *Behav. Brain Res.* **44**, 87–99 (1991).

249. Celikel, T. & Sakmann, B. Sensory integration across space and in time for decision making in the somatosensory system of rodents. *Proc. Natl. Acad. Sci.* **104**, 1395–1400 (2007).

250. Kraft, A. W., Bauer, A. Q., Culver, J. P. & Lee, J.-M. M. Sensory deprivation after focal ischemia in mice accelerates brain remapping and improves functional recovery through Arc-dependent synaptic plasticity. *Sci. Transl. Med.* **10**, eaag1328 (2018).

251. Lehmann, J. *et al.* CPP, a selective N-methyl-D-aspartate (NMDA)-type receptor antagonist: Characterization in vitro and in vivo. *J. Pharmacol. Exp. Ther.* **240**, 737–746 (1987).

252. Clem, R. L., Celike, T. & Barth, A. L. Ongoing in vivo experience triggers synaptic metaplasticity in the neocortex. *Science (80-.).* **319**, 101–104 (2008).

253. Kleim, J. A. & Jones, T. A. Principles of Experience-Dependent Neural Plasticity: Implications for Rehabilitation After Brain Damage. *J. Speech, Lang. Hear. Res.* **51**, 225–239 (2008).

254. Wittenberg, G. F. Experience, cortical remapping, and recovery in brain disease. *Neurobiol. Dis.* **37**, 252–258 (2010).

255. Lüscher, C. & Malenka, R. C. NMDA receptor-dependent long-term potentiation and long-term depression (LTP/LTD). *Cold Spring Harb. Perspect. Biol.* **4**, (2012).

256. Nicoll, R. & Roche, K. W. Long-term potentiation: peeling the onion. *Neuropharmacology* **74**, 18–22 (2013).

257. Eichenbaum, H. A cortical–hippocampal system for declarative memory. *Nat. Rev. Neurosci.* **1**, 41–50 (2000).

258. Antic, S. D., Zhou, W. L., Moore, A. R., Short, S. M. & Ikonomu, K. D. The decade of the dendritic NMDA spike. *J. Neurosci. Res.* **88**, 2991–3001 (2010).

259. Paoletti, P., Bellone, C. & Zhou, Q. NMDA receptor subunit diversity: Impact on receptor properties, synaptic plasticity and disease. *Nat. Rev. Neurosci.* **14**, 383–400 (2013).

260. Jaarsma, D., Sebens, J. B. & Korf, J. Localization of NMDA and AMPA receptors in rat barrel field. *Neurosci. Lett.* **133**, 233–236 (1991).

261. Sudhof, T. C. The presynaptic active zone. *Neuron* **75**, 11–25 (2012).

262. Regehr, W. G. Short-term presynaptic plasticity. *Cold Spring Harb. Perspect. Biol.* **4**, 1–19 (2012).

263. Castillo, P. E. Presynaptic LTP and LTD of excitatory and inhibitory synapses. *Cold Spring Harb. Perspect. Biol.* **4**, (2012).

264. Traynelis, S. F. *et al.* Glutamate Receptor Ion Channels: Structure, Regulation, and Function. *Pharmacol. Rev.* **62**, 405 LP-496 (2010).

265. Niswender, C. M. & Conn, P. J. Metabotropic Glutamate Receptors: Physiology, Pharmacology, and Disease. *Annu. Rev. Pharmacol. Toxicol.* **50**, 295–322 (2010).

266. Herring, B. E. & Nicoll, R. A. Long-Term Potentiation: From CaMKII to AMPA Receptor Trafficking. *Annu. Rev. Physiol.* **78**, 351–365 (2016).

267. Lerma, J. & Marques, J. M. Kainate receptors in health and disease. *Neuron* **80**, 292–311 (2013).

268. Lomeli, H. *et al.* The rat delta-l and delta-2 subunits extend the excitatory amino acid receptor family IQCK s GFFRHRPaPNA. *FEBS Lett.* **315**, 318–322 (1993).

269. Choquet, D. Linking Nanoscale Dynamics of AMPA Receptor Organization to Plasticity of Excitatory Synapses and Learning. *J. Neurosci.* **38**, 9318–9329 (2018).

270. Sheng, M. & Kim, E. The postsynaptic organization of synapses. *Cold Spring Harb Perspect Biol* **3**, a005678 (2011).

271. Nakahata, Y. & Yasuda, R. Plasticity of spine structure: Local signaling, translation and cytoskeletal reorganization. *Front. Synaptic Neurosci.* **10**, 1–13 (2018).

272. Ehlers, M. D. D. Dendritic trafficking for neuronal growth and plasticity. *Biochem. Soc. Trans.* **41**, 1365–82 (2013).

273. Sheng, M. & Hoogenraad, C. C. The postsynaptic architecture of excitatory synapses: a more quantitative view. *Annu. Rev. Biochem.* **76**, 823–47 (2007).

274. Kaizuka, T. & Takumi, T. Postsynaptic density proteins and their involvement in neurodevelopmental disorders. *J. Biochem.* **163**, 447–455 (2018).

275. Xu, W. PSD-95-like membrane associated guanylate kinases (PSD-MAGUKs) and synaptic plasticity. *Curr. Opin. Neurobiol.* **21**, 306–312 (2011).

276. Woods, G. F., Oh, W. C., Boudewyn, L. C., Mikula, S. K. & Zito, K. Loss of PSD-95 Enrichment Is Not a Prerequisite for Spine Retraction. *J. Neurosci.* **31**, 12129–12138 (2011).

277. El-Husseini, A. E., Schnell, E., Chetkovich, D. M., Nicoll, R. A. & Bredt, D. S. PSD-95 involvement in maturation of excitatory synapses. *Science* **290**, 1364–8 (2000).

278. Greger, I. H., Watson, J. F. & Cull-Candy, S. G. Structural and Functional Architecture of AMPA-Type Glutamate Receptors and Their Auxiliary Proteins. *Neuron* **94**, 713–730 (2017).

279. Diering, G. H. & Huganir, R. L. The AMPA Receptor Code of Synaptic Plasticity. *Neuron* **100**, 314–329 (2018).

280. Schwenk, J. *et al.* High-resolution proteomics unravel architecture and molecular diversity of native AMPA receptor complexes. *Neuron* **74**, 621–33 (2012).

281. Schwenk, J. *et al.* Regional Diversity and Developmental Dynamics of the AMPA-Receptor Proteome in the Mammalian Brain. *Neuron* 1–14 (2014). doi:10.1016/j.neuron.2014.08.044

282. Hollmann, M. & Heinemann, S. Cloned Glutamate Receptors. *Annu. Rev. Neurosci.* **17**, 31–108 (1994).

283. Shepherd, J. D. & Huganir, R. L. The cell biology of synaptic plasticity: AMPA receptor trafficking. *Annu. Rev. Cell Dev. Biol.* **23**, 613–43 (2007).

284. Sobolevsky, A. I., Rosconi, M. P. & Gouaux, E. X-ray structure, symmetry and mechanism of an AMPA-subtype glutamate receptor. *Nature* **462**, 745–56 (2009).

285. Penn, A. C., Balik, A., Wozny, C., Cais, O. & Greger, I. H. Activity-Mediated AMPA Receptor Remodeling, Driven by Alternative Splicing in the Ligand-Binding Domain. *Neuron* **76**, 503–510 (2012).

286. Plested, A. J. R. Structural mechanisms of activation and desensitization in neurotransmitter-gated ion channels. *Nat. Struct. Mol. Biol.* **23**, 494–502 (2016).

287. Armstrong, N. & Gouaux, E. Mechanisms for activation and antagonism of an AMPA-sensitive glutamate receptor: Crystal structures of the GluR2 ligand binding core. *Neuron* **28**, 165–181 (2000).

288. Colquhoun, D., Jonas, P. & Sakmann, B. Action of brief pulses of glutamate on AMPA/kainate receptors in patches from different neurones of rat hippocampal slices. *J. Physiol.* **458**, 261–287 (1992).

289. Xu-Friedman, M. A. & Regehr, W. G. Structural Contributions to Short-Term Synaptic Plasticity. *Physiol. Rev.* **84**, 69–85 (2004).

290. Rossmann, M. *et al.* Subunit-selective N-terminal domain associations organize the formation of AMPA receptor heteromers. *EMBO J.* **30**, 959–971 (2011).

291. Lu, W. *et al.* Subunit composition of synaptic AMPA receptors revealed by a single-cell genetic approach. *Neuron* **62**, 254–68 (2009).

292. Hirokawa, N., Niwa, S. & Tanaka, Y. Molecular motors in neurons: transport mechanisms and roles in brain function, development, and disease. *Neuron* **68**, 610–38 (2010).

293. Rangaraju, V., tom Dieck, S. & Schuman, E. M. Local translation in neuronal compartments: how local is local? *EMBO Rep.* **18**, 693–711 (2017).

294. Anggono, V. & Huganir, R. L. Regulation of AMPA receptor trafficking and synaptic plasticity. *Curr. Opin. Neurobiol.* **22**, 461–469 (2012).

295. Yan, D. & Tomita, S. Defined criteria for auxiliary subunits of glutamate receptors. *J. Physiol.* **590**, 21–31 (2012).

296. Letts, V. a *et al.* Genetic and physical maps of the stargazer locus on mouse chromosome 15. *Genomics* **43**, 62–8 (1997).

297. Chen, L. *et al.* Stargazin regulates synaptic targeting of AMPA receptors by two distinct mechanisms. *Nature* **408**, 936–43 (2000).

298. Kato, A. S., Gill, M. B., Yu, H., Nisenbaum, E. S. & Bredt, D. S. TARPs differentially decorate AMPA receptors to specify neuropharmacology. *Trends Neurosci.* **33**, 241–8 (2010).

299. Jackson, A. C. & Nicoll, R. The expanding social network of ionotropic glutamate receptors: TARPs and other transmembrane auxiliary subunits. *Neuron* **70**, 178–199 (2011).

300. Tomita, S. *et al.* Functional studies and distribution define a family of transmembrane AMPA receptor regulatory proteins. *J. Cell Biol.* **161**, 805–16 (2003).

301. Bats, C., Groc, L. & Choquet, D. The interaction between Stargazin and PSD-95 regulates AMPA receptor surface trafficking. *Neuron* **53**, 719–34 (2007).

302. Hafner, A.-S. *et al.* Lengthening of the Stargazin Cytoplasmic Tail Increases Synaptic Transmission by Promoting Interaction to Deeper Domains of PSD-95. *Neuron* 475–489 (2015). doi:10.1016/j.neuron.2015.03.013

303. Straub, C. & Tomita, S. The regulation of glutamate receptor trafficking and function by TARPs and other transmembrane auxiliary subunits. *Curr. Opin. Neurobiol.* **22**, 488–495 (2012).

304. Tomita, S. *et al.* Stargazin modulates AMPA receptor gating and trafficking by distinct domains. *Nature* **435**, 1052–8 (2005).

305. Yamazaki, M. *et al.* A novel action of stargazin as an enhancer of AMPA receptor activity. *Neurosci. Res.* **50**, 369–374 (2004).

306. Schwenk, J., Harmel, N., Zolles, G. & Bildl, W. Functional proteomics identify cornichon proteins as auxiliary subunits of AMPA receptors. *Science (80-.).* 1313–1319 (2009).

307. Engelhardt, J. Von, Mack, V. & Sprengel, R. CKAMP44: a brain-specific protein attenuating short-term synaptic plasticity in the dentate gyrus. *Science (80-.).* **60**, 1518–1522 (2010).

308. Klaassen, R. V. *et al.* Shisa6 traps AMPA receptors at postsynaptic sites and prevents their desensitization during synaptic activity. *Nat. Commun.* **7**, 1–12 (2016).

309. Schmitz, L. J. M. *et al.* The AMPA receptor-associated protein Shisa7 regulates hippocampal synaptic function and contextual memory. *Elife* **6**, 1–28 (2017).

310. Bissen, D., Foss, F. & Acker-Palmer, A. *AMPA receptors and their minions: auxiliary proteins in AMPA receptor trafficking*. *Cellular and molecular life sciences : CMLS* **76**, (Springer International Publishing, 2019).

311. Lin, D.-T. *et al.* Regulation of AMPA receptor extrasynaptic insertion by 4.1N, phosphorylation and palmitoylation. *Nat. Neurosci.* **12**, 879–87 (2009).

312. Kennedy, M. J., Davison, I. G., Robinson, C. G. & Ehlers, M. D. Syntaxin-4 defines a domain for activity-dependent exocytosis in dendritic spines. *Cell* **141**, 524–35 (2010).

313. Blanpied, T. A., Scott, D. B., Ehlers, M. D. & Carolina, N. Dynamics and Regulation of Clathrin Coats at Specialized Endocytic Zones of Dendrites and Spines. *Neuron* **36**, 435–449 (2002).

314. Raghavachari, S. & Lisman, J. E. Properties of Quantal Transmission at CA1 Synapses. *J. Neurophysiol.* **92**, 2456–2467 (2004).

315. Borgdorff, A. J. & Choquet, D. Regulation of AMPA receptor lateral movements. *Nature* **417**, 649–653 (2002).

316. Heine, M. *et al.* Surface mobility of postsynaptic AMPARs tunes synaptic transmission. *Science* **320**, 201–5 (2008).

317. Hoze, N. *et al.* Heterogeneity of AMPA receptor trafficking and molecular interactions revealed by superresolution analysis of live cell imaging. *Proc. Natl. Acad. Sci. U. S. A.* **109**, 17052–7 (2012).

318. Triller, A. & Choquet, D. New concepts in synaptic biology derived from single-molecule imaging. *Neuron* **59**, 359–74 (2008).

319. Nair, D. *et al.* Super-resolution imaging reveals that AMPA receptors inside synapses are dynamically organized in nanodomains regulated by PSD95. *J. Neurosci.* **33**, 13204–13224 (2013).

320. Opazo, P. *et al.* CaMKII triggers the diffusional trapping of surface AMPARs through phosphorylation of stargazin. *Neuron* **67**, 239–252 (2010).

321. Tang, A. H. *et al.* A trans-synaptic nanocolumn aligns neurotransmitter release to receptors. *Nature* **536**, 210–214 (2016).

322. Haas, K. T. *et al.* Pre-post synaptic alignment through neuroligin-1 tunes synaptic transmission efficiency. *Elife* **7**, 1–22 (2018).

323. Matsuzaki, M., Honkura, N., Ellis-Davies, G. C. R. & Kasai, H. Structural basis of long-term potentiation in single dendritic spines. *Nature* **429**, 761–766 (2004).

324. Hayashi, Y. *et al.* Driving AMPA receptors into synapses by LTP and CaMKII: requirement for GluR1 and PDZ domain interaction. *Science* **287**, 2262–7 (2000).

325. Carroll, R. C., Lissin, D. V, Zastrow, M. von, Nicoll, R. A. & Malenka, R. C. Rapid redistribution of glutamate receptors contributes to long-term depression in hippocampal cultures. *Nat. Neurosci.* **2**, 454–460 (1999).

326. Lisman, J., Yasuda, R. & Raghavachari, S. Mechanisms of CaMKII action in long-term potentiation. *Nat. Rev. Neurosci.* **13**, 169–182 (2012).

327. Derkach, V., Barria, A. & Soderling, T. R. Ca2+/calmodulin-kinase II enhances channel conductance of -amino-3-hydroxy-5-methyl-4-isoxazolepropionate type glutamate receptors. *Proc. Natl. Acad. Sci.* **96**, 3269–3274 (2002).

328. Mauceri, D., Cattabeni, F., Di Luca, M. & Gardoni, F. Printed in calmodulin-dependent protein kinase II phosphorylation drives synapse-associated protein 97 into spines. *J. Biol. Chem.* **279**, 23813–23821 (2004).

329. Howard, M. a, Elias, G. M., Elias, L. a B., Swat, W. & Nicoll, R. a. The role of SAP97 in synaptic glutamate receptor dynamics. *PNAS* **107**, 3805–10 (2010).

330. Volk, L., Kim, C.-H., Takamiya, K., Yu, Y. & Huganir, R. L. Developmental regulation of protein interacting with C kinase 1 (PICK1) function in hippocampal synaptic plasticity and learning. *Proc. Natl. Acad. Sci.* **107**, 21784–21789 (2010).

331. Opazo, P. & Choquet, D. A three-step model for the synaptic recruitment of AMPA receptors. *Mol. Cell. Neurosci.* **46**, 1–8 (2011).

332. Penn, A. C. *et al.* Hippocampal LTP and contextual learning require surface diffusion of AMPA receptors. *Nature* **549**, 384–388 (2017).

333. Lledo, P.-M., Zhang, X., Sudhof, T. C., Malenka, R. C. & Nicoll, R. A. Postsynaptic Membrane Fusion and Long-Term Potentiation. *Science (80-.).* **279**, 399–403 (1998).

334. Coultrap, S. J. *et al.* Autonomous CaMKII mediates both LTP and LTD using a mechanism for differential substrate site selection. *Cell Rep.* **6**, 431–437 (2014).

335. Yang, Y., Wang, X. -b. & Zhou, Q. Perisynaptic GluR2-lacking AMPA receptors control the reversibility of synaptic and spines modifications. *Proc. Natl. Acad. Sci.* **107**, 11999–12004 (2010).

336. Sanderson, J. L., Gorski, J. A. & Dell'Acqua, M. L. NMDA Receptor-Dependent LTD Requires Transient Synaptic Incorporation of Ca2+-Permeable AMPARs Mediated by AKAP150-Anchored PKA and Calcineurin. *Neuron* **89**, 1000–1015 (2016).

337. Plant, K. *et al.* Transient incorporation of native GluR2-lacking AMPA receptors during hippocampal long-term potentiation. *Nat. Neurosci.* **9**, 602–604 (2006).

338. Guire, E. S., Oh, M. C., Soderling, T. R. & Derkach, V. A. Recruitment of Calcium-Permeable AMPA Receptors during Synaptic Potentiation Is Regulated by CaM-Kinase I. *J. Neurosci.* **28**, 6000–6009 (2008).

339. Gray, E. E., Fink, A. E., Sariñana, J., Vissel, B. & O'Dell, T. J. Long-Term Potentiation in the Hippocampal CA1 Region Does Not Require Insertion and Activation of GluR2-Lacking AMPA Receptors. *J. Neurophysiol.* **98**, 2488–2492 (2007).

340. Adesnik, H. & Nicoll, R. A. Conservation of Glutamate Receptor 2-Containing AMPA Receptors during Long-Term Potentiation. *J. Neurosci.* **27**, 4598–4602 (2007).

341. Granger, A. J., Shi, Y., Lu, W., Cerpas, M. & Nicoll, R. LTP requires a reserve pool of glutamate receptors independent of subunit type. *Nature* **493**, 495–500 (2013).

342. Takemoto, K. *et al.* Optical inactivation of synaptic AMPA receptors erases fear memory. *Nat. Biotechnol.* **35**, 38–47 (2017).

343. Hayashi-Takagi, A. *et al.* Labelling and optical erasure of synaptic memory traces in the motor cortex. *Nature* **525**, 333 (2015).

344. Murakoshi, H. *et al.* Kinetics of Endogenous CaMKII Required for Synaptic Plasticity Revealed by Optogenetic Kinase Inhibitor. *Neuron* **94**, 37–47.e5 (2017).

345. Liu, Q. *et al.* A Photoactivatable Botulinum Neurotoxin for Inducible Control of Neurotransmission. *Neuron* **101**, 863–875.e6 (2019).

346. Adotevi, N. K. & Leitch, B. Alterations in AMPA receptor subunit expression in cortical inhibitory interneurons in the epileptic stargazer mutant mouse. *Neuroscience* **339**, 124–138 (2016).

347. Kondo, M., Sumino, R. & Okado, H. Combinations of AMPA receptor subunit expression in individual cortical neurons correlate with expression of specific calcium-binding proteins. *J. Neurosci.* **17**, 1570–81 (1997).

348. Lu, X. *et al.* Synaptic distribution of the AMPA-GluR2 subunit and its colocalization with calcium-binding proteins in rat cerebral cortex: an immunohistochemical study using a GluR2-specific monoclonal antibody. *Exp. Neurol.* **142**, 149–153 (1996).

349. Brill, J. & Huguenard, J. R. Sequential changes in AMPA receptor targeting in the developing neocortical excitatory circuit. *J. Neurosci.* **28**, 13918–28 (2008).

350. Chen, L. *et al.* Subunit-Specific Rules Governing AMPA Receptor Trafficking to Synapses in Hippocampal Pyramidal Neurons. *Cell* **105**, 331–343 (2001).

351. Gierdalski, M., Jablonska, B., Smith, A., Skangiel-Kramska, J. & Kossut, M. Deafferentation induced changes in GAD67 and GluR2 mRNA expression in mouse somatosensory cortex. *Mol. Brain Res.* **71**, 111–119 (1999).

352. He, H. Y., Rasmusson, D. D. & Quinlan, E. M. Progressive elevations in AMPA and GABAA receptor levels in deafferented somatosensory cortex. *J. Neurochem.* **90**, 1186–1193 (2004).

353. Collingridge, G. L., Kehl, S. J. & McLennan, H. Excitatory amino acids in synaptic transmission in the Schaffer collateral-commissural pathway of the rat hippocampus. *J. Physiol.* **334**, 33–46 (1983).

354. Morris, R. G. M., Anderson, E., Lynch, G. S. & Baudry, M. Selective impairment of learning and blockade of long-term potentiation by an N-methyl-D-aspartate receptor antagonist, AP5. *Nature* **319**, 774–776 (1986).

355. Whitlock, J. R., Heynen, A. J., Shuler, M. G. & Bear, M. F. Learning Induces Long-Term Potentiation in the Hippocampus. *Science (80-.).* **313**, 1093 LP-1097 (2006).

356. Nabavi, S. *et al.* Engineering a memory with LTD and LTP. *Nature* **511**, 348–352 (2014).

357. LeDoux, J. E. Emotion Circuits in the Brain. *Annu. Rev. Neurosci.* **23**, 155–184 (2000).

358. Kessels, H. W. & Malinow, R. Synaptic AMPA receptor plasticity and behavior. *Neuron* **61**, 340–50 (2009).

359. Schmitt, W. B. *et al.* Spatial reference memory in GluR-A-deficient mice using a novel hippocampal-dependent paddling pool escape task. *Hippocampus* **14**, 216–223 (2004).

360. Reisel, D. *et al.* Spatial memory dissociations in mice lacking GluR1. *Nat. Neurosci.* **5**, 868–873 (2002).

361. Humeau, Y. *et al.* A Pathway-Specific Function for Different AMPA Receptor Subunits in Amygdala Long-Term Potentiation and Fear Conditioning. *J. Neurosci.* **27**, 10947–10956 (2007).

362. Engblom, D. *et al.* Glutamate Receptors on Dopamine Neurons Control the Persistence of Cocaine Seeking. *Neuron* **59**, 497–508 (2008).

363. Letts, V. A. Stargazer—A Mouse to Seize! Verity. *Epilepsy Curr.* **5**, 161–165 (2005).

364. Caracciolo, L. *et al.* CREB controls cortical circuit plasticity and functional recovery after stroke. *Nat. Commun.* **9**, (2018).

365. Bieszczad, K. M. & Weinberger, N. M. Remodeling the cortex in memory: Increased use of a learning strategy increases the representational area of relevant acoustic cues. *Neurobiol. Learn. Mem.* **94**, 127–144 (2010).

366. Reed, A. *et al.* Cortical map plasticity improves learning but is not necessary for improved performance. *Neuron* **70**, 121–31 (2011).

367. Zepeda, A., Arias, C. & Sengpiel, F. Optical imaging of intrinsic signals: Recent developments in the methodology and its applications. *J. Neurosci. Methods* **136**, 1–21 (2004).

368. Schubert, V., Lebrecht, D. & Holtmaat, A. Peripheral Deafferentation-Driven Functional Somatosensory Map Shifts Are Associated with Local, Not Large-Scale Dendritic Structural Plasticity. *J. Neurosci.* **33**, 9474–9487 (2013).

369. Petersen, C. C. H., Hahn, T. T. G., Mehta, M., Grinvald, A. & Sakmann, B. Interaction of sensory responses with spontaneous depolarization in layer 2/3 barrel cortex. *Proc. Natl. Acad. Sci.* **100**, 13638–13643 (2003).

370. Frostig, R. D., Masino, S. A., Kwon, M. C. & Chen, C. H. Using light to probe the brain: Intrinsic signal optical imaging. *Int. J. Imaging Syst. Technol.* **6**, 216–224 (1995).

371. Svoboda, K. & Yasuda, R. Principles of Two-Photon Excitation Microscopy and Its Applications to Neuroscience. *Neuron* **50**, 823–839 (2006).

372. Grienberger, C. & Konnerth, A. Imaging Calcium in Neurons. *Neuron* **73**, 862–885 (2012).

373. Chen, T.-W. *et al.* Ultrasensitive fluorescent proteins for imaging neuronal activity. *Nature* **499**, 295–300 (2013).

374. Armstrong-James, M., Welker, E. & Callahan, C. The contribution of NMDA and non-NMDA receptors to fast and slow transmission of sensory information in the rat SI barrel cortex. *J. Neurosci.* **13**, 2149–2160 (1993).

375. Margolis, D. J., Lütcke, H. & Helmchen, F. Microcircuit dynamics of map plasticity in barrel cortex. *Curr. Opin. Neurobiol.* **24**, 76–81 (2014).

376. Haselmann, H. *et al.* Human Autoantibodies against the AMPA Receptor Subunit GluA2 Induce Receptor Reorganization and Memory Dysfunction. *Neuron* **100**, 91–105.e9 (2018).

377. Peng, X. *et al.* Cellular plasticity induced by anti-α-amino-3-hydroxy-5-methyl-4-isoxazolepropionic acid

(AMPA) receptor encephalitis antibodies. *Ann. Neurol.* **77**, 381–398 (2015).

378. Zaitsev, A. V. *et al.* Specific mechanism of use-dependent channel block of calcium-permeable AMPA receptors provides activity-dependent inhibition of glutamatergic neurotransmission. *J. Physiol.* **589**, 1587–1601 (2011).

379. Bliss, T. & Collingridge, G. Expression of NMDA receptor dependent LTP in the hippocampus. *J. Eng. Sci. Technol.* **13**, 1205–1221 (2018).

380. Neale, E. A., Bowers, L. M., Jia, M., Bateman, K. E. & Williamson, L. C. Botulinum neurotoxin a blocks synaptic vesicle exocytosis but not endocytosis at the nerve terminal. *J. Cell Biol.* **147**, 1249–1260 (1999).

381. Nishiyama, J., Mikuni, T. & Yasuda, R. Virus-Mediated Genome Editing via Homology-Directed Repair in Mitotic and Postmitotic Cells in Mammalian Brain. *Neuron* **96**, 755–768.e5 (2017).

382. Henley, J. M. & Wilkinson, K. A. Synaptic AMPA receptor composition in development, plasticity and disease. *Nat. Rev. Neurosci.* **17**, 337–350 (2016).

383. Kole, K. & Celikel, T. Neocortical Microdissection at Columnar and Laminar Resolution for Molecular Interrogation. *Curr. Protoc. Neurosci.* **86**, 1–21 (2019).

384. Major, G., Larkum, M. E. & Schiller, J. Active Properties of Neocortical Pyramidal Neuron Dendrites. *Annu. Rev. Neurosci.* **36**, 1–24 (2013).

385. Heo, C. *et al.* A soft, transparent, freely accessible cranial window for chronic imaging and electrophysiology. *Sci. Rep.* **6**, 1–11 (2016).

386. Constals, A. *et al.* Glutamate-induced AMPA receptor desensitization increases their mobility and modulates short-term plasticity through unbinding from Stargazin. *Neuron* **85**, 787–803 (2015).

387. Fortune, E. S. & Rose, G. J. Short-term synaptic plasticity as a temporal filter. *Trends Neurosci.* **24**, 381–385 (2001).

388. Zucker, R. S. & Regehr, W. G. Short-Term Synaptic Plasticity. *Annu. Rev. Physiol.* **64**, 355–405 (2002).

389. Choquet, D. Fast AMPAR trafficking for a high-frequency synaptic transmission. *Eur. J. Neurosci.* **32**, 250–260 (2010).

390. Choquet, D. & Triller, A. The dynamic synapse. *Neuron* **80**, 691–703 (2013).

391. Derdikman, D. *et al.* Layer-Specific Touch-Dependent Facilitation and Depression in the Somatosensory Cortex during Active Whisking. *J. Neurosci.* **26**, 9538–9547 (2006).

392. Reyes, A. & Sakmann, B. Developmental Switch in the Short-Term Modification of Unitary EPSPs Evoked in Layer 2/3 and Layer 5 Pyramidal Neurons of Rat Neocortex. *J. Neurosci.* **19**, 3827–3835 (1999).

393. Beierlein, M., Gibson, J. R. & Connors, B. W. Two Dynamically Distinct Inhibitory Networks in Layer 4 of the Neocortex. *J. Neurophysiol.* **90**, 2987–3000 (2003).

394. Huettner, J. E. & Bean, B. P. Block of N-methyl-D-aspartate-activated current by the anticonvulsant MK-801: Selective binding to open channels. *PNAS* **85**, 1307–1311 (1988).

395. Mathis, A. *et al.* DeepLabCut: markerless pose estimation of user-defined body parts with deep learning. *Nat. Neurosci.* **21**, 1281–1289 (2018).

Annexes

AMPAR trafficking dependent LTP initiates cortical remapping and adaptive behaviors during sensory experience

Tiago Campelo[1,2], Elisabete Augusto[1,2], Nicolas Chenouard[1,2], Aron de Miranda[1,2], Vladimir Kouskoff[1,2], Daniel Choquet[1,2,3*], and Frédéric Gambino[1,2*]

[1]Interdiscliplinary Institute for NeuroScience (IINS), CNRS, Centre Broca Nouvelle-Aquitaine, 146, rue Léo-Saignat, 33076 Bordeaux, France.

[2] UMR5297, University of Bordeaux, 146, rue Léo-Saignat, 33076 Bordeaux, France.

[3] Bordeaux Imaging Center, UMS 3420 CNRS, US4 INSERM, University of Bordeaux, Bordeaux, France

* These authors jointly supervised this work

Send correspondence to daniel.choquet@u-bordeaux.Fr or frederic.gambino@u-bordeaux.fr

Number of words: Title: 13; Abstract: 138; Main text: 1810; Caption 1: 181; Caption 2: 229; Caption 3: 172; Caption 4: 235; **Total: 2628**; Methods: 2884

Running title: LTP initiates cortical remapping and adaptive behaviors

Abstract

Cortical plasticity improves behaviors and helps recover lost functions after injury by optimizing neuronal computations. However, the underlying synaptic and circuit mechanisms remain unclear. In mice, we found that trimming all but one whisker enhances sensory responses from the spared whisker and occludes whisker-mediated long-term potentiation (w-LTP) *in vivo*. In addition, whisking-dependent behaviors that are initially impaired by single whisker experience (SWE) rapidly recover when associated cortical regions remap. Blocking the surface diffusion of AMPA receptors suppresses the expression of w-LTP in naïve mice with all whiskers intact, demonstrating that physiologically induced LTP *in vivo* also depends on AMPAR trafficking. We use this approach to demonstrate that w-LTP is required for SWE mediated strengthening of synaptic inputs and initiates the recovery of previously learned skills during the early phases of SWE. Taken together, our data reveal that w-LTP mediates cortical remapping and behavioral improvement upon partial sensory deafferentation and opens the path to controlling functional restauration of sensory maps after peripheral injury.

Functional sensory maps in the cerebral cortex reorganize in response to peripheral injury, with active modalities gaining cortical space at the expense of less active regions (*1*, *2*). While map expansion has been proposed to promote learning and to adapt behaviors (*3*–*5*), the underlying circuit and synaptic mechanisms remain poorly understood. Here, we exploited the mouse whisker-to-barrel cortex system to explore the relation between the synaptic mechanisms of sensory map plasticity and correlated adaptive behaviors (*6*–*8*). Rodents use their whiskers to explore their immediate tactile environment. Under normal conditions, neurons in each barrel-column have receptive fields in the primary somatosensory cortex (S1) that are strongly tuned towards one principal whisker (PW). Nevertheless, trimming some whiskers causes layer (L) 2/3 pyramidal neurons located in the deprived and spared-related columns to respond stronger to the spared whiskers stimulation (*6*–*10*), thereby resulting in the strengthening and expansion of the spared whisker representations within the map (*6*–*8*). Long-term synaptic potentiation (LTP) has been postulated as a synaptic mechanism for such response strengthening during learning and deprivation-induced plasticity (*6*–*15*). Initial studies reported that activation of *N*-methyl-D-aspartate receptors (NMDARs) (*14*, *16*), α-amino-3-hydroxy-5-methyl-4-isoxazolepropionic acid receptors (AMPARs) (*17*, *18*), α/δ CREB, α-CaMKII, and α-CaMKII autophosphorylation (*10*, *19*) are all involved in response potentiation in L2/3, thereby providing consistent, yet indirect, evidence for a requirement of LTP during whisker map plasticity. However, while whisker-mediated LTP (w-LTP) has been successfully achieved in S1 (*20*, *21*), a direct demonstration that synaptic plasticity is required for cortical remapping and the adaptation of sensorimotor skills is still lacking.

To explore this question, we first investigated the impact of single whisker experience (SWE) on w-LTP. We exposed mice to a brief period of SWE (2-4 days) by clipping all but the C2 whisker (**Fig. 1A**). In agreement with the potentiation of sensory-driven responses *in vivo* (*9*, *10*, *14*, *17*, *22*), the intrinsic optical signal evoked by the deflection of the spared whisker increased upon SWE within the spared whisker barrel column (**Fig. S1**). Importantly, it occurred at a time at which no alterations in activity of layer 4 granular neurons have been observed, suggesting that SWE-induced map plasticity originates primarily from changes in neural activity within L2/3 (*9*, *10*). Accordingly, when deflecting the principal C2 whisker back and forth (100 ms, 0.1 Hz),

the fraction of spiking neurons in L2/3 and the number of spikes per stimulus were increased in SWE as compared to full-whisker experience (FWE) (fraction of spiking cells, fwe: 0/20; swe: 11/13; p<0.001; spiking probability, fwe: 0; swe: 0.48 ± 0.09; p<0.001) (**Fig. 1B**). Despite a moderate increase in intrinsic excitability (**Fig. S2B**), the change of L2/3 neuronal spiking after SWE mostly resulted from an increase in peak amplitude of whisker-evoked subthreshold postsynaptic potentials (PSP; fwe: 9.88 ± 0.86 mV; swe: 17.98 ± 2.26 mV; p<0.001) (**Fig. 1C**; **Fig. S2C**). LTP-like mechanisms are prime candidates for enhancing synaptic transmission after SWE (*12–14*, *23*). To test this hypothesis, we compared w-LTP induction in FWE and SWE mice (**Fig. 1D, E**). In FWE animals, a significant potentiation of subsequent whisker-evoked PSP was elicited by stimulating the PW for 1 min at a frequency of 8 Hz (RWS, rhythmic whisker stimulation) (baseline: 8.18 ± 1.17 mV, RWS: 9.77 ± 1.11 mV; n=7; p=0.002) (**Fig. 1D, E,** light blue traces; see also **Fig. 2D**). This potentiation was in good agreement with the w-LTP induced by RWS through NMDARs-dependent plateau potentials driven by the coordinated activation of segregated thalamo-cortical circuits (**Fig. S2A**) (*20*, *21*). Conversely, in SWE mice, RWS failed to strengthen whisker-evoked PSP (baseline: 20.45 ± 2.26 mV, RWS: 19.9 ± 2.12 mV; n=7; p=0.264) (**Fig. 1D**). SWE had no effect on plateau potentials evoked by single whisker stimulation (**Fig. 1C,** see also **Fig. S4**), indicating that the NMDARs-dependent induction mechanism of w-LTP was not suppressed during SWE (*20*) (**Fig. S2F**). Taken together, our results indicate that SWE enhances synaptic response to the spared whisker and occludes w-LTP (fwe: 123.5 ± 5.9 %, n=7; swe: 97.6 ± 2.1 %, n=7; p=0.001) (**Fig. 1E**).

Next, we questioned if w-LTP was causally inducing the potentiation of whisker-evoked response during SWE (**Fig. 2, 3**). While blocking the induction of LTP with NMDARs antagonists provided the most direct evidence that synaptic plasticity at appropriate synapses is required for both potentiation of spared whisker responses and learning (*14*, *16*, *24*), it might obstruct normal sensory cortical transmission *in vivo*, which relies on NMDARs conductances (*25*). Instead, we used an antibody cross-linking approach to limit the surface diffusion of postsynaptic GluA2 (*26*) and thus block the expression of w-LTP. This subunit of AMPAR is predominantly expressed in the neocortex (*27*) and its expression in S1 is dynamically regulated upon partial sensory deafferentation (*28*, *29*). Consistent with previous studies (*26*), we found that in FWE mice with all whiskers intact, the cortical injection of immunoglobulins G (IgGs) against GluA2,

or the control anti-GFP IgG (Fig. S3A) did not affect neuronal excitability, spontaneous neuronal activity, sensory-evoked excitatory and inhibitory conductances, and NMDARs-dependent plateau potentials (Fig. 2B, C; Fig. S3). Similar to FWE mice in which no injection was done, RWS induced a significant w-LTP of PW-evoked PSP in the presence of anti-GFP IgGs (baseline: 8 ± 1.9 mV, RWS: 9.7 ± 2 mV; n=9; p=0.002) (Fig. 2D). On average, the change in PSP amplitude when RWS was applied (RWS+: 123.9 ± 1.7 %, n=9) was significantly higher than when RWS was not (RWS-: 101.6 ± 0.71 %, n=8, p<0.001) (Fig. 2 F), and positively correlated with the strength of plateau potentials (Fig. 2G; Fig. S4). In contrast, cross-linking-mediated suppression of GluA2 diffusion prevented w-LTP (baseline: 10.6 ± 1.2 mV, RWS: 11.3 ± 1.3 mV; n=8; p=0.102; RWS+ *vs.* RWS-: 107.1 ± 3.6 % *vs.* 97.5 ± 3.1 %, p>0.05) (Fig. 2E, F; Fig. S4). S1 pyramidal neurons bearing high plateau strength could not be potentiated in the presence of anti-GluA2 IgGs (plateau strength > 0.5; anti-GFP: 138.6 ± 5 %, n=4; anti-GluA2: 108 ± 4 %, n=7; p<0.001) (Fig. 2G; Fig. S4). Our results demonstrate that cross-linking surface GluA2 prevents the expression of w-LTP in living animals, thereby complementing *in vitro* observations (*26*, *30*, *31*).

We reasoned that if w-LTP increases synaptic responses during SWE, the chronic suppression of GluA2 surface diffusion during SWE would block this mechanism, thereby allowing RWS to potentiate whisker-evoked PSP. Anti-GluA2 IgGs (or anti-GFP for controls) were injected in S1 twice a day for two consecutive days while trimming all but the contra-lateral C2 whisker. L2/3 pyramidal neurons were then recorded after a 12h-clearance period to washout IgGs (X-SWE, Fig. 3A). X-SWE significantly decreased the average number of spikes per PW deflection (anti-GluA2: 0.08 ± 0.03; n=9; anti-GFP: 0.35 ± 0.14, n=8; p=0.026) (Fig. 3B, C) although it did not modify the fraction of spiking neurons (X-SWE: 6/9; SWE: 11/13; p>0.05) (Fig. 3B). The average PW-evoked PSP peak amplitude in the presence of anti-GluA2 IgGs (7 ± 1.3 mV, n=9, p<0.001), but not anti-GFP IgGs (14.2 ± 1.6 mV, n=8, p=0.126), was significantly decreased as compared to SWE (17.9 ± 2.3 mV, n=13) (Fig. 3D, E). X-SWE did not alter whisker-induced plateau potentials (Fig. S4B, C). RWS potentiated PW-evoked PSP when anti-GluA2 IgGs, but not anti-GFP IgGs, were washed-out (anti-GluA2; baseline: 7.6± 1.7 mV, RWS: 10.4± 2.6 mV; n=6; p=0.04; anti-GFP; baseline: 12.6 ± 1.6 mV, RWS: 12.2 ± 1.9 mV; n=6; p=0.436) (Fig. 3F, G). Thus X-SWE restored the expression of w-LTP in SWE mice (X-SWE: 129.8 ± 7.8 %, n=6 *vs.* SWE: 97.6 ± 2.1 %, n=7; p=0.001) to similar levels as in FWE mice (123.5± 5.9 %, n=7; p=0.4)

(Fig. 3G; Fig. S4). This indicates that chronically blocking AMPARs trafficking during SWE prevents sensory-evoked synaptic potentiation.

SWE alters various whisker-mediated behavioral tasks (*2*, *14*, *32*, *33*). We demonstrated that the chronic blockade of AMPAR trafficking prevented potentiation of whisker-evoked responses during SWE, supporting the idea that w-LTP contributes to SWE-induced cortical remapping. Thus, we reasoned that if cortical remapping improves tactile perception, blocking w-LTP during SWE should affect whisker-mediated behavioral performance. To test this hypothesis, we monitored freely behaving mice performing a binary gap-crossing task under infrared light (Fig. 4A; Fig. S5A-C). Mice were trained to reach a rewarding platform separated by a distance between 40 and 65 mm from the home platform (Fig. 4B). At a distance of 65 mm, mice used preferentially their whiskers to locate the target platform and jump onto it to receive the reward (*32*, *33*) (Fig. S5D). SWE-mediated cortical remapping was induced after mice reached expertise (4 days of training) (Fig. 4B; Fig. S5C). Gap-crossing performance decreased immediately after SWE (fraction of success; session 4: 0.96 ± 0.04; session 5: 0.68 ± 13; n=6; p=0.006) but recovered quickly after 2 days of SWE (session 6: 0.87 ± 0.09; p=0.372) (Fig. 4C), a time scale at which w-LTP has been fully occluded (Fig. 1). Importantly, mice that were not tested during SWE (sessions 5 to 7) had similar final success rate (session 8; 0.95 ±0.03, n=6; 0.89 ± 0.08, n=5; p>0.05) (Fig. 4C, D), suggesting that behavioral recovery was likely not caused by a new learning phase. The gap-crossing performance of anti-GluA2 IgGs-injected mice decreased more (session 5: -61.8 ± 12% *vs.* -22.6 ± 6.7%, p=0.016) and recovered significantly slower as compared to that of anti-GFP injected mice (Fig. 4E-G). Success rates were however similar between both groups 3 days after SWE (session7: 0.82 ± 0.09 *vs.* 0.72 ± 0.14; p=0.805) (Fig. 4G), which might reflect barrel cortex-independent behavioral strategies (*32*, *34*) and/or the existence of mechanisms that preserve a slow capacity for cortical remapping (*14*). None of the IgGs altered exploration and decision latency (Fig. S6). Altogether, our data indicate that blocking GluA2 diffusion similarly affects neuronal response potentiation *in vivo* and behavioral output at early phases of SWE, thereby providing new evidence for a critical role of w-LTP in facilitating the recovery of lost skills.

In previous studies, controlling synaptic plasticity mechanisms in rodents has been used to alter memories they have formed (*26*, *35*). Here, by manipulating the dynamics of

AMPARs *in vivo*, we demonstrate that cross-linking GluA2 inhibits w-LTP induced by physiological and behaviorally relevant stimuli, presumably by blocking GluA2 surface diffusion and preventing the increase in synaptic AMPAR content. This NMDARs-dependent form of LTP is associated during the early phases of SWE with improvements in behavioral recovery. This suggests that w-LTP occurs nearly immediately following partial sensory deafferentation, providing new important processing resources for spared inputs (*6*–*8*). In support of this hypothesis, training-related increases in cortical representations correlate with perceptual learning (*3*–*5*), suggesting that sensory deafferentation could cause behavioral gains by promoting cortical remapping. Our results are of importance for clinicians and patients, as brief periods of sensory deprivation have been proposed as therapeutic ways to promote recovery of lost function after peripheral injury or stroke (*36*).

Acknowledgements

We thank E. Normand and the IINS *in vivo* core facility for animal husbandry. We thank the IINS cell biology core facilities (LABEX BRAIN [ANR-10-LABX-43]) and in particular C. Breillat for antibody handling. We thank H. El Oussini and B. Darracq (Imetronic) for their technical expertise and support, and all the members of the Gambino and Choquet laboratories for technical assistance and helpful discussions. We thank E. Gouaux for generous gift of the 15F1 anti-GluA2 antibody.

This project has received funding from (to FG): the European Research Council (ERC) under the European Union's Horizon 2020 research and innovation program (NEUROGOAL, grant agreement n° 677878), the FP7 Marie-Curie Career Integration program (grant agreement n° 631044); the ANR JCJC (grant agreement n° 14-CE13-0012-01), the University of Bordeaux (Initiative of Excellence senior chair 2014); (to DC): the European Research Council (ERC) under the European Union's Horizon 2020 research and innovation program (ADOS, grant agreement n° 339541; DynSynMem, grant agreement n° 787340); and from the Region Nouvelle Aquitaine to DC and FG.

Author contribution

TC, EA, AM, VK performed the experiments. TC, DC and FG conceived the studies and analyzed the data with the help of EA, NC, AM and VK. DC and FG supervised the research and wrote the manuscript with the help from co-authors.

Declaration of interests

The authors declare no competing financial interests.

References

1. M. M. Merzenich *et al.*, Topographic reorganization of somatosensory cortical areas 3b and 1 in adult monkeys following restricted deafferentation. *Neuroscience*. **8**, 33–55 (1983).
2. C. Xerri, Plasticity of cortical maps: multiple triggers for adaptive reorganization following brain damage and spinal cord injury. *Neuroscientist*. **18**, 133–48 (2012).
3. A. Reed *et al.*, Cortical map plasticity improves learning but is not necessary for improved performance. *Neuron*. **70**, 121–31 (2011).
4. K. Molina-Luna, B. Hertler, M. M. Buitrago, A. R. Luft, Motor learning transiently changes cortical somatotopy. *Neuroimage*. **40**, 1748–1754 (2008).
5. K. M. Bieszczad, N. M. Weinberger, Remodeling the cortex in memory: Increased use of a learning strategy increases the representational area of relevant acoustic cues. *Neurobiol. Learn. Mem.* **94**, 127–144 (2010).
6. D. J. Margolis, H. Lütcke, F. Helmchen, Microcircuit dynamics of map plasticity in barrel cortex. *Curr. Opin. Neurobiol.* **24**, 76–81 (2014).
7. D. E. Feldman, Synaptic Mechanisms for Plasticity in Neocortex. *Annu. Rev. Neurosci.* **32**, 33–55 (2009).
8. K. Fox, Anatomical pathways and molecular mechanisms for plasticity in the barrel cortex. *Neuroscience*. **111**, 799–814 (2002).
9. S. Glazewski, K. Fox, Time course of experience-dependent synaptic potentiation and depression in barrel cortex of adolescent rats. *J. Neurophysiol.* **75**, 1714–1729 (1996).
10. S. Glazewski, C. M. Chen, A. Silva, K. Fox, Requirement for alpha-CaMKII in experience-dependent plasticity of the barrel cortex. *Science*. **272**, 421–3 (1996).
11. M. F. Bear, L. N. Cooper, F. F. Ebner, A physiological basis for a theory of synapse modification. *Science*. **237**, 42–8 (1987).
12. M. S. Rioult-Pedotti, D. Friedman, J. P. Donoghue, Learning-induced LTP in neocortex. *Science*. **290**, 533–6 (2000).
13. J. R. Whitlock, A. J. Heynen, M. G. Shuler, M. F. Bear, Learning induces long-term potentiation in the hippocampus. *Science*. **313**, 1093–7 (2006).
14. R. L. Clem, T. Celikel, A. L. Barth, Ongoing in Vivo Experience Triggers Synaptic Metaplasticity in the Neocortex. *Science (80-.).* **319**, 101–104 (2008).
15. G. T. Finnerty, L. S. Roberts, B. W. Connors, Sensory experience modifies the short-term dynamics of neocortical synapses. *Nature*. **400**, 367–71 (1999).
16. V. Rema, M. Armstrong-James, F. F. Ebner, Experience-dependent plasticity of adult rat S1 cortex requires local NMDA receptor activation. *J. Neurosci.* **18**, 10196–206 (1998).
17. R. L. Clem, A. Barth, Pathway-specific trafficking of native AMPARs by in vivo experience. *Neuron*. **49**, 663–70 (2006).
18. J. Dachtler *et al.*, Experience-Dependent Plasticity Acts via GluR1 and a Novel Neuronal Nitric Oxide Synthase-Dependent Synaptic Mechanism in Adult Cortex. *J. Neurosci.* **31**, 11220–11230 (2011).
19. S. Glazewski, K. P. Giese, A. Silva, K. Fox, The role of alpha-CaMKII autophosphorylation in neocortical experience-dependent plasticity. *Nat. Neurosci.* **3**, 911–8 (2000).
20. F. Gambino *et al.*, Sensory-evoked LTP driven by dendritic plateau potentials in vivo. *Nature*. **515**, 116–119 (2014).
21. Y. Zhang, R. H. Cudmore, D.-T. Lin, D. J. Linden, R. L. Huganir, Visualization of

NMDA receptor–dependent AMPA receptor synaptic plasticity in vivo. *Nat. Neurosci.* **18**, 402–7 (2015).
22. A. L. Barth *et al.*, Upregulation of cAMP response element-mediated gene expression during experience-dependent plasticity in adult neocortex. *J. Neurosci.* **20**, 4206–16 (2000).
23. T. P. Carvalho, D. V Buonomano, Differential effects of excitatory and inhibitory plasticity on synaptically driven neuronal input-output functions. *Neuron*. **61**, 774–85 (2009).
24. T. Takeuchi, A. J. Duszkiewicz, R. G. M. Morris, The synaptic plasticity and memory hypothesis: encoding, storage and persistence. *Philos. Trans. R. Soc. B Biol. Sci.* **369**, 20130288–20130288 (2013).
25. M. Armstrong-James, E. Welker, C. A. Callahan, The contribution of NMDA and non-NMDA receptors to fast and slow transmission of sensory information in the rat SI barrel cortex. *J. Neurosci.* **13**, 2149–60 (1993).
26. A. C. Penn *et al.*, Hippocampal LTP and contextual learning require surface diffusion of AMPA receptors. *Nature*. **549**, 384–388 (2017).
27. J. Schwenk *et al.*, Regional diversity and developmental dynamics of the AMPA-receptor proteome in the mammalian brain. *Neuron*. **84**, 41–54 (2014).
28. H.-Y. He, D. D. Rasmusson, E. M. Quinlan, Progressive elevations in AMPA and GABAA receptor levels in deafferented somatosensory cortex. *J. Neurochem.* **90**, 1186–93 (2004).
29. M. Gierdalski, B. Jablonska, A. Smith, J. Skangiel-Kramska, M. Kossut, Deafferentation induced changes in GAD67 and GluR2 mRNA expression in mouse somatosensory cortex. *Brain Res. Mol. Brain Res.* **71**, 111–9 (1999).
30. A. J. Granger, Y. Shi, W. Lu, M. Cerpas, R. A. Nicoll, LTP requires a reserve pool of glutamate receptors independent of subunit type. *Nature*. **493**, 495–500 (2012).
31. D. Choquet, Linking Nanoscale Dynamics of AMPA Receptor Organization to Plasticity of Excitatory Synapses and Learning. *J. Neurosci.* **38**, 9318–9329 (2018).
32. T. Celikel, B. Sakmann, Sensory integration across space and in time for decision making in the somatosensory system of rodents. *Proc. Natl. Acad. Sci. U. S. A.* **104**, 1395–400 (2007).
33. P. Barnéoud, M. Gyger, F. Andrés, H. van der Loos, Vibrissa-related behavior in mice: transient effect of ablation of the barrel cortex. *Behav. Brain Res.* **44**, 87–99 (1991).
34. Y. K. Hong, C. O. Lacefield, C. C. Rodgers, R. M. Bruno, Sensation, movement and learning in the absence of barrel cortex. *Nature*. **561**, 542–546 (2018).
35. S. Nabavi *et al.*, Engineering a memory with LTD and LTP. *Nature*. **511**, 348–352 (2014).
36. A. W. Kraft, A. Q. Bauer, J. P. Culver, J.-M. Lee, Sensory deprivation after focal ischemia in mice accelerates brain remapping and improves functional recovery through Arc-dependent synaptic plasticity. *Sci. Transl. Med.* **10**, eaag1328 (2018).

Figures and Legends

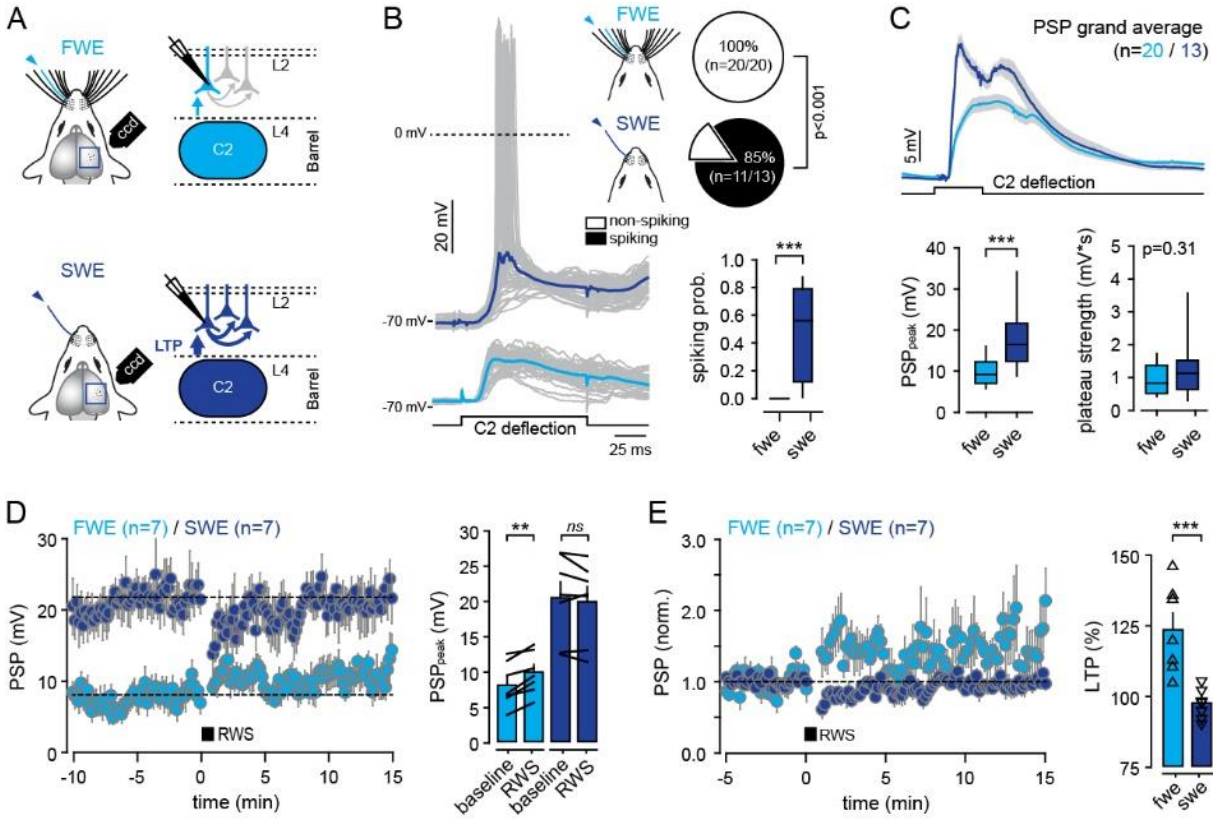

<u>Fig.1.</u> SWE increases whisker-evoked responses and occludes w-LTP.

A) Schematic of recordings of L2/3 pyramidal neurons in full-whisker experience (fwe) and single-whisker experience (swe) mice. PSPs and RWS are evoked by deflecting the principal whisker (PW). **B)** *Left*, single-cell examples of whisker-evoked responses (grey, single trials; dark and light blue, averaged traces from swe and fwe mice). Square pulse lines, C2 whisker deflection (100 ms). *Right,* fraction of spiking neurons (top) and number of spikes per whisker deflection (spiking probability; median ± interquartile range). **C)** *Top,* PW-evoked PSP grand average (all recorded cells averaged) ± sem. Square pulse lines, C2 whisker deflection (100 ms). *Bottom,* median (± interquartile range) PSP peak amplitude and plateau strength. **D)** *Left,* time-course of averaged PSP peak amplitude before and after RWS, in FWE and SWE mice. *Right,* mean (±sem) amplitude before (baseline) and after RWS. Error bars, sem; grey lines between bars, pairs. **E)** *Left,* time-course of averaged PSP amplitude normalized to baseline. *Right,* mean (±sem) amplitude normalized to baseline (% of LTP). Triangles, individual cells.

Values and statistical tests are provided in Table S1.

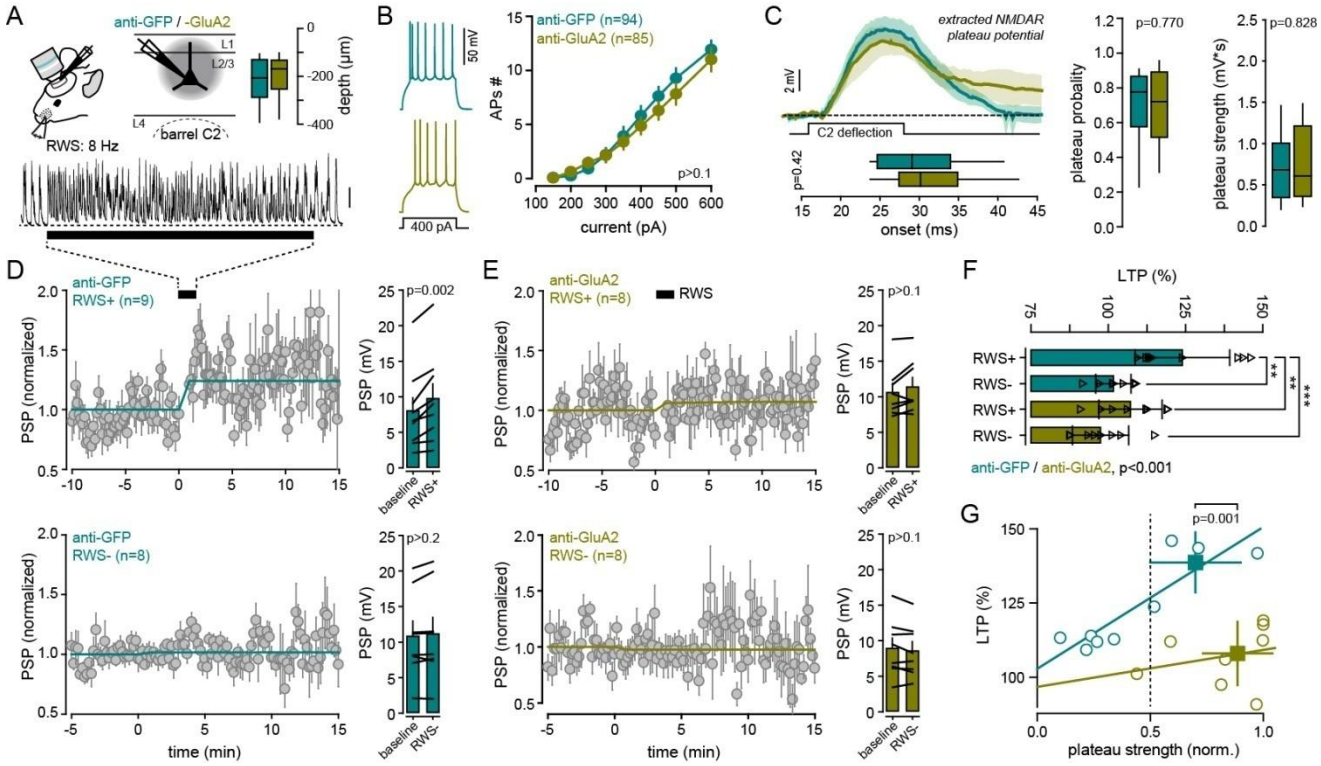

<u>Fig.2.</u> Cross-linking GluA2 subunit suppresses the expression of w-LTP without altering its induction mechanism.

A) *Top,* schematic of recordings of L2/3 pyramidal neurons in the presence of anti-GluA2 or anti-GFP IgGs. Depth of recorded cells is indicated. *Bottom,* example trace of sustained depolarization induced by RWS (8 Hz for 1 min; black bar). **B)** *Left,* example of spiking pattern in anti-GFP (green) and anti-GluA2 (magenta) injected mice upon 400pA current injection. *Right,* average (± sem) number of action potentials (APs) triggered by incremental current injections. **C)** *Left top,* grand average of PW-evoked extracted plateau potential (all recorded cells averaged ± sem). Black square pulse line, C2 whisker deflection (100 ms). *Left bottom*, median (± interquartile range) onset of plateau potentials. *Right*, median (± interquartile range) plateau probability and strength. **D)** *Left,* time-course of averaged PSP peak amplitude upon RWS (RWS+, *top*) and when RWS is not induced (RWS-, *bottom*), in anti-GFP injected mice. *Right,* mean (± sem) peak amplitude before (baseline) and after RWS+ (*top*) or RWS- (*bottom*). Black lines between bars, pairs. **E)** Same as in D) but for anti-GluA2 IgGs injected mice. **F)** Mean (± sem) peak amplitude normalized to baseline (% of LTP). Triangles, individual cells. **G)** Correlation between normalized plateau strength and the level of RWS-induced LTP in anti-GFP (green) and anti-GluA2 (magenta) IgGs injected mice.

Values and statistical tests are provided in Table S1.

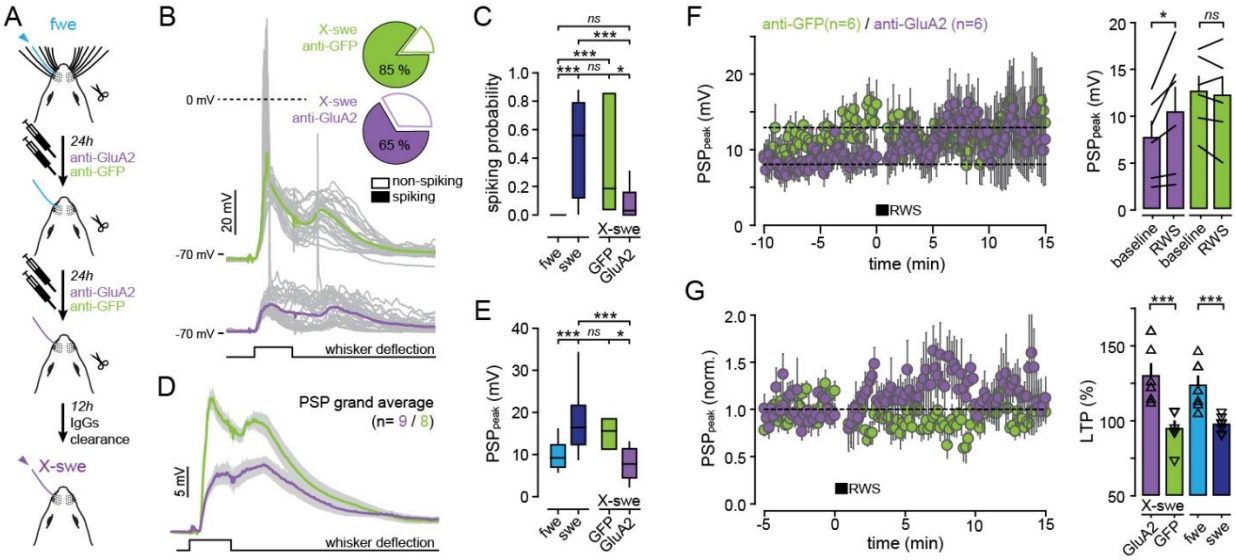

<u>Fig.3.</u> w-LTP mediates neuronal potentiation during SWE-induced cortical remapping.

A) Schematic of experimental strategy. IgGs are injected during SWE, followed by washed-out before recordings. **B)** *Left*, single-cell examples of whisker-evoked responses (grey, single traces; green and purple, averaged traces from anti-GFP and anti-GluA2 injected mice, respectively). Square pulse line, C2 whisker deflection (100 ms). *Right,* fraction of spiking neurons triggered by whisker deflection. **C)** Number of spikes per whisker deflection (spiking probability; median ± interquartile range). **D)** PW-evoked PSP grand average (all recorded cells averaged ± sem). Square pulse line, C2 whisker deflection (100 ms). **E)** Median (± interquartile range) PSP peak amplitude. **F)** *Left,* time-course of averaged PSP peak amplitude upon RWS in anti-GFP (green) and anti-GluA2 (purple) injected mice (after wash-out). *Right,* mean (± sem) PSP peak amplitude before (baseline) and after RWS. Black lines between bars, pairs. **G)** *Left,* time-course of averaged PSP amplitude normalized to baseline. *Right,* mean (±sem) amplitude normalized to baseline (% of LTP). Triangles, individual cells.

Values and statistical tests are provided in Table S1.

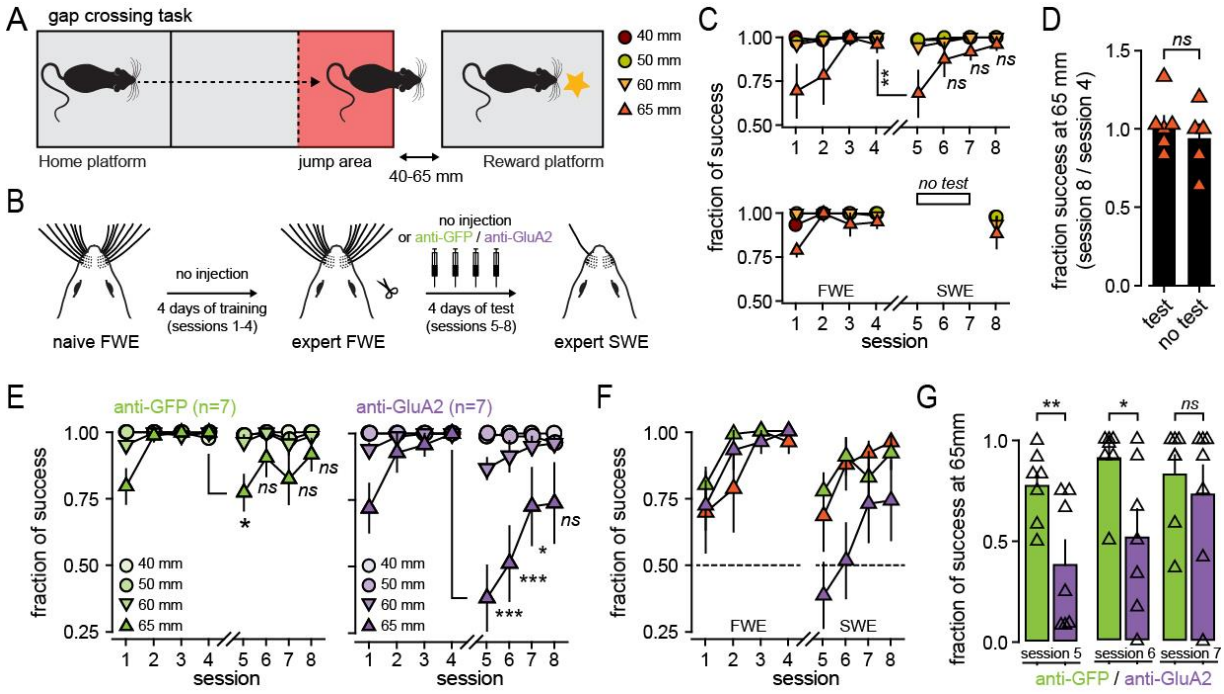

<u>Fig.4.</u> w-LTP facilitates the recovery of altered whisker-dependent behaviors during the early phases of SWE.

A) Overview of the gap-crossing task (see Fig. S5 for details). The reward platform is moved between trials to set the gap width from 40 to 65 mm. **B)** Schematic of the time-course regarding the behavior, the trimming of the whiskers and IgGs injections. Mice learn to reach the rewarding platform (4 consecutive days) before SWE is induced during which anti-GFP or anti-GluA2 IgGs are injected through implanted cannula twice a day (before and after each behavioral session). **C)** *Top,* averaged (±sem) fraction of gap-crossing success for different gap distances, in non-injected mice. *Bottom,* tests in session 5 to 7 were omitted to assess the role of learning during SWE. **D)** Mean (± sem) fraction of success in the final session (normalized to session 4 before SWE) at a distance of 65 mm for mice that are tested every day (test) and for mice that are not tested in sessions 5 to 7 (no test). Triangles, individual mice. **E)** Averaged (± sem) fraction of gap-crossing success for different gap distances, in anti-GFP (*left*) and anti-GLuA2 (*right*) injected mice. **F)** Averaged (± sem) fraction of gap-crossing success at a distance of 65 mm, in non-injected (orange), anti-GFP (green) and anti-GLuA2 (purple) injected mice. **G)** Mean (± sem) fraction of success at a distance of 65 mm after expertise in fwe mice and during swe. Triangles, individual mice.

Values and statistical tests are provided in Table S1.

Supporting Online Material

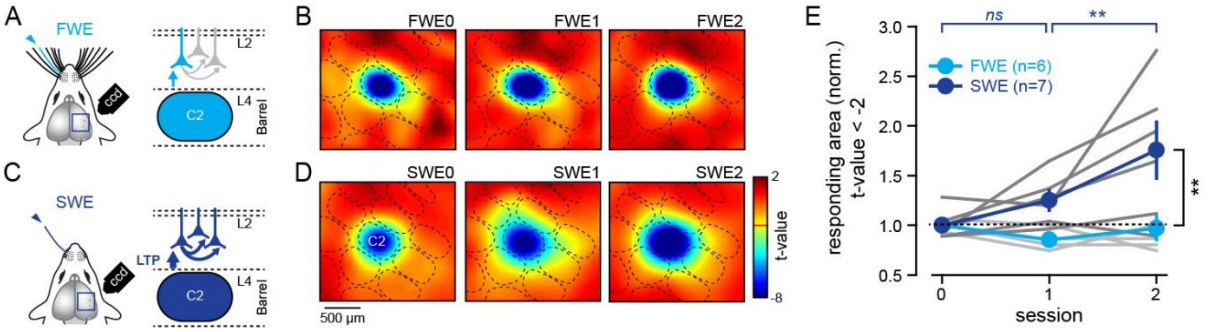

Fig. S1. SWE increases the cortical representation of the spared whisker.

A) PW-evoked intrinsic optical signals (IOS) are recorded in full-experience experience (fwe) mice (n=6). **B)** Statistical *t*-maps over 3 successive days. For each mouse, red light reflectance 100 ms-long frames were acquired during anesthesia through the skull before (frames 1-10), during (frames 11-20), and after (frames 21-50) a 1-s long train (8 Hz) of single whisker deflection. The PW-evoked response area is computed by a statistical comparison of the averaged baseline (frames 1-10) and whisker-evoked (frames 19-28) IOS over at least 10 successive trials. This is done by using a pixel-by-pixel paired *t*-test, and only pixels with a *t*-value below the threshold (t<-2) are included into the stimulus-evoked response area. **C, D)** Same representation as A and B, but for SWE mice (n=7). **E)** Averaged (± sem) PW-evoked response area (normalized to the first session). Light/dark grey lines, individual FWE/SWE mice, respectively.

Values and statistical tests are provided in Table S1.

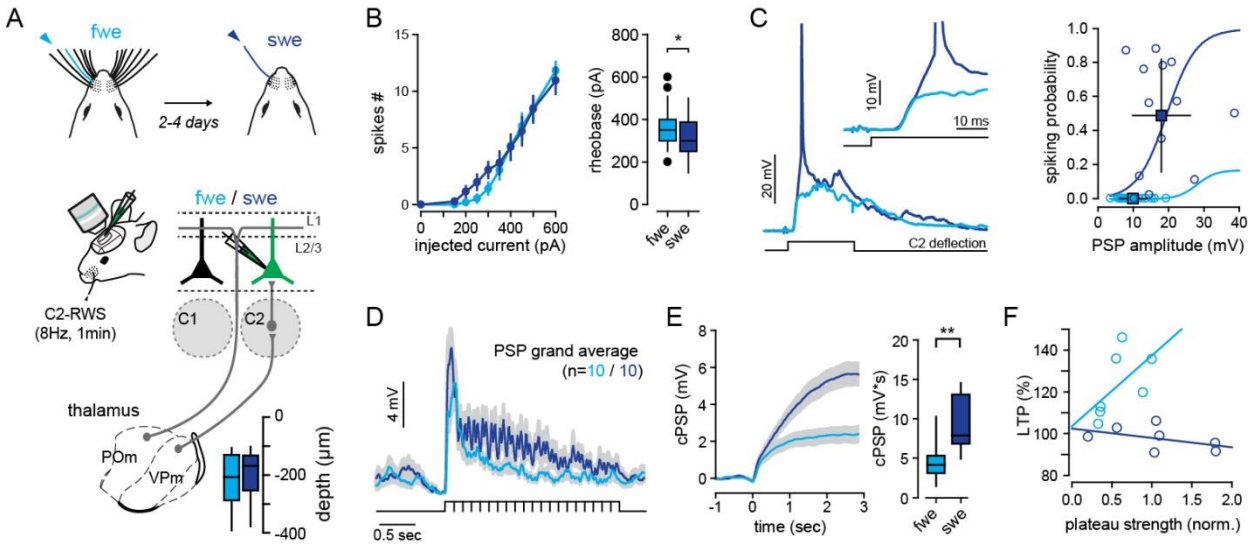

Fig. S2. Effect of SWE on L2/3 pyramidal neurons excitability and plateau potentials

A) *Top,* schematic of sensory experience protocol. *Bottom,* schematic of thalamo-cortical circuits. Sensory information from the whiskers is transmitted to S1 by two main and well-segregated thalamo-cortical projections. L2/3 pyramidal neurons are recorded in the principal barrel-related column upon deflection of the PW (C2). Depth of recorded cells is indicated. **B)** *Left,* average (± sem) number of action potentials (APs) triggered by incremental current injections in FWE (light blue) and SWE (dark blue) mice. *Right,* Median (± interquartile range) minimal current amplitude (pA) triggering action potentials (rheobase). **C)** *Left,* single-cell examples of PW-evoked responses (averaged traces from FWE (light blue) and SWE (dark blue) mice). *Right*, relationship between PW-evoked PSP amplitude and the spiking probability illustrating the increase in PSP-spike coupling upon SWE. Circles, individual cells; squares, averages. **D)** Grand average (all recorded cells averaged, ± sem) of membrane depolarization upon rhythmic whisker stimulation (20 stimuli at 8 Hz). **E)** *Left,* cumulative RWS-induced depolarization. *Right,* median (± interquartile range) cumulative depolarization measured at the end of the stimulation. **F)** Correlation between normalized plateau strength and the level of RWS-induced LTP in FWE (light blue) and SWE (dark blue) mice. SWE dissociates the induction from the expression of w-LTP by suppressing siLTP without affecting plateau strength.

Values and statistical tests are provided in Table S1.

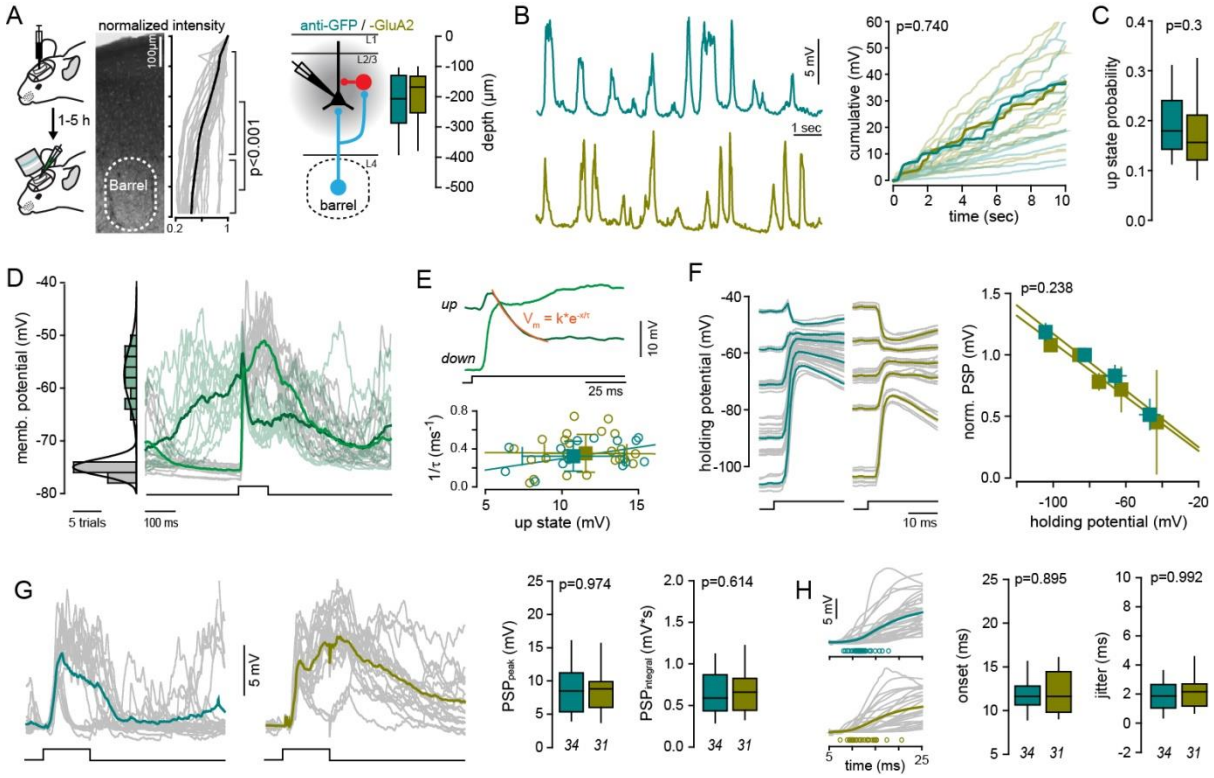

Fig. S3. Cross-linking GluA2 subunit does not affect spontaneous activity nor excitatory/inhibitory PW-evoked responses

A) *Left,* Schematic of experimental strategy. L2/3 pyramidal neurons are recorded in PW barrel-related column, 1 to 5h after IgGs injection. *Middle,* normalized intensity of anti-GluA2 IgGs signal as a function of cortical depth. IgGs are mostly targeting superficial layers. *Right,* schematic of the excitatory (light blue)/inhibitory (red) feed-forward circuit in a barrel-related column. Depth of recorded cells is indicated. **B)** *Left,* examples of single-cell spontaneous membrane potential during anesthesia in anti-GFP (top) and anti-GluA2 (bottom) IgGs injected mice. *Right,* cumulative RWS-induced depolarization. Light lines, individual cells. Bold lines, examples from B. **C)** Median (± interquartile range) probability of spontaneous up-states. **D)** *Left,* membrane potential histogram showing the average (30 ms) membrane potential before each PW stimulation. Down (grey) and up (green) states follow separated Gaussian distributions. *Right,* PW-evoked PSPs during down (green) and up (dark green) states. Individual trials are represented with light lines. **E)** *Top*, single-cell examples of PW-evoked PSP in down and up states. The decay of membrane potential during up states is fitted with an exponential, which is indicative of the amount of PW-evoked inhibition. Bottom, relation between the amplitude of up states and the exponential tau, in anti-GFP (green) and anti-GluA2 (magenta) IgGs injected mice. Circles, individual cells; squares, mean (± sem). **F)** *Left,* single-cells examples of PW-evoked PSPs at different holding potentials. Right, relation between holding potential and the amplitude of PW-PSP (normalized to the amplitude at resting membrane potential). **G)** *Left*, single-cell example of PW-evoked PSPs. Individual trials are represented with grey lines. *Right,* Median (± interquartile range) PSP peak amplitude and integrals. **H)** *Left*, single-cells examples of PW-evoked PSPs illustrating the onset of PSP. Circles, individual cells. Right, Median (± interquartile range) PSP onset and onset jitter. Square pulse line, whisker deflections (100 ms).

Values and statistical tests are provided in Table S1.

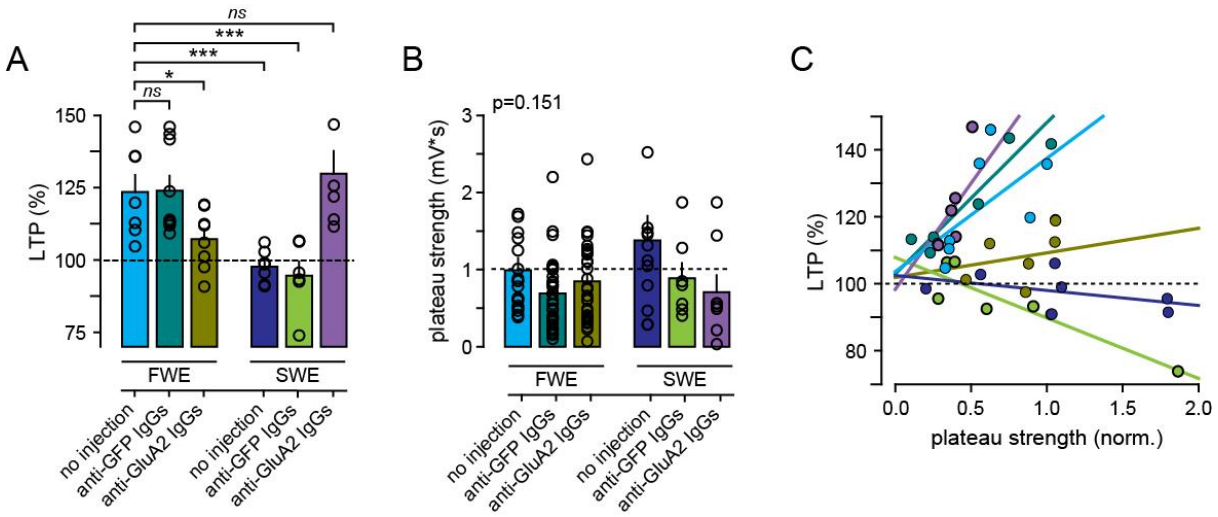

Fig. S4. Comparison between all the different treatments for LTP and plateau strength

A) Mean (± sem) amplitude normalized to baseline (% of LTP). Circles, individual cells. **B)** Mean (± sem) plateau strength. Circles, individual cells. **C)** Correlation between normalized plateau strength and the level of RWS-induced LTP for all treatments. Only the conditions SWE (dark blue) and FWE+antiGluA2 IgGs (magenta) dissociate the induction from the expression of w-LTP by suppressing w-LTP without affecting plateau strength.

Values and statistical tests are provided in Table S1.

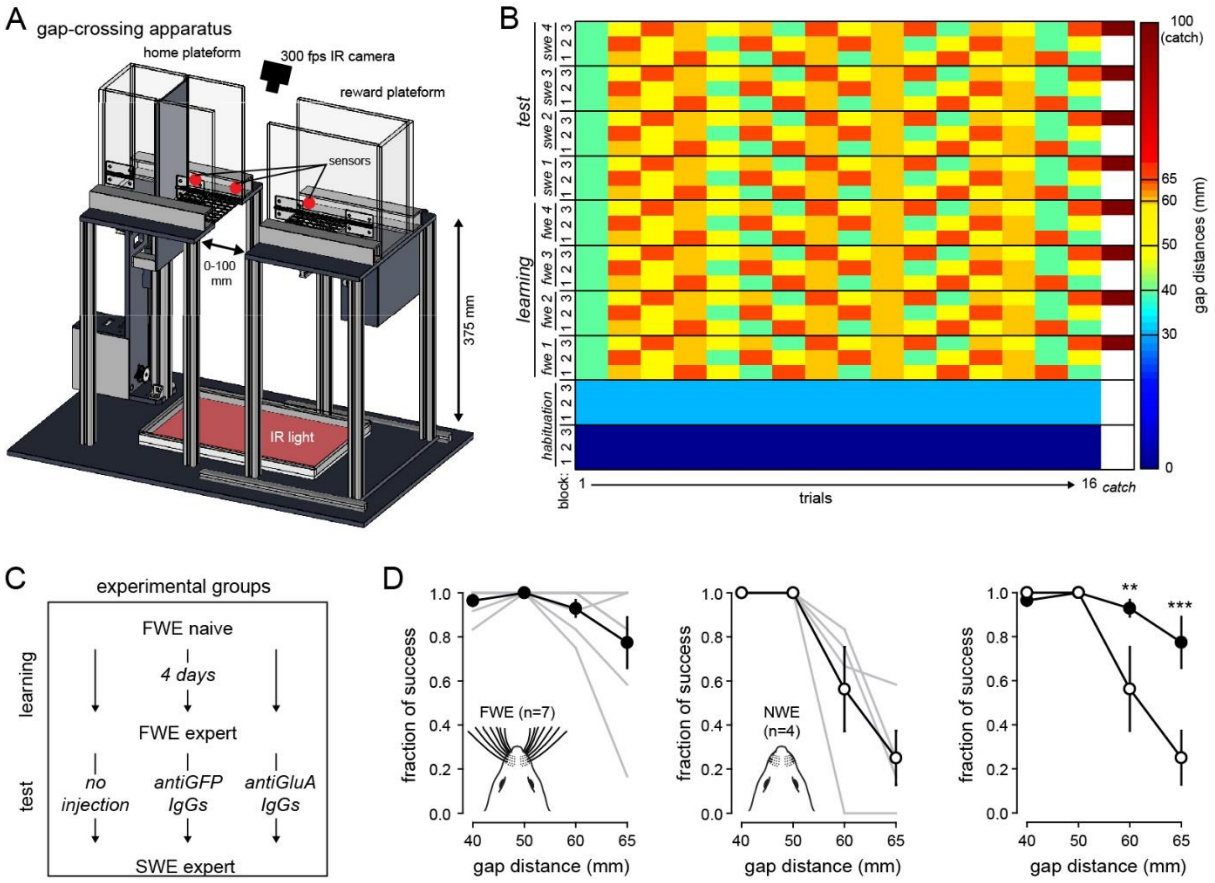

Fig. S5. The gap-crossing task relies preferentially on sensory input from whiskers

A) Overview of the gap-crossing apparatus. It consists of two individual moveable platforms: (i) a starting platform containing an automated door to precisely control the start of a trial; (ii) a reward platform containing a pellet distributor to deliver a calibrated food reward. Both platforms are elevated 374 mm from the surface and surrounded with 20-cm-high Plexiglas walls. The two platforms face each other with a high-speed 300 fps camera at the top and an infra-red pad at the bottom. The edges of the platforms close to the gap (10 x 10 cm) are made of a metal grid to allow a better grip during jump. A ruler placed in between the platforms is used to precisely define the gap distances (GD) at a given trial. Behavior is done without any sensory cues forcing mice to use their whiskers. **C)** Behavioral protocol. Food-restricted mice are first habituated to the apparatus. During test, each session consists of 3 blocks of 16 trials with pseudo-randomized GD (40, 50, 60, and 65 mm). A given trial is defined as success if mice reach the reward platform and eat the food pellet or as a failure if it takes more than 2 min to do so. At the end each trial, the animal is placed back in the home platform to start the next one. Each session ends with a catch trial where the reward platform is removed. This allows to rule out any motor habituation during jumping decision. **D)** Averaged (± sem) fraction of gap-crossing success at a distance of 65 mm, in FWE (*left*) and fully-deprived (no whiskers, NWE, *middle*). Gray lines, mice *Right,* Averaged (± sem) fraction of gap-crossing success at a distance of 65 mm, in FWE (filled circles) and NWE (open circles) mice.

Values and statistical tests are provided in Table S1.

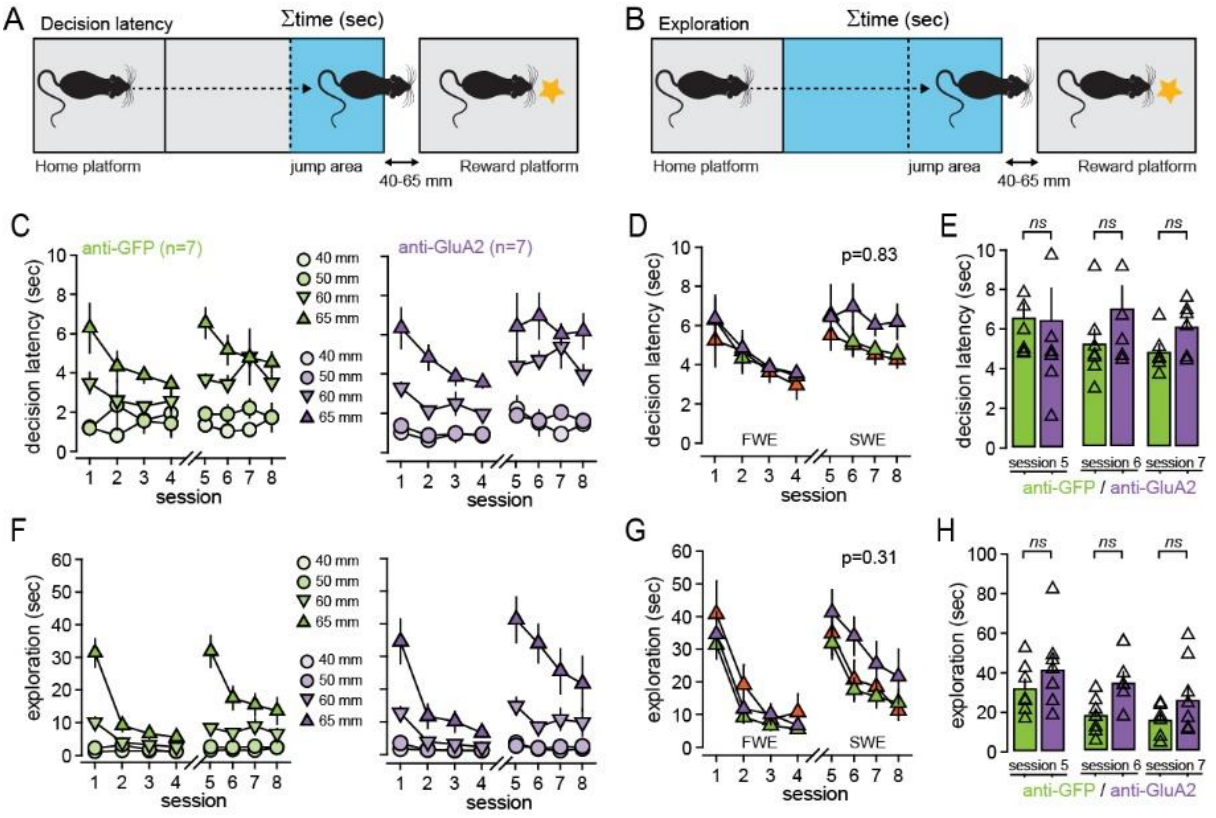

Fig. S6. IgGs do not alter exploration and decision latency

A, B) Behavioral parameters. The total time (∑time, sec) spent in the jump area (light blue in A) and in the apparatus (light blue in B, excluding the start zone) are used as metrics for decision latency and exploration, respectively. **C)** Averaged (± sem) decision latency (sec) for different gap distances, in anti-GFP (*left*) and anti-GLuA2 (*right*) injected mice. **D)** Averaged (± sem) decision latency (sec) at a distance of 65 mm, in non-injected (orange), anti-GFP (green) and anti-GLuA2 (purple) injected mice. **E)** Mean (± sem) decision latency (sec) at a distance of 65 mm after expertise in fwe mice and during swe. Triangles, individual mice. F-H), Same representation as in C-E but for exploration.

Values and statistical tests are provided in Table S1.

Table S1

fig.	variable /units	group	N	M	mean	Std dev	median	25%	75%	test	p -value
1B	fraction spiking cells non spiking (-) / spiking (+)	fwe -	20	16						*Pearson χ^2 test*	p<0.001
		fwe+	0	16							
		swe-	2	9							
		swe+	11	9							
1B	Spiking probability	fwe	20	16	0	0	0	0	0	*Mann-Whitney rank sum test*	p<0.001
		swe	13	9	0.487	0.331	0.56	0.125	0.785		
1C	PSP peak (mV)	fwe	20	16	9.883	3.883	9.209	7.093	12.041	*Mann-Whitney rank sum test*	p<0.001
		swe	13	9	17.98	8.163	16.414	12.64	21.27		
	plateau strength (mV*sec)										p=0.311
		fwe	20	16	0.994	0.705	0.812	0.514	1.325	*Mann-Whitney rank sum test*	
		swe	13	9	1.347	1.057	1.113	0.709	1.493		
1D	PSP peak (mV) fwe	baseline	7	7	8.178	3.116	6.912	6.375	11.033	*two-tailed paired t-test*	p=0.002
		RWS	7	7	9.771	2.948	9.385	7.735	12.446		
	swe									*two-tailed paired t-test*	p=0.264
		baseline	7	7	20.45	5.987	20.899	14.46	25.939		
		RWS	7	7	19.91	5.627	20.958	14.93	23.833		
1E	LTP (%) normalized to baseline	fwe	7	7	123.5	15.599	119.64	110.9	135.74	*Mann-Whitney rank sum test*	p<0.001
		swe	7	7	97.64	5.58	98.366	92.39	101.71		
2B		antiGFP	94							*two-way anova repeated measures*	p>0.1
		antiGluA2	85								
2C	plateau potentials onset (ms)	antiGFP	26	18	31.4	6.0878	30.17	27.43	34.68	*Mann-Whitney rank sum test*	p=0.420
		antiGluA2	24	16	30.03	6.2541	29.11	24.67	33.89		
	probability	antiGFP	26	18	0.702	0.2301	0.775	0.581	0.86	*Mann-Whitney rank sum test*	p=0.770
		antiGluA2	24	16	0.685	0.2341	0.72	0.522	0.887		
	strength (mV*sec)	antiGFP	26	18	0.717	0.4797	0.682	0.354	0.999	*Mann-Whitney rank sum test*	p=0.828
		antiGluA2	24	16	0.775	0.551	0.608	0.364	1.202		
2D	PSP peak (mV) anti-GFP	baseline	9	9	7.987	5.62				*two-tailed paired t-test*	p=0.002
		RWS+	9	9	9.721	6.252					
2D	PSP peak (mV) anti-GFP	baseline	8	8	10.82	6.046				*two-tailed paired t-test*	p=0.205
		RWS-	8	8	11.15	6.535					
2E	PSP peak (mV) anti-GluA2	baseline	8	8	10.59	3.531				*two-tailed paired t-test*	p=0.102
		RWS+	8	8	11.33	3.804					
	PSP peak (mV) anti-GluA2	baseline	8	8	8.899	4.072				*two-tailed paired t-test*	p=0.145
		RWS-	8	8	8.526	3.714					
2F	LTP (% of baseline)	antiGFP RWS+	9	9	123.9	15.331				*one-way anova*	p<0.001
		antiGFP RWS-	8	8	101.6	5.673				*All pairwise multiple comparisons (Holm-Sidak method)*	*p<0.001; antiGFP, RWS+ vs. RWS-*
		antiGluA2 RWS+	8	8	107.1	10.187					*p=0.085; antiGluA2, RWS+ vs. RWS-*
		antiGluA2 RWS-	8	8	97.48	9.1					*p=0.003; RWS+, antiGFP vs. antiGluA2*
											p=0.449; RWS-, antiGFP vs. antiGluA2
2G	LTP (% of baseline) plateau strength>0.5	antiGFP RWS+	4	4	138.6	10.123				*t-test*	p<0.001
		antiGluA2 RWS+	7	7	108	10.679					
3B	PSP peak (mV) anti-GluA2	baseline	6	6	7.622	4.216	8.037	3.286	11.174	*paired t-test*	p=0.041
		RWS+	6	6	10.34	6.399	11.253	3.744	14.333	*Wilcoxon signed test*	p=0.031
	PSP peak (mV) anti-GFP	baseline	6	6	12.55	3.914	12.723	9.747	16.276	*paired t-test*	p=0.436
		RWS+	6	6	12.15	4.654	12.735	9.305	15.033	*Wilcoxon signed test*	p=0.563
3F	LTP (% of baseline)	Xswe-GluA2	6	6	127.9	21.778	123.65	113.9	146.74	*one-way anova*	p<0.001
		Xswe-GFP	6	6	98.09	5.906	98.366	92.71	103.48	*All pairwise multiple comparisons (Holm-Sidak method)*	*p<0.001; Xswe, GluA2 vs. GFP*
		fwe	7	7	123.5	15.599	119.64	110.9	135.74		*p<0.001; Xswe GluA2 vs. swe*
		swe	7	7	97.64	5.58	98.366	92.39	101.71		*p<0.001; Xswe GFP vs. fwe*
											p<0.001; fwe. vs swe
											p=0.551; Xswe-GluA2 vs fwe
											p=0.945; Xswe-GFP vs. swe
3G	fraction spiking cells non spiking (-) / spiking (+)	X-swe-GFP (-)	2							*Pearson χ^2 test*	p=0.701
		X-swe-GFP (+)	6								
		X-swe-GluA2 (-)	3								
		X-swe-GluA2 (+)	6								

fig.	variable /units	group	N	M	mean	Std dev	median	25%	75%	test	p -value
3C	spiking probability	fwe	20	16	0	0	0	0	0	*one-way anova*	p<0.001
		swe	13	9	0.487	0.331	0.56	0.125	0.785	*All pairwise multiple*	*p<0.001; fwe. vs swe*
		Xswe-GFP	8	8	0.351	0.391	0.18	0.031	0.693	*comparisons*	*p<0.001; Xswe GFP vs. fwe*
		Xswe-GluA2	9	9	0.089	0.131	0.0317	0	0.124	*(Holm-Sidak method)*	*p<0.001; Xswe GluA2 vs. swe*
											p=0.026; Xswe, GluA2 vs. GFP
											p=0.351; Xswe-GluA2 vs fwe
											p=0.202; Xswe-GFP vs. swe
3D	PSP peak (mV)	fwe	20	16	9.883	3.883	9.209	7.093	12.041	*one-way anova*	p<0.001
		swe	13	9	17.98	8.163	16.414	12.64	21.27	*All pairwise multiple*	*p<0.001; fwe. vs swe*
		Xswe-GFP	8	8	14.17	4.596	14.562	10.8	17.481	*comparisons*	*p<0.001; Xswe GluA2 vs. swe*
		Xswe-GluA2	9	9	7.047	4.036	6.734	2.661	10.816	*(Holm-Sidak method)*	*p=0.01; Xswe, GluA2 vs. GFP*
											p=0.07; Xswe GFP vs. fwe
											p=0.201; Xswe-GluA2 vs fwe
											p=0.126; Xswe-GFP vs. swe
4C	fraction of success 65mm	FWE session 4		6	0.958	0.102				*one-way anova*	p=0.034
		SWE session 5		6	0.681	0.322				*repeated measures*	*swe5 vs fwe4, p=0.006*
		SWE session 6		6	0.875	0.234				*multiple comparisons*	*swe6 vs fwe4, p=0.372*
		SWE session 7		6	0.917	0.105				*vs. FWE session 4*	*swe7 vs fwe4, p=0.653*
		SWE session 8		6	0.958	0.0697				*(Holm-Sidak method)*	*swe8 vs fwe4, p=1*
4D	fraction of success			6	1.014	0.17				*t-test*	p=0.503
	normalized session8/session4			5	0.934	0.211					
4E	fraction of success anti-GFP 65mm	FWE session 4		7	1	0	1	1	1	*one-way anova*	p=0.025
		SWE session 5		7	0.774	0.178	0.833	0.625	0.896	*repeated measures*	*swe5 vs fwe4, p=0.015*
		SWE session 6		7	0.905	0.183	1	0.917	1	*multiple comparisons*	*swe6 vs fwe4, p=0.250*
		SWE session 7		7	0.826	0.252	0.917	0.667	1	*vs. FWE session 4*	*swe7 vs fwe4, p=0.125*
		SWE session 8		7	0.917	0.16	1	0.875	1	*(Holm-Sidak method)*	*swe8 vs fwe4, p=0.5*
	fraction of success anti-GluA2 65mm	FWE session 4		7	1	0	1	1	1	*one-way anova*	p<0.001
		SWE session 5		7	0.382	0.325	0.25	0.085	0.729	*repeated measures*	*swe5 vs fwe4, p<0.001*
		SWE session 6		7	0.512	0.374	0.5	0.208	0.854	*multiple comparisons*	*swe6 vs fwe4, p<0.001*
		SWE session 7		7	0.726	0.384	0.917	0.5	1	*vs. FWE session 4*	*swe7 vs fwe4, p=0.031*
		SWE session 8		7	0.739	0.396	1	0.396	1	*(Holm-Sidak method)*	*swe8 vs fwe4, p=0.059*
4G	fraction of success 65mm Session 5	antiGFP		7	0.774	0.178	0.833	0.625	0.896	*t-test*	p=0.0016
		antiGluA2		7	0.382	0.325	0.25	0.085	0.729	*Mann-Whitney test*	p=0.0026
	fraction of success 65mm Session 6	antiGFP		7	0.905	0.183	1	0.917	1	*t-test*	p=0.028
		antiGluA2		7	0.512	0.374	0.5	0.208	0.854	*Mann-Whitney test*	p=0.038
	fraction of success 65mm Session 7	antiGFP		7	0.826	0.252	0.917	0.667	1	*t-test*	p=0.577
		antiGluA2		7	0.726	0.384	0.917	0.5	1	*Mann-Whitney test*	p=0.805
	fraction of success 65mm Session 8	antiGFP		7	0.917	0.16	1	0.875	1	*t-test*	p=0.293
		antiGluA2		7	0.739	0.396	1	0.396	1	*Mann-Whitney test*	p=0.535
S1E	responding area normalized to first session	SWE0		6	1	0.149				*one-way anova*	p=0.012
		SWE1		6	1.25	0.246				*repeated measures*	*SWE0 vs SWE1, p=0.246*
		SWE2		6	1.756	0.69					*SWE0 vs SWE2, p=0.004*
		FWE0		7	1	0.0658				*one-way anova*	p=0.306
		FWE1		7	0.854	0.11				*repeated measures*	
		FWE2		7	0.97	0.304					
S2B	Rheobase (pA)	FWE	24	11	370.4	96.336	350	300	400	*t-test*	p=0.042
		SWE	27	17	308.3	115.78	300	250	375	*Mann-Whitney test*	p=0.029
S2C	PSP peak (mV)	FWE	20	16	9.883	3.883	9.209	7.093	12.041	*t-test*	p<0.001
		SWE	13	9	17.98	8.163	16.414	12.64	21.27	*Mann-Whitney test*	p<0.001
	Spiking probability	FWE	20	16	0	0	0	0	0	*t-test*	p<0.001
		SWE	13	9	0.487	0.331	0.56	0.125	0.785	*Mann-Whitney test*	p<0.001
S2E	8hZ-cumulatibe PSP mV*sec	FWE	10	10	4.637	2.63	4.147	3.587	4.727	*t-test*	p=0.004
		SWE	10	10	9.185	3.396	7.893	6.841	12.877	*Mann-Whitney test*	p=0.005
S3A	cell depth (µm)	antiGFP	34		-219.9	103.57	-206.8	-284	-130.3	*t-test*	p=0.512
		antiGluA2	31		-201.2	91.886	-168.3	-251	-134.3	*Mann-Whitney test*	p=0.631
S3B	10 sec cumulative Vm mV*sec	antiGFP	14		27.4	16.095	24.383	16.32	37.663	*t-test*	p=0.827
		antiGluA2	20		26.08	18.078	22.873	11.46	33.438	*Mann-Whitney test*	p=0.740
S3C	up states probability	antiGFP	14		0.192	0.0637	0.179	0.144	0.24	*t-test*	p=0.452
		antiGluA2	20		0.173	0.0757	0.157	0.126	0.21	*Mann-Whitney test*	p=0.319
S3E	1/τ (ms-1)	antiGFP	18		0.32	0.156	0.315	0.228	0.481	*t-test*	p=0.615
		antiGluA2	25		0.35	0.198	0.337	0.257	0.49	*Mann-Whitney test*	p=0.610
	up-state amplitude (mV)	antiGFP	18		10.72	3.32	10.372	8.244	13.923	*t-test*	p=0.396
		antiGluA2	25		11.51	2.67	11.187	9.554	13.578	*Mann-Whitney test*	p=0.675
S3F	IV curve	antiGFP	4	4	0.815	0.0357				*two-way anova*	p=0.238
		antiGluA2	2	2	0.751	0.0456				*repeated measures*	

fig.	variable /units	group	N	M	mean	Std dev	median	25%	75%	test	p -value
S3G	PSP peak amplitude (mV)	antiGFP	34		8.874	4.474	8.512	5.375	11.204	*t-test*	p=0.895
		antiGluA2	31		8.732	4.07	8.812	6.08	9.845	*Mann-Whitney test*	p=0.974
	PSP integral (mV*sec)	antiGFP	34		0.642	0.319	0.573	0.432	0.849	*t-test*	p=0.596
		antiGluA2	31		0.684	0.306	0.644	0.429	0.809	*Mann-Whitney test*	p=0.614
S3H	PSP onset (ms)	antiGFP	34		11.87	2.229	11.639	10.68	12.761	*t-test*	p=0.621
		antiGluA2	31		12.22	3.029	11.631	9.844	14.363	*Mann-Whitney test*	p=0.865
	onset jitter (ms)	antiGFP	34		1.876	1.07	1.883	1.052	2.621	*t-test*	p=0.178
		antiGluA2	31		2.444	1.77	2.159	1.279	2.677	*Mann-Whitney test*	p=0.992
S4A	LTP (% of baseline)	fwe	7	7	123.5	15.599	119.64	110.9	135.74	*one-way anova*	p<0.001
		fwe antiGFP	9	9	123.9	15.331	113.84	112.5	142.08	*repeated measures*	*fwe vs. fwe anti-GFP, p=0.951*
		fwe antiGluA2	8	8	107.1	10.187	108.91	99.25	115.54	*multiple comparisons*	*fwe vs. fwe anti-GluA2, p=0.023*
		swe	7	7	97.64	5.58	98.366	92.39	101.71	*vs. fwe*	*fwe vs. swe, p<0.001*
		swe antiGFP	6	6	94.58	11.989	94.308	92.36	106.24	*(Holm-Sidak method)*	*fwe vs. swe antiGFP, p<0.001*
		swe antiGluA2	6	6	129.8	19.188	123.65	113.9	146.74		*fwe vs. swe antiGluA2, p=0.408*
S4B	plateau strength (mV*sec)	fwe	20		0.994	0.705	0.812	0.514	1.325	*one-way anova*	p=0.151
		fwe antiGFP	34		0.693	0.449	0.682	0.354	0.999		
		fwe antiGluA2	31		0.85	0.524	0.756	0.398	1.228		
		swe	13		1.347	1.057	1.113	0.709	1.493		
		swe antiGFP	7		0.888	0.523	0.797	0.498	1.171		
		swe antiGluA2	9		0.709	0.622	0.538	0.349	0.999		
S5B	fraction of success	fwe (40)		7	0.964	0.0656	1	0.938	1	*two-way anova*	p=0.002 (interaction)
	NWE, no whisker FWE, full whiskers (gap distance,mm)	fwe (50)		7	1	0	1	1	1	*repeated measures*	*GD 40, FWE vs NWE, p=0.763*
		fwe (60)		7	0.929	0.101	1	0.854	1	*multiple comparisons*	*GD 50, FWE vs NWE, p=1*
		fwe (65)		7	0.774	0.307	0.833	0.646	1	*(Holm-Sidak method)*	*GD 60, FWE vs NWE, p=0.004*
		nwe (40)		4	1	0	1	1	1		*GD 65, FWE vs NWE, p<0.001*
		nwe (50)		4	1	0	1	1	1		
		nwe (60)		4	0.563	0.381	0.708	0.333	0.792		
		nwe (65)		4	0.25	0.245	0.208	0.083	0.417		
S6E	decision latency (sec) anti-GFP vs anti-GluA2 GD=65mm	session5 GFP		7	5.893	2.599	5.957	4.806	7.314	*t -test*	session 5, antiGFP vs antiGluA2, p=0.995
		session6 GFP		7	4.67	2.245	4.615	3.773	5.335		session 6, antiGFP vs antiGluA2, p=0.258
		session7 GFP		7	4.222	1.762	4.487	3.965	4.916		session 7, antiGFP vs antiGluA2, p=0.285
		session5 GluA2		7	5.882	4.119	4.835	3.276	7.238		
		session6 GluA2		7	6.219	3.156	5.997	4.499	8.021		
		session7 GluA2		7	5.342	2.236	6.068	4.446	6.81		
S6H	exploration (sec) anti-GFP vs anti-GluA2 GD=65mm	session5 GFP		7	28.79	14.218	26.39	20.2	38.521	*t -test*	session 5, antiGFP vs antiGluA2, p=0.286
		session6 GFP		7	15.99	9.336	17.317	8.785	21.999		session 6, antiGFP vs antiGluA2, p=0.037
		session7 GFP		7	13.92	8.121	15.58	5.836	20.437		session 7, antiGFP vs antiGluA2, p=0.181
		session5 GluA2		7	37.77	20.361	37.661	25.7	46.408		
		session6 GluA2		7	31.14	17.003	33.362	17.41	39.299		
		session7 GluA2		7	23.62	18.149	20.583	10.62	29.713		

Materials and Methods

Animals

All experiments were performed in accordance with the Guide for the Care and Use of Laboratory Animals (National Research Council Committee (2011): Guide for the Care and Use of Laboratory Animals, 8th ed. Washington, DC: The National Academic Press.) and the European Communities Council Directive of September 22th 2010 (2010/63/EU, 74). Experimental protocols were approved by the institutional ethical committee guidelines for animal research (N°50DIR_15-A) and by the French Ministry of Research (agreement N°18892). We used male C57BL6/J 5- and 6-weeks old mice from Charles River that were housed with littermates (3 mice per cage) in a 12-h light-dark cycle. Cages were enriched with tunnels, food and water were provided *ad libitum*, except during behavioral experiments (see below).

Cranial window implantation for chronic Intrinsic Optical Imaging

Anesthesia. Anesthesia was induced using isoflurane (4% containing ~0.5 l/min O2) and then continued using an intraperitoneal (i.p.) injection of a MB mixture (MB) (5 µl/g) composed of medetomidine (0.2 mg/kg), and buprenorphine (0.2 mg/kg). A heating-pad was positioned underneath the animal to keep the body temperature at 37°C. Eye dehydration was prevented by topical application of ophthalmic gel. Analgesia was achieved by local application of 100 µL of lidocaine (lurocaine, 1 %) and subcutaneous (s.c.) injection of buprenorphine (buprécare, 0.05 mg/kg). To prevent risks of inflammation and brain swelling 40 µL of dexamethasone (dexadreson, 0.1 mg/mL) were injected intramuscularly (i.m.) before the surgery. After disinfection of the skin (with modified ethanol 70% and betadine), the skull was exposed and a ~5mm plastic chamber was attached to it above the relative stereotaxic location of the C2 barrel column (-1.5 mm from bregma, + 3.3 mm mideline) using a combination of super glue (Loctite) and dental cement (Jet Repair Acrylic, Lang Dental Manufacturing). The chamber was filled with saline (0.9% NaCl) and sealed with a glass coverslip.

Intrinsic Optical Imaging (IOI) for barrel column targeting. To locate the cortical barrel column computing the whisker C2 (wC2), intrinsic optical signals (IOS) were imaged as previously described, through the intact skull using a light guide system with a 700 nm (bandwidth of 20 nm) interference filter and stable 100-W halogen light source (*1-3*). Briefly, the head of the animal was stabilized using a small stereotaxic frame and the body temperature kept constant with a heating pad. An image of the surface vascular pattern was taken using a green light (546 nm- interference filter) at the end of each imaging session. Images were acquired using the Imager 3001F (Optical Imaging, Mountainside, NJ) equipped with a large spatial 602 × 804 array, fast readout, and low read noise charge-coupled device (CCD) camera. The size of the imaged area was adjusted by using a combination of two lenses with different focal distances (upper lens: Nikon 135 mm, f2.0; bottom lens: Nikon 50 mm, f1.2). The CCD camera was focused on a plane 300 µm below the skull surface. Images were recorded at 10 Hz for 5 sec., with a spatial resolution of 4.65 µm/pixel comprising a total area of 2.9 x 3.7 mm^2. wC2 was deflected back and forth (20 stimulations at 8 Hz for 1 sec.) using a glass-capillary attached to a piezoelectric actuator (PL-140.11 bender controlled by an E-650 driver; Physik Instrumente) triggered by a pulse stimulator (Master-8, A.M.P.I.). Each trial consisted of a 1 sec. of baseline period (frames 1-10), followed by a response period (frames 11-22) and a post-stimulus period (frames 23-50). Inter-trial intervals lasted 20 sec. to avoid contamination of the current IOS by prior stimulations. IOS were computed by subtracting each individual frame of the

response period by the average baseline signal. The obtained IOS was overlapped with the vasculature image using ImageJ software to precisely identify the cortical region computing wC2.

Craniotomy and cranial window. implantation. After IOI, adequate anesthesia was assessed (absence of toe pinch reflexes, corneal reflexes, and vibrissae movement) and prolonged using supplementary isoflurane if necessary. Dehydration was prevented by injecting sterile saline by s.c. injection. A 3 mm diameter craniotomy was then made over the maximum IOS using a pneumatic dental drill. The craniotomy was covered with sterile saline and sealed with a 3 mm glass coverslip. The coverslip was sealed to the skull using dental acrylic and dental cement (Jet Repair Acrylic, Lang Dental Manufacturing). Anesthesia was reverted by a sub-cutaneous injection of an AB mixture (AB) containing atipamezole (Revertor, 2.5 mg/kg), and buprenorphine (Buprécare, 0.1mg/kg). A delay of 2-3 weeks for surgery recovery was respected before all imaging experiments, during which the body weight of mice was daily checked.

Chronic Intrinsic Optical Imaging

Imaging protocol. MB-anaesthetized mice were daily-imaged during 1 session with all their whiskers (baseline), followed by 2 sessions (SWE 1-2) with all their whiskers trimmed except wC2. A cohort group was additionally recorded for 3 days with all their whiskers (FWE 1-3) as a control for barrel expansion. During each session, wC2 was deflected back and forth (20 stimulations at 8Hz for 1 sec) and IOS recorded through a CW.

Spatiotemporal analysis of IOS. An average of 200 trials were recorded per session to quantify IOS as previously described (3). The IOS of different sessions from the same animal were spatially aligned using the animal's brain surface vasculature and spatially binned (6x6, final resolution: 27.9 µm/pixel or 3x3, final resolution: 13.95 µm/pixel). A high pass-filter was then applied by subtracting from each image-frame the same image-frame that was convolved using a 1270 µm full-width at half maximum (FWHM) Gaussian kernel. The whisker-evoked IOS were then simulated using a pixel-by-pixel paired t-test, comparing the baseline period and the response period of all trials within a session. The t maps for each individual trial were low pass-filtered with a 340 µm FWHM Gaussian kernel and averaged into a final t map response. A threshold was set to $t < -2.0$ and any signal below this value was considered to belong to the stimulus-evoked response area. If the pixel value was $t \geq -2.0$ it was considered background noise and discarded for quantification. This usually resulted in an image with a clear minimum, representing the response maximum and the barrel's center of mass. Changes on IOS pixel area caused by whisker trimming were computed as the ratio between the whisker-evoked IOS response of the baseline and SWE sessions. All data analysis was performed using a custom software written in MATLAB (MathWorks).

***In vivo* whole-cell recordings**

Acute AMPAR X-linking surgery. Anesthesia was induced using isoflurane (4% with 0.5 l min^{-1} O2) and then continue using i.p. injection of urethane (1.5 g kg^{-1}). Surgery preparation and IOI were performed as aforementioned. After imaging, adequate anesthesia was assessed and prolonged by supplementary urethane (0.15 g kg^{-1}) if necessary. A small ~1 × 1 mm craniotomy (centered above the C2 whisker maximum IOS response) was made using a pneumatic dental drill. Thee injections of either an anti-GluA2 antibody (clone 15F1, gif from E. Gouaux) or a monoclonal anti-GFP IgG1-K (Roche, 11814460001) were targeted to the L2/3 of S1 (-0.1 to 0.3 mm dorsoventral). A 30 nL

solution containing antibody diluted in sterile saline (0.05 mg/mL) was injected at maximum rate of 15nl/min, with 30 sec intervals between injection sites as described before. All the experiments were performed blind for the antibody injected.

Chronic AMPAR X-linking surgery. Anesthesia was induced using isoflurane (4% containing ~0.5 l min^{-1} O2) and continued using an i.p. injection of MB to perform IOI targeting of the wC2 cortical barrel. Adequate anesthesia was assessed and prolonged using isoflurane if necessary. Dehydration was also prevented by s.c. injection of sterile saline. A small ~ 1 mm diameter craniotomy above the maximum IOS was made using a pneumatic dental drill. The dura was left intact and a stereotaxic injection of either anti-GluA2 or anti-GFP antibody was performed as mentioned above for acute injection. After stereotaxic injection, the craniotomy was covered with sterile saline and protected with a 3 mm polydimethylsiloxane (PDMS) coverslip. PDMS was attached to the skull using an ultra-violet (U.V.) curing optical adhesive (NOA61, Norland) cured with a 50 mW U.V. laser (3755B-150-ELL-PP, Oxxius). Before reverting anesthesia using AB, all the whisker except C2 were trimmed (SWE1). Antibodies were re-injected twice on the day after (SWE2), with a 12h interval between injections using isoflurane anesthesia (4% for induction, then 2% for injection with ~0.5 l min−1 O^2). Stereotaxic injections were performed through the PDMS CW with the same injection protocol than before. After 12h of antibody washout (SWE3), mice were finally anesthetized with isoflurane (4% with 0.5 l min-1 O2) and an i.p. injection of urethane (1.5 $g.kg^{-1}$). Before the patch-clamp recordings, the PDMS C.W. was removed and the cortex protected with saline. All the experiments were performed blind for the antibody injected.

Recordings. Whole-cell patch-clamp recordings of L2/3 pyramidal neurons were obtained as describes previously (*4*). Current-clamp recordings were made using a potassium-based internal solution in mM: 135 potassium gluconate, 4 KCl, 10 HEPES, 10 Na2-phosphocreatine, 4 Mg-ATP and 0.3 Na-GTP), pH adjusted to 7.25 with KOH, 285 mOsM). High positive pressure (200–300 mbar) was applied to the pipette (5–8 MΩ) to prevent tip occlusion. After passing the pia the positive pressure was immediately reduced to prevent cortical damage. The pipette was then advanced in 1-µm steps, and pipette resistance was monitored in the conventional voltage clamp configuration. When the pipette resistance suddenly increased, positive pressure was relieved to obtain a 3–5 GΩ seal. After break-in, membrane potential (Vm) was measured, and dialysis could occur for at least 5 min before deflecting the whisker. Spiking pattern of patched cells was analyzed to identify pyramidal neurons. Action potentials were obtained by a step-increment of injected current and the number or the minimum threshold for spike represented. Spontaneous slow-have fluctuations of the resting membrane potentials were recorded as previously described (*5*). PSPs were evoked by back and forth deflection of the whisker (100 ms, 0.133 Hz) as previously described (*4*). The voltage applied to the actuator was set to evoke a displacement of 0.6 mm with a ramp of 7-8 ms of the wC2. Different frequencies of stimulation were used accordingly to the experiment (RWS-LTP: 8Hz, 1 min; cumulative PSPs: 8Hz, 2.5 sec). Series and input resistance were monitored with a 100-ms long-lasting hyperpolarizing square pulse 400 ms before each single-deflection and extracted offline by using a double-exponential fit. Recordings were discarded if the change in these parameters were larger than 30%. The bridge was usually not balanced, and liquid junction potential not corrected. All the data were acquired using a Multiclamp 700B Amplifier (Molecular Devices) and digitized at 10 kHz (National Instruments) using software. Offline analysis was performed using custom routines written in IGOR Pro (WaveMetrics).

Behavior

Gap crossing apparatus. The custom-made gap crossing (G.C.) apparatus (Imetronic, France) consists of two individual moveable platforms: (1) a starting platform containing an automated door to precisely control the start of a trial; (2) a reward platform containing a pellet distributor to deliver a calibrated food reward. Both platforms (10x20 cm) were elevated 37.4 cm from the surface and surrounded on the three sides with a 20-cm-high Plexiglas walls. The two platforms were placed facing each other with a high-speed 300 frames per second (fps) camera at the top and an infra-red pad at the bottom. This allowed us to precisely track mice behavior and whisker motion with high spatiotemporal resolution. The edges of the platforms that face each other were made of a metal grid (10 x 10 cm) to allow a better grip where the animals should jump. A ruler placed at the bottom and between the platforms was used to precisely define the gap distances (GD) at a given trial. The apparatus was placed into a light- and soundproof cage containing ventilation, and surrounding speakers with a continuous white noise background. This ensures that mice do not have neither visual nor auditory cues regarding the reward platform. Food pellet odor was saturated inside the box to avoid any olfactory-related cues.

Behavioral protocol. At least 5 days before starting behavior, mice were food restricted and handled to decrease stress. After a 15 – 20 % reduction of the initial body weight, habituation was performed during 3 days: (day 1 – Maze Habituation) mice were placed on the G.C. apparatus with a GD = 0 cm for 10 min. where the pellet distributor was randomly presented for multiple times without food reward; (day 2 – Reward Habituation) mice were placed on the start platform and trained for 3 blocks (16 trials each block, GD = 0 cm) to the distribution of a food pellet in the reward platform. A given trial was defined as success if the animal reached the reward platform and ate the food pellet or as a failure if it took more than 2 min to do so. At the end of a trial, the animal was placed back in the starting platform to beginning the next one; (day 3 – Jump Habituation) the same protocol than (2) but using a GD = 3 cm to habituate the animal for a distance between platforms. Habituation is considered successful and the test sessions started if the success rate was >95%. The test protocol had 1 session per day during 4 days where each session was composed of 16 trials containing GD = 40, 50, 60, and 65 mm. Individual blocks started with the minimal GD, had random GD sequences, and finished with a catch trial (GD: 100 mm) where the reward platform was removed. This allowed to rule out habit to jump. When addressing the effect of whisker trimming on expert mice, test sessions were performed before and after whisker trimming.

Cannula implantation for chronic AMPAR X-linking. Anesthesia was induced using isoflurane and continued by an i.p. injection of MB to perform IOI targeting of the wC2 cortical barrel as aforementioned. A small craniotomy above the maximum IOS was made using a pneumatic dental drill, preventing any cortical damage. After drilling, a guide cannula (62001, RWD Life Science Co., LTD) was stereotaxically inserted in the brain using a cannula holder through the craniotomy previously made. The size of the cannula (0.6 mm) was adjusted to target L1 of the somatosensory cortex. The guide cannula was fixed to the skull using two stainless steel screws and a mix of super glue (Loctite), dental acrylic and dental cement. Anesthesia was reverted by a s.c. injection of AB and mice left to recover over 2 weeks before starting food restriction. During food restriction, mice were additionally habituated to be restrained by a different experimenter to avoid stress during antibody injection. Mice were tested during 4 sessions with FWE followed by 4 SWE sessions, during which either an anti-GluA2 or an anti-GFP antibody (0.05 mg/mL)

was injected. Antibodies were injected twice per day, before and after each test session, using a pump (D404, RWD Life Science CO.) with an injection speed of 6nL/min for the first 120nL and 3nL/min for the remaining 30nL of antibody. Mice were freely moving in their home cage during injection. All experiments and analysis were performed blind for the antibody injected.

Histology

To evaluate the antibody injection profiles in S1, animals were intracardially perfused with PBS (1%) and PFA (4%). Fixed brains were sliced with a vibratome and sections posteriorly incubated with PBS.H202 (0.3%) during 30 min to block endogenous peroxide. Brain slices were then incubated with a secondary anti-mouse biotinylated antibody from donkey (1/200), during 2h at room temperature (RT). To finally reveal the injected primary antibody, slices were first incubated with an avidin-biotin complex (1/200 in PBS (1x) – Triton 0.1%), and then with DAB (ab64259, Abcam). Brain slices were finally mounted between slide and coverslip and imaged post-hoc using a Nanozoomer (S360, Hamamatsu). To evaluate the viral expression profiles in the barrel cortex, fixed brain slices were directly imaged post-hoc on the same microscope. Illumination was set such that the full dynamic range of the 16-bit images was utilized. A two-dimensional graph of the intensities of pixel was then plotted using a Fiji Software. 16-bit image's brightness was processed and a mask were registered to the corresponding coronal plates (ranging from -0.26 to -1.94 mm) of the mouse brain atlas using Illustrator (Adobe), at the various distances posterior to the bregma.

Statistics.

Detailed statistics are described in table S1. Statistical differences were considered at $p<0.05$. All experiments and analysis were performed blind for experimental conditions.

References

1. Gambino, F. & Holtmaat, A. Spike-timing-dependent potentiation of sensory surround in the somatosensory cortex is facilitated by deprivation-mediated disinhibition. *Neuron* **75**, 490–502 (2012).
2. Zepeda, A., Arias, C. & Sengpiel, F. Optical imaging of intrinsic signals: Recent developments in the methodology and its applications. *J. Neurosci. Methods* **136**, 1–21 (2004).
3. Schubert, V., Lebrecht, D. & Holtmaat, A. Peripheral Deafferentation-Driven Functional Somatosensory Map Shifts Are Associated with Local, Not Large-Scale Dendritic Structural Plasticity. *J. Neurosci.* **33**, 9474–9487 (2013).
4. Gambino, F. *et al.* Sensory-evoked LTP driven by dendritic plateau potentials in vivo. *Nature* **515**, 116–119 (2014).
5. Petersen, C. C. H., Hahn, T. T. G., Mehta, M., Grinvald, A. & Sakmann, B. Interaction of sensory responses with spontaneous depolarization in layer 2/3 barrel cortex. *Proc. Natl. Acad. Sci.* **100**, 13638–13643 (2003).